Universidade de São Paulo
Instituto de Física

A correspondência AdS/CFT e o plasma de quarks e glúons

Viktor Jahnke
Orientador: Diego Trancanelli

Tese de doutorado apresentada ao
Instituto de Física da Universidade de São Paulo
para obtenção do título de Doutor em Ciências

Banca examinadora:
Prof. Dr. Diego Trancanelli - IFUSP (Orientador)
Prof. Dr. Victor Oliveira Rivelles - IFUSP
Prof. Dr. Matthew Luzum - IFUSP
Prof. Dr. Horatiu Stefan Nastase - IFT/UNESP
Prof. Dr. José D. Edelstein - USC/Espanha

São Paulo, 2016

FICHA CATALOGRÁFICA
Preparada pelo Serviço de Biblioteca e Informação do Instituto de Física da Universidade de São Paulo

Jahnke, Viktor

A correspondência AdS/CFT e o plasma de quarks e glúons. São Paulo, 2016.

Tese (Doutorado) – Universidade de São Paulo. Instituto de Física. Depto. de Física Matemática.

Orientador: Prof. Dr. Diego Trancanelli

Área de Concentração: Teoria de Cordas

Unitermos: 1. Física de alta energia; 2. Física teórica; 3. Teoria de gauge.

USP/IF/SBI-081/2016

Universidade of São Paulo
Instituto de Física

The AdS/CFT correspondence and the quark-gluon plasma

Viktor Jahnke
Supervisor: Diego Trancanelli

A thesis submitted in fulfillment of
the requirements for the degree of
Doctor in Science in the Instituto de
Física da Universidade de São Paulo

Doctoral Committee:
Prof. Dr. Diego Trancanelli - IFUSP (Supervisor)
Prof. Dr. Victor Oliveira Rivelles - IFUSP
Prof. Dr. Matthew Luzum - IFUSP
Prof. Dr. Horatiu Stefan Nastase - IFT/UNESP
Prof. Dr. José D. Edelstein - USC/Spain

São Paulo, 2016

Resumo

O objetivo desse trabalho é estudar aplicações da correspondência AdS/CFT na descrição de plasmas fortemente acoplados similares ao plasma de quarks e glúons (PQG) produzido em colisões de íons pesados no RHIC e no LHC. O projeto está articulado em duas partes. Inicialmente estudamos como alguns observáveis, como a taxa de produção de fótons e diléptons, são afetados por anisotropias espaciais presentes no plasma. Isso é importante porque o PQG produzido em experimentos do mundo real tipicamente começa em configurações de alta anisotropia, que depois evoluem para configurações isotrópicas. Para modelar a anisotropia a acoplamento forte fizemos uso de uma solução de buraco negro de supergravidade do tipo IIB encontrada recentemente em arXiv:1105.3472/hep-th. Como segunda direção de pesquisa e novamente focando em aplicações da correspondência AdS/CFT na descrição do PQG, investigamos teorias de gravidade de Lovelock, que são generalizações naturais da teoria de relatividade geral de Einstein. Essas teorias contém termos com derivadas de ordem superior ao mesmo tempo que mantém equações do movimento de segunda ordem, e por isso constituem uma arena ideal para começar a entender como termos de derivada de ordem superior afetam vários observáveis físicos do plasma.

Palavras-chave: correspondência gauge-gravidade, holografia e o plasma de quarks e glúons, gravidade de curvatura de ordem mais elevada.

Abstract

The aim of this work is to study applications of the AdS/CFT correspondence to strongly coupled plasmas similar to the quark-gluon plasma (QGP) produced in heavy ion collisions at RHIC and LHC. The project is articulated in two parts. Initially, we will study how some observables, such as photon and dilepton production rates, are affected by spatial anisotropies present in the plasma. This is important, since the QGP produced in real world experiments generically starts in highly anisotropic configurations, which later evolve towards isotropy. To model anisotropy at strong coupling we will make use of an anisotropic black hole solution of type IIB supergravity which has been recently obtained in arXiv:1105.3472/ hep-th. As a second direction of research and again focusing on applications of the AdS/CFT correspondence to the QGP, we will investigate Lovelock theories of gravity, which are a natural generalizations of Einsteins general relativity. These theories contain higher derivative terms, while maintaining the equations of motion of second order, and constitute an ideal arena where to start understanding how higher derivative corrections affect various physical observables of the plasma.

Keywords: Gauge-gravity correspondence, holography and quark-gluon plasmas, Higher curvature gravity.

À minha família, Joyce e Pedrinho.

Agradecimentos

Agradeço ao meu orientador, Diego Trancanelli, pelo grande auxílio na realização desse projeto e por toda ajuda na minha formação como físico teórico.

Também agradeço aos meus colaboradores, Leonardo Patiño, Andres Luna e Anderson Misobuchi. Em especial, agradeço ao Anderson pelo companheirismo e pelas discussões que deram origem a maior parte dessa tese.

Agradeço também ao meu amigo Stefano Finazzo, por me apresentar a área de pesquisa desse trabalho e por me fornecer as referências básicas para aprender sobre esse assunto.

Agradeço ao professor Jorge Noronha, com quem aprendi muito sobre fluidos relativísticos não dissipativos e pela ajuda nos estágios iniciais desse trabalho.

Agradeço à minha irmã, Cristiane, por toda ajuda prestada ao longo de todo esse trabalho e por tudo que me ensinou sobre a fenomenologia da colisão de íons pesados. Também agradeço ao Tiago Fiorini, pelo companherismo e pelos conselhos acadêmicos de grande valia.

Agradeço ao meu irmão, Max, pelo companherismo e por todo auxílio prestado ao longo desse trabalho. Agradeço também o apoio e a amizade da Adèle.

Também agradeço aos meus amigos *simprões*, Lelas, Bruno, Ícaro, Schock, LM e Felis, pelo companherismo ao longo desses quase quatro anos de doutoramento e pelas

inúmeras discusses sobre a Vida, o Universo e Tudo Mais. Em particular, agradeço ao Brunão pela ajuda na preparação da defesa e por sempre assistir minhas prévias.

Em especial, agradeço à minha famlia, Joyce e Pedrinho, por toda a paciência e incentivo ao longo desse trabalho e pela inspiração que me proporcionam.

Agradeço aos meus pais, Horst e Gilda, por todo apoio e incentivo. Em especial, agradeço à minha mãe por educar a mim e aos meus irmãos com todo amor e dedicação. Também agradeço a todos os familiares que me apoioaram nesse período: Sr. João, Joãozinho, Natália, Manu e Bruno Jahnke.

Também não posso deixar de agradecer o grande auxílio prestado pelo pessoal da CPG: Éber, Paula e Andrea.

Agradeço aos membros da banca por todo trabalho que tiveram para ler e avaliar este trabalho.

Por fim, agradeço o apoio finaceiro da CAPES e da Fapesp (2014/01805-5).

Contents

Acknowledgements **i**

List of Figures **xvi**

List of Tables **xvii**

1 Introduction **1**

1.1 Organization of this thesis 5

2 Quark-gluon plasma **6**

2.1 QCD lagrangian and symmetries 6

2.2 QCD thermodynamics 11

2.2.1 QCD equation of state at $\mu_b = 0$ 16

2.3 The QGP and ultra-relativistic heavy-ion collisions 19

3 Conformal Field Theories **23**

3.1 Conformal Group in $d > 2$ dimensions 24

3.2 Primary fields and correlation functions 27

3.3 $d = 4$, $\mathcal{N} = 4$ Super Yang-Mills theory 29

3.3.1 Symmetries of $\mathcal{N} = 4$ SYM 32

3.3.2 Representations of the superconformal algebra 33
3.3.3 Large N limit 35

4 Basics of string theory **36**

4.1 Bosonic string theory 36
4.2 Superstring theories 39
4.3 Interactions 42
4.4 D-branes 43
4.4.1 Low energy limit 44
4.4.2 D-brane charges 46
4.4.3 N coincident Dp-branes 48
4.4.4 Dp-branes as p-branes 49

5 The AdS/CFT correspondence **52**

5.1 Motivating the AdS/CFT correspondence 52
5.1.1 First low energy limit and then strongly coupled limit 53
5.1.2 First strongly coupled limit and then low energy limit 53
5.1.3 The AdS/CFT conjecture 56
5.2 Parameters of the correspondence 57
5.3 Matching symmetries and spectrum 60
5.4 Bulk fields in AdS_5 62
5.5 Correlation functions 64
5.5.1 Euclidian correlation functions 64
5.5.2 Real-time correlators 77
5.6 Generalizations 81
5.7 Thermodynamic properties 82

5.8 Transport coefficients 83

6 Thermal probes of an anisotropic plasma 90

6.1 Photon and dilepton production in an anisotropic plasma 92

6.1.1 Gravity set-up 96

6.1.2 Quark masses 102

6.2 Photon production with massive quarks from holography 105

6.2.1 Spectral density for the polarization $\epsilon_{(1)}$ 105

6.2.2 Spectral density for the polarization $\epsilon_{(2)}$ 109

6.2.3 Total photon production rate 113

6.3 Dilepton production from holography 114

6.3.1 Isotropic limit 118

6.3.2 Dilepton spectral density $\chi_{(1)}$ 119

6.3.3 Dilepton spectral density $\chi_{(2)}$ 120

6.3.4 Total dilepton production rate 128

6.4 Discussion 128

Appendix 6.A Solutions for $\mathbf{E_1}$ and $\mathbf{E_2}$ 140

Appendix 6.B Explicit near-boundary-expansion for the action (6.68) . . . 144

7 Chern-Simons diffusion rate from higher curvature gravity 146

7.1 Topology of non-abelian gauge theories 149

7.2 Gravity setup and results 154

7.3 Discussion 159

8 Anisotropic black branes in GB gravity theory 162

8.1 Action and solution 164

8.2 Central charges 169
8.3 Boundary stress tensor 170
8.4 Observables of the dual anisotropic plasma 172
8.4.1 Shear viscosity to entropy ratios 173
8.4.2 Conductivities 177
8.4.3 Drag force 179
8.4.4 Jet quenching parameter 184
8.4.5 Quarkonium static potential 188
8.4.6 Photon production 192
8.5 Discussion 202
Appendix 8.A Derivation of the solution 206
Appendix 8.B Shear viscosity tensor 210
8.B.1 Kubo formula 210
8.B.2 Near-horizon matching technique 212
Appendix 8.C Drag force for a general background and arbitrary direction 216
Appendix 8.D Jet quenching parameter for an arbitrary motion 220
Appendix 8.E Quarkonium static potential in generic background 225

9 Conclusion **228**

References **232**

List of Figures

2.1 Contemporary view of the QCD phase diagram. Figure taken from [51]. 12

2.2 *Left*: Polyakov loop and its susceptibility as a funtion of the bare coupling. *Right*: Chiral condensate and its susceptibilty as a function of the bare coupling. Both results were obtained in QCD with two flavors. Figure taken from [62]. 16

2.3 *Left*: ϵ/T^4 and $3P/T^4$ as a function of the temperature. *Right*: entropy density divided by the corresponding ideal gas result as a function of the temperature. Results obtained from lattice calculations. SB indicates the Stefan-Boltzmman result, obtained in the ideal gas approximation. Figure taken from [64]. 18

2.4 Trace anomaly as a function of the temperature obtained from lattice calculations. Figure taken from [64]. 19

2.5 Geometry of a heavy-ion collision. The beam direction is z and xy is the transverse plane. *Left*: two Lorentz contracted gold nuclei colliding. *Right* Overlap region projected in the transverse plane. Figure taken from [93]. 21

4.1 Two-to-two amplitude expressed as a sum over topologies. Figure taken from [93]. 43

5.1 Throat geometry generated by a system of N coincident D3-branes. Figure from [93]. 55

6.1 Momentum and polarization vectors. Because of the rotational symmetry in the xy-plane, the momentum can be chosen to be contained in the xz-plane, forming an angle ϑ with the z-direction. $\vec{\epsilon}_{(1)}$ is oriented along the y-direction and $\vec{\epsilon}_{(2)}$ is contained in the xz-plane, orthogonally to $\vec{k}$. 95

6.2 Log-log plot of the entropy density as a function of a/T. The dashed blue line is a straight line with slope 1/3. 98

6.3 Ratio (6.15) as a function of a/T. The blue dots are the actual values of the ratio, and the red curve is the fit (6.16). 99

6.4 The curves correspond, from bottom to top, to $a/T = 0$, 4.41, 12.2, 86, 249. 104

6.5 The isotropic correlator χ_{iso} for $T = 0.33$ and, from top to bottom on the left side of the plot, $\psi_{\text{H}} = 0$ (black), 0.53 (blue), 0.75 (purple), 0.941(red), 0.98 (orange). Here $\tilde{\mathcal{N}}_{\text{D7}} = 4K_{\text{D7}}/u_{\text{H}}^2$ and $\mathfrak{w} = k_0/2\pi T$ is the dimensionless frequency. This color code will be respected throughout this section. 106

6.6 Plots of the spectral density $\chi_{(1)}$ corresponding to the polarization $\epsilon_{(1)}$, normalized with respect to the isotropic result at fixed temperature $\chi_{\rm iso}(T)$. The curves correspond from top to bottom to the angles $\vartheta = 0$ (solid), $\pi/4$ (dashed), $\pi/2$ (dotted). Within each group of curves the values of the mass are given, from bottom to top on the right side (black to orange), by $\psi_{\rm H} = 0$, 0.53, 0.75, 0.941, 0.98. The four plots correspond to the cases $a/T = 4.41$ (a), 12.2 (b), 86 (c), 249 (d). 108

6.7 Plot of the conductivity $\tilde{\sigma}_{(1)}$ corresponding to the polarization $\epsilon_{(1)}$ as a function of a/T for, from top to bottom, $\psi_{\rm H} = 0$, 0.53, 0.75, 0.941, 0.98. . 109

6.8 Plots of the spectral density $\chi_{(2)}$ corresponding to the polarization $\epsilon_{(2)}$, normalized with respect to the isotropic result at fixed temperature $\chi_{\rm iso}(T)$. The curves correspond from top to bottom to the angles $\vartheta = 0$ (solid), $\pi/4$ (dashed), $\pi/2$ (dotted). Within each group of curves the values of the mass are given, from bottom to top on the right side (black to orange), by $\psi_H = 0$, 0.53, 0.75, 0.941, 0.98. The four plots correspond to the cases $a/T = 4.41$ (a), 12.2 (b), 86 (c), 249 (d). 112

6.9 Plot of the conductivity $\tilde{\sigma}_{(2)}$ corresponding to the polarization $\epsilon_{(2)}$ as a function of a/T. The groups of curves correspond from top to bottom to $\psi_{\rm H} = 0$, 0.53, 0.75, 0.941. Inside each group we plot the angles $\vartheta = 0$ (solid), $\pi/4$ (dashed), and $\pi/2$ (dotted). 113

6.10 Plot of the conductivity $\tilde{\sigma}_{(2)}$ corresponding to the polarization $\epsilon_{(2)}$ as a function of the angle ϑ. The groups of curves correspond, from top to bottom, to $\psi_{\rm H} = 0$, 0.53, 0.75, 0.941, 0.98. Within each group we have, from bottom to top on the left side of the graph, a/T =1.38 (solid), 5.9 (dashed), 9.25 (dot-dashed), and 12.2 (dotted). 114

6.11 Plots of the total production rate. The groups of curves correspond from top to bottom to $\psi_{\rm H} = 0, 0.53, 0.75, 0.941, 0.98$. Within each group we plot the angles $\vartheta = 0$ (solid), $\pi/4$, (dashed), and $\pi/2$ (dotted). The four plots correspond to the cases $a/T = 4.41$ (a), 12.2 (b), 86 (c), 249 (d). The temperatures in the four cases are, respectively, $T = 0.33, 0.36, 0.49, 0.58$. The isotropic results at the same temperatures and masses are the coarsely dashed curves. 115

6.12 Plots of the spectral densities $\chi_{(1)_{\rm iso}}$ and $\chi_{(2)_{\rm iso}}$. Here we have fixed $T = 0.33$. Curves of different colors and traits denote different values of $\mathfrak{q}$ ($\mathfrak{q}$ =0 (blue), 1 (red), 1.5 (green)) and of $\psi_{\rm H}$ ($\psi_{\rm H}$ =0 (solid), 0.75 (dashed), 0.941 (dot-dashed)). The curves for $\mathfrak{q} = 0$ are identical in the two plots, up to an overall factor of 2, as it should be, considering that (6.63) and (6.64) coincide in this case. 119

6.13 Plots of the spectral density $\chi_{(1)}$ normalized with respect to the isotropic result at fixed temperature $\chi_{(1)_{\rm iso}}(T)$. Curves of different colors denote different values of a/T as follows a/T =4.41 (blue), 12.2 (red), 86 (green). The angles are $\vartheta = 0$ (solid), $\pi/4$ (dashed), $\pi/2$ (dot-dashed). Columns correspond to different values of $\mathfrak{q}$: from left to right it is $\mathfrak{q} = 0, 1, 1.5$. Rows correspond to different values of the quark mass: from top to bottom it is $\psi_{\rm H} = 0, 0.75, 0.941$. Then, for instance, (h) corresponds to $\mathfrak{q} = 1$, $\psi_{\rm H} = 0.941$. 121

6.14 Plots of the spectral density $\chi_{(1)}$ normalized with respect to the isotropic result at fixed temperature $\chi_{(1)\mathrm{iso}}(T)$. Curves of different colors denote different values of a/T as follows a/T =4.41 (blue), 12.2 (red), 86 (green). The angles are $\vartheta = 0$ (solid), $\pi/4$ (dashed), $\pi/2$ (dash-dotted). Columns correspond to different values of $\mathfrak{w}$: from left to right it is $\mathfrak{w} = 1/2, 1, 1.5$. Rows correspond to different values of the quark mass: from top to bottom it is $\psi_{\mathrm{H}} = 0, 0.75, 0.941$. Then, for instance, (f) corresponds to $\mathfrak{w} = 3/2$, $\psi_{\mathrm{H}} = 0.75$. 122

6.15 Plots of the spectral density $\chi_{(1)}$ normalized with respect to the isotropic result at fixed temperature $\chi_{(1)\mathrm{iso}}(T)$. Curves of different colors denote different values of $\mathfrak{q}$ as follows $\mathfrak{q}$ =0 (purple), 1/2 (magenta), 1 (green). The angles are $\vartheta = 0$ (solid), $\pi/4$ (dashed), $\pi/2$ (dash-dotted). Columns correspond to different values of $\mathfrak{w}$: from left to right it is $\mathfrak{w} = 0.5, 1, 1.5$. Rows correspond to different values of the quark mass: from top to bottom it is $\psi_{\mathrm{H}} = 0, 0.75, 0.941$. Then, for instance, (f) corresponds to $\mathfrak{w} = 1.5$, $\psi_{\mathrm{H}} = 0.75$. 123

6.16 Plots of the spectral density $\chi_{(1)}$ normalized with respect to the isotropic result at fixed temperature $\chi_{(1)\mathrm{iso}}(T)$. Curves of different colors denote different values of $\mathfrak{w}$ as follows $\mathfrak{w}$ =1/2 (black), 1 (brown), 3/2 (blue). The angles are $\vartheta = 0$ (solid), $\pi/4$ (dashed), $\pi/2$ (dash-dotted). Columns correspond to different values of $\mathfrak{q}$: from left to right it is $\mathfrak{q} = 0, 0.5, 1$. Rows correspond to different values of the quark mass: from top to bottom it is $\psi_0 = 0, 0.75, 0.941$. Then, for instance, (f) corresponds to $\mathfrak{q} = 1$, $\psi_{\mathrm{H}} = 0.75$. 124

6.17 Plots of the spectral density $\chi_{(2)}$ normalized with respect to the isotropic result at fixed temperature $\chi_{(2)\mathrm{iso}}(T)$. Curves of different colors denote different values of a/T as follows a/T =4.41 (blue), 12.2 (red), 86 (green). The angles are $\vartheta = 0$ (solid), $\pi/4$ (dashed), $\pi/2$ (dash-dotted). Columns correspond to different values of $\mathfrak{q}$: from left to right it is $\mathfrak{q} = 0, 1, 1.5$. Rows correspond to different values of the quark mass: from top to bottom it is $\psi_{\mathrm{H}} = 0, 0.75, 0.941$. Then, for instance, (h) corresponds to $\mathfrak{q} = 1$, $\psi_{\mathrm{H}} = 0.941$. 129

6.18 Plots of the spectral density $\chi_{(2)}$ normalized with respect to the isotropic result at fixed temperature $\chi_{(2)\mathrm{iso}}(T)$. Curves of different colors denote different values of a/T as follows a/T =4.41 (blue), 12.2 (red), 86 (green). The angles are $\vartheta = 0$ (solid), $\pi/4$ (dashed), $\pi/2$ (dash-dotted). Columns correspond to different values of $\mathfrak{w}$: from left to right it is $\mathfrak{w} = 0.5, 1, 1.5$. Rows correspond to different values of the quark mass: from top to bottom it is $\psi_{\mathrm{H}} = 0, 0.75, 0.941$. Then, for instance, (f) corresponds to $\mathfrak{w} = 1.5$, $\psi_{\mathrm{H}} = 0.75$. 130

6.19 Plots of the spectral density $\chi_{(2)}$ normalized with respect to the isotropic result at fixed temperature $\chi_{(2)\mathrm{iso}}(T)$. Curves of different colors denote different values of $\mathfrak{q}$ as follows $\mathfrak{q}$ =0 (purple), 0.5 (magenta), 1 (green). The angles are $\vartheta = 0$ (solid), $\pi/4$ (dashed), $\pi/2$ (dash-dotted). Columns correspond to different values of $\mathfrak{w}$: from left to right it is $\mathfrak{w} = 0.5, 1, 1.5$. Rows correspond to different values of the quark mass: from top to bottom it is $\psi_{\mathrm{H}} = 0, 0.75, 0.941$. Then, for instance, (f) corresponds to $\mathfrak{w} = 1.5$, $\psi_{\mathrm{H}} = 0.75$. 131

6.20 Plots of the spectral density $\chi_{(2)}$ normalized with respect to the isotropic result at fixed temperature $\chi_{(2)\mathrm{iso}}(T)$. Curves of different colors denote different values of $\mathfrak{w}$ as follows $\mathfrak{w}$ =0.5 (black), 1 (brown), 1.5 (blue). The angles are $\vartheta = 0$ (solid), $\pi/4$ (dashed), $\pi/2$ (dash-dotted). Columns correspond to different values of $\mathfrak{q}$: from left to right it is $\mathfrak{q} = 0, 0.5, 1$. Rows correspond to different values of the quark mass: from top to bottom it is $\psi_0 = 0, 0.75, 0.941$. Then, for instance, (f) corresponds to $\mathfrak{q} = 1$, $\psi_{\mathrm{H}} = 0.75$. 132

6.21 Plots of the spectral density χ^{μ}_{μ} normalized with respect to the isotropic result at fixed temperature $\chi^{\mu}_{\mu\mathrm{iso}}(T)$. Curves of different colors denote different values of a/T as follows a/T =4.41 (blue), 12.2 (red), 86 (green). The angles are $\vartheta = 0$ (solid), $\pi/4$ (dashed), $\pi/2$ (dash-dotted). Columns correspond to different values of $\mathfrak{q}$: from left to right it is $\mathfrak{q} = 0, 1, 1.5$. Rows correspond to different values of the quark mass: from top to bottom it is $\psi_{\mathrm{H}} = 0, 0.75, 0.941$. Then, for instance, (h) corresponds to $\mathfrak{q} = 1$, $\psi_{\mathrm{H}} = 0.941$. 133

6.22 Plots of the spectral density χ^{μ}_{μ} normalized with respect to the isotropic result at fixed temperature $\chi^{\mu}_{\mu\mathrm{iso}}(T)$. Curves of different colors denote different values of a/T as follows a/T =4.41 (blue), 12.2 (red), 86 (green). The angles are $\vartheta = 0$ (solid), $\pi/4$ (dashed), $\pi/2$ (dash-dotted). Columns correspond to different values of $\mathfrak{w}$: from left to right it is $\mathfrak{w} = 0.5, 1, 1.5$. Rows correspond to different values of the quark mass: from top to bottom it is $\psi_{\mathrm{H}} = 0, 0.75, 0.941$. Then, for instance, (f) corresponds to $\mathfrak{w} = 1.5$, $\psi_{\mathrm{H}} = 0.75$. 134

6.23 Plots of the spectral density χ^{μ}_{μ} normalized with respect to the isotropic result at fixed temperature $\chi^{\mu}_{\mu\mathrm{iso}}(T)$. Curves of different colors denote different values of $\mathfrak{q}$ as follows $\mathfrak{q}$ =0 (purple), 0.5 (magenta), 1 (green). The angles are $\vartheta = 0$ (solid), $\pi/4$ (dashed), $\pi/2$ (dash-dotted). Columns correspond to different values of $\mathfrak{w}$: from left to right it is $\mathfrak{w} = 0.5, 1, 1.5$. Rows correspond to different values of the quark mass: from top to bottom it is $\psi_{\mathrm{H}} = 0, 0.75, 0.941$. Then, for instance, (f) corresponds to $\mathfrak{w} = 1.5$, $\psi_{\mathrm{H}} = 0.75$. 135

6.24 Plots of the trace of spectral density χ^{μ}_{μ} normalized with respect to the isotropic result at fixed temperature $\chi^{\mu}_{\mu\mathrm{iso}}(T)$. Curves of different colors denote different values of $\mathfrak{w}$ as follows $\mathfrak{w}$ =0.5 (black), 1 (brown), 1.5 (blue). The angles are $\vartheta = 0$ (solid), $\pi/4$ (dashed), $\pi/2$ (dash-dotted). Columns correspond to different values of $\mathfrak{q}$: from left to right it is $\mathfrak{q} = 0, 0.5, 1$. Rows correspond to different values of the quark mass: from top to bottom it is $\psi_{\mathrm{H}} = 0, 0.75, 0.941$. Then, for instance, (f) corresponds to $\mathfrak{q} = 1$, $\psi_{\mathrm{H}} = 0.75$. 136

7.1 Schematic representation of the vacuum of non-abelian gauge theories. The Chern-Simons number, N_{CS}, labels the different classical vacua states. . . 153

7.2 (Left) The factors $H^{(0)}(\lambda_{\mathrm{GB}})$ (red, solid curve) and $H^{(1)}(\lambda_{\mathrm{GB}})$ (blue, dashed curve) as functions of λ_{GB}. (Right) The same factors as functions of η/s. The plots are exact in λ_{GB} and in η/s, whose allowed ranges are obtained from eqs. (7.24) and (7.31). In these ranges, the corrections to eq. (7.2) are finite and cannot make the diffusion rate arbitrarily small. 160

8.1 The metric functions at order $O(a^2)$. Here we have set $\lambda_{\mathrm{GB}} = 0.2$. 167

8.2 Drag force normalized by the isotropic result as a function of $(\lambda_{\rm GB}, \frac{a}{T})$. Here we have fixed $v = 0.3$. Left: Motion along the anisotropic direction. Right: Motion along the direction transversal to the anisotropy. 183

8.3 Drag force normalized by the isotropic result as a function of $(\lambda_{\rm GB}, v)$. Here we have fixed $\frac{a}{T} = 0.2$. Left: Motion along the anisotropic direction. Right: Motion along the direction transversal to the anisotropy. For other values of $\frac{a}{T}$ the results were qualitatively the same. 184

8.4 Left: Jet quenching parameter as a function of (θ, φ). We have set $\lambda_{\rm GB} = 0.1$ and $a/T = 0.33$. Right: The jet quenching parameter as a function of $(\lambda_{\rm GB}, \frac{a}{T})$. We have set $\theta = \varphi = \pi/4$. Both plots were normalized by the isotropic result (8.60). 187

8.5 Quark-antiquark potential $V_{Q\bar{Q}}$ as a function of their separation L for different values of the Gauss-Bonnet coupling: $\lambda_{\rm GB} = -0.1$ (red, dotted), $\lambda_{\rm GB} = 0$ (black, solid) and $\lambda_{\rm GB} = 0.1$ (blue, dashed). For all curves $a/T \approx 0.3$ and $\theta = \pi/4$. 190

8.6 (a) Screening length $L_s(\lambda_{\rm GB}, a)$ normalized with respect to the isotropic result $L_{\rm iso} = L_s(\lambda_{\rm GB} = 0, a = 0)$ for $\theta = 0$. (b) Ratio $L_\perp/L_{||}$, where $L_\perp$ is the screening length calculated at $\theta = \pi/2$, and $L_{||}$ is the screening length calculated at $\theta = 0$. 191

8.7 Screening length L_s as a function of a/T for three different quarkonium orientations: $\theta = 0$ (black, solid), $\theta = \pi/4$ (purple, dashed) and $\theta = \pi/2$ (blue, dotted). The Gauss-Bonnet coupling is fixed $\lambda_{\rm GB} = 0$. . . . 192

8.8 Momentum $\vec{k}$ and polarization vectors $\vec{\epsilon}_{(1)}$ and $\vec{\epsilon}_{(2)}$. The $SO(2)$ rotational symmetry in the xy-plane allows us to choose the momentum lying in the xz-plane, forming an angle ϑ with the z-direction. Both polarization vectors are orthogonal to $\vec{k}$. We chose $\vec{\epsilon}_{(1)}$ oriented along the y-direction and $\vec{\epsilon}_{(2)}$ contained in the xz-plane. 194

8.9 The trace of the spectral density $\chi^{\mu}_{\mu}(\lambda_{\rm GB}, a, \vartheta)$ normalized with respect to the isotropic result (8.87). All the spectral densities were calculated at the same temperature $T_0 = 0.316698$. The colors of the curves identify the value of the $\lambda_{\rm GB}$ parameter as: red curves ($\lambda_{\rm GB} = -0.1$), brown curves ($\lambda_{\rm GB} = -0.05$), black curves ($\lambda_{\rm GB} = 0$), purple curves ($\lambda_{\rm GB} = 0.05$) and blue curves ($\lambda_{\rm GB} = 0.1$). In (a), the angle of emission is fixed ($\vartheta = 0$) and we have solid curves ($a = 0.2$), dashed curves ($a = 0.1$) and dotted curves ($a = 0$). In (b), the anisotropy is fixed ($a = 0.2$) and we have solid curves ($\vartheta = 0$), dot-dashed curves ($\vartheta = \pi/4$), and dotted curves ($\vartheta = \pi/2$). 200

8.10 Total photon production rate as a function of $\mathfrak{w} = k^0/2\pi T_0$. From top to bottom, the value of the Gauss-Bonnet coupling is identified as $\lambda_{\rm GB} = 0.1$ (blue), $\lambda_{\rm GB} = 0.05$ (purple), $\lambda_{\rm GB} = 0$ (black), $\lambda_{\rm GB} = -0.05$ (brown), $\lambda_{\rm GB} = -0.1$ (red). We have fixed $\vartheta = 0$ and $a = 0.2$. The results for different angles are very similar to the plot above due to the smallness of the anisotropy. 202

List of Tables

4.1 Massless and tachyonic spectrum of closed and open strings. 37

4.2 Massless spectrum of type IIB string theory. 40

8.1 Summary of the effect of the Gauss-Bonnet coupling $\lambda_{\rm GB}$ on several observables. We also present the finite 't Hooft corrections of type $\alpha'^3 R^4$ [185, 248, 261, 262]. The comparison is taken w.r.t. the respective $\mathcal{N} = 4$ SYM result at same temperature. 204

Chapter 1

Introduction

The AdS/CFT correspondence [1–3] is the best known example of a gauge/gravity duality. These dualities are realizations of the Holographic Principle, which asserts that a gravity theory in $d+1$ dimensions is equivalent to a d-dimensional gauge theory. As the gauge theory can be thought as living on the boundary of the space where the gravity theory is defined, these dualities also goes under the name of holography. Given this holographic interpretation, the gravity theory and the gauge theory are usually referred to as the *bulk theory* and the *boundary theory*, respectively. The particular case of AdS/CFT correspondence proposes an equilvalence between conformal field theories (CFT) in four dimensional Minkowski space and string theory in five dimensional Anti-de Sitter (AdS) space.

In the best undestood example of the AdS/CFT correspondence the gravity theory is type IIB string theory in $AdS_5 \times S^5$ and the dual gauge theory is the so-called $\mathcal{N} = 4$ Super Yang-Mills (SYM) theory with gauge group $SU(N)$ in four dimensions. The realization of the holographic principle is clear when one performs a compactification on S^5 and obtains an effective five-dimensional gravity theory in AdS_5. In this case,

the gauge theory lives in the four-dimensional boundary of AdS_5.

The power of the AdS/CFT correspondence resides in the fact that it is a strong/weak coupling duality. That means that, when one side of the duality is strongly coupled, the other is weakly coupled, and vice-versa. This allows one to reformulate difficult non-perturbative problems in one side of the duality in the language of the dual weakly coupled theory.

Remarkably, the AdS/CFT correspondence has found applications in the study of the "quark-gluon plasma" (QGP) produced in heavy-ion collisions, at RHIC [4, 5] and LHC [6]. This plasma cannot be well described by perturbative QCD because it behaves as a strongly coupled fluid at the typical temperatures in which it is produced [7, 8]. Lattice techniques can be use for studying thermodynamic properties of this plasma, but such approach is poorly suited to compute dynamical quantities such as transport coefficients. With this in view, the AdS/CFT correspondence seems to be one of the few alternatives to study strongly coupled systems. Indeed, besides providing us with many tools and insights to understand qualitative features of strongly coupled dynamics, such approach has allowed the computation of some quantities, called *universal*, that are independent of the fine details of the microscopic theory. The most notable example is the shear viscosity to entropy density ratio [9].

In the most simple applications, the stronlgy coupled plasma of the $\mathcal{N} = 4$ SYM theory at finite temperature is used as a model for the QGP phase of Quantum Chromodynamics (QCD). Of course, these two theories are very different at zero temperature. The $\mathcal{N} = 4$ SYM is highly supersymmetric, conformal and only have fields in the adjoint representation of the gauge group, which $SU(N)$ with N large, while QCD has no supersymmetries and it is a confining theory, with flavored fields in the fundamental and adjoint representation of the color gauge group $SU(3)$. However,

slightly above the deconfinement temperature of QCD, that is the typical temperatures explored at RHIC and LHC, many of these differences disappear [95]. It is then interesting to use the AdS/CFT correspondence to gain insights about the QGP phase of QCD and, hopefully, calculate some model independent quantities of this plasma.

The QGP produced in heavy-ion collisions at RHIC and LHC is highly anisotropic in the initial stages of its evolution. This is due to the fact that the system expands mainly along the beam axis at the earliest times after the collision.This anisotropy is a very important characteristic of the plasma and can be holographically described at strong coupling via a type IIB supergravity black brane solution with an anisotropic horizon [10, 11].[1] The effects this anisotropy in various physical observables has recently received some attention. Quantities that have been studied include the shear viscosity to entropy density ratio [13, 14], the drag force experienced by a heavy quark [15, 16], the energy lost by a quark rotating in the transverse plane [17], the stopping distance of a light probe [18], the jet quenching parameter of the medium [16, 19, 20], the potential between a quark and antiquark pair, both static [16, 20–22] and in a plasma wind [22], including its imaginary part [23], Langevin diffusion and Brownian motion [24, 25], chiral symmetry breaking [26], and the production of thermal photons [27–29].[2]

In this thesis we study the effects of anisotropy in the production of thermal photons and dileptons in a strongly coupled anisotropic medium with massive quarks. This study was published in JHEP [31] and is presented in Chapter 6.

In order to consider more realistic gauge theories, we consider, as a second direc-

[1] This geometry is the finite temperature generalization of the geometry found in [12].

[2] For a review of many of these studies, see [30].

tion of research, gravity theories that incorporate higher derivatives corrections, as we explain below.

Two important parameters that characterize the $\mathcal{N} = 4$ SYM theory are the rank of the gauge group N and the 't Hooft coupling λ. For generic values of these parameters this theory is conjectured to be dual to type IIB string theory. However, the AdS/CFT correspondence is best undestood in the limit where both N and λ are infinite. This is because the large N limit suppress quantum or loop corrections in the gravity side while the large λ limit suppress the appearance of higher curvature terms (α' corrections). As a result IIB string theory reduces to classical type IIB supergravity in this limit.

To investigate departures from this limit one have to consider more general gravity theories, including α' and loop corrections to the supergravity action, which is generally very difficult. The first α' correction to type IIB supergravity, for example, has the schematic form $\alpha'^3 R^4$.

A possible approach is to consider toy models that incorporates higher curvatures corrections while maintaining the calculations under control, in the hope to gain qualitative insigths about the effects these terms might have in the physical observables of the dual gauge theory. A possible family of toy models is constituted by the so-called Lovelock theories of gravity [32–35].[3] These theories are generalizations of the Einstein's general relativity to dimensions higher than four. Despite contain higher curvature terms these theories are free of pathologies, because they are defined in such a way that the equations of motion for the metric are still of second order. Another important characteristic of the Lovelock theories of gravity is the fact that they admit exact black hole solutions with AdS asymptotics; for a comprehensive review, see e.g.

[3]Reviews on Lovelock theories in the context of AdS/CFT can be found in, e.g., [36–38].

[39, 40] and [41]. The first Lovelock correction is the so-called Gauus-Bonnet (GB) term. This term appears in five dimensions and it is quadratic in the curvature.

In this thesis we consider higher curvature corrections to the Chern-Simons diffusion rate in Chapter 7. The results were published in PRD [42]. In Chapter 8 we also consider a bottom up model which incorporates both higher curvature corrections and anisotropy. We compute several physical observables in this model. The results were published in JHEP [43] and EPJC [44].

1.1 Organization of this thesis

This thesis is organized as follows. Chapter 2 provides a brief introduction to QCD, explains the QGP phase from the theoretical point of view and discuss how it is produced in heavy ion collisions. Chapter 3 presents some basic results about CFTs and give some details about the $\mathcal{N} = 4$ SYM theory. In Chapter 4 we present some basic concepts of string theory that are relevant in AdS/CFT applications. We then motivate and discuss the AdS/CFT correspondence in Chapter 5. These first chapters aim to provide the reader some basic knowledge useful to apply the AdS/CFT correspondence to study the QGP. The subsequent chapters present the original work of this thesis. In Chapter 6 we calculate the production rate of photons and dileptons in a stronlgy coupled anisotropic plasma. The results were published in JHEP [31]. Chapter 7 presents the computation of the sphaleron rate in higher derivative gravity theories. The results were published in PRD [42]. We then consider a bottom up model that incorporate both anisotropy and higher derivative corrections in Chapter 8. The studies of this chapter were publish in JHEP [43] and EPJC [44]. The conclusions of this thesis are presented in Chapter 9.

Chapter 2

Quark-gluon plasma

In this chapter we will discuss some basic properties of the quark-gluon plasma formed in ultra-relativistic heavy-ion collisions. We first made a brief review of quantum chromodynamics (QCD) and its phase diagram. We also present some lattice results regarding the equation of state of QCD. We then explain the production of the QGP from the experimental point of view, discussing the evidence for its existence and the probes used to study it.

2.1 QCD lagrangian and symmetries

QCD is the theory that describes the hadrons and the nuclear physics. This theory is based on the principle of local $SU(3)_c$ color symmetry. For later purposes, let t_a, with $a = 1, ..., 8$ denote the generators of this group of symmetry.

The basic fields of QCD are quarks and gluons. The quark fields are described by 4-component Dirac spinors ψ_{cf}, where $c = 1, 2, 3$ is a color index of $SU(3)_c$ and

$f = u, d, s, c, b, t$ is a flavor index[1]. The gluon fields are described by a Lorentz vector A^a_μ, where $a = 1, ..., 8$ is an adjoint color index of $SU(3)_c$.

Given the number of flavors and the quark masses m_f, the QCD lagrangian is completely fixed by requiring local $SU(3)_c$ color symmetry and is given by

$$\mathcal{L}_{QCD} = -\frac{1}{2}\mathrm{Tr}\left[G_{\mu\nu}G^{\mu\nu}\right] + \sum_f \bar{\psi}_f(i\gamma_\mu D^\mu - m_f)\psi_f \tag{2.1}$$

where g denotes the QCD coupling,

$$D_\mu = \partial_\mu - igA_\mu(x), \quad \text{with} \quad A_\mu(x) = \sum_{a=1}^{8} t_a A^a_\mu \tag{2.2}$$

is the gauge covariant derivative and

$$G_{\mu\nu} \equiv \sum_{a=1}^{8} t_a G^a_{\mu\nu} = \frac{i}{g}[D_\mu, D_\nu] \tag{2.3}$$

is the gluonic field strengh. As we said above, the QCD lagrangian is invariant under local gauge transformations $V(x) = e^{-i\theta^a(x)\,t_a}$ of $SU(3)_c$, under which the fields transforms as

$$\begin{aligned} \psi &\to \psi' = V\psi, \\ A_\mu &\to A'_\mu = VA_\mu V^\dagger + \frac{1}{g}V(\partial_\mu V^\dagger) \end{aligned} \tag{2.4}$$

At low temperatures all the excitations of QCD are color singlets under the gauge group. These excitations are observed in nature as mesons, which are composed of

[1]Here, u, d, s, c, b and t stands for *up, down, strange, charm, bottom* and *top*, respectively, which are the names of the different flavors (types) of quarks.

a quark and an anti-quark $q\bar{q}$, and baryons, composed of three quarks qqq. These bound states of quarks are held together by the exchange of gluons. In other words, at ordinary temperatures, quarks and gluons cannot be observed as free particles. They only appears as bounds states, like mesons and baryons. This phenomenom is known as color confinement.

QCD is invariant under scale transformations $x \to \lambda x$ at the classical level, but this symmetry is broken when quantum effects are taken into account. This happens because the renormalization of the theory requires the running of its coupling g, that, in a given process, becomes a function of the characteristic momentum transfer Q

$$g^2(Q^2) \sim \frac{1}{\log\left(\frac{Q^2}{\Lambda^2_{QCD}}\right)}.$$

As a consequence the scale invariance is broken by the introduction of a scale Λ_{QCD}, which is known as the QCD scale. One can think of Λ_{QCD} as the scale at which g becomes large. The numerical value of this scale is $\Lambda_{QCD} \simeq 200\,\mathrm{MeV} \simeq 1\,\mathrm{fm}^{-1}$[45]. Note that g is large in the infrared, but becomes small at large Q. In fact, for sufficiently large values of Q, QCD is a free theory. This phenomenom is known as asymptotic freedom [46, 47].

QCD also has some approximate flavor symmetries. This depends on the active number of flavors that we take into account. As the quarks, c, b and t are very heavy ($m_c, m_b \sim 1$ GeV and $m_t \approx 170$ GeV) we can consider, for many purposes, that they are infinite massive, and work with only three flavors of quarks u, d and s.

To appreciate the power of the approximate flavor symmetry, let us first ignore the s quark, and work only with two flavors, u and d. We write the QCD lagrangian

as

$$\mathcal{L}_{QCD} = \bar{\psi}_u(i\gamma_\mu D^\mu - m_u)\psi_u + \bar{\psi}_d(i\gamma_\mu D^\mu - m_d)\psi_d + ... \tag{2.5}$$

where the dots represent the omitted bosonic part. We can write the quark fields in terms of right-handed and left-handed fields as

$$\psi_f^L = \frac{(1+\gamma_5)}{2}\psi_f, \quad \psi_f^R = \frac{(1-\gamma_5)}{2}\psi_f \tag{2.6}$$

where $f = u, d$. In terms of this fields the lagrangian becomes

$$\mathcal{L}_{QCD} = \sum_{f=u,d}\left(\bar{\psi}_f^L i\gamma_\mu D^\mu \psi_f^L + \bar{\psi}_f^R i\gamma_\mu D^\mu \psi_f^R + \bar{\psi}_f^L m_f \psi_f^R + \bar{\psi}_f^R m_f \psi_f^L\right) + ... \tag{2.7}$$

Note that in the massless limit $m_u = m_d = 0$, the left and right-handed fields decouple and are independently invariant under $SU(2)$ flavor rotations

$$\begin{aligned} \psi_f^L &\to L_{fg}\,\psi_g^L \\ \psi_f^R &\to R_{fg}\,\psi_g^R \end{aligned} \tag{2.8}$$

where $(L, R) \in SU(2)_L \times SU(2)_R$. This is the so-called chiral symmetry. This symmetry is espontaneously broken at the quantum level because, even if we start with massless quarks in the lagrangian, the quarks inside the hadrons interacts with the gluonic medium and this generates a dynamic mass for them [48, 49]. This mass is independent of flavor and is given by a non-zero value of the so-called chiral condensate $\langle\bar{\psi}\psi\rangle \sim M_q$.

So, if we start with a lagrangian with massless u and d quarks the QCD dynamics

generates a non-zero mass for them[2] that breaks the chiral symmetry to a $SU(2)_f$ flavor symmetry

$$\psi_f \to V_{fg}\,\psi_g, \quad V \in SU(2)_f \tag{2.9}$$

As we know from Goldstone's theorem, for every spontaneously broken global symmetry, there exists a massless state that carries the quantum numbers of the corresponding symmetry charge. Since the quark condensate breaks the approximate chiral symmetry there must be (approximate) massless Goldstone bosons associated to this symmetry breaking. It turns out that these are the pions (π^+, π^0, π^-). This fields are not massless because the chiral symmetry is only approximate, since the quarks in the QCD lagrangian are not massless and we are ignoring the s, c, t and b quarks.

If we start with massless u, d and s quarks the associated chiral symmetry is $SU(3)_L \times SU(3)_R$. The chiral condensate breaks this symmetry to a $SU(3)_f$ flavor symmetry. The Goldstone theorem implies the appearance of eight approximately massless Goldstone bosons, which turn out to be the pseudoscalar meson octet $(\pi, K, \bar{K}, \eta)$. Again, this fields are not massless because the chiral symmetry of QCD is only approximate. These flavor symmetry groups discussed above are the famous isospin group of the strong interactions. The observed spectrum of hadrons can be approximately associated to representations of $SU(3)_f$, and the low energy effective lagrangian for them is partially fixed by this group of symmetry [50].

Finally, $\mathcal{L}_{QCD}$ is also invariant under the $U(1)_B$ global symmetry $\psi_f \to e^{i\theta}\psi_f$. The Noether current associated to this symmetry is $J^\mu_B = \bar{\psi}(x)\gamma^\mu\psi(x)$ and the associated conserved charge is the baryon number $B = \int d^3x\, \psi^\dagger(x)\psi(x)$, which can also be

[2] As we will see in the following, this only happens below the QCD critical temperature. Above this temperature the chiral condensate is approximately zero

calculated as

$$B = \frac{1}{3}(n_q - n_{\bar{q}}) \tag{2.10}$$

where n_q is the number of quarks and $n_{\bar{q}}$ is the number of anti-quarks.

2.2 QCD thermodynamics

The study of QCD thermodynamics, besides being interesting from the purely theoretical point of view, its also important in the description of natural phenomena, like the early universe, compact stars, heavy ion collisions, etc. Indeed, lattice calculations at zero chemical potential allows the determination of the QCD equation of state, which is used as an input in hydrodynamical models used in the description of these phenomena.

The static thermodynamic properies of QCD at zero chemical potential can be obtained by taking derivatives of the partition function $Z(T) = \mathrm{Tr}\, e^{-H/T}$, where H is the QCD hamiltonian and T is the temperature. This corresponds to use the *canonical ensemble*.

In the presence of a conserved charge, like the baryon number B in QCD, and particles with non-zero chemical potential, it is appropriate to use the *grand canonical ensemble*. In this case, the partition function is characterized by the temperature T and the baryon chemical potential μ_b as

$$Z(T, \mu_b) = \mathrm{Tr}\, e^{-(H - \mu_b B)/T} \tag{2.11}$$

In principle, the above partition function allows the determination of a phase diagram $T - \mu_b$ for QCD. Each point of this diagram corresponds to a stable thermodynamic

state, with well defined pressure, baryon density, kinetic coefficients, etc.

Unfortunally, full analytical treatment of QCD is only possible at weak coupling, what requires large values for T and/or μ_b [51]. This leaves a large part of phase space unexplored and, as will see in the following, this is precisely the most interesting part of the phase diagram.

Lattice methods can be used to study QCD thermodynamics at $\mu_b = 0$ [52] and also for small values of μ_b [53], but they encounter difficulties for generic values of μ_b. On can access regions of larger values of μ_b in the phase diagram of QCD using phenomenological models, like the linear sigma model (see, e.g., [54] and references therein).

Figure 2.1 shows the conjectured QCD phase diagram. The sketch is based on lattice calculations, phenomenological models and calculations in asymptotic regions [51, 55].

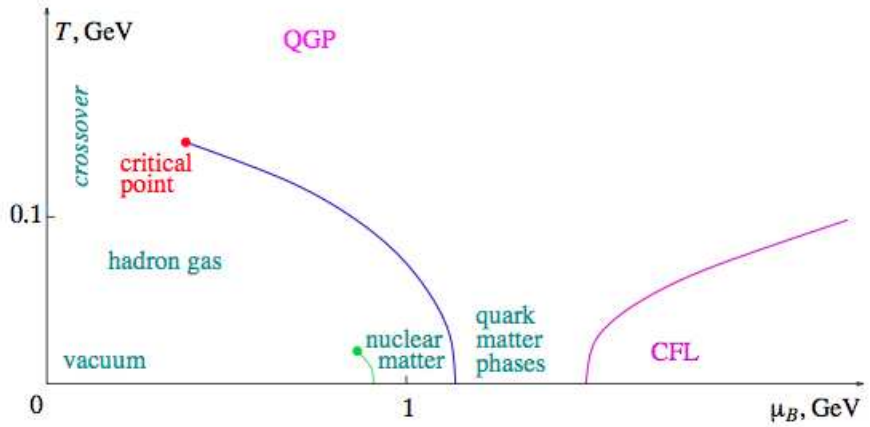

Figure 2.1: Contemporary view of the QCD phase diagram. Figure taken from [51].

Let us now discuss some basic features of this phase diagram. At low temperatures and low chemical potential the quarks and gluons are confined in color-singlet

combinations inside hadrons with masses of order Λ_{QCD}. As we increase the temperature, the QCD coupling decreases and, for sufficiently high temperature $T >> \Lambda_{QCD}$, asymptotic freedom implies that we have a weakly interacting plasma of deconfined quarks and gluons [56–58].

It is then clear that at some intermediate temperature there must be some kind of phase transition, in which the hadrons melt giving rise to deconfined quarks and gluons. The blue line in Fig. 2.1 indicates a first order transition that ends at the critical point of QCD. In the region between this line and the origin, the quarks and gluons are confinend inside hadrons. Outside this region we have a deconfined phase known as *Quark-Gluon Plasma* (QGP). Lattice calculations performed with realistic quark masses shows that, for $\mu_b = 0$, the transition from hadrons to deconfined quarks and gluons is an analytic crossover [59]. The transition temperature, also known as critical temperature, is obtained as $T_c \approx 150$ MeV. The precise determination of the QCD critical point (T, μ_b) has not been done yet and it is a subject of intense study. The difficult lies in the fact that lattice techniques can only be applied for small values of μ_b. The exploration of the QCD phase diagram for larges value of μ_b must rely on phenomenological models, like linear sigma models. For more details, see, for instance, the reference [54].

We briefly comment that for asymptotically large chemical potential QCD has a color superconducting phase, called CFL (color- flavor locked) phase. We will not be interested in this superconducting phase in this work. A good reference to study it is [55]. We also comment the existence of a phase transition between the nuclear matter to a strongly correlated superfluid, composed of protons and neutrons [56].

Phase transitions are associated to a change in the global symmetries of the system under study. The confinement/deconfinement transitions in QCD with zero flavors

are associated to a break of a global Z_{N_c} discrete symmetry of $SU(N_c)$ gauge theory. The associated order parameter is related to the Polyakov loop, which is defined as [60]

$$L(\vec{x}) = \frac{1}{N_c}\mathrm{Tr}\,\mathcal{P}\exp\left[ig\int_0^{1/T} A_0(\tau,\vec{x})\,d\tau\right] \tag{2.12}$$

where $\mathcal{P}$ is the path-ordered product and the trace is taken over the color indices. Although the full QCD don't have the Z_{N_c} symmetry, the Polyakov loop is still a good quantity to characterize the crossover between the confinement and the deconfinement phase. On can show that the average value of the Polyakov loop is given by

$$\langle L(T)\rangle \sim \exp\left[-F_{q\bar{q}}\,(r\to\infty,T)\right] \tag{2.13}$$

where $F_{q\bar{q}}\,(r,T)$ is the free energy of a static quark-antiquark pair sepated by a distance r. In a confining medium $F_{q\bar{q}}\,(r,T)\sim r$ and $\langle L(T)\rangle_{\text{confined}} = 0$. In a deconfined medium screening prevents the interaction between the quar-antiquark pair beyond certain distance and $\langle L(T)\rangle_{\text{deconfined}} \neq 0$. In summary, we can write

$$\langle L(T)\rangle = \begin{cases} 0 & T < T_L \\ \text{non-zero} & T > T_L \end{cases} \tag{2.14}$$

where T_L denotes the temperature of the confinement/deconfinement transition.

Actually, $\langle L(T)\rangle_{\text{confined}} = 0$, only in the limit of infinitely heavy quarks, where the symmetry Z_{N_c} is present. For finite quark masses this quantity is small, but non-zero. As a result the order parameter $\langle L(T)\rangle$ is no longer discontinuous at T_L, presenting a continuous behaviour with respect to T along the confinement/deconfinement transition.

QCD also exibits a phase transition characterized in terms of the chiral symmetry breaking. As we explain before, QCD has an approximate chiral symmetry that is spontaneouly broken at low energies by a non-zero value of the chiral condensate $\chi(T) = \langle\bar{\psi}\psi\rangle$. At temperatures above the chiral phase transition the thermal fluctuations melt the gluon cloud around the quarks and their dynamical masses disappears $M_q \sim \langle\bar{\psi}\psi\rangle = 0$. It is then clear that

$$\chi(T) = \begin{cases} \text{non-zero} & T < T_\chi \\ 0 & T > T_\chi \end{cases} \tag{2.15}$$

where T_χ is the temperature of the phase transition. In this context, this quantity is also known chiral symmetry restoration temperature. This makes evident that the chiral condensate can also be used as an order parameter for the chiral phase transition. As the chiral symmetry is only approximate, χ is small, but not exactly zero for $T > T_\chi$. So, like the Polyakov loop, the chiral condensate also presents a smooth behaviour with respect to T in the region of the chiral symmetry restoration.

Note that, if $\langle L(T)\rangle$ or $\chi(T)$ really have the form of a step function, their derivatives $\partial_T L(T)$ or $\partial_T \chi(T)$ would diverge at the critical temperature. In more realistic situations, instead of diverging, these derivatives present a peak around the critical temperature T_c. $\partial_T L(T)$ and $\partial_T \chi(T)$ are known as Polyakov loop and chiral condensate susceptibilities, respectively. This quantities were extensively studied using lattice techniques (Fig. 2.2 shows an example) and the results shows that, at zero chemical potential, chiral symmetry restorarion and deconfinement happens at the same temperature $T_L = T_\chi \simeq 175$ MeV. This number is usually used as the definition of the critical temperature. For non-zero chemical potential it is not likely that de-

confinement and chiral symmetry restoration happens at the same temperature, but this is still a subject of investigation [61].

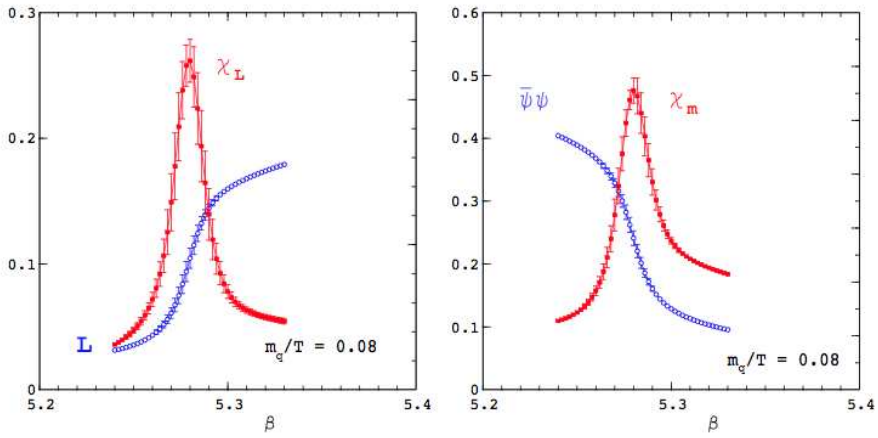

Figure 2.2: *Left*: Polyakov loop and its susceptibility as a funtion of the bare coupling. *Right*: Chiral condensate and its susceptibilty as a function of the bare coupling. Both results were obtained in QCD with two flavors. Figure taken from [62].

2.2.1 QCD equation of state at $\mu_b = 0$

In this section we discuss the equation of state of QCD at zero chemical potential. This information it is important in phenomenological applications, like the description of elliptic flow in heavy-ion collisions, for example, where it enters as an input in hydrodynamical models.

We will be interested in study the equation of state of QCD near of the critical temperature T_c, where the most interesting phenomena takes place. To do that, it will be useful to compare the thermodynamic quantities near of the crtical temperature with the corresponding quantities at very high temperature $T >> T_c$, where QCD can be approximately described as an ideal gas of quarks and gluons. In this approximation the only scale with dimension of energy is T. This implies, by dimensional

analysis, that

$$\epsilon_{\rm gas} \approx T^4, \quad P_{\rm gas} \approx T^4 \tag{2.16}$$

where $\epsilon_{\rm gas}$ and $P_{\rm gas}$ are the energy density and the pressure of the gas of quarks and gluons. In fact, the ratio $P_{\rm gas}/T^4$ defines the so-called Stefan-Boltzmman constant, which only depends on the number of degrees of freedom of the system. For a $SU(N_c)$ gauge theory with N_f massless quark flavors one obtains [63]

$$\frac{P_{\rm gas}}{T^4} = \Big[2(N_c^2-1) + 2N_cN_f\frac{7}{4}\Big]\frac{\pi^2}{90} \tag{2.17}$$

The energy-momentum tensor of a ideal gas is given by $T_{\mu\nu} = {\rm diag}[\epsilon_{\rm gas}, P_{\rm gas}, P_{\rm gas}, P_{\rm gas}]$ and the corresponding equation of state is obtained from the condition $T^\mu_\mu = 0$ as $\epsilon_{\rm gas} = 3P_{\rm gas}$.

As $T_c \sim \Lambda_{QCD}$, QCD is strongly coupled near of the critical temperature. As a result, the computation of thermodynamics quantity must rely on lattice techniques. Figure 2.3 shows the ratios ϵ/T^4 and $3P/T^4$ as a function of the temperature obtained from lattice calculations. The figure also shows the results for the entropy density divided by the corresponding ideal gas result as a funtion of the temperature. The sudden jump in the curves corresponds to the latent heat of confinement/deconfinement transition.

The deviation from the ideal gas approximation is best measure by the *trace anomaly*

$$\Delta = \frac{\epsilon - 3P}{T^4} \tag{2.18}$$

which is identically zero in an ideal gas. Figure 2.4 shows the behaviour of the trace anomaly as a function of the temperature obtained from lattice calculations

[64]. The result makes clear that the plasma of quarks and gluons formed after the deconfinement transition is strongly coupled in the region approximately given by $T_c \leq T \leq 5T_c$.

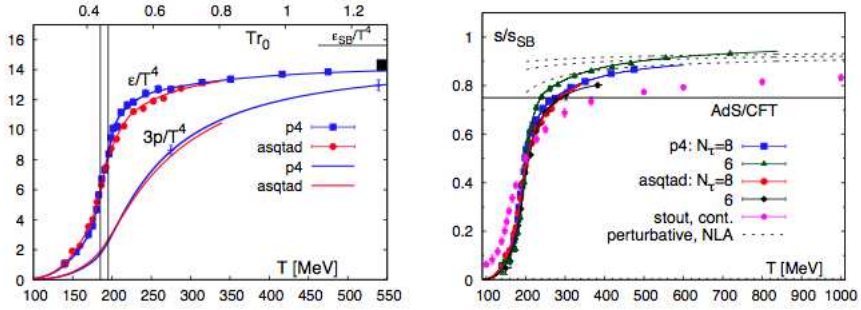

Figure 2.3: *Left*: ϵ/T^4 and $3P/T^4$ as a function of the temperature. *Right*: entropy density divided by the corresponding ideal gas result as a function of the temperature. Results obtained from lattice calculations. SB indicates the Stefan-Boltzmman result, obtained in the ideal gas approximation. Figure taken from [64].

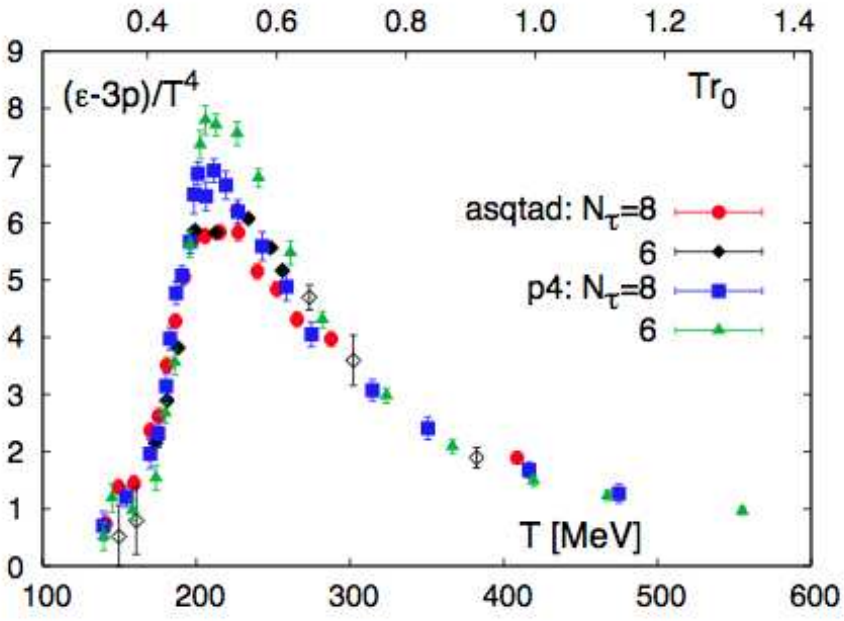

Figure 2.4: Trace anomaly as a function of the temperature obtained from lattice calculations. Figure taken from [64].

2.3 The QGP and ultra-relativistic heavy-ion collisions

For small values of temperature T and chemical potential μ_B quarks and gluons are confined in color-singlet combinations inside hadrons. As we increase T or μ_B we reach a new state of matter in which the quarks and gluons are no longer confined inside hadrons, appearing as individual particles. This deconfined phase is known as the Quark-Gluon Plasma (see Fig. 2.1 and the discussion below it).

The extreme conditions required to produce the QGP are expected to have existed in the early universe and may exist in the dense core of neutron stars [66]. The

controlled reproduction of these conditions can be achieved in ultra-relativistic heavy-ion collisions. The recent experimental efforts with the aim of study the QGP phase of QCD were realized at the RHIC and LHC [4–6]. In both cases the experiment involves the collision of counter-circulating beams of ultra-relativistic heavy-ions (gold nuclei at RHIC and lead nuclei at the LHC).

The collision of two nuclei produces regions of very high energy densities and temperatures in which the QGP is formed. As the produced plasma it is hotter than the enviroment it expands and, as a consequence, the temperature falls. When the falling temperature reaches the critical temperature the plasma undergoes a hadronization process, in which the deconfined quarks and gluons join together forming hadrons. The hadrons produced, or the product of their decay, can be observed at the detectors placed in the region of collision. This radiation does not provide information about the properties of the QGP, but only about the hadronization process [67]. However, the asymmetric flow of hadrons provides evidence for the existence of the QGP, as we explain below.

The Fig. 2.5 shows a non-central collision of two heavy nuclei, where we define z as the beam direction, and the plane xy as the transverse plane. As seen from the laboratory, the two nuclei are Lorentz contracted in the beam direction and they interact in an almond-shaped region.

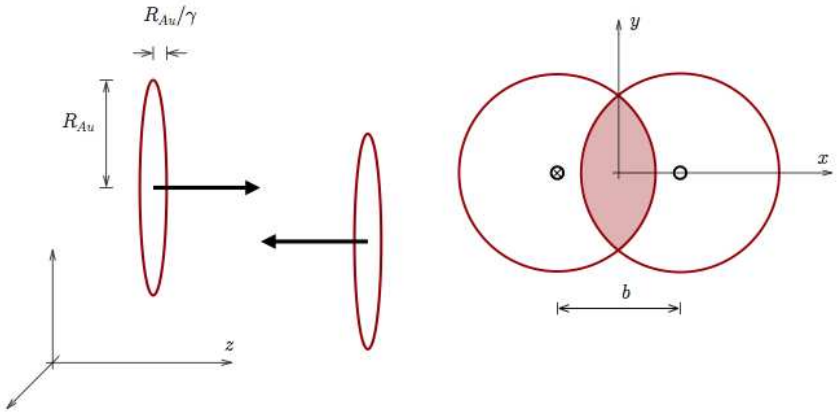

Figure 2.5: Geometry of a heavy-ion collision. The beam direction is z and xy is the transverse plane. *Left*: two Lorentz contracted gold nuclei colliding. *Right* Overlap region projected in the transverse plane. Figure taken from [93].

If the QGP were not produced in ultra-relativistic heavy ion collisions and the hadrons observed after the collision were produced in nucleon-nucleon interactions in the almond-shaped region, the flow of hadrons would be symmetric along the transverse plane and unrelated to the form of the overlap region. On the other hand, if the QGP were produced in the overlap region, we would expect, with base in hydrodynamical models, an asymmetric flow of hadrons after the hadronization process [68]. Indeed, this asymmetric flow was observed in the results of RHIC and this provides strongly indication that the QGP is indeed produced in ultra-relativistic heavy ion collisions [68]. Other evidences for the formation of the QGP are provided by some probes that we describe below.

Jet quenching parameter. Results from RHIC [69–72] indicate a strong suppression of particles with high transversal momentum p_{T} in Au-Au collisions, but not in d-Au collisions. The explanation for this phenomenon is that in Au-Au collisions the hot and dense quark gluon plasma is produced, and the jets lose energy due to

the interaction with this medium before hadronizing. This energy loss effect is called "jet quenching" and it can give valuable information as regards the properties of the plasma.

Thermal production of photons and dileptons. The limited extension of the QGP created in heavy ion collisions and the weakness of the electromagnetic interactions imply that this medium should be optically thin. Therefore, the photons produced in the plasma escape from it without subsequent interactions, providing an excellent probe of the conditions of the medium.

Quarkonium. Quarkonium mesons are produced in the early stages of heavy ion collisions, before the creation of the QGP. As they are much more tightly bound and smaller than ordinary 'light' hadrons, they can survive as bound states in the QGP at temperatures above the deconfinement temperature up to some dissociation temperature. This property, together with the fact that their interaction with the thermal medium is comparatively stronger than their interaction with the hadronic matter formed after hadronization, makes the quarkonium mesons excellent probes to study the QGP formed in heavy ion collisions [67].

There are, of course, several other probes that can be used to study the QGP. Here we only describe the probes that (together with other more abstract quantities) were studied in this thesis. Along with these probes, other quantities that are very important in the study of the properties of the QGP are the **transport coefficients** of the plasma, which are necessary inputs in hydrodynamic models.

Chapter 3

Conformal Field Theories

In this chapter we present some general properties of conformal field theories (CFTs) in spacetimes with $d > 2$[1]. In particular, we present some basic aspects of the $\mathcal{N} = 4$ SYM theory, which is the CFT relevant in the most known and studied example of the AdS/CFT correspondence.

The so-called conformal field theories are quantum field theories which are invariant under conformal tranformations. Besides being very important in the context of AdS/CFT correspondence and in string theory, CFT also has applications in more applied fields of physics, like statistical physics and condensed matter physics.

Before adressing CFTs let us discuss some basic properties of quantum field theories (QFTs). The basic observables of a QFT are correlation functions of a product of local operators

$$\langle O_1(x_1)O_2(x_2)...O_n(x_n)\rangle \tag{3.1}$$

the operator are made out of fields that define the QFT and are characterized by

[1]The conformal group is infinite dimensional for $d = 2$. In this special case the symmetry group is $SL(2, \mathbb{C})$. The standard references for CFT in two-dimensional spacetimes are [65, 73]

their Lorentz structure, charges and scaling dimensions. All information regarding the correlation functions is encoded in the partition function of the QFT, $Z_{\rm QFT}[J_i(x)]$, which is given by

$$Z_{\rm QFT}[J_i(x)] = \left\langle \exp \int d^d x J_i(x) O_i(x) \right\rangle \tag{3.2}$$

where $J_i(x)$ represent the sources for the operators $O_i(x)$. The correlation function can be calculated taking derivatives of the partition function

$$\langle O_1(x_1) O_2(x_2) ... O_n(x_n) \rangle = \frac{\delta^n \log Z_{\rm QFT}[J_i(x)]}{\delta J_1(x_1) \delta J_2(x_2) ... \delta J_n(x_n)} \Big|_{J_i=0} \tag{3.3}$$

The scaling dimension and the Lorentz structure of the sources J_i are completely determined by those of O_i.

A QFT is said to be solved if all the correlation functions are known. In general, the determination of the correlation functions is difficult, specially for strongly interacting theories, where we cannot use perturbation theory. However, this task is easier if the theory has some symmetries. As we will se in the next section, the conformal symmetry is so strong that it fix the form of the 2- and 3-point functions of local operators.

3.1 Conformal Group in $d > 2$ dimensions

Consider a d-dimensional spacetime ($d > 2$) with flat metric $g_{\alpha\,\beta} = \eta_{\alpha\,\beta}$ of signature $(1, d-1)$. Under a general coordinate transformation, $x \to x'$, the metric transforms as a two-tensor

$$g_{\mu\nu}(x) \to g'_{\mu\nu}(x) = \frac{\partial x^\alpha}{\partial x'^\mu} \frac{\partial x^\beta}{\partial x'^\nu} g_{\alpha\beta}(x) \tag{3.4}$$

The group of conformal transformations are a subclass of the group of general coordinate transformations that preserve the angle between two arbitrary vectors. Mathematically, this corresponds to a transformation, $x \to x'$, under which the metric is invariant up to a scale factor $\Omega(x)$,

$$g_{\mu\nu}(x) \to g'_{\mu\nu}(x') = \Omega(x) g_{\mu\nu}(x) \tag{3.5}$$

To find the infinitesimal generators of the conformal group we consider a infinitesimal coordinate transformation $x \to x' = x - \epsilon$ respecting Eq. (3.5). Under this transformation we have, using Eq. (3.4),

$$g'_{\mu\nu}(x') = g_{\mu\nu} + \partial_\mu \epsilon_\nu + \partial_\nu \epsilon_\mu \tag{3.6}$$

Using Eq. (3.5) we find

$$g_{\mu\nu}(\Omega(x) - 1) = \partial_\mu \epsilon_\nu + \partial_\nu \epsilon_\mu \tag{3.7}$$

Contracting both sides with $g^{\mu\nu}$ we obtain

$$\Omega(x) = 1 + \frac{2}{d}(\partial \cdot \epsilon) \tag{3.8}$$

Substituting (3.8) in (3.7) we find a differential equation for ϵ

$$\partial_\mu \epsilon_\nu + \partial_\nu \epsilon_\mu = \frac{2}{d}(\partial \cdot \epsilon) \tag{3.9}$$

which is known as the conformal Killing vector equation. Solutions of (3.9) charac-

terize the possible type of conformal transformations, which are

$$\begin{aligned}
\epsilon^\mu &= a^\mu && \text{translations} \\
\epsilon^\mu &= \omega^\mu_\nu x^\nu && \text{rotations} \quad (\omega_{\mu\nu} = -\omega_{\nu\mu}) \\
\epsilon^\mu &= \lambda x^\mu && \text{dilations} \\
\epsilon^\mu &= b^\mu x^2 - 2x^\mu (b \cdot x) && \text{special conformal transformations}
\end{aligned} \tag{3.10}$$

Integrating the infinitesimal generators we find the finite conformal trasformations

$$\begin{aligned}
x' &= x + a && \text{translations} \\
x' &= \Lambda\, x && \text{rotations} \\
x' &= \lambda\, x && \text{dilations} \\
x' &= \tfrac{x + b x^2}{1 + 2b\cdot x + b^2 x^2} && \text{special conformal transformations}
\end{aligned} \tag{3.11}$$

These transformations form the conformal group in d dimensions. The corresponding generators are

$$P_\mu = -i\partial_\mu, \quad J_{\mu\nu} = i(x_\mu \partial_\nu - x_\nu \partial_\mu), \quad K_\mu = -i[x^2 \partial_\mu - 2x_\mu (x\cdot\partial)], \quad D = -ix\cdot\partial \tag{3.12}$$

These generators satisfy the following commutation relations

$$\begin{aligned}
[J_{\mu\nu}, P_\alpha] &= -i(\eta_{\mu\alpha}P_\nu - \eta_{\nu\alpha}P_\mu), \\
[P_\mu, K_\nu] &= 2i(J_{\mu\nu} - \eta_{\mu\nu}D), \\
[J_{\mu\nu}, J_{\alpha\beta}] &= -i(\eta_{\mu\alpha}J_{\nu\beta} - \eta_{\mu\beta}J_{\nu\alpha} - \eta_{\nu\alpha}J_{\mu\beta} + \eta_{\nu\beta}J_{\mu\alpha}), \\
[J_{\mu\nu}, K_\alpha] &= -i(\eta_{\mu\alpha}K_\nu - \eta_{\nu\alpha}K_\mu), \\
[D, K_\mu] &= iK_\mu, \quad [D, P_\mu] = -iP_\mu, \quad [J_{\mu\nu}, D] = 0.
\end{aligned} \tag{3.13}$$

The total number of parameters of the conformal group is $d+d(d-1)/2+1+d = (d+2)(d+1)/2$. The algebra of the above generators is locally isomorphic to $SO(2,d)$. This can be seen defining the generators

$$M_{\mu\nu} = J_{\mu\nu}, \quad M_{\mu,d} = \frac{1}{2}(K_\mu - P_\mu), \quad M_{\mu,d+1} = \frac{1}{2}(K_\mu + P_\mu), \quad M_{d,d+1} = D \tag{3.14}$$

and checking that they satisfy the algebra of $SO(2,d)$.

3.2 Primary fields and correlation functions

The fields and operators of a CFT are usually classified by their Lorentz quantum numbers (j_L, j_R) and scaling dimension Δ. To have a well defined scaling dimension an operator $O(x)$ must be a eingenstate of D

$$[D, O(x)] = i(-\Delta + x^\mu \partial_\mu)O(x) \tag{3.15}$$

Under dilations, $x \to \lambda x$, this operator transforms as

$$O(x) \to \lambda^{\Delta} O(\lambda x) \tag{3.16}$$

Imposing that all states in a given representation have positive norm (unitarity condition) implies the existence of a lower bound on the dimesion of all operators [74]

$$\Delta \geq \epsilon(j_L, j_R) \tag{3.17}$$

where $\epsilon(j_L, j_R)$ is a lower bound that depends on the Lorentz quantum numbers of the operators in question. For supersymmetric theories ϵ also depends on the R-symmetry quantum numbers.

Observing the commutation relations between P_μ and K_μ with D it is easy to verify that P_μ raises the dimension of the operator while K_μ lowers it. As there is a lower bound on the dimension of all operators, there must be an operator which is annihilated by K_μ. Such an operator is called a *conformal primary operator*. In a (j_L, j_R) representation of the Lorentz group, this operator is defined as

$$[D, O_{(\Delta, j_L, j_R)}(0)] = i\Delta\, O_{(\Delta, j_L, j_R)}(0) \tag{3.18}$$

$$[K_\mu, O_{(\Delta, j_L, j_R)}(0)] = 0 \tag{3.19}$$

Acting on a primary operator with the other generators of the conformal group we obtain a infinite dimensional representation of this group specified by the numbers (Δ, j_L, j_R).

Classically, the scaling dimension of the fields or operators of a QFT can be determined by dimensional analysis, as they correspond to the enginering dimension

of these fields. At the quantum level, however, the scaling dimensions can get quantum corrections in interacting theories.

The conformal symmetry is so strong that it fix the form of the 2- and 3-point functions of CFTs. Using the conformal algebra one can show that: 2-point functions vanish if the operators have different dimensions; The 2-point function of a single operator O with dimension Δ is

$$O(0)O(x) \propto \frac{1}{|x|^{2\Delta}}; \tag{3.20}$$

The 3-point function of O_i, O_j and O_k with dimensions Δ_1, Δ_2 and Δ_3 is given by

$$O_i(x_1)O_j(x_2)O_k(x_3) = \frac{c_{ijk}}{|x_1 - x_2|^{\Delta_1+\Delta_2-\Delta_3}|x_1 - x_3|^{\Delta_1+\Delta_3-\Delta_2}|x_2 - x_3|^{\Delta_2+\Delta_3-\Delta_1}}. \tag{3.21}$$

The conformal symmetry is even more powerfull when it can be mix with supersymmetry. In this case, the conformal group is enlarged to the superconformal group. Special representations of the superconformal group are extremely important in tests of the AdS/CFT duality. In the next section we will discuss the superconformal group in the special case of the four-dimensional $\mathcal{N} = 4$ SYM theory.

3.3 $d = 4$, $\mathcal{N} = 4$ Super Yang-Mills theory

The most general renormalizable theory consistent with $\mathcal{N} = 4$ global supersymmetries in four dimensions is the so-called $\mathcal{N} = 4$ Super Yang-Mills (SYM) theory. In the case relevant for AdS/CFT correspondence, the gauge group G of this theory $SU(N)$. For now we let G be a generic Lie group. Later we will discuss the special

properties of $G = SU(N)$ case.

This theory can be obtained by dimensional reduction of the $\mathcal{N} = 1$ SYM theory in ten dimensions [75, 76]. The action of this ten dimensional theory is given by

$$S_{\mathcal{N}=1} = \int d^{10}x \mathrm{Tr}\Big(-\frac{1}{4} F_{MN} F^{MN} + \frac{i}{2} \bar{\lambda}\, \Gamma^M D_M\, \lambda \Big) \tag{3.22}$$

where $D_M \lambda = \partial_M \lambda + i g_{\mathrm{YM}} [A_M, \lambda]$, $F_{MN} = \partial_M A_N - \partial_N A_M + i g_{\mathrm{YM}} [A_M, A_N]$, and λ is a Majorana-Weyl spinor. The indices M and N run from 0 to 9 and Γ^M is a ten-dimensional Dirac matrix. Both F_{MN} and λ are written in matrix notation. g_{YM} is the coupling of the theory.

The above action is invariant under the supersymmetry transformation

$$\begin{aligned} \delta A_M &= -i \bar{\zeta}\, \Gamma_M \lambda, \\ \delta \lambda &= \frac{1}{2} F_{MN} \Gamma^{MN} \zeta \end{aligned} \tag{3.23}$$

where ζ is the supersymmetry generator, which is also a Majorana-Weyl spinor, and $\Gamma^{MN} = \Gamma^M \Gamma^N - \Gamma^N \Gamma^M$.

Performing a Kaluza-Klein compactification in a six-dimensional torus, T^6, the action becomes

$$S_{\mathcal{N}=4} = \int d^4x \mathrm{Tr}\Big[-\frac{1}{4} F_{\mu\nu} F^{\mu\nu} + 2 D_\mu A_m D^\mu A_m - g^2_{\mathrm{YM}} [A_m, A_n]^2 - \frac{i}{2} \big(\bar{\lambda}\, \Gamma^\mu D_\mu\, \lambda + \bar{\lambda} \Gamma_m [A_m, \lambda] \big) \Big] \tag{3.24}$$

where μ, ν run from 0 to 3 and m, n run from 4 to 9. The coordinates x^m label the

compact space T^6. The supersymmetry transformation becomes

$$\begin{aligned}
\delta A_\mu &= -i\bar{\zeta}\,\Gamma_\mu\lambda, \\
\delta A_m &= -i\bar{\zeta}\,\Gamma_m\lambda, \\
\delta\lambda &= \Big(\frac{1}{2}F_{\mu\nu}F^{\mu\nu} + D_\mu A_n\Gamma^{\mu n} + \frac{ig_{\rm YM}}{2}[A_m, A_n]\Gamma^{mn}\Big)\zeta.
\end{aligned} \tag{3.25}$$

The ten-dimensional gauge field gives rise to a four-dimensional gauge field A_μ and six scalars A_m. The Majorana-Weyl spinor λ (with sixteen components) gives rise to four four-dimensional Weyl spinors. These fileds form the vector multiplet of $\mathcal{N} = 4$ SUSY and all of them transform in the adjoint representation of the gauge group G. The ten-dimensional SUSY generator separates into four four-dimensional SUSY generators, giving rise to $\mathcal{N} = 4$ SUSY.[2]

Under the Kaluza-Klein compactification is convenient to consider the following decomposition of the ten-dimensional Lorentz group

$$SO(9,1) \to SO(3,1) \times SO(6) \tag{3.26}$$

where $SO(3,1)$ is the Lorentz group in four dimensions and $SO(6)$ is the isometry group of the compact space (a six dimensional torus).

From the point of view of the four-dimensional theory, the fields have a $SO(6)$ global symmetry under which A_μ is a singlet and A_m is a vector. This global symmetry is identified with the R-symmetry group of the $\mathcal{N} = 4$ SUSY algebra.

[2]In a d-dimensional spacetime, $\mathcal{N}$ denotes the ratio of the number of supercharges to the smallest spinor representation.

3.3.1 Symmetries of $\mathcal{N} = 4$ SYM

In this section we discuss the symmetries of the $\mathcal{N} = 4$ SYM theory. This theory is invariant under:

- *Conformal transformations*: genetared by D, P_μ, K_μ and $J_{\mu\nu}$. The corresponding symmetry group is $SO(2,4) \sim SU(2,2)$;
- *R-symmetry transformations*: the symmetry group is $SO(6) \sim SU(4)$. Let T^A, with $A = 1, ..., 15$, be the generators of this symmetry;
- *Poincare supersymmetries*: the supercharges Q^a_α and $\bar{Q}_{\dot{\alpha}a}$ with $a = 1, ..., 4$, generates the $\mathcal{N} = 4$ SUSY;
- *Superconformal symmetries* generated by the supercharges S^a_α and $\bar{S}_{\dot{\alpha}a}$ with $a = 1, ..., 4$. This charges arise from the non-vanishing commutator between Q and $\bar{Q}$ with K_μ. Schematically, we have: $[K, Q] \sim S$ and $[K, \bar{Q}] \sim \bar{S}$. As both operators inside the commutator generate symmetries, their commutator (S or $\bar{S}$) also generate symmetries.

Together, all these symmetries form the *superconformal group* $SU(2,2|4)$.[3] Supressing the indices of the generators, the non-trivial part of the superconformal algebra is schematically given by[4]

$$\begin{aligned} [D, Q] &= -\frac{i}{2}Q, \quad [D, S] = \frac{i}{2}S, \quad [K, Q] \sim S, \quad [P, S] \sim Q, \\ Q, \bar{Q} &\sim P, \quad S, \bar{S} \sim K, \quad Q, S \sim J + D + T, \end{aligned} \tag{3.27}$$

[3] In $d = 4$, the superconformal group of a theory with $\mathcal{N}$ supersymmetries is denoted as $SU(2,2|\mathcal{N})$.

[4] For more details about the superconformal algebra in $\mathcal{N} = 4$ SYM, see [77].

Remarkably, the superconformal symmetry remains unbroken after the quantization of $\mathcal{N} = 4$ SYM theory. As a consequence, the β-function of this theory vanishes identically and the coupling of the theory is constant

$$\beta = E\frac{dg}{dE} = 0 \;\Rightarrow\; g = \text{constant} \tag{3.28}$$

where E is some scale of energy and g is the coupling of theory.

3.3.2 Representations of the superconformal algebra

The commutation relation between S and D show us that the operator S lowers the dimension of the operator where it is applied. As there is a lower bound on the dimension of all operator in unitary CFTs, there must be an operator that is annihilated by S. We define a *superconformal primary operator* O to be a non-vanishing operator such that

$$[S, O] \quad = 0, \quad [\bar{S}, O] = 0, \quad \text{for } O \text{ bosonic} \tag{3.29}$$

$$\{S, O\} \quad = 0, \quad \{\bar{S}, O\} = 0, \quad \text{for } O \text{ fermionic} \tag{3.30}$$

Since $S, \bar{S} \sim K_\mu$, a superconformal primary operator is also a conformal primary operator, but the converse is not necessarily true.

Given a superconformal primary operator we can construct descendant operators by applying any generator of the superconformal algebra. A superconformal primary operator and all its descendant operators form a infinite dimensional representation of $SU(2,2|4)$.

A special type of superconformal primary operators are the so-called *chiral pri-*

mary operators. Besides being annihilated by S, this operators are also annihilated by at least one of the supercharges

$$[Q^a_\alpha, O] = 0, \quad \text{for } O \text{ bosonic} \tag{3.31}$$

$$\{Q^a_\alpha, O\} = 0, \quad \text{for } O \text{ fermionic} \tag{3.32}$$

for at least one $a = 1, ..., 4$, and one $\alpha = 1, 2$. As they are annihilated by some of the supercharges, the chiral primary operators are BPS states of the $\mathcal{N} = 4$ SUSY.[5]

By acting with the other generators of the conformal algebra in a chiral primary operator we obtain a multiplet (representation) of the superconformal group which is short than generic multiplets obtained from generic superconformal primary operators. Because of that, representations obtained from chiral primary operators are also called *short multiplets*.

The chiral primary operators are very important because their scaling dimension Δ does not receive quantum corrections. Δ is fixed by the superconformal algebra.

From the superconformal algebra on can deduce that all the superconformal primary operators of the $\mathcal{N} = 4$ SYM theory are built from gauge-invariant symmetric combinations of the scalar fields A_m's. The simplest example are the single trace operators given by

$$O(x) = \text{Tr}\left(A^{(i_1} A^{i_2} ... A^{i_k)}\right) - \text{traces} \tag{3.33}$$

where $i_1, i_2, ..., i_k$ are indices of the fundamental representation of $SO(6)$. The subtraction of all the traces ensures that $O(x)$ corresponds to an irreducible representation of the superconformal algebra. Operators with the above form are chiral primary operators of the theory. This operators are very useful in tests of the AdS/CFT du-

[5]For a good introduction to BPS states in $\mathcal{N} = 4$ SYM theory, see the Appendix J of [78].

ality, because we can use them to compare the spectrum of the $\mathcal{N} = 4$ SYM theory with the spectrum of type IIB supergravity. We will discuss tests of the AdS/CFT correspondence in the Chapter 5.

3.3.3 Large N limit

Now we discuss some basic properties of this theory at large N. As pointed out by 't Hooft [79], in the large N limit of a non-abelian gauge theory, with $N \times N$ matrices, the physical quantities can be expanded in powers of $1/N$. Let Z be the partition function of the non-abelian gauge theory and $g_{\rm YM}$ its coupling constant. Defining the 't Hooft coupling, $\lambda = g_{\rm YM}^2 N$, one can show that the vacuum-to-vacuum amplitude, $\log Z$, can be written as

$$\log Z = \sum_{h=0}^{\infty} N^{2-2h} f_h(\lambda) = N^2 f_0(\lambda) + f_1(\lambda) + \frac{1}{N^2} f_2(\lambda) + ... \tag{3.34}$$

where $f_h(\lambda)$ are functions of the 't Hooft coupling that includes the contributions of all diagrams which can be drawn in a two-dimensional surface with h holes without crossing any lines. Therefore, the Feynman diagrams are organized by their topologies: planar diagrams are included in $f_0(\lambda)$ and are proportional to N^2; Non-planar diagrams that can be drawn on a torus are included in $f_1(\lambda)$ and are proportional to $N^0 = 1$; Non-planar diagrams that can be drawn on a donut with two holes are included in $f_2(\lambda)$ and are proportional to $1/N^2$, etc. Note that, in the large N limit, only planar diagrams contribute. The same holds for other physical observables, the only difference is an overall factor of N^m multipling the expansion, where m is some number that depends on the observable in question.

Chapter 4

Basics of string theory

In this chapter we present very basic concepts of string theory necessary to understand the AdS/CFT correspondence. String theory is a relativistic quantum theory in which the basic objects are: closed strings, open strings and D-branes. D-branes (short for Dirichlet-branes) are non-perturbative solitonic objects where open strings can end and closed string can break into open strings. The only free parameter in string theory is a lengh scale ℓ_s known as string lengh. It is also customary to use another parameters like $\alpha' = \ell_s^2$ or the *string tension*, $T_{\rm str} = 1/(2\pi\alpha')$.

4.1 Bosonic string theory

Let us first consider the dynamics of a single string propagating in a flat d-dimensional spacetime. In analogy with the case of a point particle, whose action is given by the lengh of its wordline, in string theory the action is defined as proportional to the area of the surface swept by the string in the spacetime. This surface is known as string worldsheet. Parametrizing the string worldsheet with the coordinates (σ^0, σ^1), this

action can be written as

$$S_{\rm str} = -T_{\rm str} \int d^2\sigma \sqrt{-\det g_{\alpha\beta}} \tag{4.1}$$

where $d^2\sigma = d\sigma^0\, d\sigma^1$ and $g_{\alpha\beta}$ is the metric induced on the worldsheet and α, $\beta = 0$, 1. This action was first proposed in 1970 [80, 81] and is known as *Nambu-Goto action*. The quantization of the above action requires d =26. This is necessary to avoid negative-norm states and the anomaly of the Lorentz group at the quantum level. We emphasize that we consider here the "first-quantizatized" point of view, which means that we consider different statets of a single string. Creation and anihilation of strings are possible with a "second quantized" point of view known as *string field theory* which we will not adress here.

After quantization we get a spectrum that corresponds to the different vibration modes of the string. It turns out that the vibration modes have properties of the usual elementary particles with interger spin. The spectrum contains a finite number of massless modes and an infinity tower of massive modes with mass of the order $m_s = \ell_s^{-1}$. The spectrum of closed and open string for the tachyonic and massless modes is summarized in Table 4.1.

Table 4.1: Massless and tachyonic spectrum of closed and open strings.

Mass	Closed string	Open string
$M < 0$	tachyon	tachyon
$M = 0$	$g_{\mu\nu}$, $B_{\mu\nu}$, Φ	A_μ

The spectrum of open string with free endpoints[1] has a tachyon (particle with

[1]In order to assume that the string's endpoint are free, we have to assume the existence of a space

negative squared mass) as the fundamental state, with $M^2 = -1/\alpha'$. The first excited state is massless vector boson and the first massive state is a spin-two particle with $M^2 = 1/\alpha'$. Then we have states with higher mass and spin.

The spectrum of closed strings also contains a tachyon as the fundamental state, with $M^2 = -4/\alpha'$. In the first excited state we have a massless spin-two particle, the graviton $g_{\mu\nu}$; a massless scalar Φ called dilaton and a antisymmetric second rank tensor $B_{\mu\nu}$, called *Kalb-Ramond field*. Again, the massive modes corresponds to particles of higher mass and spin. As this theory contains a graviton its spacetime is not fixed, as we assume in the begining, being actually dynamical.

An unsatisfactory feature of this theory is the presence of tachyons. Tachyons are unphysical because they imply the instability of the vacuum. The open-string tachyon can be understood in terms of the decay of D-branes, but the closed string tachyon is still a problem for this theory [82]. Besides that, another unsatisfactory feature of open and closed string theories is that in both cases the spectrum only contains bosons. Because of that this theory is usually known as *bosonic string theory*.

At low energies $E << m_s$ string theory massive modes are not excited and one can obtain a effective low energy action that describes the massless fields. This can be done by considering strings propagating in the background of the massless fields $g_{\mu\nu}$, $B_{\mu\nu}$ and Φ and requiring conformal invariance of the worldsheet. The resulting low energy theory is basically the general theory of relativity with some additional fileds[2]

$$S_{\text{eff}} = \int d^{26}x\sqrt{-g}e^{-2\Phi}\Big(R - \frac{1}{12}H_{\mu\nu\lambda}H^{\mu\nu\lambda} + 4\,\partial_\mu\Phi\,\partial^\mu\Phi\Big) \tag{4.2}$$

filling D-brane, that is, a D25-brane. This is necessary because the string's endpoints are confined to move in the world-volume of the branes where it ends.

[2]A detailed derivation of this effective action can be found in [83].

where $g = \det(g_{\mu\nu})$, R is the scalar of curvature derived from $g_{\mu\nu}$, and $H_{\mu\nu\lambda} = \partial_\mu B_{\nu\lambda} + \partial_\nu B_{\lambda\nu} + \partial_\lambda B_{\mu\nu}$ is the field strength associated to $B_{\mu\nu}$. This procedure of deducing an effective action by requiring conformal invariance can also be used in superstring theories to show that the low energy limit of this theories are supergravity theories.

4.2 Superstring theories

To describe fermions it is necessary to add fermionic degrees of freedom to the action (4.1). There are at least three ways of doing that. In the RNS formalism [84, 85], this is done imposing supersymmetry in the string worldsheet. In the Green-Schwarzs (GS) formalism [86, 87], one requires supersymmetry in the d-dimensional spacetime. In the pure spinor formalism one covariantly quantize the superstring in a manifestly super-Poincaré covariant manner [88].

The quantization of the supersymmetric generalization of (4.1) gives rise to the so-called superstring theories.[3] As before, the vibration modes of the superstrings will give rise to different particles, but this time including bosons nd fermions. There are five types of superstring theory and all these theories live in 10-dimensional spacetimes, as required for anomaly cancellation. These five theories are: type I, type IIA, type IIB, heterotic $SO(32)$ and heterotic $E_8 \times E_8$. The type of theory we get after quantization depends on the boundary conditions chosen for the fermionic degrees of freedom and on the way we built the closed string theories. These theories have different properties like: spectrum, gauge group, chirality, etc. Despite these differences all these theories are related to each other by dualities and are belived to be part of

[3] In general, the term "string theory" is used refering to "superstring theories". The string theory that only contain bosons is usually known as "bosonic string theory".

a single theory called M-theory [82].

In thesis we will focus on type IIB string theory, that is the superstring theory relevant for the AdS/CFT correspondence. Table 4.2 shows the massless spectrum of type IIB string theory.

Table 4.2: Massless spectrum of type IIB string theory.

Sector	Fields
R-R	$C_0, C_{2\mu\nu}, C^+_{4\mu\nu\lambda\rho}$
NS-NS	$g_{\mu\nu}$, $B_{2\mu\nu}$, Φ
R-NS	λ_{1+}, ψ^{μ}_{1-}
NS-R	λ_{2+}, ψ^{μ}_{2-}

The letters R-R, NS-NS, R-NS and NS-R in the rows of Table 4.2 indicate different sectors of the supestring spectrum. R stands for Ramond and NS for Neveu-Schwarz. The R-R and NS-NS sectors contains the bosons of the theory, while the R-NS and NS-R contains the fermions.[4] The fields in the R-R sectors are a 0-form C_0 (the axion field), a 2-form $C_{2\mu\nu}$ and a 4-form $C^+_{4\mu\nu\lambda\rho}$. The superscript + indicate that C_4 has a self-dual field strength. The NS-NS sectors contains the same fields of the bosonic string theory, that is, a rank two symmetric tensor $g_{\mu\nu}$ (the metric tensor), a rank two antisymmetric tensor $B_{2\mu\nu}$ (the Kalb-Ramond field) and a scalar field Φ (the dilaton).

The fields of the R-NS sector are a left-handed Majorana-Weyl dilatino λ_{1+}, and a right-handed Majorana-Weyl gravitino ψ^{μ}_{1-}. The NS-R sector contains a right-handed Majorana-Weyl dilatino λ_{2+}, and a left-handed Majorana-Weyl gravitino ψ^{μ}_{2-}. The numbers 1 e 2 indicate whether the fermionic fields are in the R-NS or in the NS-R

[4]For more details regarding the precise definition of these sectors, see for instance [82].

sector, respectively, while the sign +(-) indicate a positive (negative) chirality. As the two gravitinos and the two dilatinos have the same chirality, this theory is said to be chiral or parity violating.

Type IIB string theory is supersymmetric, so it must have the same number of degrees of freedom at each mass level, in particular, at the massless level. Indeed, we can check that we have the same number of fermionic and bosonic degrees of freedom in the massless part of the IIB spectrum:

$$\text{Type IIB bosons:} \quad \overbrace{\underbrace{1}_{\Phi}+\underbrace{28}_{B_{\mu\nu}}+\underbrace{35}_{g_{\mu\nu}}}^{\text{NS-NS sector}}+\overbrace{\underbrace{1}_{C_0}+\underbrace{28}_{C_2}+\underbrace{35}_{C_4}}^{\text{R-R sector}}=128$$

$$\text{Type IIB fermions:} \quad \overbrace{\underbrace{8}_{\lambda_{1+}}+\underbrace{56}_{\psi^{\mu}_{1-}}}^{\text{R-NS sector}}+\overbrace{\underbrace{8}_{\lambda_{2+}}+\underbrace{56}_{\psi^{\mu}_{2-}}}^{\text{NS-R sector}}=128$$

The low energy limit of this theory, as in the case o bosonic string theory, the massive modes are not excited and one can obtain a effective low energy theory for the massless fields. As in the case of bosonic string theory, this is done by considering superstring propagating in the background of the bosonic fields and requiring conformal invariance of the worldsheet.

Before writing the action of low energy type IIB string theory we introduce the field strengths $H_3 = dB_2$, $F_1 = dA_0$, $F_3 = dC_2$ and $F_5 = dC_4$ and other convenient quantities

$$\begin{aligned} \tilde{F}_3 &= F_3 - C_0 \wedge H_3, \\ \tilde{F}_5 &= F_5 - \frac{1}{2} C_2 \wedge H_3 + \frac{1}{2} B_2 \wedge F_3 \end{aligned} \tag{4.3}$$

With the quantities defined above one can write the bosonic part of the effective low energy action as [82]

$$\begin{aligned} S_{\rm IIB} &= S_1 + S_2, \\ S_1 &= \frac{1}{2\kappa_{10}^2}\int d^{10}x\sqrt{-g}e^{-2\Phi}\Big(R - \frac{1}{2}|H_3|^2 + 4(\partial\phi)^2\Big), \\ S_2 &= -\frac{1}{4\kappa_{10}^2}\int d^{10}x\Big[\sqrt{-g}\Big(|F_1|^2 + |\tilde{F}_3|^2 + \frac{1}{2}|\tilde{F}_5|^2\Big) + C_4 \wedge H_3 \wedge F_3\Big] \end{aligned} \tag{4.4}$$

where $\kappa_{10}^2 = 8\pi G_{(10)}$ ($G_{(10)}$ is the ten-dimensional Newton constant), $g = \det(g_{\mu\nu})$, and R is the scalar of curvature. Along with the action $S_{\rm IIB}$ it is also necessary to require $\tilde{F}_{(5)}$ to be self-dual, that is, $\tilde{F}_{(5)} = \star\tilde{F}_{(5)}$. The low-energy theory resulting from this action has $\mathcal{N} = 2$ spacetime supersymmetries and is known as type IIB supergravity [89, 90].

As we will discuss in the Chapter 5, the AdS/CFT correspondence is mostly understood in the low energy limit of type IIB string theory, in which these theory is effectively described by a supergravity theory. In the section 4.4 we will describe special solutions of the supergravity field equations that will be useful in the context of the AdS/CFT correspondence.

4.3 Interactions

The interaction between two closed strings can be introduced postulating that two strings can join together forming a single string which, by its turn, can split in two strings. Scattering amplitudes are given by a sum over the topologies of two-dimensional surfaces formed by the worldsheets of the strings in interaction as shown in Figure 1.

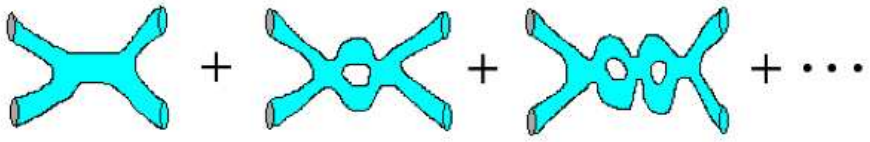

Figure 4.1: Two-to-two amplitude expressed as a sum over topologies. Figure taken from [93].

In the above sum the contribution of surfaces with h holes is weighted by a factor g_s^{2h-2}, where g_s is the *string coupling constant*. Surprisingly, g_s is not a independent parameter of the theory. One can show that $g_s = \langle e^{\phi} \rangle$, that is, g_s is dynamical parameter related to the expectation value of the dilaton field.

4.4 D-branes

Besides open and closed strings, string theory also contains higher dimensional objects known as D-branes[5] (or Dp-branes). A Dp-brane is a hypersurface with p spatial directions where the open strings endpoints can move freely, but these endpoints are not aloud to move outside the brane volume. Mathematicaly, this implies that coordinates of open strings endpoints must respect Neumann boundary conditions along the $(p+1)$ spacetime coordinates of the brane worldvolume and $(9-p)$ Dirichlet boundary conditions for the other coordinates.

The presence of a Dp-brane breaks the Lorentz group $SO(9,1)$ to $SO(p,1) \times SO(9-p)$, with $SO(p,1)$ being the Lorentz group of the brane world-volume and $SO(9-p)$ the rotational group of the space transverse to the brane.

The quantization of open strings ending on a Dp-brane gives rise to a spectrum

[5]This section is based on the section 4.4 of [91].

of fields that lives inside the brande world-volume and transform under its $SO(p,1)$ Lorentz group. At the massless level there is a photon field A_a, $(a = 1, 2, ..., p)$ and $(9-p)$ scalars fields ϕ^I, $(I = p+1, ..., 9)$. The number of scalar fields is equal to the number of directions transverse to the brane and these fields represent fluctuations of the branes in these directions [83]. Note that while ϕ^I are scalar under the $SO(p,1)$ Lorentz group of the brane, they behave as vectors under the $SO(9-p)$ rotational symmetry of the directions transverse to the brane. In the brane world-volume the $SO(9-p)$ symmetry appears as a global symmetry.

As before, there is also massive excitations that we will not consider because they are not excited at the low energy limit, which is the limit that we will always work.

The above results indicate that Dp-branes are dynamical objects rather than just geometrical objects that encode boundary conditions. Indeed, the open strings ending on a Dp-brane can be viewed as excitations of the brane itself [92].

4.4.1 Low energy limit

As in the case of closed strings we can obtain an effective low energy theory that describes the massless open string excitations that lives insides the Dp-brane by requiring the conformal invariance of the world-sheet of these strings in the presence of the background field of these massless excitations. One can show that the bosonic part of the efffective low energy action of a Dp-brane is given by

$$S_{Dp} = S_{DBI} + S_{WZ} \tag{4.5}$$

where S_{DBI} is the Dirac-Born-Infeld (DBI) action and S_{WZ} is the Wess-Zumino (WZ) term. We will describe these two terms below.

Let x^M, $(M = 0, 1, ..., 9)$ denote the space-time coordinates and σ^a, $(a = 1, ..., p)$ denote the coordinates of the D-brane world-volume. In terms of these coordinates the DBI action reads

$$S_{DBI} = -\tau_p \int d^{p+1}\sigma \, e^{-\phi} \sqrt{-\det\big(P[g]_{ab} + P[B]_{ab} + 2\pi\alpha' F_{ab}\big)} \tag{4.6}$$

where $\tau_p = (2\pi)^{-p}\alpha'^{-(p+1)/2}$ is a constant, F_{ab} is the field strength associated to the gauge field A_a that lives inside the Dp-brane and

$$P[g]_{ab} = \frac{\partial x^M}{\partial \sigma^a}\frac{\partial x^N}{\partial \sigma^b}\, g_{MN}, \quad P[B]_{ab} = \frac{\partial x^M}{\partial \sigma^a}\frac{\partial x^N}{\partial \sigma^b}\, B_{MN}. \tag{4.7}$$

denotes the pullback of g_{MN} and B_{MN}, respectively.

To better understand the DBI action let us consider some special cases of it. Consider that $B_{ab} = F_{ab} = 0$, and the dilaton field ϕ is constant $e^{\phi} = g_s$. In this case the DBI action reduces to

$$S_{DBI} = \frac{\tau_p}{g_s} \int d^{p+1}\sigma \sqrt{\det\big(P[g]_{ab}\big)} \tag{4.8}$$

which is proportional to the Dp-brane world-volume. This shows that the DBI action is a generalization of the Nambu-Goto action to objects of higher dimensions. As the action is dimensionless and the Dp-brane world-volume has units of $(\text{length})^{p+1}$ the prefactor τ_p/g_s must have units of $(\text{length})^{-p-1}$, or, equivalently, units of $\text{mass}/(\text{length})^p$. Hence this prefactor has units of mass divided by the spatial volume of the Dp-brane and be viewed as a tension, $T_p = \tau_p/g_s$. Therefore, unlike the fundamental string, which has a tension proportional do α'^{-2}, the Dp-brane tension is proportional to $1/g_s$, what makes it a non-perturbative object.

Le us now investigate another special case of the DBI action in which, as before, the dilaton field is constant $e^{\phi} = g_s$ and $B_{ab} = 0$, but now $g_{MN} = \eta_{MN}$ and $F_{ab} \neq 0$. In this case the DBI action can be expanded in powers of α' and the first non-trivial contribution is

$$-(2\pi\alpha')^2 \frac{\tau_p}{4g_s} \int d^{p+1}\sigma \, F_{ab}F^{ab} \tag{4.9}$$

this shows that the DBI action for a singles Dp-brane is a generalization of the Yang-Mills action with gauge group $U(1)$ and coupling $g_{\rm YM} = (2\pi)^{p-2}\alpha'^{(p-3)/2}g_s$. The Yang-Mills theory lives in the Dp-brane world-volume.

The Wess-Zumino term describe a non-trivial coupling between the NS-NS fields, F_{ab} and the R-R forms,

$$S_{WZ} = T_p \int \sum_p P[C_{p+1}] \wedge e^{P[B]+2\pi\alpha' F} \tag{4.10}$$

where the sum extends over the forms present in the superstring theory in question (for type IIB theory, for instance, we have C_0, C_2 and C_4) and the exponential has to be understood in terms of the wedge product.

4.4.2 D-brane charges

The Dp-brane word-volume Σ_{p+1} is a $(p+1)$-dimensional hypersurface tha naturally couples to the pullback of a $(p+1)$-form

$$S_p = T_p \int_{\Sigma_{p+1}} P[C_{p+1}] \tag{4.11}$$

this can be viewed as a generalization of the coupling of a charged particle world-line Σ_1 to a Maxwell one-form $S_1 = q\int_{\Sigma_1} P[A] = q\int A_\mu \frac{dx^\mu}{d\tau} d\tau$, where q is the charge of

the particle. The action S_1 represents the action of a external electric field provided by A_μ over a charged particle, while S_p represent the action of a external eletric field provided by C_{p+1} over the Dp-brane. This shows that a Dp-brane is charged with respect to a $(p+1)$-form C_{p+1}.

The action S_p is invariant under diffeomorphisms and under Abelian gauge transformations Λ_p of rank p

$$A_{p+1} \to A_{p+1} + d\Lambda_p \tag{4.12}$$

There is a gauge invariant field strength associated to A_{p+1}, defined as $F_{p+2} = dA_{p+1}$, whose flux is conserved when appropriately integrated in the coordinates of the space transverse to the brane world-volume.

The $(p+1)$-orm C_{p+1} has a magnetic dual C_{7-p}^{magn} which is a $(7-p)$-form defined by the relation

$$dC_{7-p}^{\text{magn}} = \star dC_{p+1} \tag{4.13}$$

Therefore, a Dp-brane associated to C_{p+1} has a magnetic dual D$(6-p)$-brane that couples to the gauge field C_{7-p}^{magn}. The type IIB theory has a 0-form, a 2-form and a 4-form. The magnetic dual of the 0-form and of the 2-form are a 8-form and a 6-form, respectively. The 4-form is said to be self-dual because it is equal to its magnetic dual form.

In principle D-branes can decay into lighter objetcs, like closed strings, for example. However, a Dp-brane will be stable if it is charged with respect to eletric or magnetic R-R fields. This is because there isn't any lighter object which is also charged with respect to the R-R fields and then the Dp-brane cannot decay without violating a conservation law. Thus, whether or not a superstring theory have stables Dp-branes depends on the R-R fields present in the theory. Type IIB string theory has

a 0-form, a 2-form, and a 4-form along with their magnetic duals 8-form and 6-form, respectively. These forms allow the stability of the D1-brane, D3-brane, D5-brane, D7-brane and of the D9-brane[6] in type IIB theory.

4.4.3 N coincident Dp-branes

In the last section we saw that open strings ending on a single Dp-brane can be described, at low energy, by a $U(1)$ abelian gauge theory.

Non-abelian gauge theories can be introduced in string theory by considering a stack of N coincident Dp-branes. Indeed, the quantization of open strings stretching between the Dp-branes gives rise to $U(N)$ massless gauge fields that live in the world-volume of the branes. The two indices of non-abelian gauge fields can be visualized as labeling in which Dp-brane the open string is ending. The excitations of the $U(1)$ subgroup of $U(N)$ describe motion of the center of mass of the branes. Because of the overall translation invariance, these excitations decouple from the other excitations (motions of the branes relative to one another) that can be described by the $SU(N)$ subgroup of $U(N)$.

In summary, at the low energy, the massless open strings excitations between the D-branes can be described by a Yang-Mills theory with gauge group $SU(N)$. By considering unoriented strings one can obtain other gauge groups like $SO(N)$ or $USp(N)$ [91].

[6]The D9-brane is usually disregarded because it requires additional conditions [92].

4.4.4 Dp-branes as p-branes

Dp-branes can also be viewed as solutions of the supergravity field equations known as p-branes. A p-brane is a solution that carry a charge with respect to a $(p+1)$-form A_{p+1}. If this $(p+1)$-form is one of the R-R fields of supestring theories this p-brane is called a Dp-brane[7].

A p-brane has a flat $(p+1)$-dimensional hypersurface with invariance under the group of translations $\mathbb{R}^{p+1}$ and under the Lorentz group $SO(p,1)$. One can always loook for a solution of the supergravity field equation with maximal rotational symmetry $SO(9-p)$ in the transverse directions [101]. The group of symmetry of a p-brane is then $\mathbb{R}^{p+1} \times SO(p,1) \times SO(9-p)$.

Because of the the Poincaré symmetry the world-volume metric has to be a rescaling of the Minkowski metric while the metric in the transverse direction has to be a rescaling of the Euclidean metric. An anzats which incorporates the above restrictions and solves the equations of motion is [91]

$$
\begin{aligned}
ds^2 &= H_p(r)^{-1/2}\eta_{ab}dx^a dx^b + H_p(r)^{1/2}dy^I dy^I, && (4.14)\\
e^{\phi} &= g_s H_p(r)^{(3-p)/4}, && (4.15)\\
C_{p+1} &= \big(H_p(r)^{-1} - 1\big)dx^0 \wedge dx^1 \wedge ... \wedge dx^p, && (4.16)\\
B_{MN} &= 0, && (4.17)\\
r^2 &= \sum_{I=p+1}^{9} y^I y^I, && (4.18)
\end{aligned}
$$

where x^a, $(a = 0, 1, ..., p)$ denotes coordinates of the brane world-volume and y^I, $(I = p+1, ..., 9)$ denotes coordinates perpendicular to the brane. The function $H_p(r)$

[7]Other p-branes include the fundamental string F1 and its magnetic dual brane NS5, that couples to the Kalb-Ramond two-form B_2, and to its magnetic dual form, respectively.

has to be an harmonic function

$$\sum_{I=p+1}^{9} \frac{\partial}{\partial y^I} \frac{\partial}{\partial y^I} H_p(r) = 0 \tag{4.19}$$

This is the Laplace equation in the $(9-p)$ transverse directions. A solution of this equation has the form $H_p = A + B\, r^{p-7}$, where A and B are constants. The constant A can be set equal to 1 by requiring the solution to recover the ten dimensional Minkowski spacetime in the limit $r \to \infty$ (far away from the brane). One usually writes the other constante as $B = L_p^{7-p}$, where L_p is another constant with units of length. In terms of L_p the function $H_p(r)$ reads [91]

$$H_p(r) = 1 + \Big(\frac{L_p}{r}\Big)^{7-p}. \tag{4.20}$$

The constant L_p can be determined in terms of the charge of the Dp-brane solution, as we explain below. To calculate the charge of the Dp-brane one must note that the brane appears as pointlike charge in the space transverse to itself. Therefore, the charge Q of the brane can be calculated by integrating the R-R flux through a $(8-p)$-dimensional sphere at the infinity

$$Q = \frac{1}{\kappa_{10}^2} \int_{S^{8-p}} \star F_{p+2}, \quad F_{p+2} = dC_{p+1}. \tag{4.21}$$

For a supergravity solution representing N coincidents Dp-branes we have $Q = N\, T_p$. Calculating Q for the above solution and imposing the result to be equal to N fixes the constant L_p to be [91]

$$L_p^{7-p} = (4\pi)^{(5-p)/2}\, \Gamma\Big(\frac{7-p}{2}\Big)\, g_s\, N\, \alpha'^{(7-p/2)} \tag{4.22}$$

Note that the mass of the N coincident Dp-branes is proportional to their charge Q,

$$M = \mathrm{Vol}(\mathbb{R}^{p,1})\, N\, T_p = \mathrm{Vol}(\mathbb{R}^{p,1})\, Q. \tag{4.23}$$

this represents an *extremal p-brane solution*, because it saturates a BPS bound $M \geq c_p Q$, where c_p is some numerical constant. Because of that these solutions are also refered to as BPS solutions [100].

There are also non-BPS solutions, also known as *near-extremal solutions*, for which the dilaton and the R-R forms are the same as in the extremal case, the charge is also given by $Q = N\, T_p$, but the mass is no longer proportional to Q. These solutions are given by [91]

$$ds^2 = H_p(r)^{-1/2}\big(-f(r)dt^2 + dx^i dx^i\big) + H_p(r)^{1/2}\Big(\frac{dr^2}{f(r)} + r^2 d\Omega^2_{8-p}\Big), \tag{4.24}$$

$$f(r) = 1 - \frac{r_h^{7-p}}{r^{7-p}}. \tag{4.25}$$

where $i = 1, 2, ..., p$ and the transverse coordinates are written as $dy^I dy^I = dr^2 + r^2 d\Omega^2_{8-p}$. These solutions represent *black p-branes*, which are basically black-holes that extend in p spatial directions but are localized (in the sense that they do not extend to infinity). Since $f(r_h) = 0$ the parameter r_h represents the radial position of the black p-brane horizon.

Chapter 5

The AdS/CFT correspondence

In this chapter we present an introduction to the AdS/CFT correspondence[1]. We first give a motivation for the correspondence and discuss some basic checks of it. We then explain how to use holographic techniques to compute correlation functions and transport coefficients of a strongly coupled system.

5.1 Motivating the AdS/CFT correspondence

In this section we motivate the AdS/CFT correspondence studying a system of N D3-branes, with N fixed e large, in type IIB string theory. Let g be the string coupling constant. We start with g such that $gN << 1$[2]. We will take the strongly coupled and low energy limits of this system. Depending on the order in which these limits are taken we obtain different pictures described by different theories, as shown in figure 1. One of this theories is $\mathcal{N} = 4$ super Yang-Mills (SYM) with gauge group

[1] What follows is based on [93–97]

[2] g is related to the expectation value of the dilaton. In this case, because of the conformal symmetry of the SYM theory, we can tune the g for any value we want.

$SU(N)$ in $\mathbb{R}^{3,1}$ e the other is type IIB string theory in $AdS_5 \times S^5$. As theses two theories are obtained from the same basic objects, is natural to conjecture that they are equivalent descriptions of the same system. In what follows we give more details of what happens in these two limits.

5.1.1 First low energy limit and then strongly coupled limit

At the begining $gN << 1$ so that we can ignore the backreaction of the spacetime geometry. In this picture we have closed strings in $\mathbb{R}^{9,1}$ and open strings that begin and end on the D3-branes. The strengh of the interaction of the closed strings with each other and with the open strings is controlled by the dimensionless coupling constant GE^8, where G is the Newton constant and E is the scale of energy in which the interaction takes place. Hence, at low energies, the closed strings are free and the interacting sector is described by the open strings excitations of the branes. If the energy is suficiently small the massive open strings modes will not be excited and only the massless modes will be relevant. The dynamics of these massless modes is described by the $\mathcal{N} = 4$ SYM with gauge group $SU(N)$ in $\mathbb{R}^{3,1}$. Note that, as long as we stay at the low energy limit, the closed string sector is always decoupled from the open string sector, so, if we take the strong coupling limit $gN >> 1$ we will obtain two decoupled sectors: closed strings in $\mathbb{R}^{9,1}$ and the strongly interacting $\mathcal{N} = 4$ theory in $\mathbb{R}^{3,1}$.

5.1.2 First strongly coupled limit and then low energy limit

When we take the strong coupling limit, $gN >> 1$, the presence of the branes will deform the space-time around them. In this case, the D3-branes are described by a

nontrivial solution of the massless field equations of type IIB string theory (supergravity). This solution is given by [98, 99]:

$$ds^2 = H^{-1/2}(-dt^2 + d\vec{x}^2) + H^{1/2}(dr^2 + r^2 d\Omega_5^2) \tag{5.1}$$

where $\vec{x}$ are the coordinates along the D3-branes and the second parenteses is the metric of the directions transverse to the D3-branes. $H(r)$ is given by

$$H = 1 + \frac{L^4}{r^4} \tag{5.2}$$

where

$$L^4 = 4\pi g N \ell_s^4 \tag{5.3}$$

For $r >> L$ the metric reduces to that of a flat space-time, $\mathbb{R}^{9,1}$. In the strong gravity region, $r << L$, we have

$$ds^2 = ds^2_{AdS_5} + L^2 d\Omega_5^2 \tag{5.4}$$

where

$$ds^2_{AdS_5} = \frac{r^2}{L^2}(-dt^2 + d\vec{x}^2) + \frac{L^2}{r^2} dr^2 \tag{5.5}$$

So, we see that very close to the D3-branes the 10-dimensional metric factorizes into $AdS_5 \times S^5$. This solution is well represented by a throat geometry, as ilustrated in Fig. 2. In this description there are no open strings and the D3-branes correspond to a space-time geometry where closed strings propagate.

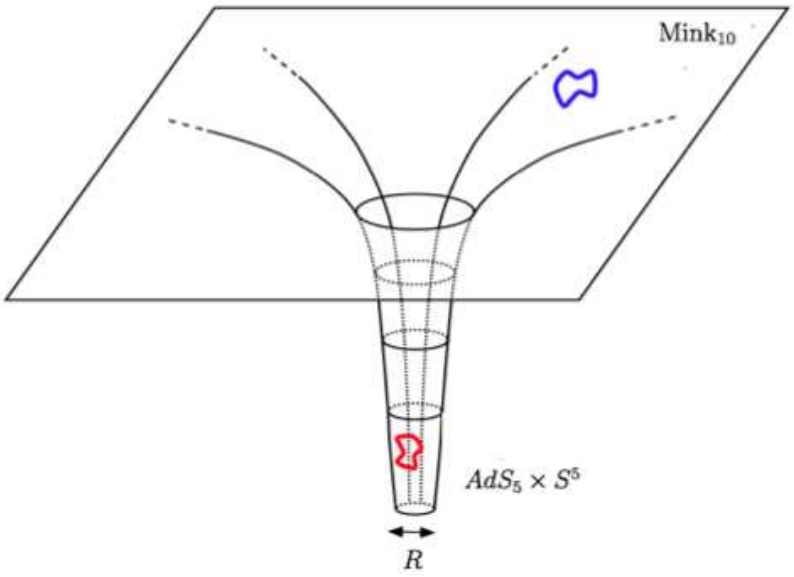

Figure 5.1: Throat geometry generated by a system of N coincident D3-branes. Figure from [93].

Now, let's take the low energy limit of this system from the point of view of a observer far away from the branes, at $r >> L$, where the space is asymptotically flat. To this observer, the low energy excitations are of two types: low energy excitations of the asymptotically flat region and finite energy excitations from the throat part of the geometry. Low energy excitations from the flat region correspond to massless modes of closed strings. These excitations decouple from each other at low energies because their interactions are proportional to GE^8. The finite energy excitations from the throat have to climb a gravitational potential to reach the flat region where they are perceived as low energy excitations. For this reason, the whole tower of massive string excitations are relevant from the point of view of the observer in the flat region. Finally, it can be shown that these two types of excitations decoupled at small energies [96, 100]. In conclusion, we have two decoupled system: free closed

strings in the asymptotically flat region and closed strings in $AdS_5 \times S^5$.

5.1.3 The AdS/CFT conjecture

As we have seen in the last two subsections, a system of N D3-branes have two completely different descriptions at the low energy and strongly coupled limits, depending on the order in which these limits are taken. In both descriptions we have free closed strings in flat space-time. The interacting parts are $\mathcal{N} = 4$ SYM theory in $\mathbb{R}^{3,1}$, with gauge group $SU(N)$, in one of these descriptions, and type IIB string theory in $AdS_5 \times S^5$ in the other description. It is then natural to conjecture that these two pictures describe the same physics which implies that the two theories are equivalent.

As the gravity theory is defined in ten dimensions and the gauge theory (the $\mathcal{N} = 4$ theory) is defined in four dimensions, it is necessary to clarify the role of the six extra dimensions. The string theory lives in $AdS_5 \times S^5$. In general, we consider situations where we do a compactification on S^5 in such a way that we deal with a 5 dimensional gravity theory. Nevertheless, the gravity theory still have one dimension more than the gauge theory, this extra dimension corresponds to the AdS radial coordinate r.

For each constant value of the AdS radial coordinate the corresponding subspace is conformally flat. Therefore, one can say that we have a 4-dimensional Minkowski spacetime for each constant value of r. The boundary of AdS, in particular, is also a 4-dimensional Minkowski spacetime. It is possible to show that the AdS radial coordinate is related to the renormalization group (RG) scale of the $\mathcal{N} = 4$ theory. This fact provides a geometrical visualization of the RG flow, since one can picture different 4-dimensional effective theories, each one corresponding to a given value of r. Using this geometrization of the RG flow together with the holographic principle,

which asserts that a theory of quantum gravity in a region of space should be described by a non-gravitational theory living on the boundary of that region, the $\mathcal{N} = 4$ theory can be thought as living on the boundary of AdS. Because of that, the gravitational theory (string theory), which is defined in the interior of AdS, is also called bulk theory, and the $\mathcal{N} = 4$ theory is also called boundary theory. In what follows we also refer to the $\mathcal{N} = 4$ theory as the gauge theory.

5.2 Parameters of the correspondence

To analyse the situations where the duality is useful it is important to study the relations between the parameters in both theories (the gauge theory and the gravity theory). The relevant parameters in the $\mathcal{N}$ =4 theory are coupling constant $g_{\rm YM}$ and the constant N. For type IIB string theory in $AdS_5 \times S^5$ the relevant parameters are the string coupling g and radius L of S^5. In order to deal only with dimensionless parameters we will express L in units of the string length ℓ_s.

As we said before, the $\mathcal{N} = 4$ theory appears in the low energy limit of a system of N D3-branes. The precise relation between the parameter $g_{\rm YM}$ and g is

$$g^2_{\rm YM} = 4\pi g \tag{5.6}$$

the relation between the other parameters is given by the black-brane solution for the system of D3-branes in the limit $gN >> 1$. According to Eq. (5.3) we have

$$L^4 = 4\pi g N \ell_s^4 = g^2_{\rm YM} N \ell_s^4 \tag{5.7}$$

in terms of the 't Hooft coupling we have

$$\frac{L^4}{\ell_s^4} = \lambda \tag{5.8}$$

$$g = \frac{\lambda}{4\pi N} \tag{5.9}$$

It is also interesting to express this relation in terms of the 10-dimensional Newton constant $G_{(10)}$. In string theory this constant can be written in terms of the string length ℓ_s and the string coupling g by the relation[3]

$$16\pi G_{(10)} = (2\pi)^7 g^2 \ell_s^2 \tag{5.10}$$

Using the relations above it is easy to show that

$$G_{(10)} = \frac{\pi^4 L^8}{2N^2} \tag{5.11}$$

As $G_{(10)} = \ell_p^8$, where ℓ_p is the Planck length, we can write

$$\left(\frac{\ell_p}{L}\right)^8 = \frac{\pi^4}{2N^2} \tag{5.12}$$

The equations (5.8) and (5.12) will be relevant for us because the ratio ℓ_s/L tell us whether stringy correction are important and, in the same way, the ratio ℓ_p/L tell us wheter quantum corrections are important.

Let us now discuss some limits of these parameters that are relevant in applications involving the AdS/CFT correspondence. If $\ell_p/L << 1$ the system can be treated

[3]It is also very common to use the symbol κ_{10}, which is related to $G_{(10)}$ by the equation $\kappa_{10}^2 = 8\pi G_{(10)}$.

classically, which means that we can ignore the quantum fluctuations of the spacetime. From the relations above we can see that this happens in the large N limit. Therefore, gravitational quantum corrections can be incorporated in a power series of ℓ_p^8/L^8, which corresponds to corrections in a power series of $1/N^2$ in the $\mathcal{N} = 4$ theory.

Stringy corretions, which are related to the difference between point particles and strings, are controlled by the dimensionless parameter ℓ_s/L. The limit $\ell_s/L << 1$ means that, for the system under consideration, the strings can be treated as point particles. In this case, the massive modes, with masses of the order $m_s = \ell_s^{-2}$, require to much energy to be excited and only the massless modes will be relevant. For the particular case of type of type IIB string theory, this limit leads to type IIB supergravity theory. As the scale of curvature of the system is given by $1/L^2$, corrections in a power series of ℓ_s^2/L^2 corresponds to addition of higher curvatures terms in the lagrangian of the effective low-energy gravity theory. As we can see from the relations above, this corresponds to corrections in a power series of $1/\sqrt{\lambda}$ in the gauge theory.

Note that, if we take both limits, that is $\ell_p/L << 1$ and $\ell_s/L << 1$, the theory obtained is classical type IIB supergravity. On the other side of the duality we get the $\mathcal{N}$ =4 with gauge group $SU(N)$ at strong coupling and in the large N limit. This limit is relevant because we can investigate non-perturbative aspects of the $\mathcal{N} = 4$ theory using a classical gravity theory in a perturbative regime[4].

[4]The classical gravity theory is weakly coupled because taking the large N limit with the 't Hoot coupling fixed requires a small g

5.3 Matching symmetries and spectrum

Both sides of the duality share the same group of global symmetry. The $\mathcal{N} = 4$ SYM theory have: the conformal symmetry, with group $SO(2,4)$; the R-symmetry, with group $SU(4) \sim SO(6)$; Poincare supersymmetries, generated by 16 supercharges, and superconformal symmetries, generated by 16 supercharges. The total number of supercharges is 32, as discussed in 3.3.1. All these symmetries can be join together forming the supergroup $SU(2,2|4)$.

The symmetries of type IIB string theory in $AdS_5 \times S^5$ are: the isometry of AdS_5, with group $SO(2,4)$, the isometry of S^5, with group $SO(6)$, and the supersymmetry transformations generated by 32 supercharges. Again, the supergroup which join all these symmetries is $SU(2,2|4)$.[5]

The spectrum of both theories can be organized in terms of representations of the superconformal group $SU(2,2|4)$. From the point of view of the $\mathcal{N} = 4$ SYM theory, the spectrum can be organized in terms of superconformal primary operators and theirs descendants, as discussed in 3.3.2. A generic operator $O(x)$ in this representation is characterized by a scaling dimension, Δ, by a Lorentz structure, and by R-symmetry quantum numbers.

In the supergravity side, after compactification in S^5, each SUGRA field gives rise to a tower of KK modes with a given mass that depends on the Lorentz structure and on the $SO(6)$ quantum numbers of the fields. The resulting spectrum can be organized in terms of the mass, Lorentz structure and $SO(6)$ quantum numbers of this fields.

As will see in the following, the AdS/CFT correspondence predictcs a one-to-

[5]Both theories have also the so-called S duality, with gauge group $SL(2,\mathbb{Z})$.

one correspondence between fields of the gravity theory and operators of the gauge theory. The field and the operator must have the same quantum numbers and there is a relation between the scaling dimension Δ of the operator and the mass m of the bulk field. For the case of a scalar bulk field, for instance, the relation is $\Delta(\Delta-4) = m^2L^2$.

Thus, if the correspondence is true, given a gauge theory operator $O(x)$ with scaling dimension Δ, there must be a corresponding field in the gravity theory, with the same quantum numbers, and with a mass equal to the one predicted by the AdS/CFT, which is determined by Δ.

However, this matching between fields and operators is not easy to verify, because the scaling dimension of generic operators of the gauge theory receives quantum corrections. As the AdS/CFT duality is useful when the gauge theory is strongle coupled, this quantum corrections are difficult to calculate. A way to circumvent this difficult is to work with chiral primary operators (discussed in Section 3.3.2), whose scaling dimensions are protected against quantum corrections. From the point of view of the gravity theory, one must look for the corresponding short representations. It turns out that the supergravity KK modes in AdS_5 are in such short representations and, by consequence, they are dual to chiral primary operators.

In fact, a perfect matching between chiral primary operators and all the KK modes of type IIB supergravity was verified [101]. As an example of how this maching is done, consider an operator of the form

$$O(x) = \mathrm{Tr}\left[F_{\mu\nu}F^{\mu\nu}\right] \tag{5.13}$$

as $O(x)$ is a Lorentz scalar, has $\Delta = 4$ and a singlet under the $SO(6)$ symmetry, there must be a dual field with the same quantum numbers and with mass $m^2L^2 =$

$4(4-4) = 0$. The dual field is the zero mode of the dilaton, $\phi_{n=0}$, with mass $m_{n=0} = 0$[6], which is also a Lorentz scalar and a singlet under $SO(6)$. Consider now an operator of the form

$$O^{i_1 \ldots i_n} = \mathrm{Tr}\left[F_{\mu\nu} F^{\mu\nu} A^{(i_1} \ldots A^{i_n)}\right] \tag{5.14}$$

where $A^{(i_1 \ldots i_n)}$ is the traceless symmetric product of the scalar fields A'_ms. This operator has scaling dimension $\Delta = 4 + n$, and transforms as a product of **6**'s under $SO(6)$. The corresponding bulk field must have mass given by $m^2 L^2 = n(n+4)$. In fact, the associated bulk field is ϕ_n, which also transforms as a traceless symmetric product of **6**'s under $SO(6)$ and have mass $m^2 L^2 = n(n+4)$ (as given by (5.21)).

5.4 Bulk fields in AdS_5

In this section we describe some general properties of the fields of type IIB supergravity in $AdS_5 \times S^5$. Let x be a coordinate on AdS_5 and y a coordinate on S^5. A generic bilk field $\phi(x, y)$ can be expanded in terms of spherical harmonics in S^5

$$\phi(x, y) = \sum_{n=0}^{\infty} \phi_n(x) Y^n(y) \tag{5.15}$$

where $Y^n(y) \sim y^{(I_1} y^{I_2} \ldots y^{I_n)}$ are spherical harmonics in S^5. They satisfy the equation

$$\nabla^2_{S^5} Y^n(y) = -\frac{n(n+4)}{L^2} Y^n(y) \tag{5.16}$$

[6] ϕ_n and m_n will be defined in Section 5.4

The type IIB SUGRA action, after the dimensional reduction on S^5, has the following form

$$S_5 = \frac{1}{16\pi G_{(5)}} \int d^5x \Big[\sqrt{-g}\Big(R + \frac{12}{L^2}\Big) + \mathcal{L}_{\text{matter}}\Big] \tag{5.17}$$

where R is the 5-dimensional scalar of curvature and $\mathcal{L}_{\text{matter}}$ is the lagrangian for the matter fields, which includes the infinite tower $\phi_n(x)$ of components of the SUGRA fields coming from the expansion on S^5. The 5-dimensional Newton constant $G_{(5)}$ can be obtained from the 10-dimensional Newton constant by the equation $G_{(5)} = G_{(10)}/(L^5\Omega_5)$, where Ω_5 is the volume of the unity S^5. Using that $G_{(10)} = \pi^4 L^8/(2N^2)$ one can show that

$$G_{(5)} = \frac{\pi}{2N^2} L^3 \tag{5.18}$$

If we set all the matter fields to zero, the maximally-symmetric solution of the equations of motion derived from the action (5.17) is given by

$$ds^2_{AdS} = \frac{L^2}{z^2}\big(-dt^2 + d\vec{x}^2 + dz^2\big) \tag{5.19}$$

which is the AdS_5 metric of Eq. (5.5) with $z = L^2/r$. In these coordinates the boundary is located at $z = 0$.

The fields ϕ_n, viewed as living in AdS_5, aquire a mass equal to the eigenvalue of the laplacian on S^5.

Consider, for example, a scalar field $\varphi(x, y)$ in $AdS_5 \times S^5$. The equation of motion for this field is

$$\nabla^2 \varphi(x, y) = 0 \tag{5.20}$$

Decomposing the ten-dimensional laplacian as $\nabla^2 = \nabla^2_{AdS_5} + \nabla^2_{S^5}$, and expanding

the scalar field in terms of spherical harmonics, $\varphi(x,y) = \sum_k \varphi_n(x) Y^n(y)$, we have

$$(\nabla^2_{AdS_5} + m_n^2) \sum_n \varphi_n(x) = 0, \quad m_n^2 = n(n+4)/L^2. \tag{5.21}$$

Note that ϕ_n transforms as traceless symmetric products of **6**'s under the $SO(6)$ symmetry group.

5.5 Correlation functions

5.5.1 Euclidian correlation functions

In this section we explain how to obtain the gauge theory correlators from gravity in the Euclidean formulation of the AdS/CFT correspondence. The Euclidean version of the AdS_5 metric is

$$ds^2_{AdS} = \frac{L^2}{z^2}\left(d\tau^2 + d\vec{x}^2 + dz^2\right) \tag{5.22}$$

where $x = (\tau, \vec{x})$ denote coordinates of the gauge theory, and z is the AdS radial coordinate. In these coordinates, the boundary of AdS_5 is located at $z = 0$.

According to [2, 3], there is a one-to-one correspondence between bulk fields $\Phi(x,z)$ and operators $O(x)$ of the gauge theory. The boundary value of the bulk field (properly renormalized) act as a source $J(x)$ for the operator $O(x)$. The field and the operator identified under this map must have the same quantum numbers under the global symmetries of the theory. The mass m of the bulk fields is related to the scaling dimension Δ of the gauge theory operators. This relation depends on the Lorentz

structure of Φ and O, as shown in the equation below

$$\begin{aligned} \text{scalars} \qquad & m^2 = \Delta(\Delta - 4) \\ \text{spin } 1/2,\ 3/2 \qquad & |m| = \Delta - 2 \\ p - \text{form} \qquad & m^2 = (\Delta - p)(\Delta + p - 4) \\ \text{spin } 2 \qquad & m^2 = \Delta(\Delta - 4) \end{aligned} \tag{5.23}$$

where the scaling dimension Δ corresponds to the largest root of the above equations.

Given this map, known as the field/operator correspondence, the AdS/CFT correspondence can be state as

$$\left\langle e^{\int d^4x J(x) O(x)} \right\rangle_{\text{CFT}} = Z_{\text{string}}\big[\phi_{\text{bdry}}(x) = J(x)\big] \tag{5.24}$$

where the left-hand side is the generating functional for the correlators of $O(x)$ calculated in the SYM theory and the right-hand side is the partition function of type IIB string theory with the condition that $\phi_{\text{bdry}}(x) = J(x)$ at the boundary of AdS_5. In the above equation, $\phi_{\text{bdry}}(x)$ is not the boundary value of the bulk field $\Phi(x, z)$, because this quantity generaly diverges at $z = 0$. In fact, the the near-boundary behaviour of this field is of the form

$$\Phi(x, z) \approx f(z)\, \phi_{\text{bdry}}(x), \tag{5.25}$$

where $f(z)$ is a function that diverges at the boundary $z = 0$ when $m \neq 0$. Therefore, $\phi_{\text{bdry}}(x)$ can be defined as

$$\phi_{\text{bdry}}(x) = \lim_{z \to 0} \frac{\Phi(x, z)}{f(z)} \tag{5.26}$$

The right-hand side of Eq. (5.24) can be simplified in the large-N and large-λ limit, in which type IIB string theory can be effectively described by type IIB SUGRA. In this limit we can write

$$Z_{\text{string}}[\phi] = e^{-S_{\text{SUGRA}}[\phi_{\text{class}}]} \tag{5.27}$$

where $S_{\text{SUGRA}}[\phi_{\text{class}}]$ is the classical supergravity action evaluated on a classical solution ϕ_{class}. Here, ϕ denotes a collection of bulk fields of type IIB string theory and ϕ_{class} denotes a collection of bulk fields satisfying the classical equations of motion of type IIB SUGRA.

Using the Eq. (5.27), the connected correlators of the SYM theory can be calculated as

$$\left\langle \prod_n O(x_n) \right\rangle = \prod_n \frac{\delta}{\delta J(x_n)} S_{\text{SUGRA}}\big[\phi_{\text{bdry}} = J\big]_{J=0} \tag{5.28}$$

where $\phi_{\text{bdry}}(x)$ satisfies the classical equations of motion and is regular everywhere in AdS_5.

One- and Two-point functions

Now we exemplify how the calculation of one- and two-point functions using the AdS/CFT prescription. We will consider a gravity theory in AdS_{d+1} space. Let φ be a bulk field with the following effective action

$$S = \iint_{AdS} dz\, d^d x\, \mathcal{L}[\varphi, \partial\varphi] \tag{5.29}$$

where z is the AdS radial coordinate and $\mathcal{L}[\varphi, \partial\varphi]$ is the lagrangian density for the field φ. We will use as system of coordinates in which the AdS boundary is located

at $z = 0$. To avoid complications, we will introduce a IR cuttof and put the boundary at $z = \epsilon$. In the end of the calculations we set $\epsilon \to 0$.

According to (5.28), if φ is the source of the operator $O(x)$, the one point function of this operator in the presence of the source φ is given by

$$\langle O(x) \rangle_\varphi = \frac{\delta S_{\text{on-shell}}}{\delta \varphi} \tag{5.30}$$

We now explain how to calculate the the action on-shell, $S_{\text{on-shell}}$, and its functional derivative $\frac{\delta S_{\text{on-shell}}}{\delta \varphi}$.

Under a general transformation $\varphi \to \varphi + \delta\varphi$, tha action changes as

$$\delta S = \iint_{AdS} dz\, d^d x \left[\frac{\partial \mathcal{L}}{\partial \varphi} \delta\varphi + \frac{\partial \mathcal{L}}{\partial(\partial_\mu \varphi)} \delta(\partial_\mu \varphi) \right] \tag{5.31}$$

using integration by parts and the equations of motion, it is easy to show that the variation of the action on-shell is

$$\delta S_{\text{on-shell}} = \iint_{AdS} dz\, d^d x\, \partial_\mu \Big(\frac{\partial \mathcal{L}}{\partial(\partial_\mu \varphi)} \Big) = - \int_{\partial AdS} d^d x\, \frac{\partial \mathcal{L}}{\partial(\partial_z \varphi)}\, \delta\varphi \Big|_{z=\epsilon} \tag{5.32}$$

where we required that $[\partial \mathcal{L} / \partial(\partial_z \varphi)]\, \delta\varphi$ vanishes at $z \to \infty$.

In analogy we classical mechanics, we define the canonical momentum conjugated to φ as

$$\Pi \equiv - \frac{\partial \mathcal{L}}{\partial(\partial_z \varphi)} \tag{5.33}$$

where z plays the role of time. With this notation, the variation of the action on-shell can be written as

$$\delta S_{\text{on-shell}} = \iint_{AdS} dz\, d^d x\, \Pi(x, \epsilon)\, \delta\varphi(x, \epsilon) \tag{5.34}$$

Then, we find the on-shell action

$$S_{\mathrm{on-shell}} = \iint_{AdS} dz\, d^d x\, \Pi(x,\epsilon)\, \varphi(x,\epsilon) \tag{5.35}$$

and its functional derivative

$$\frac{\delta S_{\mathrm{on-shell}}}{\delta \varphi(x,\epsilon)} = \Pi(x,\epsilon) = -\frac{\partial \mathcal{L}}{\partial(\partial_z \varphi)} \tag{5.36}$$

As we are dealing with an effective action, the on-shell action generally diverges and needs to be renormalized. This is done with the addition of a conter term S_{ct} defined at the boundary of AdS. The renormalized action is defined as

$$S_{\mathrm{ren}} = S_{\mathrm{on-shell}} + S_{\mathrm{ct}} \tag{5.37}$$

and the associated functional derivative is

$$\frac{\delta S_{\mathrm{ren}}}{\delta \varphi(x,\epsilon)} \equiv \Pi_{\mathrm{ren}}(x,\epsilon) = \Pi(x,\epsilon) + \frac{\delta S_{\mathrm{ct}}}{\delta \varphi(x,\epsilon)} \tag{5.38}$$

where we defined the renormalized conjugated momentum $\Pi_{\mathrm{ren}}(x,\epsilon)$ as the functional derivative of the renormalized S_{ren} action with respect to the boundary field $\varphi(x,\epsilon)$.

Finally, the renormalized one-point function of $O(x)$ in the presence of a source φ is given by

$$\langle O(x) \rangle_{\varphi} = \lim_{\epsilon \to 0} \Pi_{\mathrm{ren}}(x,\epsilon) \tag{5.39}$$

Once obtained the one-point function, one can use linear response theory to determine the two-point function. From the point of view of the gauge theory, the one-point

function is calculated as

$$\langle O(x)\rangle_{\varphi} = \int [\mathcal{D}A]\, O(x) e^{S_E[A] + \int d^d y\, \varphi(y)\, O(y)} \tag{5.40}$$

where A denote a collection of fields of the gauge theory ad S_E is the Euclidean gauge theory action. Expanding the exponent in a power series of φ, we have

$$\langle O(x)\rangle_{\varphi} = \langle O(x)\rangle_{\varphi=0} + \int d^d y\, \langle O(x)O(y)\rangle\, \varphi(y) + ... \tag{5.41}$$

wihtout loss of generality, we can put $\langle O(x)\rangle_{\varphi=0} = 0$ in such a way that $\langle O(x)\rangle_{\varphi}$ measures the fluctuations of $O(x)$ away from its vacuum expectation value. Thus, at linear order in φ, we have

$$\langle O(x)\rangle_{\varphi} = \int d^d y\, G_E(x-y)\varphi(y) \tag{5.42}$$

where $G_E(x-y)$ is the Euclidean two-point function, defined as

$$G_E(x-y) = \langle O(x)O(y)\rangle \tag{5.43}$$

Using the Fourier representations

$$\begin{aligned} \varphi(y) &= \int \frac{d^d k}{(2\pi)^d} \varphi(k) e^{ik\cdot y}, \\ G_E(x-y) &= \int \frac{d^d q}{(2\pi)^d} G_E(q) e^{iq\cdot(x-y)}, \\ \langle O(x)\rangle_{\varphi} &= \int \frac{d^d k}{(2\pi)^d} \langle O(k)\rangle_{\varphi} e^{ik\cdot x}, \end{aligned} \tag{5.44}$$

one can check that

$$\langle O(k)\rangle_{\varphi} = G_E(k)\,\varphi(k) \tag{5.45}$$

We then find that, in momentum space, the two-point function is given by the simple formula

$$G_E(k) = \frac{\langle O(k)\rangle_{\varphi}}{\varphi(k)} \tag{5.46}$$

Performing the inverse Fourier transformation, we finally obtain

$$\langle O(x)O(y)\rangle = \int \frac{d^d k}{(2\pi)^d} \frac{\langle O(k)\rangle_{\varphi}}{\varphi(k)} e^{ik\cdot(x-y)}. \tag{5.47}$$

Exemple: a scalar field in Euclidean AdS

Now we discuss the particular case of a massive scalar field ϕ in Euclidean AdS_{d+1}. The metric in this case is

$$ds^2 = \frac{L^2}{z^2}(dz^2 + \delta_{\mu\nu}dx^\mu dx^\nu) \tag{5.48}$$

Let us consider that the scalar field have an effective action of the form

$$S = -\frac{1}{2}\int d^d x\sqrt{g}\Big[g^{MN}\partial_M\phi\partial_N\phi + m^2\phi^2\Big] \tag{5.49}$$

The equation of motion for this field is

$$\frac{1}{\sqrt{g}}\partial_M\Big(\sqrt{g}g^{MN}\partial_N\phi\Big) + m^2\phi^2 = 0 \tag{5.50}$$

Using the Fourier representation

$$\phi(x,z) = \int \frac{d^d x}{(2\pi)^d}\, \phi_k(z)\, e^{ik\cdot x} \tag{5.51}$$

the equation of motion can be written as

$$z^{d+1}\partial_z(z^{1-d}\partial_z\phi_k) - z^2k^2\phi_k - m^2L^2\phi_k = 0 \tag{5.52}$$

where $k^2 = \omega_E^2 + \vec{k}^2$ is the Euclidean momentum. Near of the boundary, at $z \approx 0$, it is easy to see that ϕ_k has the following behaviour

$$\phi_k = A(k)z^{d-\Delta} + B(k)z^{\Delta} \tag{5.53}$$

where

$$\Delta = \frac{d}{2} + \sqrt{\frac{d^2}{4} + m^2L^2} \tag{5.54}$$

We present this near-boundary solution in this asymmetric form because the quantity Δ has physical meaning that we will clarify later. For later purposes, let us define the quantity $\nu = \sqrt{\frac{d^2}{4} + m^2L^2} = 2\Delta - d$. Going back to position space, we can write

$$\phi(x,z) = A(x)z^{d-\Delta} + B(x)z^{\Delta} \tag{5.55}$$

Note that, as $d-\Delta = \frac{d}{2} - \sqrt{\frac{d^2}{4} + m^2L^2} < 0 < \Delta$, the dominant term very close to the boundary is $A(x)\, z^{d-\Delta}$, which diverges as $z \to 0$. Thus, the renormalized boundary value of $\phi(x,z)$, which we denote as ϕ_{bdry}, is defined as

$$\phi_{\text{bdry}} = \lim_{z\to\epsilon} z^{\Delta-d}\phi(x,z) = A(x). \tag{5.56}$$

As discussed in section 5.5.1, this quantity acts as a source for the operator $O(x)$.

From the point of view of the boundary theory, the correlation functions of the operator $O(x)$ are obtained by adding to the boundary action a term of the form

$$\int d^d x \sqrt{\gamma}\, \phi(x,\epsilon)\, O(x,\epsilon) \tag{5.57}$$

where $\gamma = (L/\epsilon)^{2d}$ is the determinant of the induced metric on the boundary. Using that $\phi(x,\epsilon) = \epsilon^{d-\Delta}\phi_{\text{bdry}}$, we obtain

$$\int d^d x (L/\epsilon)^d\, \epsilon^{d-\Delta}\phi_{\text{bdry}}\, O(x,\epsilon) \tag{5.58}$$

in order to make this term independent of the cutoff ϵ, we need to absorve the multiplicative factor $\epsilon^{-\Delta}$ into $O(x,\epsilon)$. This can be done considering that $O(x,\epsilon) = O(\epsilon x) = \epsilon^{\Delta} O(x)$, where the last property comes from that fact that the boundary theory is scale invariant. This make evident that Δ corresponds to the scalar dimension of the operator $O(x)$, and also show us that the AdS radial coordinate can be used to make a change of scale in the boundary theory.

Using (5.33), the momentum conjugated to $\phi(x,z)$ is $\Pi(x,z) = \sqrt{g}\, g^{zz}\, \partial_z \phi(x,z)$. The on-shell action is given (5.34) and is equal to

$$S_{\text{on-shell}} = \frac{1}{2}\int d^d x \Big(\sqrt{g}\, g^{zz}\, \phi\, \partial_z \phi\Big)_{z=\epsilon} \tag{5.59}$$

As the on-shell action is calculated at the boundary, one can use the near-boundary expression for $\phi(x,z)$, given by (5.55), to calculate this quantity. The result is the

following

$$S_{\rm on-shell} = \frac{L^{d-1}}{2}\int d^dx\left[(d-\Delta)A^2(x)\epsilon^{-2\nu} + dA(x)B(x) + \Delta B^2(x)\epsilon^{2\nu}\right] \tag{5.60}$$

Note that, as $2\nu > 0$, the first term in the integral is divergent, and the above action needs to be renormalized. This is done with the addition of a boundary term that cancels the divergente term. One could naively guess that this is easily done with the additon of a term of the form

$$-\frac{1}{2}\int d^dx\,(d-\Delta)A^2(x)\epsilon^{-2\nu} \tag{5.61}$$

but this is not the case. In order to maintain the invariance under diffeomorphisms of the theory, the counter-terms need to be expressed in terms of the bulk fields living at the regulated surface $z = \epsilon$. It turns out that the appropriate counter-term for this action is [102]

$$S_{\rm ct} = -\frac{1}{2}\frac{d-\Delta}{L}\int_{\partial AdS} d^dx\,\sqrt{\gamma}\,\phi^2 \tag{5.62}$$

where γ is the determinant of $\gamma_{\mu\nu}$, the metric induced at $z = \epsilon$, which is given by

$$ds^2_{z=\epsilon} = \gamma_{\mu\nu}dx^\mu dx^\nu = \frac{L^2}{\epsilon^2}\delta_{\mu\nu}dx^\mu dx^\nu \tag{5.63}$$

In the calculation of the counter-term above we assume that 2ν is not an integer. If that is the case there will be an extra logaritmic term, as explained in [102]. The renormalized action is then given by

$$S_{\rm ren} = S_{\rm on-shell} + S_{\rm ct} = \frac{L^{d-1}}{2}(2\Delta - d)\int d^dx\,A(x)\,B(x) \tag{5.64}$$

one should be carefull in calculating the functional derivatives of this action with respect to $\phi_{\rm bdry}(x) = A(x)$, because $B(x)$ also depends functionally of $A(x)$. Indeed, we will show below that

$$B(k) = \chi(k)\, A(k) \tag{5.65}$$

In position space, this relation is written as

$$B(x) = \int d^d y\, \chi(x-y)\, A(y) \tag{5.66}$$

Thus, the on-shell action becomes

$$S_{\rm ren} = \frac{L^{d-1}}{2}(2\Delta - d) \int d^d x \int d^d y\, \chi(x-y) A(x) A(y) \tag{5.67}$$

We emphasize that, as $\phi_{\rm bdry}(x) = A(x)$, is this quantity that acts as a source for the dual operator $O(x)$, and the n-point functions are calculated by taking derivatives of the renormalized action with respect to $A(x)$. The one-point function in the presence of the source A, for example, is calculated as

$$\langle O(x) \rangle_A = \frac{\delta S_{\rm ren}}{\delta A(x)} = \frac{L^{d-1}}{2}(2\Delta - d) \int d^d y\, \chi(x-y) A(y) = 2\nu L^{d-1} B(x) \tag{5.68}$$

where we use $2\Delta - d = 2\nu$ in the last equatity. In momentum space, this relation is written as

$$\langle O(k) \rangle_A = 2\nu L^{d-1} B(k) \tag{5.69}$$

from this relation we can easily calculate the two-point function in momentum space as

$$G_E(k) = \frac{\langle O(k) \rangle_A}{A(k)} = 2\nu L^{d-1} \frac{B(k)}{A(k)} \tag{5.70}$$

For this particular case of a scalar field in AdS_{d+1} we can calculate $A(k)$ and $B(k)$ analitically, as we will show below. The equation of motion for $\phi_k(z)$ is

$$z^{d+1}\partial_z(z^{1-d}\partial_z\phi_k) - z^2k^2\phi_k - m^2L^2\phi_k = 0 \tag{5.71}$$

The general solution of this equation is

$$\phi_k(z) = z^{d/2}\big[C_1J_\nu(-ikz) + C_2Y_\nu(-ikz)\big] \tag{5.72}$$

Where C_1 and C_2 are constants. However, to analize the behaviour of $\phi_k(z)$ for large z, is more convenient to work with the Hankel functions

$$\phi_k(z) = z^{d/2}\big[B_1H_\nu^{(1)}(-ikz) + B_2H_\nu^{(2)}(-ikz)\big] \tag{5.73}$$

where B_1 and B_2 are also constants. The asymptotic behavior of the Hankel functions for large argument is

$$H_\nu^{(1,2)}(x) \approx \frac{e^{\pm ix}}{\sqrt{x}} \tag{5.74}$$

This implies that

$$H_\nu^{(1,2)}(-ikz) \approx \frac{e^{\pm kz}}{\sqrt{z}} \tag{5.75}$$

Thus, to require regularity for large z we choose $B_1 = 0$, and the solutions becomes

$$\phi_k(z) = z^{d/2}H_\nu^{(2)}(-ikz) \tag{5.76}$$

Near of the boundary the above solutions has the form

$$\phi_k(z) = \underbrace{-\frac{(-i)^{-\nu}2^{\nu}k^{-\nu}}{i\sin(\nu\pi)\Gamma(1-\nu)}}_{A(k)} z^{d-\Delta} + \underbrace{\frac{e^{i\pi\nu}k^{\nu}2^{-\nu}(-i)^{\nu}}{i\sin(\nu\pi)\Gamma(1+\nu)}}_{B(k)} z^{\Delta} \tag{5.77}$$

from this expression one can see that

$$\frac{B(k)}{A(k)} = -\frac{\Gamma(1-\nu)}{\Gamma(1+\nu)}\Big(\frac{k}{2}\Big)^{2\nu} = \frac{\Gamma(-\nu)}{\Gamma(\nu)}\Big(\frac{k}{2}\Big)^{2\nu} \tag{5.78}$$

With the above result we can calculated the two-point function in momentum space

$$G_E(k) = 2\nu\frac{\Gamma(-\nu)}{\Gamma(\nu)}\Big(\frac{k}{2}\Big)^{2\nu} \tag{5.79}$$

The two-point function in position space is finally given by

$$G_E(x) = \langle O(x)O(0)\rangle = \int \frac{d^dk}{(2\pi)^d}e^{ik\cdot x}G_E(k) = \frac{2\nu L^{d-1}}{\pi^{d/2}}\frac{\Gamma(\frac{d}{2}+\nu)}{\Gamma(-\nu)}\frac{1}{|x|^{2\Delta}} \tag{5.80}$$

where we use the formula

$$\int \frac{d^dk}{(2\pi)^d}e^{ik\cdot x}k^n = \frac{2^n}{\pi^{d/2}}\frac{\Gamma(\frac{d+\nu}{2})}{\Gamma(\frac{n}{2})}\frac{1}{|x|^{2\Delta}} \tag{5.81}$$

The result for the two-point function $\langle O(x)O(0)\rangle \sim |x|^{-2\Delta}$ is expected from the fact that the operator $O(x)$ has scaling dimension Δ.

5.5.2 Real-time correlators

In this section we describe the recipe to calculate real time correlators in AdS/CFT. One could naively guess that we could obtain this correlators by applying the same procedures of the Euclidean case, but this is not the case. In fact, as discussed in [103, 104], the real-time correlators cannot be obtained by an action principle. This happens because, while in the Euclidean case a solution is completely fixed by its value at the boundary and by the condition of regularity at the horizon, in Lorentzian signature these two conditions are not enough, because there is an ambiguity related to the fact that we can have incoming-waves and outgoing-waves at the horizon of the black brane. It turns out that the solution representing incoming-waves is related to the retarded correlator, while the solution representing an outgoing-wave is related to advanced correlators. We will only focus on retarded correlators, because this quantity is important in determination of transport coefficients.

Real-time correlators are usually discussed when we have a black brane in AdS_5. In this case, the metric is

$$ds^2 = \frac{L^2}{z^2}\big(-f dt^2 + d\vec{x}^2\big) + \frac{L^2}{z^2 f} dz^2, \quad f(z) = 1 - \frac{z^4}{z_{\text{H}}^4} \tag{5.82}$$

where the boundary of the space is at $z = 0$ and the black brane horizon is located at $z = z_{\text{H}}$. Note that we can easily recover the pure AdS case by taking the limit $z_{\text{H}} \to \infty$.

Retarded correlators can be obtained by performing an analytic continuation of the Euclidean correlators. However, this is difficult to do when we only have numerical results, what unfortunately corresponds to the most cases.

The way to circunvent this is to perform an analytic continuation of the classical

Euclidean solution $\phi_E(\omega_E, \vec{k})$ and of the associated conjugated momentum $\Pi_E(\omega_E, \vec{k})$ as

$$\begin{aligned} \phi_R(\omega, \vec{k}) &= \phi_E(-i(\omega + i\epsilon), \vec{k}) \\ \Pi_R(\omega, \vec{k}) &= \Pi_E(-i(\omega + i\epsilon), \vec{k}) \end{aligned} \tag{5.83}$$

where $\phi_R(\omega, \vec{k})$ and $\Pi_R(\omega, \vec{k})$ are the corresponding quantities in Lorentzian signature. As before, the one- and two-point functions in momentum space are given by

$$\begin{aligned} \langle O(k) \rangle_A &= 2\nu L^{d-1} B(k), \\ G_R(k) &= 2\nu L^{d-1} \frac{B(k)}{A(k)} \end{aligned} \tag{5.84}$$

where A and B are obtained from the near-boundary expansion of ϕ_R

$$\phi_R(k, z) \approx A(k) z^{d-\Delta} + B(k) z^{\Delta} \tag{5.85}$$

With the above prescription, the $\phi_R(\omega, \vec{k})$ satisfy an in-falling boundary condition at the horizon. Let us verify that for the case of a massive scalar field in a black brane background which is asymptotically AdS_{d+1}

The equation of motion for this field in momentum space and in Euclidean signature is

$$z^{d+1} \partial_z (z^{1-d} f \partial_z \phi_E) - \frac{\omega_E^2 z^2}{f} \phi_E - \vec{k}^2 z^2 \phi_E - m^2 L^2 \phi_E = 0 \tag{5.86}$$

The two independent solutions of this equation in the near-horizon limit are

$$\phi^{(+)} \approx (z - z_{\rm H})^{\omega_E z_{\rm H}/4}, \quad \phi^{(-)} \approx (z - z_{\rm H})^{-\omega_E z_{\rm H}/4} \tag{5.87}$$

For $\omega_E > 0$, the solution that is regular at $z = z_{\rm H}$ is $\phi_E = \phi^{(+)}$. Performing the analytic continuation we find

$$\phi_R(\omega, \vec{k}) = \phi_E(-i(\omega + i\epsilon), \vec{k}) = (z - z_{\rm H})^{-i\omega z_{\rm H}/4}, \tag{5.88}$$

that indeed corresponds to an incoming-wave at the horizon, as we can easily see by writing this near-horizon solution in position space

$$\phi_R(x, z) \approx e^{i(k\cdot x - \omega\rho)}, \quad \text{where} \quad \rho = \frac{z_{\rm H}}{4}\log(z - z_{\rm H}) \tag{5.89}$$

Of course, it is not necessary to first calculate the Euclidean classical solutions and then perform an analytic continuation to obtain the retarded correlators. One can solve directly the equations of motion in Lorentzian signature, impose the incoming-wave boundary condition, find the near-boudary behaviour (5.85) and then apply the prescription (5.84).

Example: a scalar field in Lorentzian AdS

The metric of AdS_{d+1} in Lorentzian signature is

$$ds^2 = \frac{L^2}{z^2}(dz^2 + \eta_{\mu\nu}dx^\mu dx^\nu) \tag{5.90}$$

In Lorentzian signature, the scalar field have an effective action of the form

$$S = \frac{1}{2}\int d^d x\sqrt{-g}\Big[g^{MN}\partial_M\phi\partial_N\phi + m^2\phi^2\Big] \tag{5.91}$$

The equation of motion for this field in momentum space is

$$z^{d+1}\partial_z(z^{1-d}\partial_z\phi_k) - z^2(-\omega^2 + \vec{k}^2)\phi_k - m^2L^2\phi_k = 0 \tag{5.92}$$

This equation have a different solution depending on whether $k = (\omega, \vec{k})$ is space-like on time-like. We will consider the time-like case, since the space-like case provides the same solution (and the same one- and two-point functions) as the Euclidean case. Defining $q = \sqrt{-k^2}$, the general solution of the above equation is

$$\phi_k(z) = C_1 z^{d/2} H_\nu^{(1)}(qz) + C_2 z^{d/2} H_\nu^{(2)}(qz) \tag{5.93}$$

where C_1 and C_2 are arbitray constants. Assuming $\omega > 0$, the solution that represents an incoming-wave at the horizon ($z \to \infty$) is

$$\phi_k(z) = z^{d/2} H_\nu^{(1)}(qz) \approx \frac{e^{iqz}}{\sqrt{qz}} \tag{5.94}$$

The near-boundary behaviour of this solution is

$$\phi_k(z) = \underbrace{-\frac{2^\nu q^{-\nu}}{i\sin(\nu\pi)\Gamma(1-\nu)}}_{A(q)} z^{d-\Delta} + \underbrace{\frac{e^{-i\pi\nu} q^\nu 2^{-\nu}}{i\sin(\nu\pi)\Gamma(1+\nu)}}_{B(q)} z^\Delta \tag{5.95}$$

The ratio B/A becomes

$$\frac{B(q)}{A(q)} = \frac{\Gamma(-\nu)}{\Gamma(\nu)}\Big(\frac{q}{2}\Big)^{2\nu} e^{-i\nu} \tag{5.96}$$

With the above result it is then clear that, as in the Euclidean case, the two-point function is given by $\langle O(x)O(0)\rangle \sim |x|^{-2\Delta}$.

5.6 Generalizations

The AdS/CFT correspondence, as described in this chapter as an equivalence between $\mathcal{N} = 4$ SYM theory and type IIB superstring theory, can be extended in several ways. The most basic type of extensions is the ones whose the bulk theory lives in a space which is not exactly $AdS_5 \times S^5$, but is asymptotically $AdS_5 \times S^5$. The most important case is the one in which we have a black-brane in the interior of AdS_5. In this case, the metric is given by

$$ds^2_{\text{BB}} = \frac{r^2}{L^2}\big(- f dt^2 + d\vec{x}^2\big) + \frac{L^2}{r^2 f} dr^2 + L^2 d\Omega_5^2 \tag{5.97}$$

where

$$f(r) = 1 - \frac{r_0^4}{r^4} \tag{5.98}$$

The constant r_0 represents the coordinate of the black brane horizon. We can associate a Hawking temperature T_{H} to this solution. This temperature is given by

$$T_{\text{H}} = \frac{r_0}{\pi L^2} \tag{5.99}$$

Note that, for $r \to \infty$, the above solution is asymptotically $AdS_5 \times S^5$. From the point of view of th boundary theory we still have the $\mathcal{N} = 4$ theory, but in a non-zero temperature $T = T_{\text{H}}$.

Another class of generalizations consists in considering bulk theories that lives in spaces which are asymptotically $AdS_5 \times \mathcal{M}$, where $\mathcal{M}$ is a compact manifold. In this generalizations we can have less symmetries (and supersymmetries), what allows us to consider more realistic situations. Finally, it is also possible to consider dualities

that holds for different dimensions, like d-dimensional CFTs dual to gravity theories in AdS_{d+1} [74].

5.7 Thermodynamic properties

In the non-zero temperature generalization of the duality we can can calculate the thermodynamic properties of our system. From the point of view of the boundary theory, our system is a strongly coupled plasma. This plasma can be used as a toy model to study the QGP formed in heavy ion collisions. Besides the temperature of the plasma, which is easily obtained as the Hawking temperature of the black hole of the boundary theory, the thermodynamic quantity that is very easy to calculate is the entropy, which is given by the Bekenstein-Hawking formula

$$S = \frac{A_{\rm H}}{4G_{(5)}} \tag{5.100}$$

where $A_{\rm H}$ is the horizon area, which is given by

$$A_{\rm H} = \int d^3x \sqrt{g^3_{xx}}\Big|_{z=z_{\rm H}} = \frac{L^3}{z^3_{\rm H}} V_3 \tag{5.101}$$

where $g_{xx} = L^2/z^2$ and V_3 is the volume of the space of the boundary theory. From the above formulas one obtains the entropy density as

$$s = \frac{S}{V_3} = \frac{1}{4G_{(5)}} \frac{L^3}{z^3_{\rm H}} \tag{5.102}$$

as $z_{\rm H} = 1/(\pi T)$ and $G_{(5)} = \pi L^3/(2N^2)$, this expressions can be written as

$$s = \frac{\pi^2}{2} N^2 T^3 \tag{5.103}$$

Using standard theormodynamic relations

$$\begin{aligned} s &= \frac{\partial p}{\partial T} \\ \epsilon &= -p + Ts \end{aligned} \tag{5.104}$$

we obtain the pressure p and the energy density ϵ as

$$\begin{aligned} p &= \frac{\pi^2}{8} N^2 T^4 \\ \epsilon &= \frac{3\pi^2}{8} N^2 T^4 \end{aligned} \tag{5.105}$$

The results we obtain for s, p and ϵ at strong coupling are $3/4$ times the corresponding quantities at zero coupling, that can be calculated by standard techniques of statistical physics. This is in qualitative agreement with the results obtained for other gauge theories using lattice techniques [97].

5.8 Transport coefficients

In this section we consider the calculation of transport coefficients using holographic techniques. We assume that the boundary theory lives in a d-dimensional Minkowski spacetime and consider the following deformation of the boundary theory action

$$\int d^d x \, O(x) \, \varphi(x) \tag{5.106}$$

In linear response theory, the one-point function of $O(x)$ in the presence of the source $\varphi(x)$ is given by

$$\langle O(x)\rangle_{\varphi} = -\int d^d y\, G_R(x-y)\,\varphi(y) \tag{5.107}$$

where we assume $\langle O(x)\rangle_{\varphi=0} = 0$ and $G_R(x-y)$ is the retarded Green's function, given by

$$iG_R(x-y) \equiv \theta(x^0-y^0)\,\langle [O(x),O(y)]\rangle \tag{5.108}$$

Causality implies that the linear response theory is determined by the retarded correlator. This happens because the influence of the source in the system will only take place after it is been turn on. In momentum space the above equation is written as

$$\left\langle O(\omega,\vec{k})\right\rangle_{\varphi} = -G_R(\omega,\vec{k})\,\varphi(\omega,\vec{k}) \tag{5.109}$$

The transport coefficients are relevant in the long wavelengh hydrodynamical limit, in which we take the limits $\omega,\vec{k}\to 0$. We will assume a transport coefficient defined by the following relation

$$\langle O\rangle_{\varphi} \approx -\chi\,\partial_t\varphi, \qquad (\omega\to 0) \tag{5.110}$$

Note tha χ basically specifies the response of the system to the presence of a source φ. In the frequency space the above relation is written as

$$\langle O\rangle_{\varphi} \approx i\,\omega\,\chi\,\varphi(\omega), \qquad (\omega\to 0) \tag{5.111}$$

In linear response theory the same relation is written as

$$\langle O \rangle_{\varphi} = -G_R(\omega, \vec{k} = 0)\, \varphi(\omega), \qquad (\omega \to 0) \tag{5.112}$$

Comparing (5.111) and (5.112) we have

$$G_R(\omega, \vec{k} = 0) = -i\, \omega\, \chi \tag{5.113}$$

The transport coefficient, χ, is then given by the following ordered limit

$$\chi = \lim_{\omega \to 0} \lim_{\vec{k} \to 0} \frac{1}{\omega} \mathrm{Im}\, G_R(\omega, \vec{k}) \tag{5.114}$$

Let us now explain how one can calculate χ using holography. We will assume a $(d+1)$-dimensional metric of the form

$$ds^2 = g_{tt} dt^2 + g_{zz} dz^2 + g_{ij} dx^i dx^j \tag{5.115}$$

where $g_{ij} = \delta_{ij} g_{xx}$ and all the metric component only depends on z. We will assume the presence of a horizon at $z = z_{\mathrm{H}}$, that is

$$g_{tt} \approx -c_0\, (z_{\mathrm{H}} - z), \quad g_{zz} \approx \frac{c_z}{(z_{\mathrm{H}} - z)}, \quad (z \to z_{\mathrm{H}}) \tag{5.116}$$

where c_0 and c_z are positive constants.

Let ϕ be a scalar field with action effective action

$$S = -\frac{1}{2} \int d^{d+1}x\, \sqrt{-g} \frac{1}{q(z)} \partial_M \phi\, \partial^M \phi \tag{5.117}$$

where $\phi(z)$ is some effective coupling for ϕ. We take ϕ as massless because several transport coefficients are obtained by massless modes with effective action like the action above. The equation of motion for ϕ is

$$\partial_M\Big(\frac{\sqrt{-g}}{q(z)}g^{MN}\partial_M\phi\Big)=0 \tag{5.118}$$

The canonical momentum cojugated to ϕ is

$$\Pi\equiv-\frac{\partial\mathcal{L}}{\partial(\partial_z\phi)}=\frac{\sqrt{-g}}{q(z)}g^{zz}\partial_z\phi \tag{5.119}$$

Written in terms of the canonical momentum, the equation of motion is written as

$$\partial_z\Pi=-\frac{\sqrt{-g}}{q(z)}\Big(\frac{\partial_t^2\phi}{g_{tt}}+\frac{\partial_i^2\phi}{g_{xx}}\Big) \tag{5.120}$$

Working in Fourier space

$$\phi(z,t,\vec{x}) = \int\frac{d\omega d^{d-1}\vec{k}}{(2\pi)^d}e^{i(\vec{k}\cdot\vec{x}-\omega t)}\phi(z,\omega,\vec{k}) \tag{5.121}$$

$$\Pi(z,t,\vec{x}) = \int\frac{d\omega d^{d-1}\vec{k}}{(2\pi)^d}e^{i(\vec{k}\cdot\vec{x}-\omega t)}\Pi(z,\omega,\vec{k}) \tag{5.122}$$

the equation of motion can be written as

$$\partial_z\Pi=-\frac{\sqrt{-g}}{q(z)}\Big(\frac{\omega^2}{g_{tt}}+\frac{\vec{k}^2}{g_{xx}}\Big)\phi \tag{5.123}$$

It is then clear that, in the limits where $\omega\to0$ and $\vec{k}\to0$, Π is independent of z.

As ϕ is massless, we have $\Delta = d$, and the retarded correlator is simply given by

$$G_R(\omega, \vec{k}) = \frac{\Pi(z, \omega, \vec{k})}{\phi(z, \omega, \vec{k})}\Big|_{z=0} \tag{5.124}$$

from the retarded correlator one can calculated χ as

$$\chi = \lim_{\omega \to 0} \lim_{\vec{k} \to 0} \frac{\Pi(z, \omega, \vec{k})}{\omega\, \phi(z, \omega, \vec{k})}\Big|_{z=0} \tag{5.125}$$

One can check this quantity does not depend on z. Because of that, it can be calculated for any convenient value of z. In particular, it can be calculated at the horizon, where we know the behaviour of the metric components for a large class of black hole backgrounds.

The near-horizon equation of motion for ϕ is

$$\partial_z\big[(z_{\text{H}} - z)\partial_z\phi\big] + c_z\Big[\frac{\omega^2}{c_0(z_{\text{H}} - z)} - \frac{\vec{k}^2}{g_{xx}(z_{\text{H}})}\Big]\phi = 0 \tag{5.126}$$

Looking for a solution of the form $\phi = (z_{\text{H}} - z)^\beta$ we found two solutions

$$\phi_\pm \approx (z_{\text{H}} - z)^{\pm\sqrt{\frac{c_z}{c_0}}\omega} \tag{5.127}$$

where ϕ_+ represents a outgoing wave and ϕ_- represents an incoming wave at the horizon. Causality implies that we must chose ϕ_- as our solution. The corresponding conjugated momentum is

$$\Pi_- = \frac{1}{c_z}\frac{\sqrt{-g}}{q(z_{\text{H}})}(z_{\text{H}} - z) \underbrace{\partial_z\phi_-}_{\sqrt{c_z/c_0}\, i\,\omega\,\phi_-} \tag{5.128}$$

From this expression one can easily calculate the near-horizon retarded correlator

$$G_R = \frac{\Pi_-}{\phi_-} = \frac{i\,\omega}{q(z_{\rm H})}\sqrt{\frac{g}{c_0 c_z}}\,\Big|_{z=z_{\rm H}} \tag{5.129}$$

The transport coefficient, χ, is finally determined as

$$\chi = \frac{1}{q(z_{\rm h})}\sqrt{\frac{g}{g_{tt}g_{zz}}}\,\Big|_{z=z_{\rm H}} \tag{5.130}$$

where we use the fact that $g_{tt}\,g_{zz} = c_0\,c_z$ at the horizon.

Note that the horizon area is given by

$$A_{\rm H} = \int d^d x \sqrt{g_{xx}^{d-1}} = \sqrt{\frac{g}{g_{tt}g_{zz}}}\,\Big|_{z=z_{\rm H}} \underbrace{\int d^d x}_{V_{d-1}} \tag{5.131}$$

Thus, we can write

$$\frac{A_{\rm H}}{V_{d-1}} = \sqrt{\frac{g}{g_{tt}g_{zz}}}\,\Big|_{z=z_{\rm H}} \tag{5.132}$$

where V_{d-1} is the volume of the space of the boundary theory. Written in terms of this geometrical quantities, the transport coefficient reads

$$\chi = \frac{1}{q(z_{\rm H})}\frac{A_{\rm H}}{V_{d-1}} \tag{5.133}$$

The boundary theory entropy density is also proportional to $A_{\rm H}/V_{d-1}$

$$s = \frac{A_{\rm H}}{4G_N V_{d-1}} \tag{5.134}$$

where G_N is the d-dimensional Newton constant. Therefore, the ratio χ/s is simply

given by

$$\frac{\chi}{s} = \frac{4G_N}{q(z_{\rm H})} \tag{5.135}$$

The above formula also holds for more general actions provided that the equation of motion remains trivial in the zero frequency and zero momentum limit.

Chapter 6

Thermal probes of an anisotropic plasma

In this chapter[1] we study the production of thermal photons and dileptons in a strongly coupling anisotropic background. In particular, we study how the anisotropy and the quark mass affects these observables.

This quantity is particularly interesting since it furnishes valuable data about the conditions of the in-medium location of production of the photons. This is because, given the limited spatial extend of the plasma and the weakness of the electromagnetic interaction, photons produced in the plasma escape from it virtually unperturbed. Some of the holographic studies of this quantity include [105–117].[2] Here we extend the analysis started in [27] in two different directions.

First, we consider non-equatorial embeddings of the flavor D7-branes introduced in [27], corresponding to quarks with non-vanishing masses, thus making our analysis

[1] In parts of this chapter we reproduce the text of arXiv:1311.5513v3 [hep-th], which is one of the papers published in this work.

[2] At weak coupling, this has been studied in the presence of anisotropy in, for example, [148].

closer to the real-world system. We allow for arbitrary values of the anisotropy parameter a/T and for arbitrary angles between the photon wave vectors and the anisotropic direction, or beam direction. We also study the DC conductivity as a function of the quark mass. We find that, in general, an anisotropic plasma glows brighter than its isotropic counterpart at the same temperature. This holds for all values of the quark masses and for all angles between the anisotropic direction and the photon wave vector. This same computation for a specific value of the anisotropy and for wave vectors either parallel or perpendicular to the anisotropic direction has already been performed in [28], where a strong, external magnetic field was also included.

As a second extension of [27], we study thermal production, via virtual photon decay, of lepton/antilepton pairs (*dileptons*) in the same background. This quantity is also of phenomenological interest and is obtained by considering time-like momenta for the emitted particles, which can be massive. Compared to the photon production calculation, there is now an extra parameter, namely the magnitude of the spatial momentum. We find that the dilepton production rate is generically larger than the corresponding rate of an isotropic plasma at the same temperature, except for a small range of anisotropies, if the quark mass and the frequency are sufficiently large. These quantities are generically monotonically dependent (either increasing or decreasing) on the angle between the momentum and the anisotropic direction.

This chapter is organized as follows. In Sec. 6.1 we review how to compute the production rate of photons and dileptons in an anisotropic plasma first in the gauge theory side and then via holography using the anisotropic background of [10, 11]. In Sec. 8.1 we present our results for the spectral densities, conductivities, and total production rates for photons in a plasma with massive quarks. In Sec. 6.3 we do the

same for dileptons, which is essentially the extension of the previous computation to the case in which the emitted particles have a time-like momentum, rather than a light-like one. We discuss our results in Sec. 8.4. We relegate to two appendices some technical details of the computation.

6.1 Photon and dilepton production in an anisotropic plasma

Here we briefly recall the basic setup of [27]. The gauge theory we shall consider is obtained via an isotropy-breaking deformation of four-dimensional $\mathcal{N} = 4$ super Yang-Mills (SYM) with gauge group $SU(N_c)$, at large N_c and large 't Hooft coupling $\lambda = g^2_{\rm YM} N_c$. The deformation consists in including in the action a theta-term which depends linearly on one of the spatial directions, say z, [12]

$$S_{SU(N_c)} = S_{\mathcal{N}=4} + \frac{1}{8\pi^2} \int \theta(z)\, {\rm Tr} F \wedge F \,, \qquad \theta(z) \propto z \,, \tag{6.1}$$

where the proportionality constant in $\theta(z)$ has dimensions of energy and will be related to the parameter a that we shall introduce in the next subsection. The rotational $SO(3)$ symmetry in the space directions is broken by the new term down to $SO(2)$ in the xy-plane. For this reason we shall call the z-direction the longitudinal (or anisotropic) direction, while x and y will be the transverse directions. This theory has matter fields in the adjoint representation of the gauge group. We can also introduce N_f flavors of scalars Φ^a and fermions Ψ^a in the fundamental representation, with the index $a = 1, \ldots, N_f$. With an abuse of language, we will refer to these fundamental fields indistinctly as 'quarks'.

To study photon production we turn on a dynamical photon by including a $U(1)$ kinetic term in the action (6.1) and a coupling to the fields that we want to be charged under this Abelian symmetry. In order to realize a situation as similar to QCD as possible, we require that only the fundamental fields be charged, while the adjoint fields are to remain neutral. We do not know the gravitational dual of the full $SU(N_c) \times U(1)$ theory, but fortunately this will not be necessary for our purposes. It was in fact shown in [105] that to compute the two-point correlation function of the electromagnetic current to leading order in the electromagnetic coupling $\alpha_{\rm EM}$, it is enough to consider the $SU(N_c)$ theory only, whose dual is known from [10, 11]. Our computation will then be to leading order in $\alpha_{\rm EM}$, since the coupling of the photons to the surrounding medium is small, but fully non-perturbative in the 't Hooft coupling λ of the $SU(N_c)$ theory.

In general, photon production in differential form is given by the expression [105, 107, 119]

$$\frac{d\Gamma_\gamma}{d\vec{k}} = \frac{e^2}{(2\pi)^3 2|\vec{k}|}\Phi(k)\eta^{\mu\nu}\,\chi_{\mu\nu}(k)\Big|_{k^0=|\vec{k}|}\,, \tag{6.2}$$

with $\eta^{\mu\nu}$ the Minkowski metric (our convention is $(-+++)$), $k^\mu = (k^0, \vec{k})$ the photon null momentum and $\Phi(k)$ the distribution function, which for thermal equilibrium, as in our case, reduces to the Bose-Einstein distribution $n_B(k^0) = 1/(e^{k^0/T} - 1)$. The spectral density is $\chi_{\mu\nu}(k) = -2\ \mathrm{Im}\ G^{\rm R}_{\mu\nu}(k)$, with

$$G^{\rm R}_{\mu\nu}(k) = -i\int d^4x\, e^{-ik\cdot x}\,\Theta(t)\big\langle[J^{\rm EM}_\mu(x), J^{\rm EM}_\nu(0)]\big\rangle \tag{6.3}$$

the retarded correlator of two electro-magnetic currents $J^{\rm EM}_\mu$.

If the theory also includes fermions bearing electric charge e_ℓ, these can be produced in particle/antiparticle pairs (called *dileptons* in the following) via virtual photon decay processes. The spectral density above can then be used to compute the dilepton production rate by means of the expression [119]

$$\frac{d\Gamma_{\ell\bar{\ell}}}{dk} = \frac{e^2 {e_\ell}^2}{(2\pi)^4 6\pi |k|^5} \Phi(k)\, \Theta(k_0) \Theta(-k^2 - 4{m_\ell}^2)(-k^2 - 4{m_\ell}^2)^{1/2}(-k^2 + 2{m_\ell}^2)\eta^{\mu\nu}\, \chi_{\mu\nu}(k)\,, \tag{6.4}$$

where m_ℓ is the mass of the lepton/antilepton and the spectral function is now evaluated on the time-like four-momentum k^μ of the virtual photon.

A consequence of the Ward identity $k^\mu \chi_{\mu\nu} = 0$ for null k^μ is that, for the photon production rate, only the transverse spectral functions contribute. A simple way to extract this contribution is by not taking the whole trace as in (8.65), but by summing over the projections into the polarization vectors for the photon that are mutually orthogonal and orthogonal to $\vec{k}$:

$$\frac{d\Gamma_\gamma}{d\vec{k}} = \frac{e^2}{(2\pi)^3 2|\vec{k}|} \Phi(k) \sum_{s=1,2} \epsilon^\mu_{(s)}(\vec{k})\, \epsilon^\nu_{(s)}(\vec{k})\, \chi_{\mu\nu}(k)\Big|_{k^0=|\vec{k}|}\,. \tag{6.5}$$

Each term of the sum stands for the number of photons emitted with polarization vector $\vec{\epsilon}_{(s)}$.

Given the $SO(2)$ symmetry in the xy-plane, we can choose without loss of generality $\vec{k}$ to lie in the xz-plane, forming an angle ϑ with the z-direction – see Fig. 8.8. Specifically, we set

$$\vec{k} = q(\sin\vartheta, 0, \cos\vartheta)\,. \tag{6.6}$$

In the photon production computation it will be $q = k_0$, while in the dilepton pro-

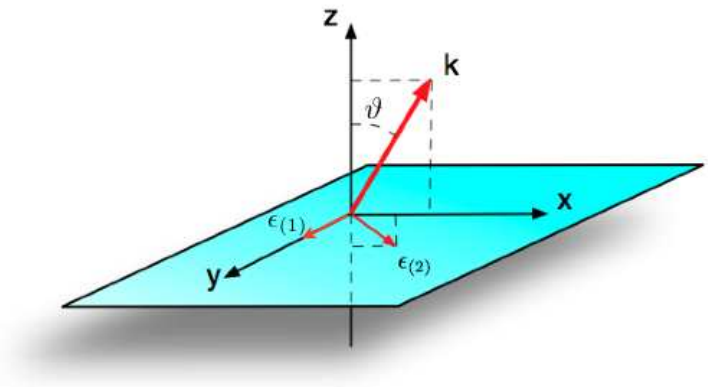

Figure 6.1: Momentum and polarization vectors. Because of the rotational symmetry in the xy-plane, the momentum can be chosen to be contained in the xz-plane, forming an angle ϑ with the z-direction. $\vec{\epsilon}_{(1)}$ is oriented along the y-direction and $\vec{\epsilon}_{(2)}$ is contained in the xz-plane, orthogonally to $\vec{k}$.

duction computation q will be an independent parameter. This means that we can choose the polarization vectors as

$$\vec{\epsilon}_{(1)} = (0, 1, 0)\,, \qquad \vec{\epsilon}_{(2)} = (\cos\vartheta, 0, -\sin\vartheta)\,. \tag{6.7}$$

Production of photons with polarization $\vec{\epsilon}_{(1)}$ is then proportional to $\chi_{yy} \sim \mathrm{Im}\,\langle J_y^{\mathrm{EM}} J_y^{\mathrm{EM}}\rangle$, whereas for those with polarization $\vec{\epsilon}_{(2)}$ it is proportional to[3]

$$\epsilon^{\mu}_{(2)}\,\epsilon^{\nu}_{(2)}\,\chi_{\mu\nu} = \cos^2\vartheta\,\chi_{xx} + \sin^2\vartheta\,\chi_{zz} - 2\cos\vartheta\sin\vartheta\,\chi_{xz}\,. \tag{6.8}$$

For the dilepton production, on the other hand, we will just compute the trace of the spectral density, as it appears in (6.4). We see then that we need to compute the different correlators $\chi_{\mu\nu}$ of the current for both null and time-like momenta, and plug them in the production densities described above. In the following section we will see

[3]Note that $\chi_{xz} = \chi_{zx}$; see e.g. [105].

how these correlators can be obtained from gravity.

6.1.1 Gravity set-up

The dual gravitational background for the theory (6.1) at finite temperature is the type IIB supergravity geometry found in [10, 11], whose string frame metric reads

$$ds^2 = \frac{L^2}{u^2}\left(-\mathcal{B}\mathcal{F}\,dt^2 + dx^2 + dy^2 + \mathcal{H}dz^2 + \frac{du^2}{\mathcal{F}}\right) + L^2\, e^{\frac{1}{2}\phi} d\Omega_5^2\,, \tag{6.9}$$

with $\mathcal{H} = e^{-\phi}$ and Ω_5 the volume form of a round 5-sphere. The gauge theory coordinates are (t, x, y, z) while u is the AdS radial coordinate, with the black hole horizon lying at $u = u_{\rm H}$ (where $\mathcal{F}$ vanishes) and the boundary at $u = 0$. As mentioned already, we refer to the z-direction as the longitudinal direction and to x and y as the transverse directions. L is set to unity in the following. Besides the metric and the dilaton ϕ, the forms

$$F_5 = 4\,(\Omega_5 + \star\Omega_5)\ , \qquad F_1 = a\,dz \tag{6.10}$$

are also turned on, with a being a parameter with units of energy that controls the degree of anisotropy of the system. The potential for the 1-form is a linear axion, $\chi = a\,z$. This acts as an isotropy-breaking external source that forces the system into an anisotropic equilibrium state.

The functions $\mathcal{B}, \mathcal{F}$, and ϕ depend solely on u. They are known analytically in limiting regimes of low and high temperature, and numerically in intermediate regimes [11]. For $u \to 0$ (independently of the value of a) they asymptote to the $AdS_5 \times S^5$ metric, $\mathcal{F} = \mathcal{B} = \mathcal{H} = 1$ and $\phi = 0$, while for $a = 0$ they reduce to the black D3-brane

solution

$$\mathcal{B} = \mathcal{H} = 1\,, \qquad \phi = \chi = 0\,, \qquad \mathcal{F} = 1 - \frac{u^4}{u_{\rm H}^4}\,, \tag{6.11}$$

which has temperature and entropy density given by [120]

$$T_{\rm iso} = \frac{1}{\pi u_{\rm H}}\,, \qquad s_{\rm iso} = \frac{\pi^2}{2} N_{\rm c}^2 T^3\,. \tag{6.12}$$

The temperature and entropy density of the anisotropic geometry are given by [11]

$$T = \frac{e^{-\frac{1}{2}\phi_{\rm H}}\sqrt{\mathcal{B}_{\rm H}}(16 + a^2 u_{\rm H}^2 e^{\frac{7}{2}\phi_{\rm H}})}{16\pi u_{\rm H}}\,, \qquad s = \frac{N_{\rm c}^2}{2\pi u_{\rm H}^3} e^{-\frac{5}{4}\phi_{\rm H}}\,, \tag{6.13}$$

where $\phi_{\rm H} \equiv \phi(u = u_{\rm H})$ and $\mathcal{B}_{\rm H} \equiv \mathcal{B}(u = u_{\rm H})$. As depicted in Fig. 6.2, the entropy density of the system interpolates smoothly between the isotropic scaling above for small a/T and the scaling [11, 12]

$$s \simeq 3.21\, N_{\rm c}^2 T^3 \left(\frac{a}{T}\right)^{\frac{1}{3}}\,, \tag{6.14}$$

for large a/T, the transition between the two behaviors taking place at approximately $a/T \simeq 3.7$. The space can then be interpreted as a domain-wall-like solution interpolating between an AdS geometry in the UV and a Lifshitz-like geometry in the IR, with the radial position at which the transition takes place being set by the anisotropic scale a: when $T \gg a$ the horizon lies in the asymptotic AdS region with scaling (6.12), whereas for $T \ll a$ it lies in the anisotropic region with scaling (6.14).

It might be useful to compare the anisotropy introduced in this setup with the anisotropy of other holographic models, or even weak coupling computations. To do

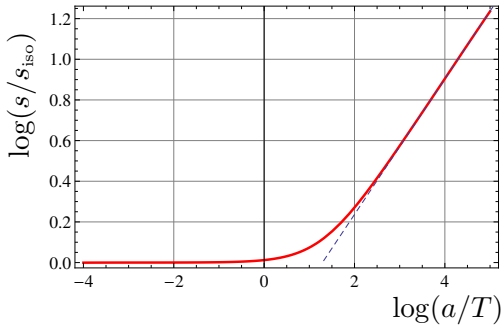

Figure 6.2: Log-log plot of the entropy density as a function of a/T. The dashed blue line is a straight line with slope 1/3.

this one could consider the following ratio [22]

$$\alpha = \frac{4E + P_\perp - P_\text{L}}{3Ts}\,, \tag{6.15}$$

where E is the energy density and $P_\perp$, P_L are the transverse and longitudinal pressures, respectively. These quantities are presented in great detail in [11]. For the isotropic $\mathcal{N} = 4$ super Yang-Mills plasma $\alpha = 1$, whereas for $0 < a/T \lesssim 20$ the ratio is well approximated by the expression

$$\alpha \simeq 1 - 0.0036 \left(\frac{a}{T}\right)^2 - 0.000072 \left(\frac{a}{T}\right)^4\,, \tag{6.16}$$

as shown in Fig. 6.3.

A feature of the anisotropic geometry of [10, 11] is the presence of a conformal anomaly that appears during the renormalization of the theory, introducing a reference scale μ. This anomaly implies that some physical quantities (such as, for example, the energy density and pressures) do not depend only on the ratio a/T, but on two independent dimensionless ratios that can be built out of a, T, and μ.

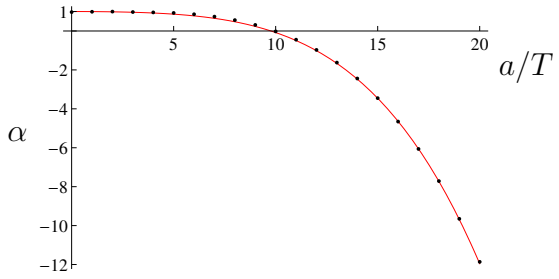

Figure 6.3: Ratio (6.15) as a function of a/T. The blue dots are the actual values of the ratio, and the red curve is the fit (6.16).

Fortunately, as we shall see in the following, all the quantities computed in this paper are not affected by this anomaly and will be independent of μ.[4]

The introduction of $N_{\rm f}$ flavors of quarks is achieved by placing $N_{\rm f}$ probe D7-branes in the background (6.9). To keep the system in a deconfined phase we will work with 'black-hole embeddings' [121] for the D7 branes. The complete system can then be thought of as a D3/D7 system with two different kinds of D7-branes, one kind sourcing the anisotropy [11, 12][5] and the other kind sourcing flavor [122, 123]; see [27]. As argued in [105], at leading order in $\alpha_{\rm EM}$ it suffices to evaluate the correlators needed for (8.65) and (6.4) in the $SU(N_{\rm c})$ gauge theory with no dynamical photons. At strong 't Hooft coupling and large $N_{\rm c}$, these correlators can be calculated holographically, as we explain now.

Let A_m $(m = 0, \ldots, 7)$ be the gauge field associated to the overall $U(1) \subset U(N_{\rm f})$ gauge symmetry on the D7-branes. Upon dimensional reduction on the 3-sphere wrapped by the flavor D7-branes, A_m gives rise to a massless gauge field (A_μ, A_u),

[4]The same happens for the quantity α introduced in (6.15), which does not depend on a and T separately, but only on the combination a/T.

[5]These $N_{\rm D7}$ branes are smeared homogeneously along the z-direction and can be thought of as giving rise to a density $n_{\rm D7} = N_{\rm D7}/L_z$ of extended charges, with L_z being the (infinite) length of the z-direction. This charge density is related to the anisotropy parameter a through $a = g^2_{\rm YM} n_{\rm D7}/4\pi$ [11].

three massless scalars, and a tower of massive Kaluza-Klein (KK) modes. All these fields propagate on the five non-compact dimensions of the D7-branes. We will work in the gauge $A_u = 0$,[6] and we will consistently set the scalars and the higher KK modes to zero, since these are not of interest here. According to the prescription of [2, 3], correlation functions of $J^{\rm EM}_\mu$ can be calculated by varying the string partition function with respect to the value of A_μ at the boundary of the spacetime (6.9).

We now proceed to write down the action for the D7-branes. It is easy to realize that there is no Wess-Zumino coupling of the branes to the background F_5, because of the particular brane orientation that has been chosen, nor a coupling to the background axion, which would be quartic in the $U(1)$ field strength $F = dA$ [27]. This means that the Dirac-Born-Infeld (DBI) action is all we need to consider:

$$S \;=\; -N_{\rm f}\, T_{\rm D7} \int_{\rm D7} d^8\sigma\, e^{-\phi} \sqrt{-\det\left(g + 2\pi\ell_s^2 F\right)}\,, \tag{6.17}$$

where g is the induced metric on the D7-branes and $T_{\rm D7} = 1/(2\pi\ell_s)^7 g_s \ell_s$ is the D7-brane tension. To obtain the equations of motion for A_μ, it suffices to expand the action above and use the quadratic part only:

$$S = -N_{\rm f} T_{\rm D7} \int_{\rm D7} d^8\sigma\, e^{-\phi} \sqrt{-\det g}\, \frac{(2\pi\ell_s^2)^2}{4} F^2\,, \tag{6.18}$$

where $F^2 = F_{mn}F^{mn}$. The embedding of the branes inside the S^5 of the geometry can be parametrized by the polar angle ξ of the S^5 with $\cos\xi \equiv \psi(u)$. The induced

[6] This gauge choice will be immaterial in the following, since we shall switch to gauge invariant quantities, but it has the advantage of simplifying our formulas.

metric on the branes is then given by

$$\begin{aligned} ds^2_{\rm D7} &= \frac{1}{u^2}\left(-\mathcal{F}\mathcal{B}\,dt^2+dx^2+dy^2+\mathcal{H}\,dz^2\right)+\frac{1-\psi^2+u^2\mathcal{F}e^{\frac{1}{2}\phi}\psi'^2}{u^2\mathcal{F}(1-\psi^2)}du^2 \\ &\quad +e^{\frac{1}{2}\phi}(1-\psi^2)d\Omega_3^2\,. \end{aligned} \tag{6.19}$$

After the dimensional reduction on the three-sphere, the action reduces to

$$S=-K_{\rm D7}\int dt\,d^3\vec{x}du\,M\,F^{mn}F_{mn} \tag{6.20}$$

where

$$\begin{aligned} M &= \frac{e^{-\frac{3}{4}\phi}\sqrt{\mathcal{B}}}{u^5}\left(1-\psi^2\right)\sqrt{1-\psi^2+u^2\mathcal{F}e^{\frac{\phi}{2}}\psi'^2}, \\ K_{\rm D7} &= 2\pi^4 N_{\rm f}T_{\rm D7}\ell_s^4=\frac{1}{16\pi^2}N_{\rm c}N_{\rm f}\,, \end{aligned} \tag{6.21}$$

and F_m is restricted to the components $m=(\mu,u)$.

As argued in [107, 121], in order to calculate the photon emission rate, we may consistently proceed by finding the embedding of the D7-branes that extremizes (6.17) in the absence of the gauge field, and then solving for the gauge field perturbations propagating on that embedding considered as a fixed background. By checking that the gauge field obtained in this way does not grow beyond the perturbation limit, we can ensure that no modes of the metric or of the background fields will be excited when following this procedure. We set to zero the components of the gauge field on the three-sphere wrapped by the D7-branes and Fourier decompose the remaining as

$$A_\mu(t,\vec{x},u)=\int\frac{dk^0d\vec{k}}{(2\pi)^4}\,e^{-ik^0t+i\vec{k}\cdot\vec{x}}\,A_\mu(k^0,\vec{k},u)\,,\qquad \vec{k}=(k_x,0,k_z)=q(\sin\vartheta,0,\cos\vartheta)\,. \tag{6.22}$$

This is possible because the state we consider, although anisotropic, is translationally invariant along the gauge theory directions [11]. As mentioned above, in the photon production computation it will be $q = k_0$, while in the dilepton production computation q will be an independent parameter.

Doing so, the equations for the gauge field deriving from (6.20) split into the following decoupled equation for A_y (primes denote derivatives with respect to u)

$$\left(Mg^{uu}g^{yy}A_y'\right)' - Mg^{yy}\left(g^{tt}k_0^2 + g^{xx}k_x^2 + g^{zz}k_z^2\right)A_y = 0\,, \tag{6.23}$$

together with a coupled system of three equations for the remaining components $A_{t,x,z}$:

$$(Mg^{uu}g^{tt}A_t')' - Mg^{tt}\left[g^{xx}k_x(k_xA_t - k_0A_x) + g^{zz}k_z(k_zA_t - k_0A_z)\right] = 0\,, \tag{6.24}$$

$$(Mg^{uu}g^{xx}A_x')' - Mg^{xx}\left[g^{tt}k_0(k_0A_x - k_xA_t) + g^{zz}k_z(k_zA_x - k_xA_z)\right] = 0\,, \tag{6.25}$$

$$(Mg^{uu}g^{zz}A_z')' - Mg^{zz}\left[g^{tt}k_0(k_0A_z - k_zA_t) + g^{xx}k_x(k_xA_z - k_zA_x)\right] = 0\,. \tag{6.26}$$

The inverse metric can be read off directly from (6.19). Equations (6.23)-(6.26) constitute the set of equations that we shall solve in the next sections, with the appropriate boundary conditions, to obtain the correlation functions of the electromagnetic currents $J_\mu^{\rm EM}$.

6.1.2 Quark masses

Given that both M and g^{uu} depend on ψ, we need to know this embedding function of the D7-branes to solve (6.23)-(6.26). The action (6.20) for the D7-branes in the

absence of the gauge field, takes the form

$$S_\psi = -K_{\rm D7}\int dt\, d\vec{x}\, du\, M_0\left(1-\psi^2\right)\sqrt{1-\psi^2+u^2\mathcal{F}e^{\frac{\phi}{2}}\psi'^2}, \tag{6.27}$$

where

$$M_0 = \frac{e^{-\frac{3}{4}\phi}\sqrt{\mathcal{B}}}{u^5}\,. \tag{6.28}$$

By varying S_ψ with respect to $\psi(u)$ one obtains the equation for the D7-branes embedding

$$\left(\frac{M_0\left(1-\psi^2\right)u^2\mathcal{F}e^{\frac{\phi}{2}}\psi'}{\sqrt{1-\psi^2+u^2\mathcal{F}e^{\frac{\phi}{2}}\psi'^2}}\right)' + M_0\frac{3\psi\left(1-\psi^2\right)+2u^2\mathcal{F}e^{\frac{\phi}{2}}\psi\psi'^2}{\sqrt{1-\psi^2+u^2\mathcal{F}e^{\frac{\phi}{2}}\psi'^2}} = 0\,. \tag{6.29}$$

This equation can be solved near the boundary $u=0$ using the near-boundary expansions of the metric [11]

$$\begin{aligned}
\mathcal{F} &= 1+\frac{11}{24}a^2u^2+\mathcal{F}_4u^4+\frac{7}{12}a^4u^4\log u+O\left(u^6\right)\,,\\
\mathcal{B} &= 1-\frac{11}{24}a^2u^2+\mathcal{B}_4u^4-\frac{7}{12}a^4u^4\log u+O\left(u^6\right)\,,\\
\phi &= -\frac{a^2}{2}u^2+\left(\frac{1152\mathcal{B}_4+121a^4}{4032}\right)u^4-\frac{a^4}{6}u^4\log u+O\left(u^6\right)\,,
\end{aligned} \tag{6.30}$$

where $\mathcal{F}_4$ and $\mathcal{B}_4$ are integration constants which are undetermined by the boundary equations of motion, but that can be read off from the numerics [11]. The result for the near-boundary expansion of $\psi(u)$ is

$$\psi = \psi_1 u+\left(\psi_3+\frac{5}{24}a^2\psi_1\log u\right)u^3+O\left(u^5\right)\,, \tag{6.31}$$

where ψ_1 and ψ_3 are related to the quark mass and condensate, respectively. To solve (6.29), we follow [107] and specify the boundary conditions at the horizon as $\psi(u_{\rm H}) = \psi_{\rm H}$ and $\psi'(u_{\rm H}) = 0$. We determine ψ_1 and ψ_3 by fitting the numerical solution near the boundary. The relation between ψ_1 and the quark mass is given by [107]

$$M_{\rm q} = \sqrt{\lambda}\, T\, u_{\rm H} \frac{\psi_1}{\sqrt{2}}\,, \tag{6.32}$$

and the explicit dependence of the dimensionless ratio $M_{\rm q}/\sqrt{\lambda}T$ for given $\psi_{\rm H}$ and a/T is detailed in Fig. 6.4.

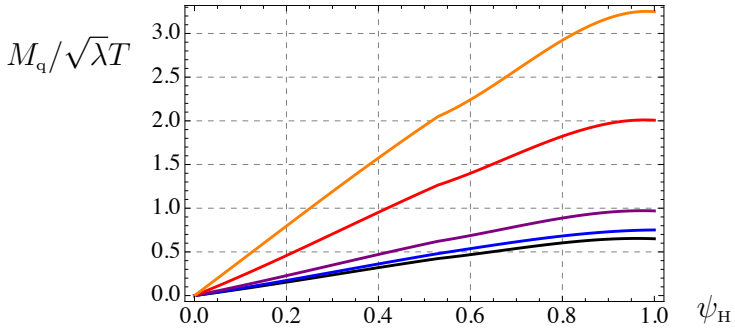

Figure 6.4: The curves correspond, from bottom to top, to $a/T = 0$, 4.41, 12.2, 86, 249.

Note that in the isotropic case the maximum value of $\psi_{\rm H}$ corresponding to a stable embedding of the D7-branes was $\psi_{\rm H} = 0.941$ [121]. In the presence of anisotropy this will presumably change and some of the higher values of $\psi_{\rm H}$ might correspond to metastable or unstable embeddings.[7] To settle this issue one should analyze phase transitions between black-hole and Minkowski embeddings in the presence of anisotropy, which is something that goes beyond the scope of the present paper.

[7] All the values of $\psi_{\rm H}$ we have considered result, however, in numerically stable evaluations.

6.2 Photon production with massive quarks from holography

In this section we extend the massless quark analysis of [27] to non-vanishing quark masses and we refer the reader to that reference for more details. The motivation for this extension is to bring our analysis closer to the real-world system studied in the RHIC and LHC experiments.

To compute the various correlation functions,[8] we start by writing the boundary action as

$$S_\epsilon = -2K_{\rm D7}\int dt\, d\vec{x}\left[Mg^{uu}\left(g^{tt}A_tA_t' + g^{xx}A_xA_x' + g^{yy}A_yA_y' + g^{zz}A_zA_z'\right)\right]_{u=\epsilon}\,, \quad (6.33)$$

where the limit $\epsilon \to 0$ is intended.

6.2.1 Spectral density for the polarization $\epsilon_{(1)}$

As in the massless case, the spectral density $\chi_{yy} \equiv \chi_{(1)}$ is the easiest to compute, since A_y does not couple to any other mode. The calculation is very similar to the one in [27], the only difference being that now the induced metric has a non-trivial brane embedding, $\psi(u) \neq 0$, contained in the new expression for M and g^{uu}.

Before proceeding further, we recall the isotropic result of [107], since ultimately we want to understand whether the presence of an anisotropy increases or decreases the isotropic photon production and conductivity. Unfortunately, it does not seem possible to obtain analytical results for the spectral density when the quark mass is not zero. One then needs to resort to numerics. In order to compare an anisotropic

[8] The original references for this prescription include [103, 124–126].

plasma with the isotropic one, we need that both be at the same temperature. We fix the temperature in the isotropic case by adjusting the position of the black hole horizon, since $T_{\rm iso} = 1/\pi u_{\rm H}$. We then obtain isotropic plots corresponding to the particular temperatures used in the anisotropic geometry. More specifically, we are using $T = 0.33$, 0.36, 0.48, 0.58 which are the temperatures for the geometries with $a/T = 4.41$, 12.2, 86, and 249, respectively, that we consider below. The results for $T = 0.33$ are plotted in Fig. 6.5, for the various masses of interest.

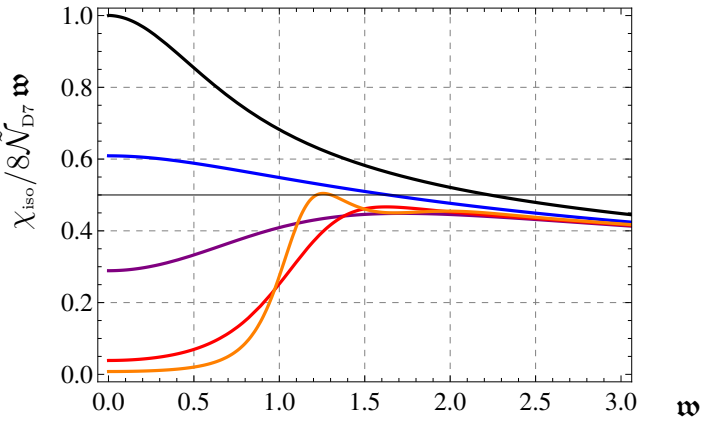

Figure 6.5: The isotropic correlator $\chi_{\rm iso}$ for $T = 0.33$ and, from top to bottom on the left side of the plot, $\psi_{\rm H}$ =0 (black), 0.53 (blue), 0.75 (purple), 0.941(red), 0.98 (orange). Here $\tilde{\mathcal{N}}_{\rm D7} = 4K_{\rm D7}/u_{\rm H}^2$ and $\mathfrak{w} = k_0/2\pi T$ is the dimensionless frequency. This color code will be respected throughout this section.

In principle we could also compare the anisotropic plasma with an isotropic plasma at the same entropy density but different temperature. We have checked that the quantities studied in this paper do not depend strongly on whether the comparison is made at the same temperature or at the same entropy density, unlike what happened for other observables, as the ones studied in [15, 19, 22]. For this reason we do not include here plots with curves normalized with an isotropic plasma with the same entropy density.

The correlation function is given by

$$G^{\rm R}_{yy} = -\frac{4K_{\rm D7}}{|A_y(k_0,0)|^2}\lim_{u\to 0} Q(u)\, A_y^*(k_0,u)\, A_y'(k_0,u)\,, \tag{6.34}$$

where

$$Q(u) \equiv M g^{uu} g^{yy}. \tag{6.35}$$

The spectral density then reads

$$\chi_{(1)} = \frac{N_{\rm c}N_{\rm f}}{2\pi^2\,|A_y(k_0,0)|^2}{\rm Im}\lim_{u\to 0} Q(u)\, A_y^*(k_0,u)\, A_y'(k_0,u)\ , \tag{6.36}$$

and is plotted in Fig. 6.6. The curves are normalized with the results for an isotropic plasma at the same temperature.

The zero-frequency limit of the spectral density gives the electric DC conductivity. For photons with polarization $\epsilon_{(1)}$ this would be the conductivity along the transverse y-direction. The quantity

$$\sigma_{(1)}(T) = \lim_{k_0\to 0}\frac{\chi_{(1)}}{\chi_{(1),{\rm iso}}(T)} = \lim_{k_0\to 0} 2\frac{\chi_{(1)}}{\chi_{\rm iso}(T)} \tag{6.37}$$

is mass independent, and therefore given by Fig. 8 of [27]. In Fig. 6.7 we plot the conductivity

$$\tilde{\sigma}_{(1)} = 2\lim_{\mathfrak{w}\to 0}\frac{\chi_{(1)}}{8\tilde{\mathcal{N}}_{\rm D7}\mathfrak{w}} \tag{6.38}$$

not normalized with the isotropic result, for the various values of the quark mass. Here $\tilde{\mathcal{N}}_{\rm D7} = N_{\rm c}N_{\rm f}T^2/4$ and $\mathfrak{w} = k_0/2\pi T$. We observe that the conductivity decreases as the quark mass increases.

It is worth pointing out that, as it will be discussed in Appendix 6.A, the imaginary

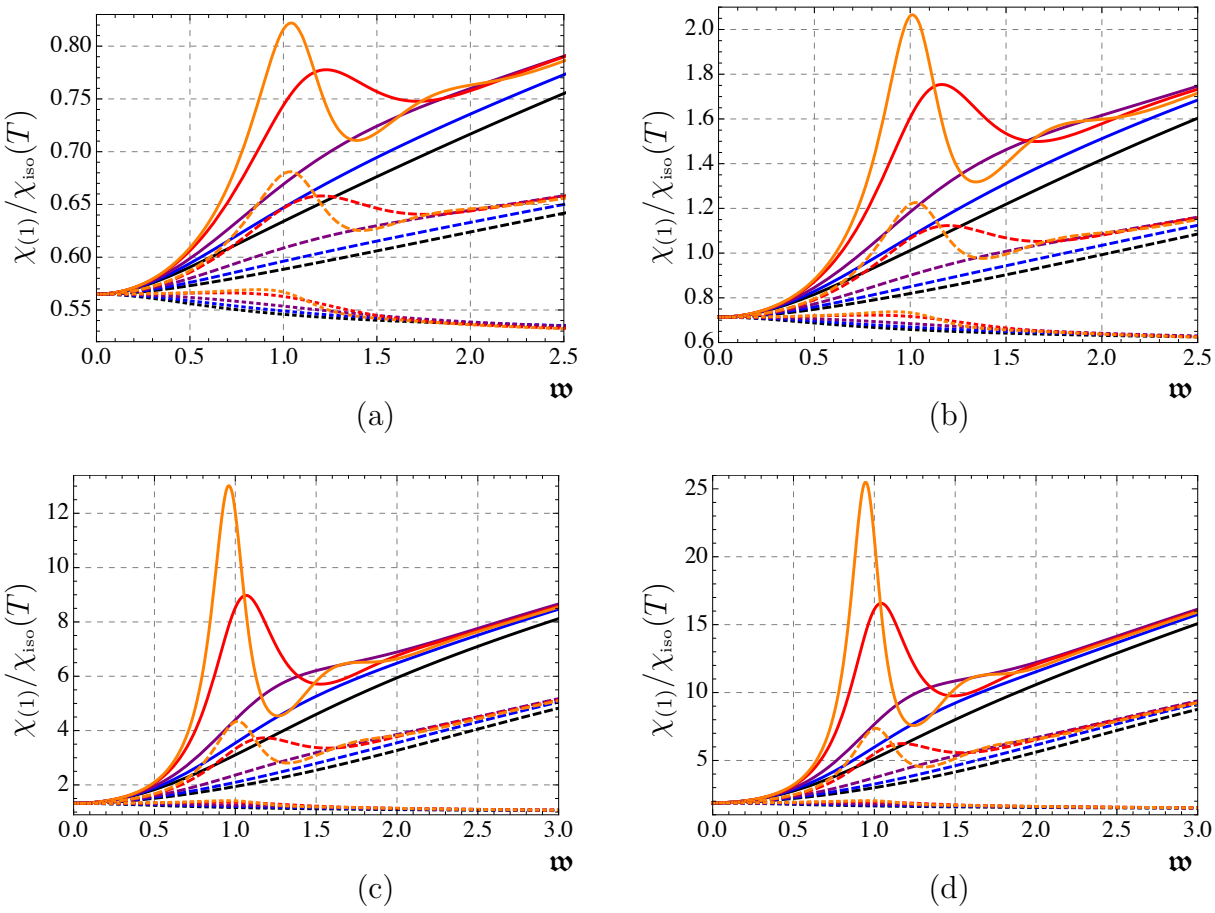

Figure 6.6: Plots of the spectral density $\chi_{(1)}$ corresponding to the polarization $\epsilon_{(1)}$, normalized with respect to the isotropic result at fixed temperature $\chi_{\rm iso}(T)$. The curves correspond from top to bottom to the angles $\vartheta = 0$ (solid), $\pi/4$ (dashed), $\pi/2$ (dotted). Within each group of curves the values of the mass are given, from bottom to top on the right side (black to orange), by $\psi_{\rm H} = 0$, 0.53, 0.75, 0.941, 0.98. The four plots correspond to the cases $a/T = 4.41$ (a), 12.2 (b), 86 (c), 249 (d).

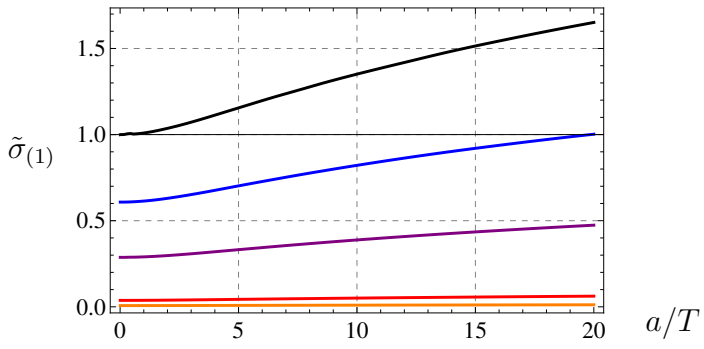

Figure 6.7: Plot of the conductivity $\tilde{\sigma}_{(1)}$ corresponding to the polarization $\epsilon_{(1)}$ as a function of a/T for, from top to bottom, $\psi_{\rm H} = 0$, 0.53, 0.75, 0.941, 0.98.

part of (6.36) is independent of u. Numerical accuracy can then be improved by evaluating this quantity at the horizon instead of at the boundary, since we know the analytic values for the metric functions and the ingoing fields at $u_{\rm H}$.

6.2.2 Spectral density for the polarization $\epsilon_{(2)}$

We now move on to compute $\chi_{(2)}$, the correlator corresponding to $\epsilon_{(2)}$. To obtain this, it is easier to work in terms of the gauge invariant fields $E_i \equiv \partial_i A_t - \partial_t A_i$. Equations (6.23)-(6.26) can be rewritten in terms of E_i with the aid of the constraint

$$-g^{tt}k_0 A_t' + g^{xx}k_x A_x' + g^{zz}k_z A_z' = 0\,, \tag{6.39}$$

resulting in

$$E_x'' + \left[(\log M g^{uu} g^{xx})' + \left(\log\frac{g^{xx}}{g^{tt}}\right)' \frac{k_x^2}{u^2\overline{k}^2} g^{xx}\right] E_x' + \frac{u^2\overline{k}^2}{g^{uu}} E_x + \left(\log\frac{g^{xx}}{g^{tt}}\right)' \frac{k_z k_x}{u^2\overline{k}^2} g^{zz} E_z' = 0\,, \tag{6.40}$$

$$E_z''+\left[(\log Mg^{uu}g^{zz})'+\left(\log\frac{g^{zz}}{g^{tt}}\right)'\frac{k_z^2}{u^2\overline{k}^2}g^{zz}\right]E_z'+\frac{u^2\overline{k}^2}{g^{uu}}E_z+\left(\log\frac{g^{zz}}{g^{tt}}\right)'\frac{k_zk_x}{u^2\overline{k}^2}g^{xx}E_x'=0\,, \tag{6.41}$$

where $u^2\overline{k}^2\equiv -g^{tt}k_0^2-g^{xx}k_x^2-g^{zz}k_z^2$. The action (6.33) can also be written in terms of these fields as

$$S_\epsilon=-2K_{\rm D7}\int dt\,d\vec{x}\,\frac{Mg^{uu}}{-k_0^2u^2\overline{k}^2}\Big[\left(-g^{tt}k_0^2-g^{zz}k_z^2\right)g^{xx}E_xE_x'+u^2\overline{k}^2g^{yy}E_yE_y'+ \\ +g^{xx}g^{zz}k_xk_z\left(E_xE_z\right)'+\left(-g^{tt}k_0^2-g^{xx}k_x^2\right)g^{zz}E_zE_z'\Big]_{u=\epsilon}\,. \tag{6.42}$$

Since we need to take the limit $\epsilon\to 0$, before proceeding any further, we need to verify that the correlators will remain finite in this limit. To this end we use the near-boundary expansion of the metric (6.30) and of the embedding ψ (6.31) to solve the equations (6.40) and (6.41) perturbatively. We find

$$E_x=E_x^{(0)}+E_x^{(2)}\cos\vartheta\,u^2-\frac{1}{24}\left(\frac{3}{4}E_x^{(0)}k_0^2\cos\vartheta+\left(5-\frac{24\psi_1^2}{a^2}\right)E_x^{(2)}\right)\cos\vartheta\,a^2\,u^4+O\left(u^6\right)\,, \tag{6.43}$$

$$E_z=E_z^{(0)}+E_x^{(2)}\sin\vartheta\,u^2+E_z^{(4)}u^4-\frac{a^2k_0^2\cos\vartheta}{16}\left(E_z^{(0)}\cos\theta+E_x^{(0)}\sin\vartheta\right)u^4\log u+O\left(u^6\right)\,. \tag{6.44}$$

Using these expressions, we can rewrite (8.79) as

$$S_\epsilon=-2K_{\rm D7}\int dt\,d\vec{x}\left[\mathcal{L}_1+\mathcal{L}_2+\mathcal{L}_3+\mathcal{L}_{\rm m}+\ldots+O\left(u^2\right)\right]_{u=\epsilon}\,, \tag{6.45}$$

where

$$\mathcal{L}_1 \;=\; -\frac{3}{4}\sin^2\vartheta\,E_x^{(0)2}-\frac{1}{4}\cos^2\vartheta\,E_z^{(0)2}-\sin\vartheta\cos\vartheta\,E_x^{(0)}E_z^{(0)}\,,$$

$$
\begin{aligned}
\mathcal{L}_2 &= \frac{1}{3k_0^2}\left[\frac{1+5\cos 2\vartheta}{\cos\vartheta}\,E_x^{(0)}E_x^{(2)} + \frac{48}{a^2}\tan\vartheta\,E_x^{(0)}E_z^{(4)} - 10\sin\vartheta\,E_z^{(0)}E_x^{(2)} + \frac{48}{a^2}E_z^{(0)}E_z^{(4)}\right], \\
\mathcal{L}_3 &= -\left(E_x^{(0)}\sin\vartheta + E_z^{(0)}\cos\vartheta\right)^2\log u\,, \\
\mathcal{L}_{\rm m} &= \frac{16\psi_1^2}{a^2k_0^2}\tan\vartheta\left(E_x^{(0)}E_x^{(2)}\sin\vartheta + E_z^{(0)}E_x^{(2)}\cos\vartheta\right), \qquad (6.46)
\end{aligned}
$$

and the ellipsis stands for the terms in the y-components that have been already dealt with. Notice that $\mathcal{L}_1$, $\mathcal{L}_2$, $\mathcal{L}_3$ are the same as in the $\psi = 0$ case of [27].

The contribution of $\mathcal{L}_{\rm m}$ to the production of photons with polarization $\epsilon_{(2)}$ is proportional to

$$
\cos^2\vartheta\frac{\delta^2\mathcal{L}_{\rm m}}{\delta E_x^{(0)2}} + \sin^2\vartheta\frac{\delta^2\mathcal{L}_{\rm m}}{\delta E_z^{(0)2}} - 2\sin\vartheta\cos\vartheta\frac{\delta^2\mathcal{L}_{\rm m}}{\delta E_z^{(0)}\delta E_x^{(0)}} = 0\,, \qquad (6.47)
$$

and therefore vanishes identically, and so does the divergent term $\mathcal{L}_3$, as shown in [27]. We obtain then the simple result

$$
\chi_{(2)} \equiv \epsilon_{(2)}^{\mu}\epsilon_{(2)}^{\nu}\chi_{\mu\nu} = 16K_{\rm D7}{\rm Im}\left[\cos\vartheta\frac{\delta E_x^{(2)}}{\delta E_x^{(0)}} - \sin\vartheta\frac{\delta E_x^{(2)}}{\delta E_z^{(0)}}\right]. \qquad (6.48)
$$

We can now proceed as in [27] to determine how $E_x^{(2)}$ varies with respect of $E_x^{(0)}$ and $E_z^{(0)}$. Alternatively, we will explain in Appendix 6.A how to apply the technology developed in [127] to obtain $\chi_{(2)}$ using the values of the fields at the horizon. As a check of our results, we have verified that we obtain the same results using both methods. We display the results in Fig. 6.8 for various values of the anisotropy, of the angles, and of the quark masses.

For photons with polarization along $\epsilon_{(2)}$, the conductivity

$$
\sigma_{(2)}(T) = \lim_{k_0\to 0}\frac{\chi_{(2)}}{\chi_{(2),{\rm iso}}(T)} = \lim_{k_0\to 0} 2\frac{\chi_{(2)}}{\chi_{\rm iso}(T)} \qquad (6.49)
$$

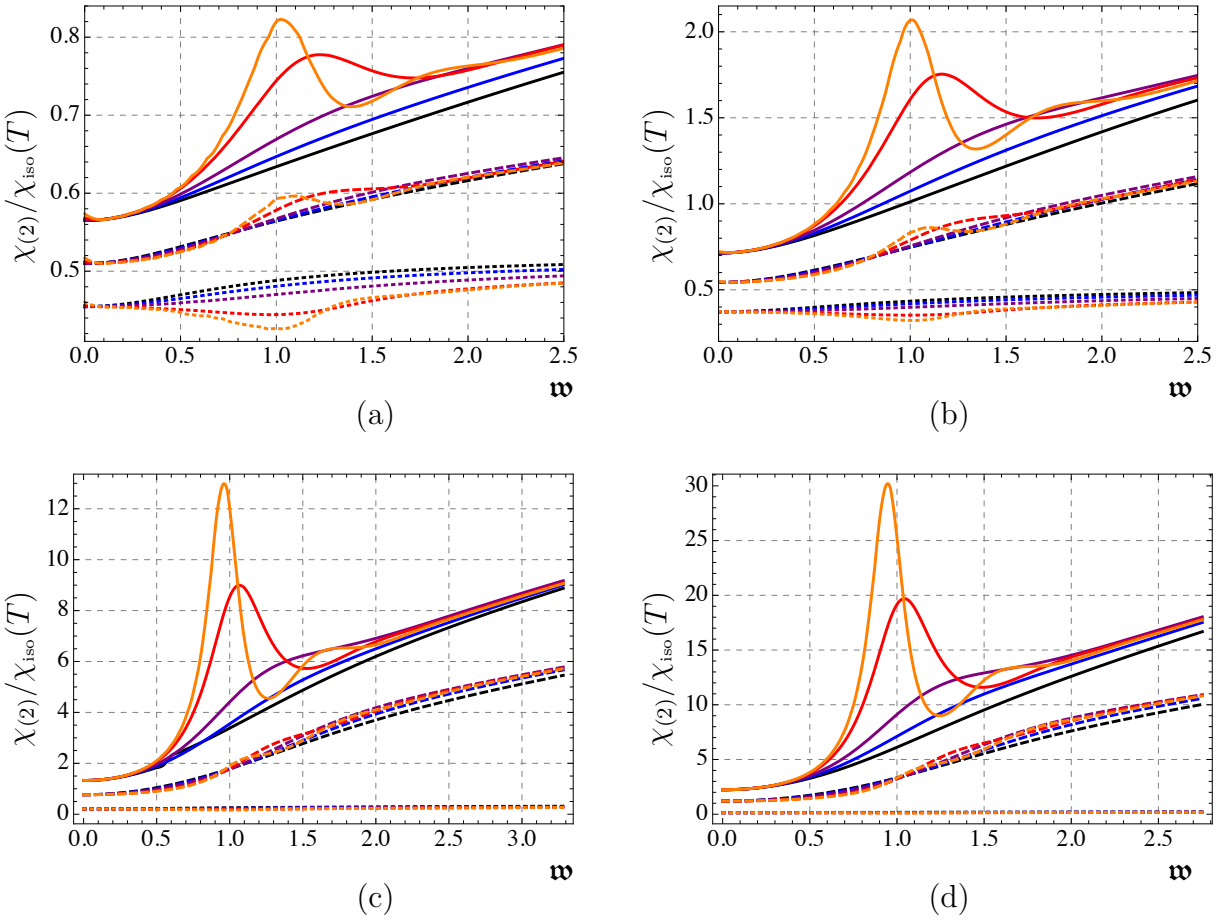

Figure 6.8: Plots of the spectral density $\chi_{(2)}$ corresponding to the polarization $\epsilon_{(2)}$, normalized with respect to the isotropic result at fixed temperature $\chi_{\rm iso}(T)$. The curves correspond from top to bottom to the angles $\vartheta = 0$ (solid), $\pi/4$ (dashed), $\pi/2$ (dotted). Within each group of curves the values of the mass are given, from bottom to top on the right side (black to orange), by $\psi_H = 0$, 0.53, 0.75, 0.941, 0.98. The four plots correspond to the cases $a/T = 4.41$ (a), 12.2 (b), 86 (c), 249 (d).

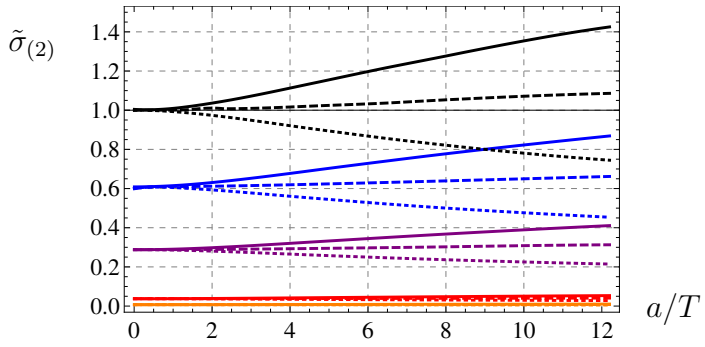

Figure 6.9: Plot of the conductivity $\tilde{\sigma}_{(2)}$ corresponding to the polarization $\epsilon_{(2)}$ as a function of a/T. The groups of curves correspond from top to bottom to $\psi_{\rm H} = 0,\ 0.53,\ 0.75,\ 0.941$. Inside each group we plot the angles $\vartheta = 0$ (solid), $\pi/4$ (dashed), and $\pi/2$ (dotted).

depends not only on the anisotropy and quark mass, as was the case for the polarization along the y-direction, but also on the angle ϑ. If we normalize with respect to the isotropic case, the conductivity does not depend on the quark masses and is therefore identical to the one depicted in Figs. 11 and 12 of [27]. We can then define unnormalized conductivities, as done above for $\tilde{\sigma}_{(1)}$,

$$\tilde{\sigma}_{(2)} = 2 \lim_{\mathfrak{w}\to 0} \frac{\chi_{(2)}}{8\tilde{\mathcal{N}}_{\rm D7}\mathfrak{w}}\,, \tag{6.50}$$

which do depend on the masses and are reported in Figs. 6.9 (as a function of a/T for fixed ϑ) and 6.10 (as a function of ϑ for fixed a/T).

6.2.3 Total photon production rate

We have now all the ingredients to calculate the total emission rate (8.69). We convert this quantity to the emission rate per unit photon energy in a infinitesimal

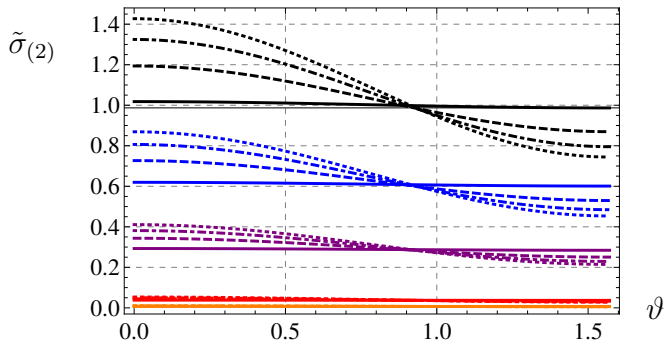

Figure 6.10: Plot of the conductivity $\tilde{\sigma}_{(2)}$ corresponding to the polarization $\epsilon_{(2)}$ as a function of the angle ϑ. The groups of curves correspond, from top to bottom, to $\psi_{\rm H} = 0$, 0.53, 0.75, 0.941, 0.98. Within each group we have, from bottom to top on the left side of the graph, a/T =1.38 (solid), 5.9 (dashed), 9.25 (dot-dashed), and 12.2 (dotted).

angle around ϑ. Using that the photon momentum is light-like, we have

$$\frac{-1}{2\alpha_{\rm EM}N_{\rm c}N_{\rm f}T^3}\frac{d\Gamma_\gamma}{d\cos\vartheta\, dk^0} = \frac{\mathfrak{w}}{2N_cN_fT^2}\frac{1}{e^{2\pi\mathfrak{w}}-1}\left(\chi_{(1)}+\chi_{(2)}\right)\,, \tag{6.51}$$

which is plotted in Fig. 6.11 for different values of a/T, ϑ and $\psi_{\rm H}$. The isotropic result at the same temperature cannot be calculated analytically, since we only have a numerical solution for ψ. So, we calculated this quantity numerically and the results are shown in the figures as coarsely dashed curves. We observe that, even in the massive quark case, the anisotropic plasma emits more photons, in total, than the corresponding isotropic plasma at the same temperature.

6.3 Dilepton production from holography

The same electromagnetic current considered above, if evaluated for time-like momenta, allows to compute the rate of emission of lepton/antilepton pairs, which are

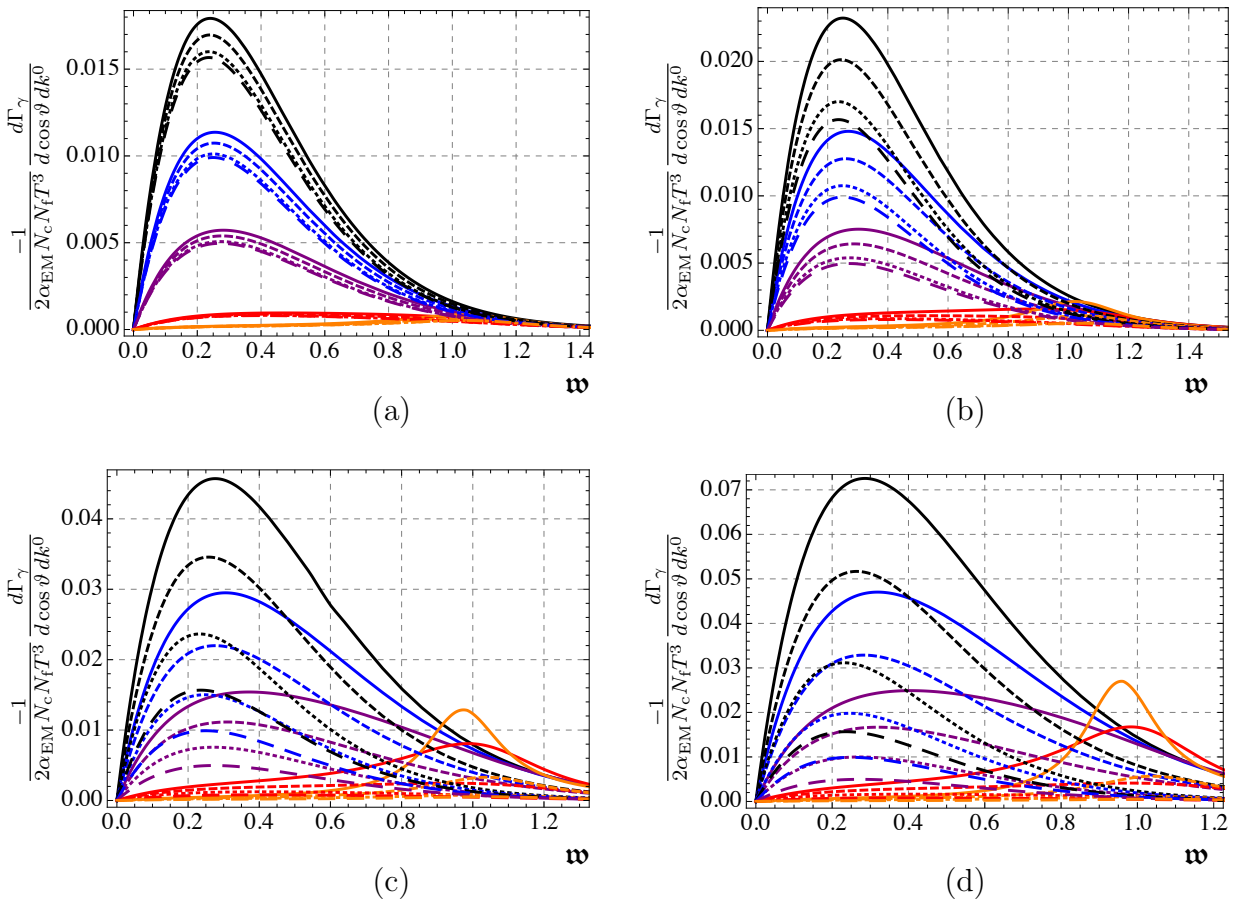

Figure 6.11: Plots of the total production rate. The groups of curves correspond from top to bottom to $\psi_{\rm H} = 0,\ 0.53,\ 0.75,\ 0.941,\ 0.98$. Within each group we plot the angles $\vartheta = 0$ (solid), $\pi/4$, (dashed), and $\pi/2$ (dotted). The four plots correspond to the cases $a/T = 4.41$ (a), 12.2 (b), 86 (c), 249 (d). The temperatures in the four cases are, respectively, $T = 0.33,\ 0.36,\ 0.49,\ 0.58$. The isotropic results at the same temperatures and masses are the coarsely dashed curves.

produced via decay of virtual photons. From (6.4) we see that the total dilepton production rate is proportional to the trace of the spectral density

$$\eta^{\mu\nu}\chi_{\mu\nu} = -\chi_{tt} + \chi_{xx} + \chi_{yy} + \chi_{zz}\,. \tag{6.52}$$

Since the equation of motion for the y-component of the gauge field is decoupled from the equations for the other components, we can split the trace as

$$\eta^{\mu\nu}\chi_{\mu\nu} = \chi_{(1)} + \chi_{(2)}\,, \tag{6.53}$$

where

$$\chi_{(1)} \equiv \chi_{yy}\,, \qquad \chi_{(2)} \equiv -\chi_{tt} + \chi_{xx} + \chi_{zz}\,. \tag{6.54}$$

The spectral densities are calculated again as $\chi_{\mu\nu} = -2\,\mathrm{Im}\,G^{\mathrm{R}}_{\mu\nu}$. We will obtain the retarded Green functions $G^{\mathrm{R}}_{\mu\nu}$ by varying the boundary action (8.79) with respect to the values of the gauge fields at the boundary $A^{(0)}_{\mu}$:

$$G^{\mathrm{R}}_{\mu\nu} = \frac{\delta^2 S_\epsilon}{\delta A^{\mu(0)}\,\delta A^{\nu(0)}}.$$

As in the previous section, it will prove convenient to work with the gauge invariant quantities $E_i = \partial_i A_t - \partial_t A_i$ instead of the gauge fields. The Green functions can be

obtained as

$$G^{\rm R}_{ii} = -k_0^2 \, \frac{\delta^2 S_\epsilon}{\delta E_i^{(0)\,2}} \,, \qquad i = x, y, z \,, \tag{6.55}$$

$$G^{\rm R}_{tt} = -k_x^2 \, \frac{\delta^2 S_\epsilon}{\delta E_x^{(0)\,2}} - k_z^2 \, \frac{\delta^2 S_\epsilon}{\delta E_z^{(0)\,2}} - 2 k_x \, k_z \, \frac{\delta^2 S_\epsilon}{\delta E_x^{(0)} \delta E_z^{(0)}}, \tag{6.56}$$

where $E_i^{(0)}$ are the values of the gauge invariant fields evaluated at the boundary. In writing (6.56) we have already used the fact that k_y is zero and that the equation for E_y decouples from the rest. We arrive at

$$\chi_{(1)} = 2 \, {\rm Im} \left[k_0^2 \, \frac{\delta^2 S_\epsilon}{\delta E_y^{(0)\,2}} \right] \,, \tag{6.57}$$

$$\chi_{(2)} = -2 \, {\rm Im} \left[(k_x^2 - k_0^2) \, \frac{\delta^2 S_\epsilon}{\delta E_x^{(0)2}} + (k_z^2 - k_0^2) \, \frac{\delta^2 S_\epsilon}{\delta E_z^{(0)2}} + 2 \, k_x \, k_z \, \frac{\delta^2 S_\epsilon}{\delta E_x^{(0)} \delta E_z^{(0)}} \right] . \tag{6.58}$$

In terms of the spectral densities the latter equation is

$$\chi_{(2)} = \left(1 - \frac{k_x^2}{k_0^2} \right) \chi_{xx} + \left(1 - \frac{k_z^2}{k_0^2} \right) \chi_{zz} - 2 \frac{k_x k_z}{k_0^2} \chi_{xz} \,. \tag{6.59}$$

When light-like momentum is considered, the previous calculation coincides, as it should, with the one for the photon production. For dilepton production, the spatial part of the momentum will be given by $\vec{k} = q(\sin\vartheta, 0, \cos\vartheta)$ for $q < k_0$, and the equation (6.58) will read

$$\chi_{(2)} = -2 \, {\rm Im} \left[(q^2 \sin^2\vartheta - k_0^2) \, \frac{\delta^2 S_\epsilon}{\delta E_x^{(0)2}} + (q^2 \cos^2\vartheta - k_0^2) \, \frac{\delta^2 S_\epsilon}{\delta E_z^{(0)2}} + 2 \, q^2 \sin\vartheta \cos\vartheta \, \frac{\delta^2 S_\epsilon}{\delta E_x^{(0)} \delta E_z^{(0)}} \right] . \tag{6.60}$$

As a warm up, we will begin by performing the calculation in the isotropic limit.

This will be used to normalize the results for the anisotropic plasma.

6.3.1 Isotropic limit

In the isotropic limit (6.11) we can use the $SO(3)$ symmetry to set $\vartheta = \pi/2$, fixing the spatial component of k in the x-direction. We have $k_x = q$, $k_y = k_z = 0$ which simplifies the equations above to

$$\chi_{(1)\text{iso}} = \chi_{yy,\text{iso}}\,, \qquad \chi_{(2)\text{iso}} = \left(1 - \frac{q^2}{k_0^2}\right)\chi_{xx,\text{iso}} + \chi_{zz,\text{iso}}. \tag{6.61}$$

We will compute χ_{yy} repeating the same steps used in the photon production for polarization $\epsilon_{(1)}$. This spectral density reads

$$\frac{\chi_{(1)\text{iso}}}{8\tilde{\mathcal{N}}_{D7}\,\mathfrak{w}} = \frac{1}{2\pi T k_0\left|A_{y,\text{iso}}(k,0)\right|^2}\text{Im}\lim_{u\to u_\text{H}} Q(u)A'_{y,\text{iso}}(k,u)A^*_{y,\text{iso}}(k,u) \tag{6.62}$$

where $Q(u)$ was defined in (6.35) and $A_{y,\text{iso}}$ solves equation (6.23), in the isotropic limit (6.11) but with $q \neq k_0$.

To compute $\chi_{xx,\text{iso}}$ and $\chi_{zz,\text{iso}}$, we make two observations. First, for $\vartheta = \pi/2$, equations (6.40) and (6.41) decouple from each other. Second, the action (8.79) will have no mixed terms, so we can vary the action with respect to $E_{x,\text{iso}}$ and $E_{z,\text{iso}}$ in a similar fashion to what has been done for $A_{y,\text{iso}}$, and get

$$\frac{\chi_{xx,\text{iso}}}{8\tilde{\mathcal{N}}_{D7}\,\mathfrak{w}} = \frac{k_0}{2\pi T\left|E_{x,\text{iso}}(k,0)\right|^2}\text{Im}\lim_{u\to u_\text{H}} Q_x(u)E'_{x,\text{iso}}(k,u)E^*_{x,\text{iso}}(k,u)\,, \tag{6.63}$$

$$\frac{\chi_{zz,\text{iso}}}{8\tilde{\mathcal{N}}_{D7}\,\mathfrak{w}} = \frac{k_0}{2\pi T\left|E_{z,\text{iso}}(k,0)\right|^2}\text{Im}\lim_{u\to u_\text{H}} Q_z(u)E'_{z,\text{iso}}(k,u)E^*_{z,\text{iso}}(k,u)\,, \tag{6.64}$$

where $Q_x(u) = \frac{Mg^{uu}}{u^2\overline{k}^2}g^{tt}g^{xx}$ and $Q_z(u) = \frac{Mg^{uu}}{-k_0^2u^2\overline{k}^2}\left(-g^{tt}k_0^2 - g^{xx}q^2\right)g^{zz}$ are, respectively,

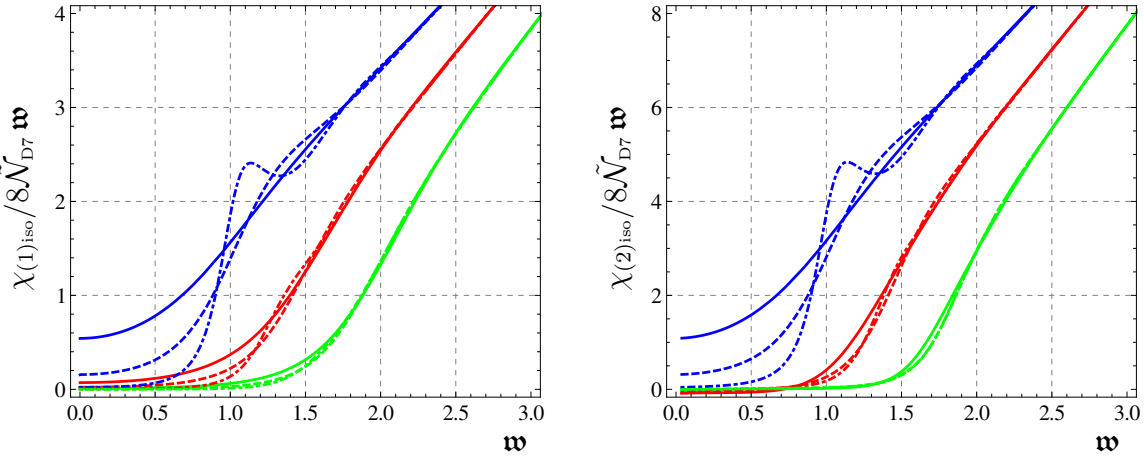

Figure 6.12: Plots of the spectral densities $\chi_{(1)\rm iso}$ and $\chi_{(2)\rm iso}$. Here we have fixed $T = 0.33$. Curves of different colors and traits denote different values of $\mathfrak{q}$ ($\mathfrak{q}$ =0 (blue), 1 (red), 1.5 (green)) and of $\psi_{\rm H}$ ($\psi_{\rm H}$ =0 (solid), 0.75 (dashed), 0.941 (dot-dashed)). The curves for $\mathfrak{q} = 0$ are identical in the two plots, up to an overall factor of 2, as it should be, considering that (6.63) and (6.64) coincide in this case.

the coefficients multiplying the $E_x E_x'$ and $E_z E_z'$ terms in the boundary action (8.79). $E_{x,\rm iso}$ and $E_{z,\rm iso}$ are solutions to (6.40) and (6.41) in the isotropic limit (6.11). These quantities reduce to the expressions in [105] and are plotted as a function of $\mathfrak{w} \equiv k_0/2\pi T$ for various values of $\mathfrak{q} \equiv q/2\pi T$ in Fig. 6.12.

6.3.2 Dilepton spectral density $\chi_{(1)}$

The equation to solve is (6.23)) with $\vec{k} = q(\sin\vartheta, 0, \cos\vartheta)$. Using the results obtained for different values of q, $\psi_{\rm H}$, and ϑ we compute the spectral density from

$$\chi_{(1)} = -\frac{4K_{\rm D7}}{|A_y(k,0)|^2}\,{\rm Im}\lim_{u\to u_{\rm H}} Q(u)A_y^*(k,u)A_y'(k,u)\,, \tag{6.65}$$

where $Q(u)$ was defined in (6.35). The imaginary part of (6.65) does not depend on u, as we shall prove in Appendix 6.A. This justifies the fact that we evaluate the limit

at $u = u_{\rm H}$, where the numerics are under better control. The results are plotted in Fig. 6.13 for the spectral density $\chi_{(1)}$ as a function of $\mathfrak{w}$, and in Fig. 6.14 as a function of $\mathfrak{q}$. In Figs. 6.15 and 6.16 we plot $\chi_{(1)}$ as a function of the anisotropy a/T.

6.3.3 Dilepton spectral density $\chi_{(2)}$

The gauge invariant fields satisfy equations (6.40)-(6.41). Solving such equations for E_x and E_z close to the boundary we find

$$\begin{aligned} E_x &= E_x^{(0)} + \left(E_x^{(2)} \cos\vartheta + \frac{1}{2} E_x^{(0)} (q^2 - k_0^2) \log u \right) u^2 \\ &\quad + \frac{1}{192} \Big(8 \left(24\psi_1^2 - 5a^2 + 3(q^2 - k_0^2) \right) E_x^{(2)} \cos\vartheta \\ &\qquad -3 \left(3(q^2 - k_0^2)^2 + 3a^2 q^2 - 2a^2 k_0^2 + a^2 q^2 \cos 2\vartheta \right) E_x^{(0)} \Big) u^4 \\ &\quad + \frac{1}{48} \left(24\psi_1^2 - 5a^2 + 3(q^2 - k_0^2) \right) (q^2 - k_0^2) u^4 \log u + O\left(u^6\right) , \end{aligned} \tag{6.66}$$

and

$$\begin{aligned} E_z &= E_z^{(0)} + \frac{1}{2} E_x^{(0)} (q^2 - k_0^2)\, u^2 \log u \\ &\quad - \frac{3(q^2 - k_0^2)[64\, E_z^{(4)} + 3\, E_z^{(0)} (q^2 - k_0^2)(a^2 + q^2 - k_0^2)]}{8\left[(q^2 - k_0^2)(2\,a^2 - 3\,(q^2 + 8\,\psi_1^2 - k_0^2)) + 3\,a^2\, q^2 \cos^2\vartheta \right]} u^2 \\ &\quad + \frac{a^2\, E_z^{(0)}\, q^2\, (q^2 - k_0^2) \cos^2\vartheta - a^2\, q^2\, \cos\vartheta \sin\vartheta \left[E_x^{(0)} (q^2 - k_0^2) - 8\, E_x^{(2)} \cos\vartheta \right]}{8\left[(q^2 - k_0^2)(2\,a^2 - 3\,(q^2 + 8\,\psi_1^2 - k_0^2)) + 3\,a^2\, q^2 \cos^2\vartheta \right]} u^2 \\ &\quad + \left(E_z^{(4)} - \frac{1}{96} E_z^{(0)} (a^2 (7q^2 - 4k_0^2) - 6(q^2 - k_0^2)(q^2 + 8\psi_1^2 - k_0^2)) \log u \right) u^4 \\ &\quad + 3a^2 q^2 \left(E_x^{(0)} \sin 2\vartheta + E_z^{(0)} \cos 2\vartheta \right) u^4 \log u + O\left(u^6\right) , \end{aligned} \tag{6.67}$$

where $E_x^{(0)}$, $E_x^{(2)}$, $E_z^{(0)}$, and $E_z^{(4)}$ are expansion coefficients which are not determined by the boundary equations, but that can be extracted from the numerical solutions, as we shall explain presently.

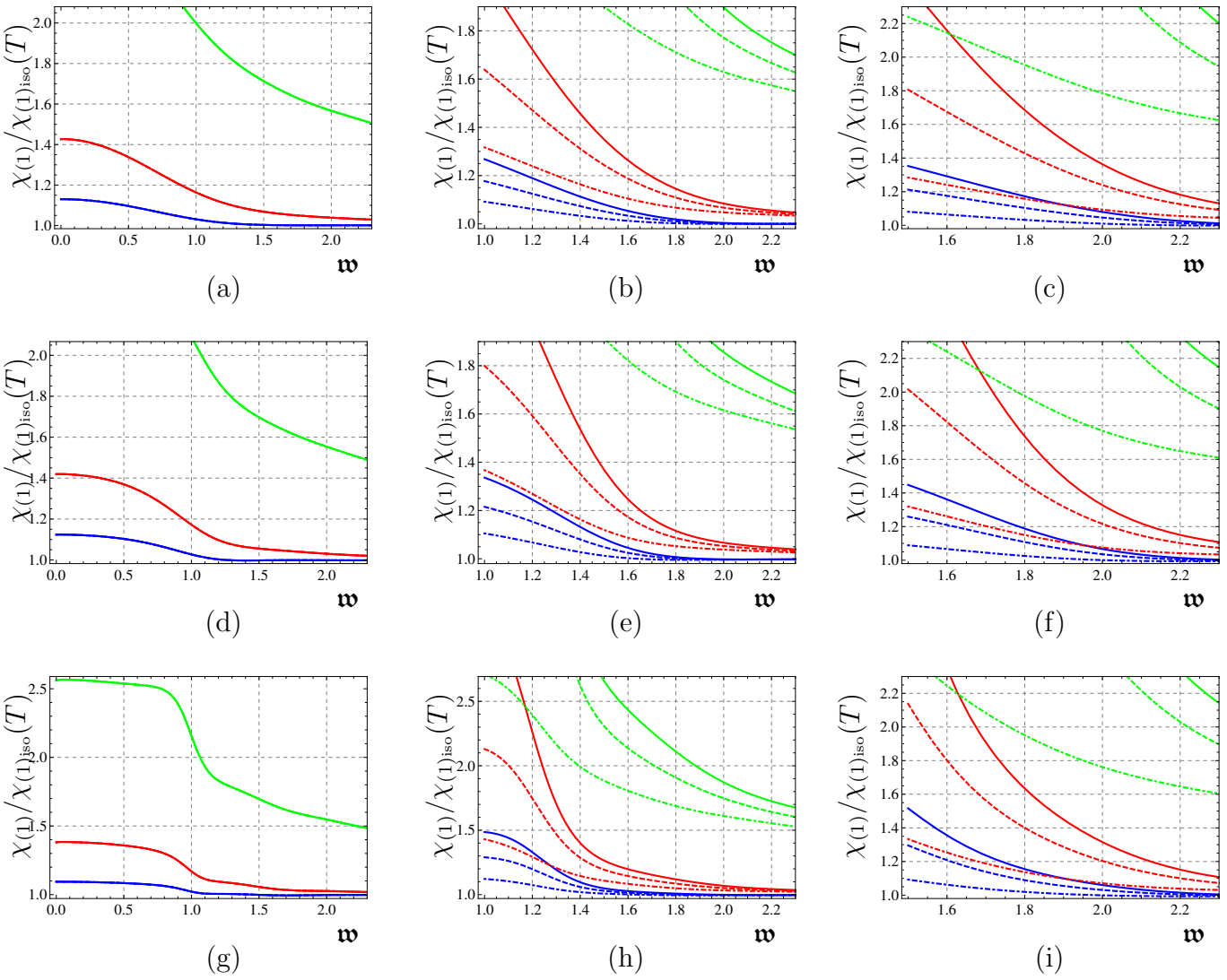

Figure 6.13: Plots of the spectral density $\chi_{(1)}$ normalized with respect to the isotropic result at fixed temperature $\chi_{(1)\rm iso}(T)$. Curves of different colors denote different values of a/T as follows a/T =4.41 (blue), 12.2 (red), 86 (green). The angles are $\vartheta = 0$ (solid), $\pi/4$ (dashed), $\pi/2$ (dot-dashed). Columns correspond to different values of $\mathfrak{q}$: from left to right it is $\mathfrak{q} = 0, 1, 1.5$. Rows correspond to different values of the quark mass: from top to bottom it is $\psi_{\rm H} = 0, 0.75, 0.941$. Then, for instance, (h) corresponds to $\mathfrak{q} = 1$, $\psi_{\rm H} = 0.941$.

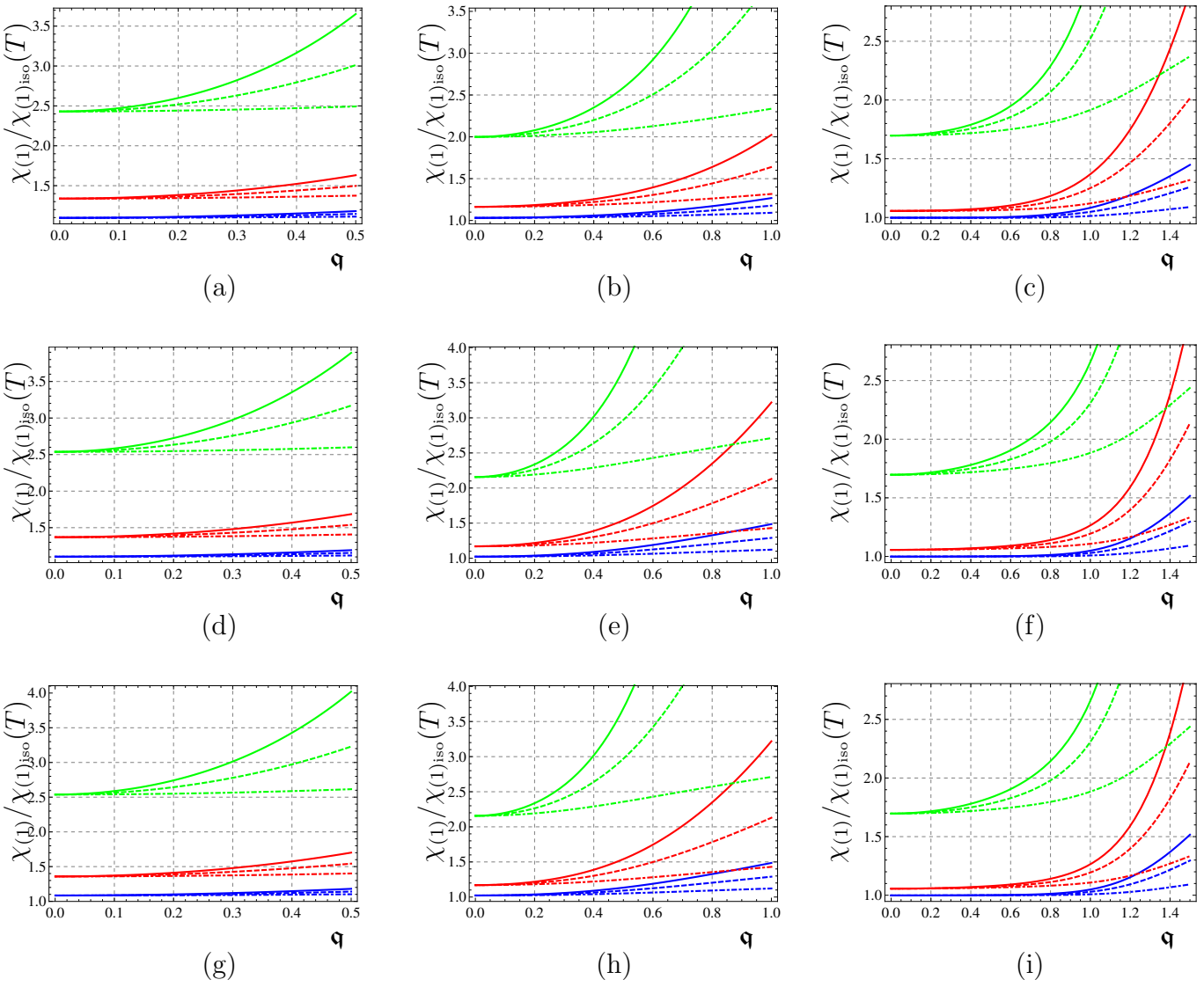

Figure 6.14: Plots of the spectral density $\chi_{(1)}$ normalized with respect to the isotropic result at fixed temperature $\chi_{(1)\mathrm{iso}}(T)$. Curves of different colors denote different values of a/T as follows a/T =4.41 (blue), 12.2 (red), 86 (green). The angles are $\vartheta = 0$ (solid), $\pi/4$ (dashed), $\pi/2$ (dash-dotted). Columns correspond to different values of $\mathfrak{w}$: from left to right it is $\mathfrak{w} = 1/2, 1, 1.5$. Rows correspond to different values of the quark mass: from top to bottom it is $\psi_{\mathrm{H}} = 0, 0.75, 0.941$. Then, for instance, (f) corresponds to $\mathfrak{w} = 3/2$, $\psi_{\mathrm{H}} = 0.75$.

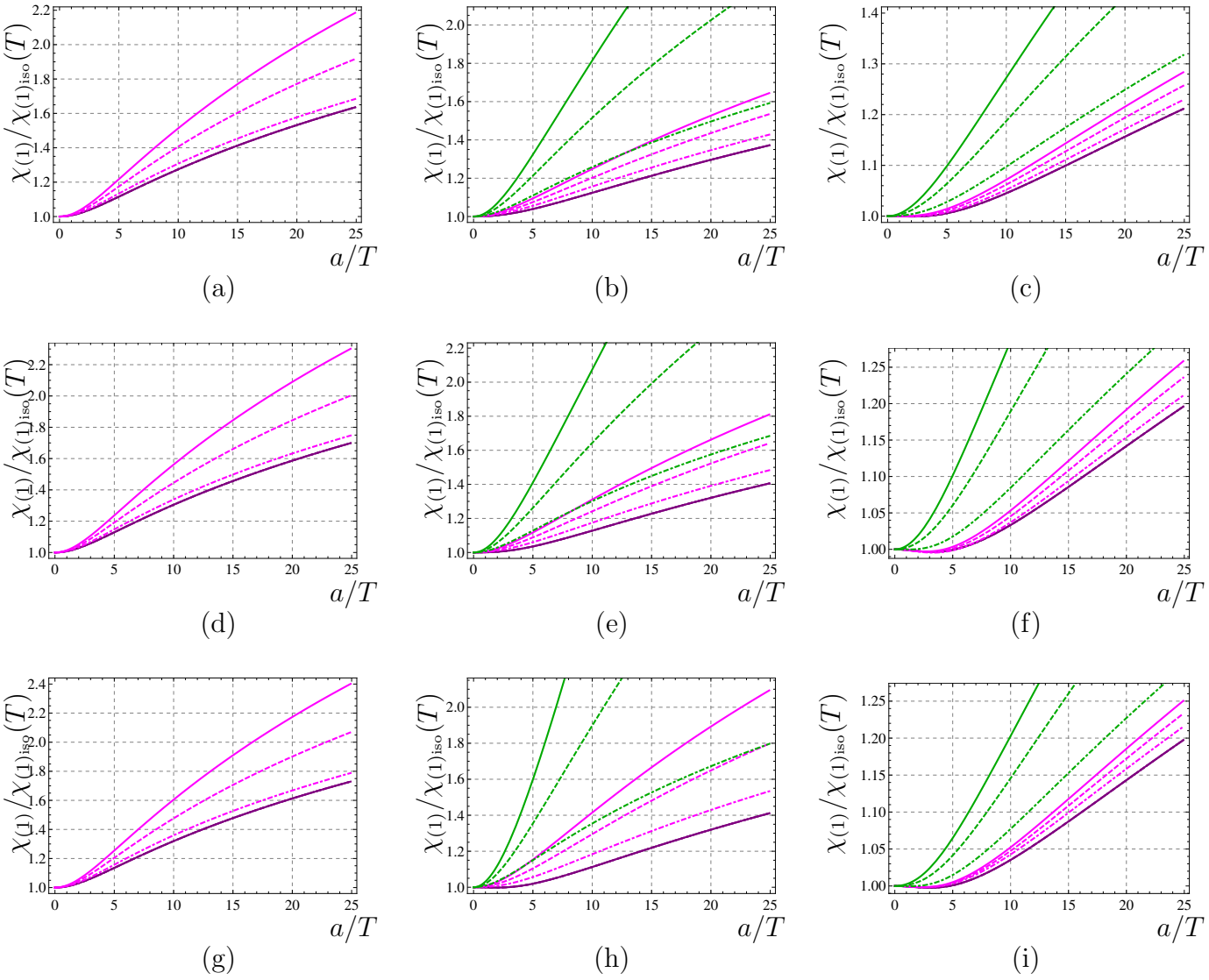

Figure 6.15: Plots of the spectral density $\chi_{(1)}$ normalized with respect to the isotropic result at fixed temperature $\chi_{(1)\mathrm{iso}}(T)$. Curves of different colors denote different values of $\mathfrak{q}$ as follows $\mathfrak{q}$ =0 (purple), 1/2 (magenta), 1 (green). The angles are $\vartheta = 0$ (solid), $\pi/4$ (dashed), $\pi/2$ (dash-dotted). Columns correspond to different values of $\mathfrak{w}$: from left to right it is $\mathfrak{w} = 0.5, 1, 1.5$. Rows correspond to different values of the quark mass: from top to bottom it is $\psi_{\mathrm{H}} = 0, 0.75, 0.941$. Then, for instance, (f) corresponds to $\mathfrak{w} = 1.5$, $\psi_{\mathrm{H}} = 0.75$.

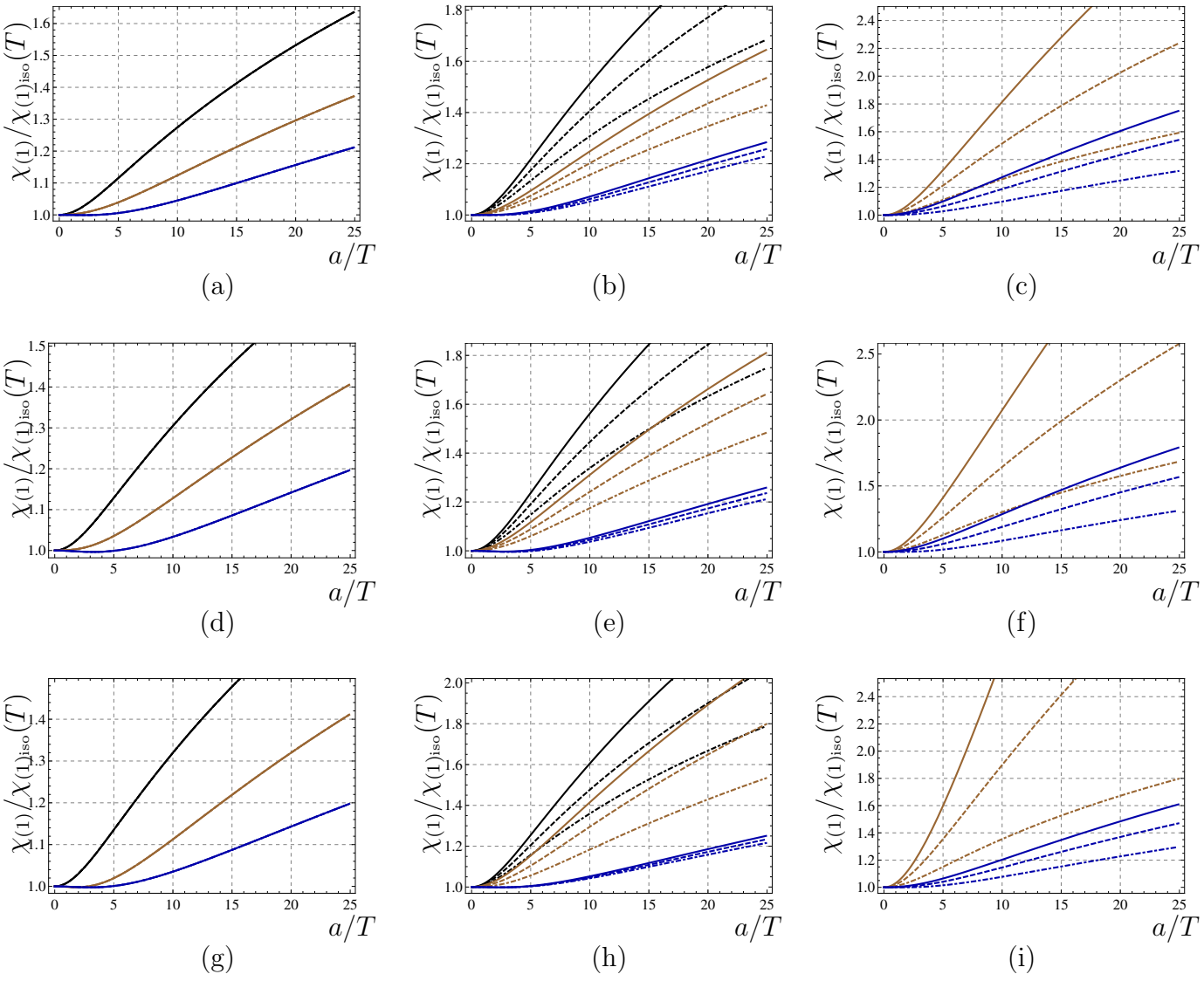

Figure 6.16: Plots of the spectral density $\chi_{(1)}$ normalized with respect to the isotropic result at fixed temperature $\chi_{(1)\mathrm{iso}}(T)$. Curves of different colors denote different values of $\mathfrak{w}$ as follows $\mathfrak{w}$ =1/2 (black), 1 (brown), 3/2 (blue). The angles are $\vartheta = 0$ (solid), $\pi/4$ (dashed), $\pi/2$ (dash-dotted). Columns correspond to different values of $\mathfrak{q}$: from left to right it is $\mathfrak{q} = 0, 0.5, 1$. Rows correspond to different values of the quark mass: from top to bottom it is $\psi_0 = 0, 0.75, 0.941$. Then, for instance, (f) corresponds to $\mathfrak{q} = 1$, $\psi_{\mathrm{H}} = 0.75$.

Using these expressions, we can write the boundary action as

$$S_\epsilon = -2K_{\text{D7}} \int dt\, d\vec{x} \left[\mathcal{L}_1 + \mathcal{L}_2 + \mathcal{L}_3 + \ldots + O\left(u^2\right)\right]_{u=\epsilon} , \tag{6.68}$$

where

$$\begin{aligned}
\mathcal{L}_1 &= A_1\, E_x^{(0)\,2} + B_1\, E_z^{(0)\,2} + C_1\, E_x^{(0)}\, E_z^{(0)} \,, \\
\mathcal{L}_2 &= A_2\, E_x^{(0)}\, E_x^{(2)} + B_2\, E_x^{(0)}\, E_x^{(2)} + C_2\, E_x^{(0)}\, E_x^{(2)} + D_2\, E_x^{(0)}\, E_x^{(2)} \,, \\
\mathcal{L}_3 &= -\frac{\log u}{k_0^2} \left[(E_x^{(0)\,2} + E_z^{(0)\,2})\, k_0^2 + (E_x^{(0)}\, \cos\vartheta - E_z^{(0)}\, \sin\vartheta)^2\, q^2\right] ,
\end{aligned} \tag{6.69}$$

and A_i, B_i, C_i $(i = 1, 2)$ and D_2 are given by (6.99) in Appendix 8.B. The contributions of $\mathcal{L}_1$ and $\mathcal{L}_3$ to the Green's functions are real, so they don't enter in the computation of $\chi_{(2)}$. Defining

$$S_2 = -2K_{\text{D7}} \int dt\, d\vec{x}\, \mathcal{L}_2 \,,$$

we can write

$$\begin{aligned}
\frac{\delta^2 S_2}{\delta E_x^{(0)\,2}} &= 2A_2 \frac{\delta E_x^{(2)}}{\delta E_x^{(0)}} + 2B_2 \frac{\delta E_z^{(4)}}{\delta E_x^{(0)}} \,, \\
\frac{\delta^2 S_2}{\delta E_z^{(0)\,2}} &= 2C_2 \frac{\delta E_x^{(2)}}{\delta E_z^{(0)}} + 2D_2 \frac{\delta E_z^{(4)}}{\delta} \,, \\
\frac{\delta^2 S_2}{\delta E_x^{(0)} \delta E_z^{(0)}} &= A_2 \frac{\delta E_x^{(2)}}{\delta E_z^{(0)}} + B_2 \frac{\delta E_z^{(4)}}{\delta E_z^{(0)}} + C_2 \frac{\delta E_x^{(2)}}{\delta E_x^{(0)}} + D_2 \frac{\delta E_z^{(4)}}{\delta E_x^{(0)}} \,.
\end{aligned} \tag{6.70}$$

Using the explicit expressions for the coefficients, one can show that

$$\chi_{(2)} \;=\; 16\,K_{\rm D7}\,{\rm Im}\left(\cos\vartheta\,\frac{\delta E_x^{(2)}}{\delta E_x^{(0)}}+\frac{6a^2q^2\cos^2\vartheta\,\sin\vartheta\,\frac{\delta E_x^{(2)}}{\delta E_z^{(0)}}+48(q^2-k_0^2)\,\frac{\delta E_z^{(4)}}{\delta E_z^{(0)}}}{6(q^2-k_0^2)(q^2-k_0^2+8\psi_1^2)-a^2(7q^2-4k_0^2)-3a^2q^2\cos 2\vartheta}\right). \tag{6.71}$$

When $q=k_0$ this expression reduces to (6.48), the expression used to calculate the photon production rate.

Having checked that there will be no divergent contributions for the correlators, we can now proceed as in [27] to find the way in which $E_x^{(2)}$ and $E_z^{(4)}$ vary with respect to $E_x^{(0)}$ and $E_z^{(0)}$. To calculate the functional derivative $\frac{\delta^2 S_\epsilon}{\delta E_i^{(0)}\delta E_j^{(0)}}$, we can use the fields E_x and E_z to construct the column

$$\mathbf{E}\equiv\begin{pmatrix}E_x\\ E_z\end{pmatrix}, \tag{6.72}$$

so that (6.40) and (6.41) can be written as the matrix equation

$$\mathcal{M}^{-1}\left(\mathcal{M}\mathbf{E}'\right)'+f(u)\mathbf{E}=0, \tag{6.73}$$

where

$$\mathcal{M}\equiv\frac{M\,g^{uu}}{k_0^2u^2\bar{k}^2}\begin{pmatrix}(g^{tt}k_0^2+g^{zz}k_z^2)k_x^2 & -g^{xx}g^{zz}k_xk_z\\ -g^{xx}g^{zz}k_xk_z & (g^{tt}k_0^2+g^{xx}k_x^2)k_z^2\end{pmatrix}, \qquad f(u)\equiv\frac{u^2\bar{k}^2}{g^{uu}}. \tag{6.74}$$

We can also write the boundary action (excluding the part with $A_y A'_y$) as

$$S_\epsilon = -2K_{\rm D7} \int dt\, d\vec{x}\, [\mathbf{E}^{\rm T} \mathcal{M} \mathbf{E}']_{u=\epsilon}\,. \tag{6.75}$$

Notice that if we can find two linearly independent solutions to (6.73), $\mathbf{E_1}$ and $\mathbf{E_2}$, such that at the boundary they reduce to $\mathbf{E_1}|_{\rm bdry} = (1\ \ 0)^{\rm T}$ and $\mathbf{E_2}|_{\rm bdry} = (0\ \ 1)^{\rm T}$, and we arrange them as the columns of a 2×2 matrix $\mathcal{E} \equiv (\mathbf{E_1}\ \ \mathbf{E_2})$, then, given that (6.73) is linear, its general solution $\mathbf{E}_{\rm sol}$ will be given by

$$\mathbf{E}_{\rm sol} = E_x^{(0)} \mathbf{E_1} + E_z^{(0)} \mathbf{E_2} = \mathcal{E} \begin{pmatrix} E_x^{(0)} \\ E_z^{(0)} \end{pmatrix}. \tag{6.76}$$

Using (6.76) we can write the boundary action (6.75) as

$$S_\epsilon = -2K_{\rm D7} \int dt\, d\vec{x} \left[(E_x^{(0)}\, E_z^{(0)}) \mathcal{M} \mathcal{E}' \begin{pmatrix} E_x^{(0)} \\ E_z^{(0)} \end{pmatrix} \right]_{u=\epsilon}, \tag{6.77}$$

where the fact that $\mathcal{E}$ becomes the identity matrix at the boundary has been used. From (6.77) we see that the variation $\frac{\delta^2 S_\epsilon}{\delta E_i^{(0)} \delta E_j^{(0)}}$, and hence the Green's function $G^{\rm R}_{ij}$, is given by the ij component of the matrix $\mathcal{M}\mathcal{E}'$. As will be seen in Appendix 6.A, this way of writing the variation of the action permits to express the imaginary part of the integrand in (6.77), which is all we need to compute the spectral densities, in terms of u-independent quantities. The evaluation can then be done at the horizon, where the numerics are under better control. In Appendix 6.A we also elaborate on how to construct the solutions necessary to carry out this procedure.

With this ground work in place, we use these expressions to numerically obtain

the dilepton production rate for different values of q, $\psi_{\rm H}$, and ϑ. In Fig. 6.17 we plot the spectral density $\chi_{(2)}$ as a function of $\mathfrak{w}$, normalized with the corresponding spectral density $\chi_{(2)_{\rm iso}}$ for an isotropic plasma at the same temperature. The same quantity as a function of $\mathfrak{q}$ is plotted in Fig. 6.18. In Figs. 6.19 and 6.20 we plot $\chi_{(2)}$ as a function of the anisotropy a/T.

6.3.4 Total dilepton production rate

In Fig. 6.21 we plot the trace of the spectral density χ^{μ}_{μ} as a function of $\mathfrak{w}$, normalized with the corresponding trace $\chi^{\mu}_{\mu_{\rm iso}}$ for an isotropic plasma at the same temperature. The same quantity as a function of $\mathfrak{q}$ is plotted in Fig. 6.22, and in Figs. 6.23 and 6.24 as a function of the anisotropy parameter a/T.

6.4 Discussion

In this paper we have studied two important phenomenological probes of a strongly coupled anisotropic plasma, namely the in-medium production of photons and of dileptons. In order to model the plasma at strong coupling, we have used the dual anisotropic black brane solution found in [10, 11]. This geometry is static, regular on and outside the horizon, and asymptotically AdS. The anisotropic equilibrium is due to a bulk axion field, corresponding on the gauge theory side to a marginally relevant deformation of the $\mathcal{N} = 4$ SYM action. The insertion of flavor D7-branes in this background has allowed us to couple the $\mathcal{N} = 4$ adjoint fields to fields in the fundamental representation, which we have called 'quarks'.

First, we have completed the computation of the photon production rate initiated in [27], where the plasma of the adjoint $\mathcal{N} = 4$ fields was coupled to *massless* quarks.

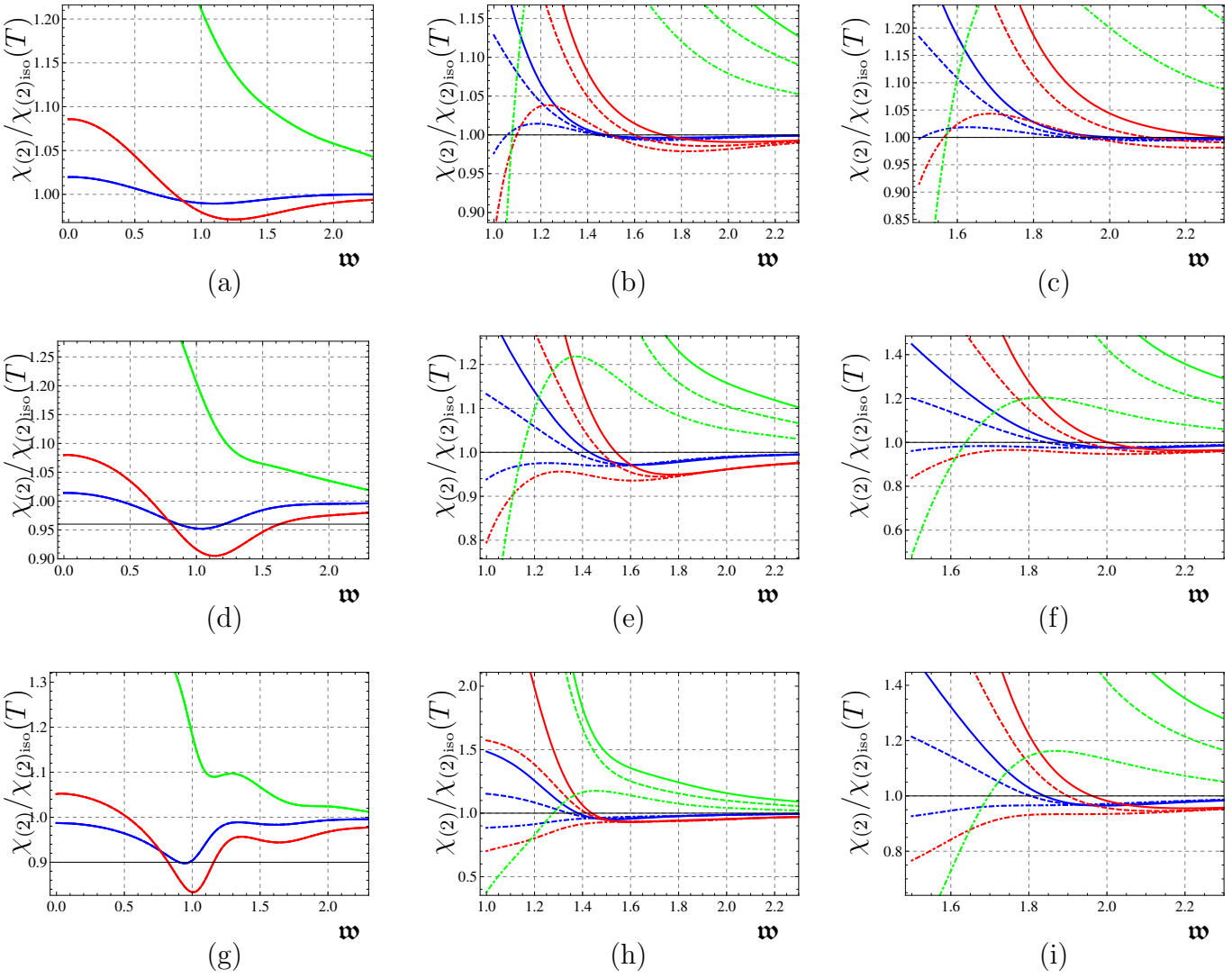

Figure 6.17: Plots of the spectral density $\chi_{(2)}$ normalized with respect to the isotropic result at fixed temperature $\chi_{(2)\mathrm{iso}}(T)$. Curves of different colors denote different values of a/T as follows a/T =4.41 (blue), 12.2 (red), 86 (green). The angles are $\vartheta = 0$ (solid), $\pi/4$ (dashed), $\pi/2$ (dash-dotted). Columns correspond to different values of $\mathfrak{q}$: from left to right it is $\mathfrak{q} = 0, 1, 1.5$. Rows correspond to different values of the quark mass: from top to bottom it is $\psi_{\mathrm{H}} = 0, 0.75, 0.941$. Then, for instance, (h) corresponds to $\mathfrak{q} = 1$, $\psi_{\mathrm{H}} = 0.941$.

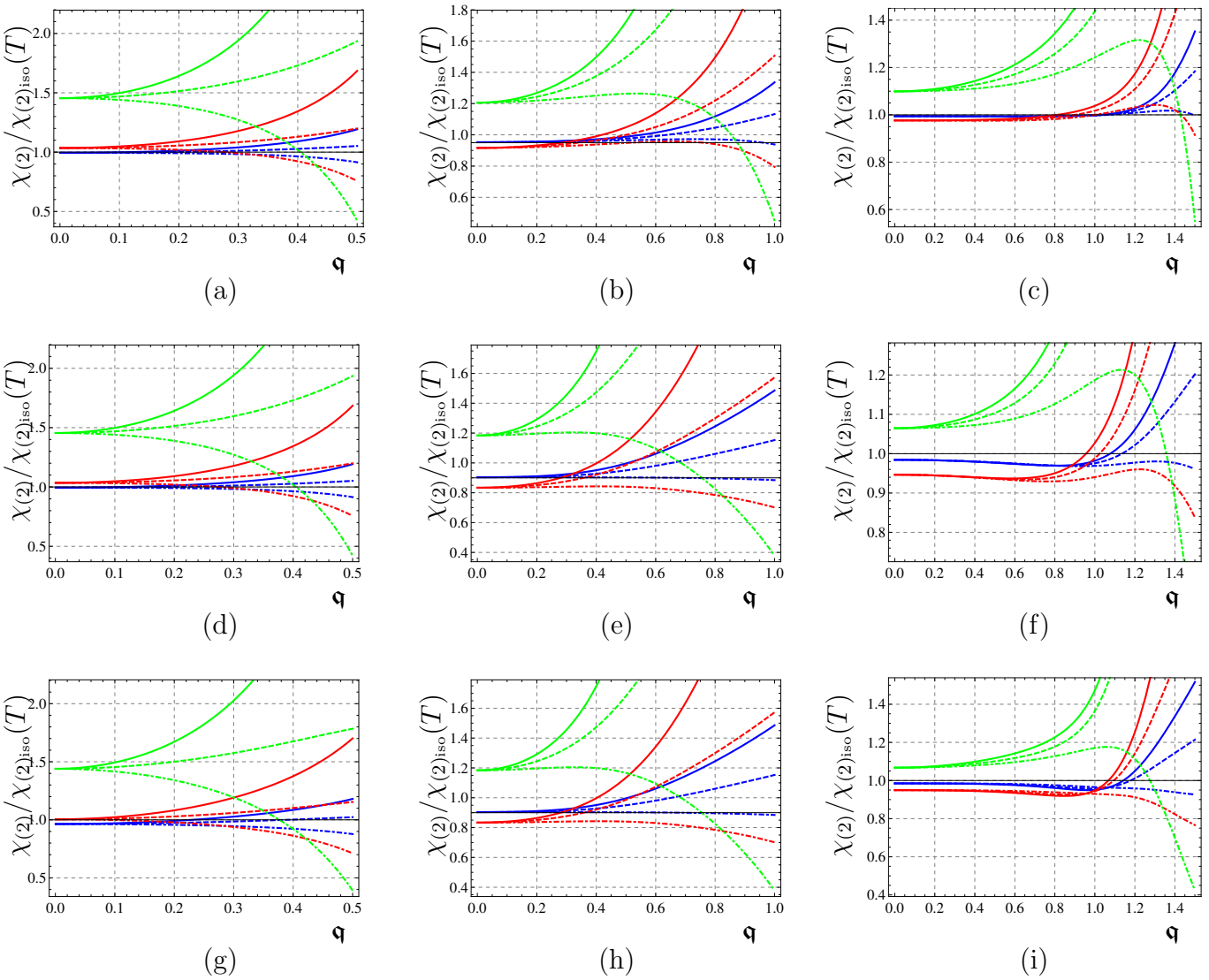

Figure 6.18: Plots of the spectral density $\chi_{(2)}$ normalized with respect to the isotropic result at fixed temperature $\chi_{(2)\mathrm{iso}}(T)$. Curves of different colors denote different values of a/T as follows a/T =4.41 (blue), 12.2 (red), 86 (green). The angles are $\vartheta = 0$ (solid), $\pi/4$ (dashed), $\pi/2$ (dash-dotted). Columns correspond to different values of $\mathfrak{w}$: from left to right it is $\mathfrak{w} = 0.5, 1, 1.5$. Rows correspond to different values of the quark mass: from top to bottom it is $\psi_{\mathrm{H}} = 0, 0.75, 0.941$. Then, for instance, (f) corresponds to $\mathfrak{w} = 1.5$, $\psi_{\mathrm{H}} = 0.75$.

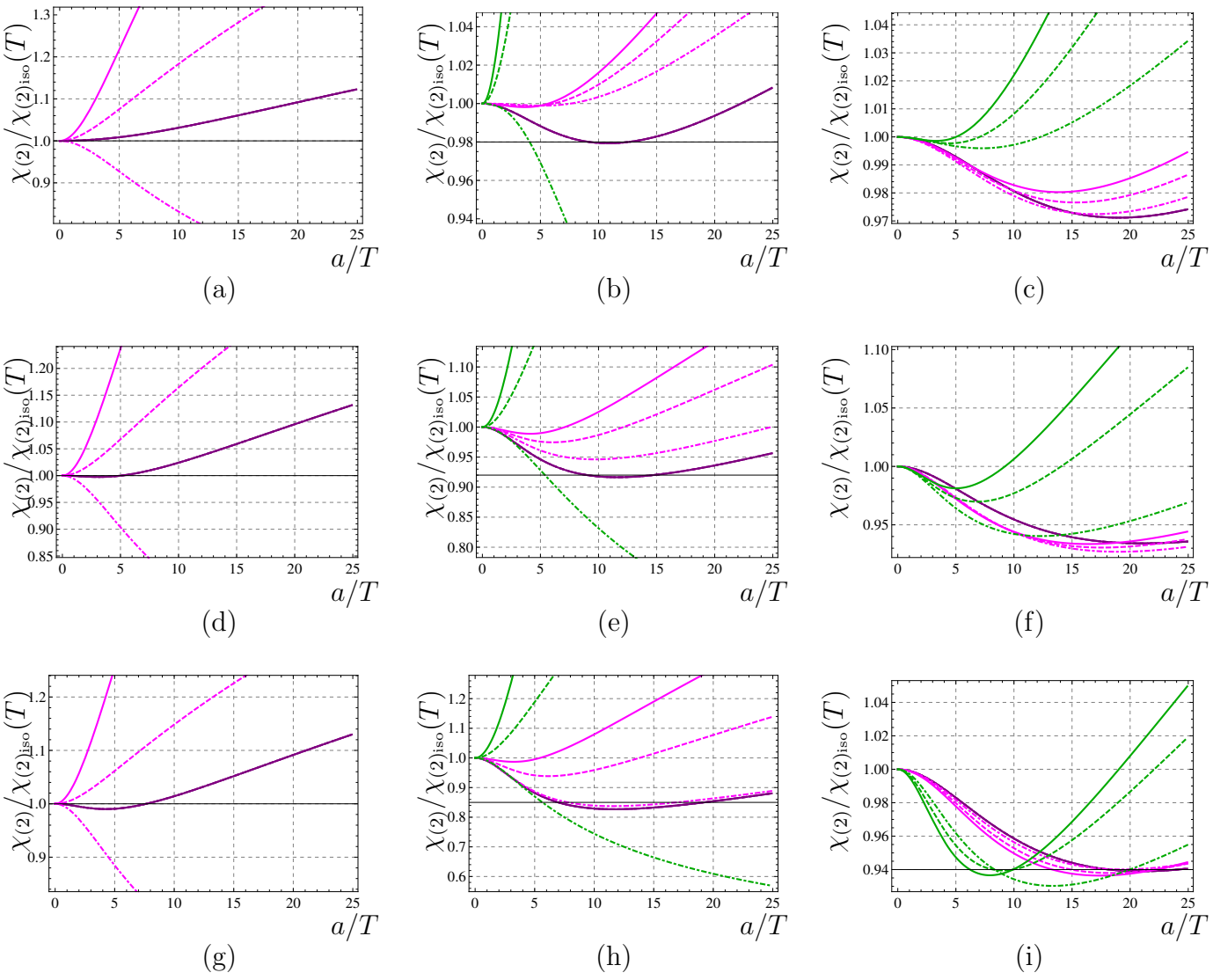

Figure 6.19: Plots of the spectral density $\chi_{(2)}$ normalized with respect to the isotropic result at fixed temperature $\chi_{(2)_{\rm iso}}(T)$. Curves of different colors denote different values of $\mathfrak{q}$ as follows $\mathfrak{q}$ =0 (purple), 0.5 (magenta), 1 (green). The angles are $\vartheta = 0$ (solid), $\pi/4$ (dashed), $\pi/2$ (dash-dotted). Columns correspond to different values of $\mathfrak{w}$: from left to right it is $\mathfrak{w} = 0.5, 1, 1.5$. Rows correspond to different values of the quark mass: from top to bottom it is $\psi_{\rm H} = 0, 0.75, 0.941$. Then, for instance, (f) corresponds to $\mathfrak{w} = 1.5$, $\psi_{\rm H} = 0.75$.

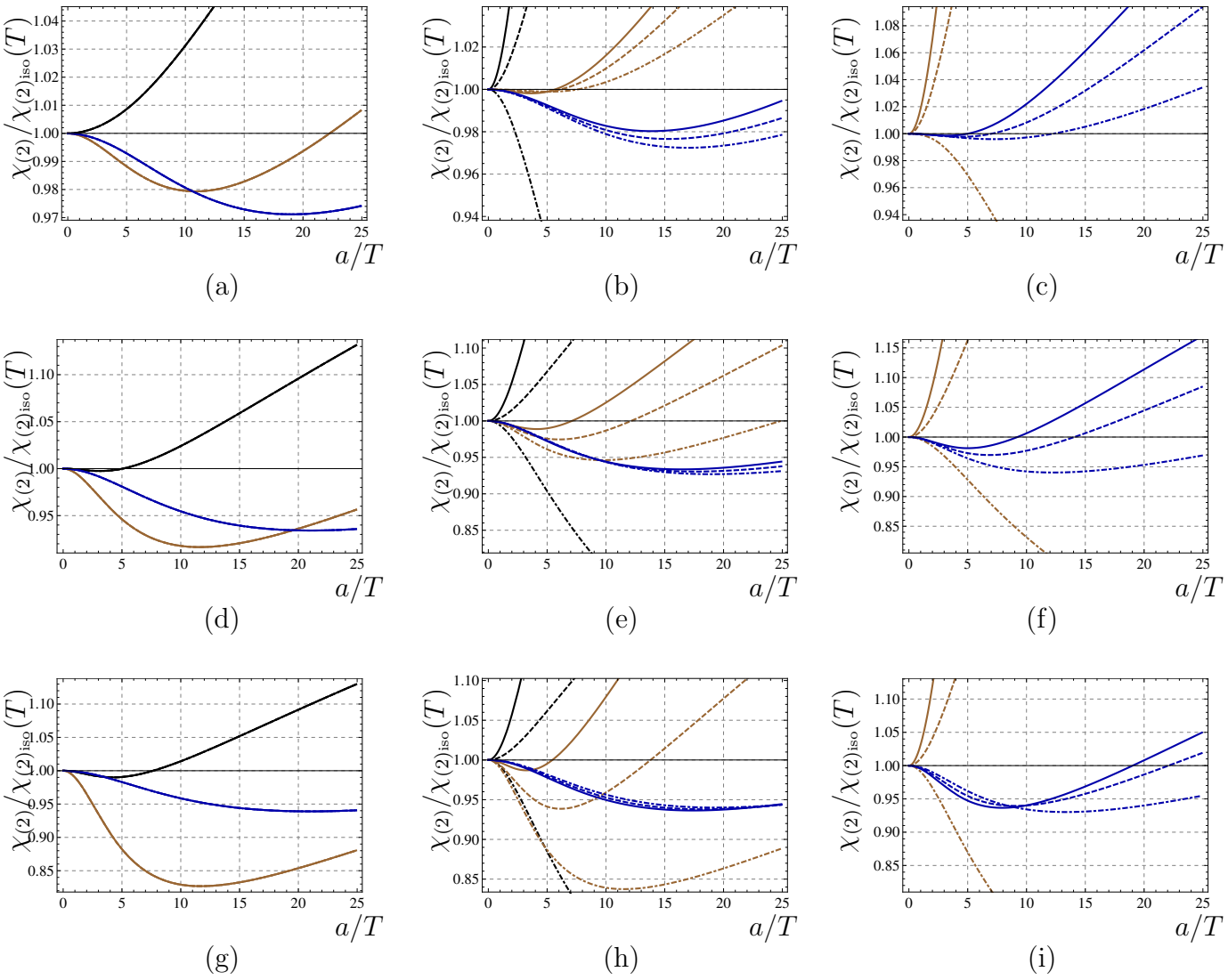

Figure 6.20: Plots of the spectral density $\chi_{(2)}$ normalized with respect to the isotropic result at fixed temperature $\chi_{(2)\mathrm{iso}}(T)$. Curves of different colors denote different values of $\mathfrak{w}$ as follows $\mathfrak{w}$ =0.5 (black), 1 (brown), 1.5 (blue). The angles are $\vartheta = 0$ (solid), $\pi/4$ (dashed), $\pi/2$ (dash-dotted). Columns correspond to different values of $\mathfrak{q}$: from left to right it is $\mathfrak{q} = 0, 0.5, 1$. Rows correspond to different values of the quark mass: from top to bottom it is $\psi_0 = 0, 0.75, 0.941$. Then, for instance, (f) corresponds to $\mathfrak{q} = 1$, $\psi_{\mathrm{H}} = 0.75$.

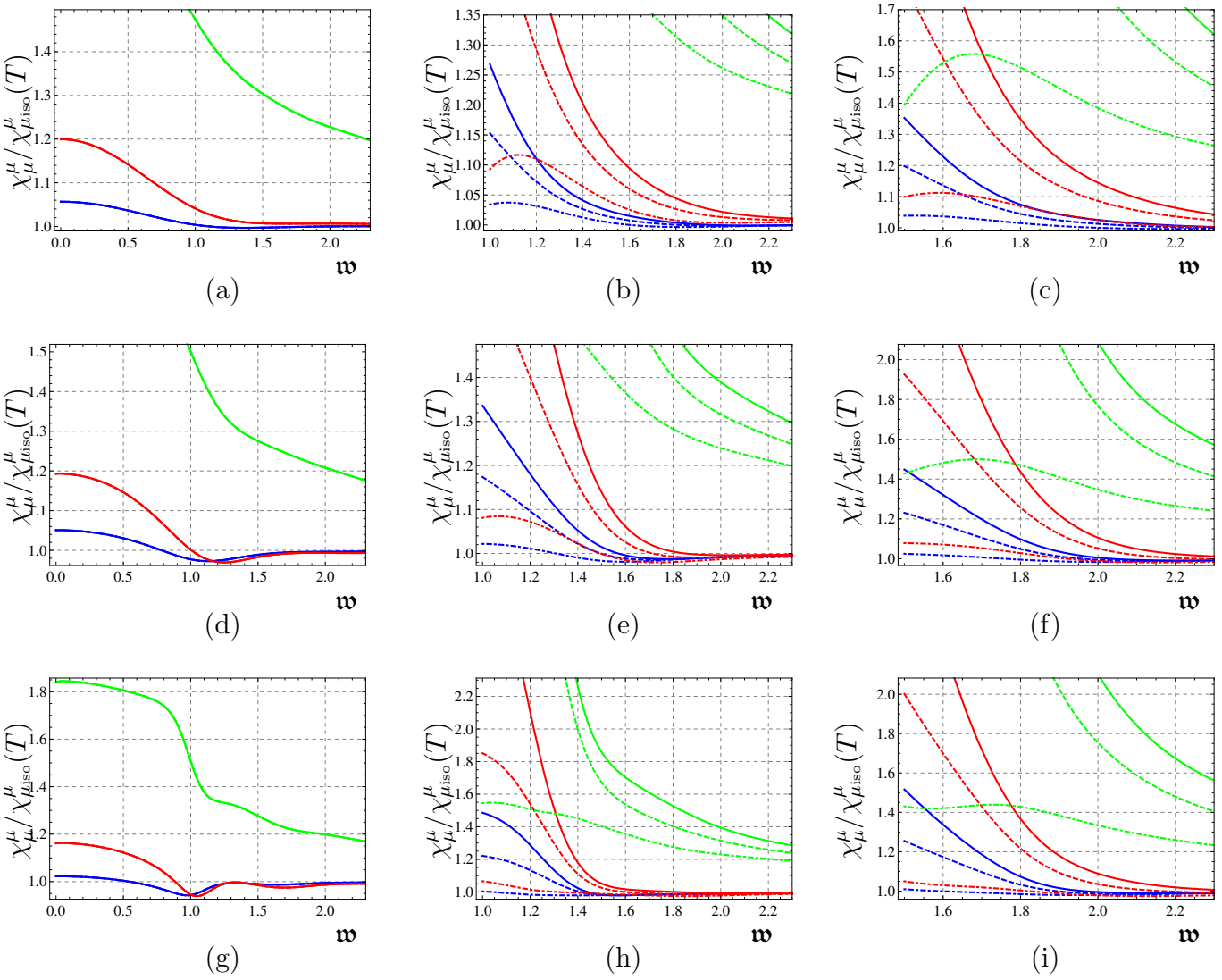

Figure 6.21: Plots of the spectral density χ^μ_μ normalized with respect to the isotropic result at fixed temperature $\chi^\mu_{\mu\mathrm{iso}}(T)$. Curves of different colors denote different values of a/T as follows a/T =4.41 (blue), 12.2 (red), 86 (green). The angles are $\vartheta = 0$ (solid), $\pi/4$ (dashed), $\pi/2$ (dash-dotted). Columns correspond to different values of $\mathfrak{q}$: from left to right it is $\mathfrak{q} = 0, 1, 1.5$. Rows correspond to different values of the quark mass: from top to bottom it is $\psi_{\mathrm{H}} = 0, 0.75, 0.941$. Then, for instance, (h) corresponds to $\mathfrak{q} = 1$, $\psi_{\mathrm{H}} = 0.941$.

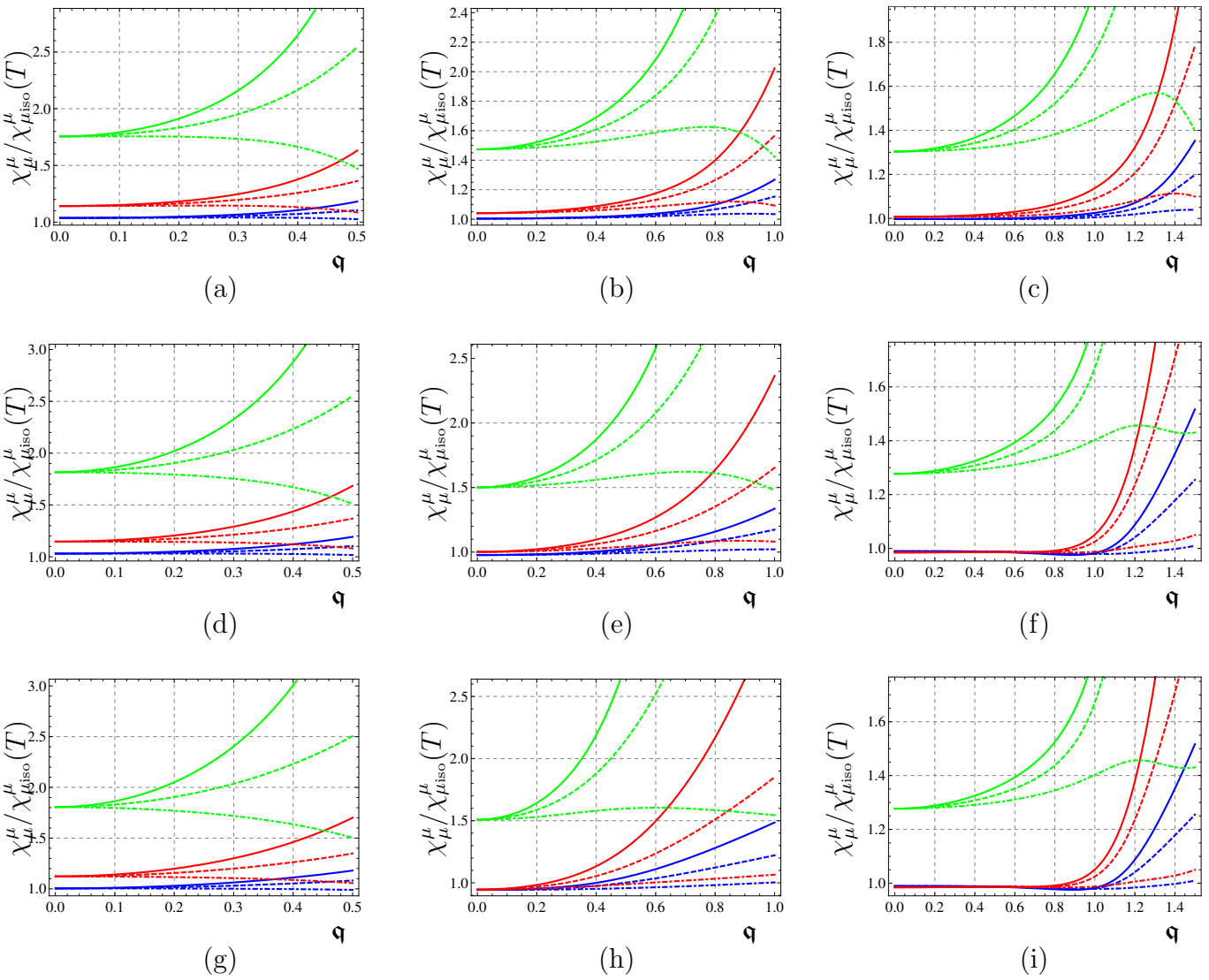

Figure 6.22: Plots of the spectral density χ^{μ}_{μ} normalized with respect to the isotropic result at fixed temperature $\chi^{\mu}_{\mu\mathrm{iso}}(T)$. Curves of different colors denote different values of a/T as follows a/T =4.41 (blue), 12.2 (red), 86 (green). The angles are $\vartheta = 0$ (solid), $\pi/4$ (dashed), $\pi/2$ (dash-dotted). Columns correspond to different values of $\mathfrak{w}$: from left to right it is $\mathfrak{w} = 0.5, 1, 1.5$. Rows correspond to different values of the quark mass: from top to bottom it is $\psi_{\mathrm{H}} = 0, 0.75, 0.941$. Then, for instance, (f) corresponds to $\mathfrak{w} = 1.5$, $\psi_{\mathrm{H}} = 0.75$.

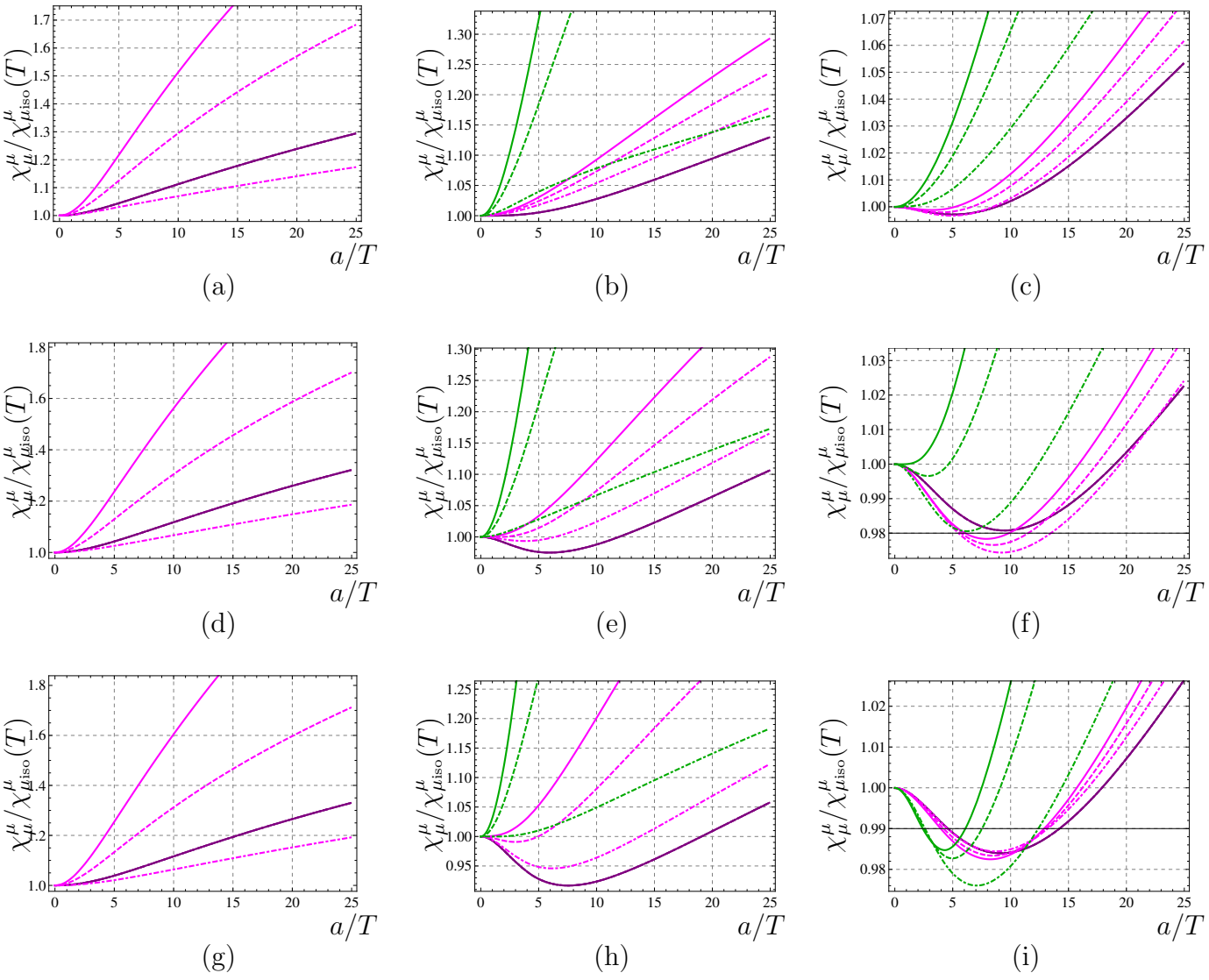

Figure 6.23: Plots of the spectral density χ^μ_μ normalized with respect to the isotropic result at fixed temperature $\chi^\mu_{\mu\mathrm{iso}}(T)$. Curves of different colors denote different values of $\mathfrak{q}$ as follows $\mathfrak{q}$ =0 (purple), 0.5 (magenta), 1 (green). The angles are $\vartheta = 0$ (solid), $\pi/4$ (dashed), $\pi/2$ (dash-dotted). Columns correspond to different values of $\mathfrak{w}$: from left to right it is $\mathfrak{w} = 0.5, 1, 1.5$. Rows correspond to different values of the quark mass: from top to bottom it is $\psi_{\mathrm{H}} = 0, 0.75, 0.941$. Then, for instance, (f) corresponds to $\mathfrak{w} = 1.5$, $\psi_{\mathrm{H}} = 0.75$.

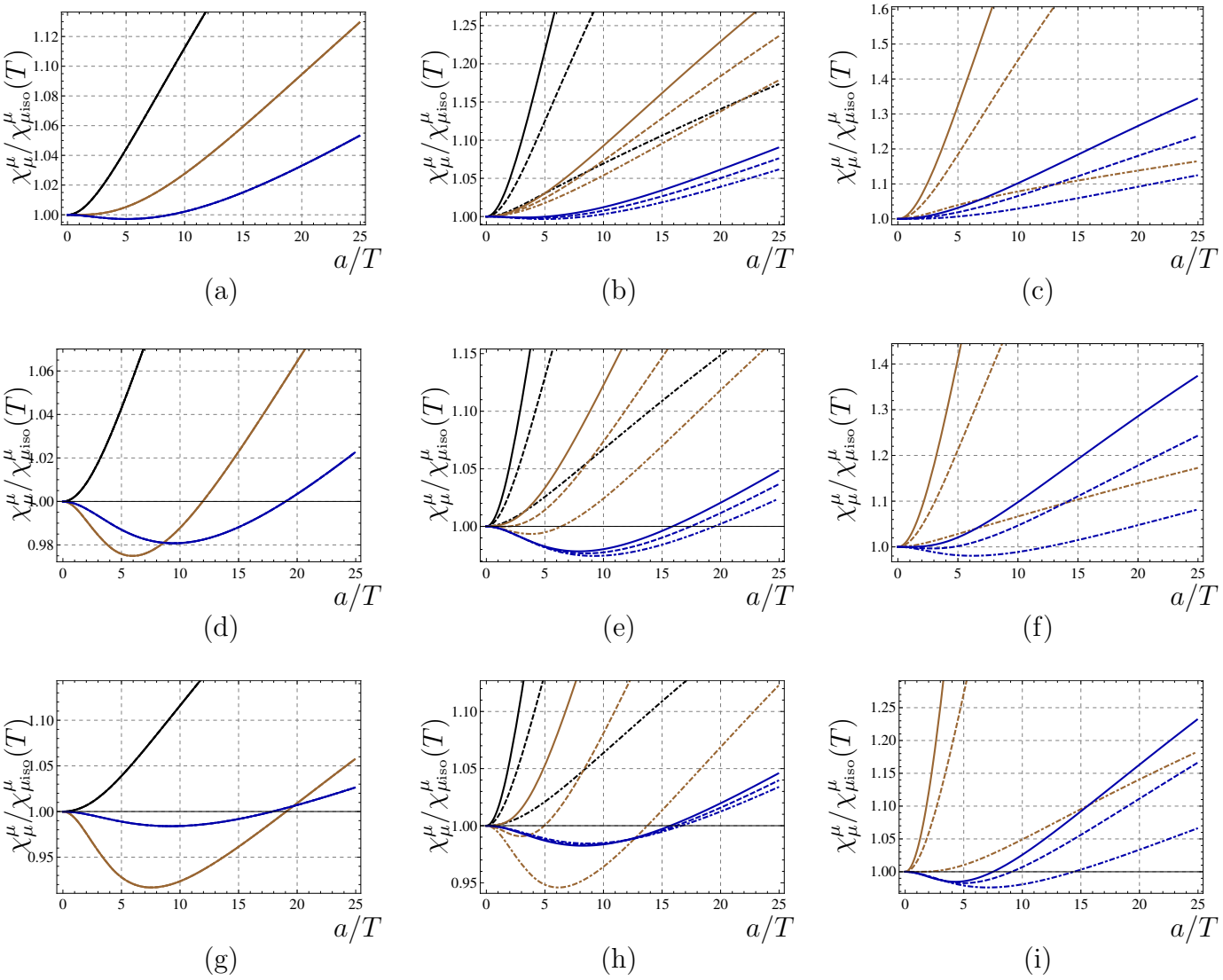

Figure 6.24: Plots of the trace of spectral density χ^{μ}_{μ} normalized with respect to the isotropic result at fixed temperature $\chi^{\mu}_{\mu\mathrm{iso}}(T)$. Curves of different colors denote different values of $\mathfrak{w}$ as follows $\mathfrak{w}$ =0.5 (black), 1 (brown), 1.5 (blue). The angles are $\vartheta = 0$ (solid), $\pi/4$ (dashed), $\pi/2$ (dash-dotted). Columns correspond to different values of $\mathfrak{q}$: from left to right it is $\mathfrak{q} = 0, 0.5, 1$. Rows correspond to different values of the quark mass: from top to bottom it is $\psi_{\mathrm{H}} = 0, 0.75, 0.941$. Then, for instance, (f) corresponds to $\mathfrak{q} = 1$, $\psi_{\mathrm{H}} = 0.75$.

Here we have allowed these fields to have a non vanishing mass, thus bringing the analysis closer to the real world experiments performed at RHIC and LHC. Secondly, we have considered the possibility of the plasma emitting these massive fundamental fields in pairs, which with a slight abuse of notation we have called 'dileptons', and we have computed their production rate.

The main results of our analysis may be summarized as follows. As for the photon production rate, we have seen that, in general, an anisotropic plasma glows brighter than its isotropic counterpart at the same temperature, both in the case of massless fundamental fields, as found in [27], and in the case of massive fundamental fields. Moreover, increasing the mass of these fields results in a decrease of the photon production rate and the DC conductivity of the plasma, as can be anticipated on general grounds. This also happens in the isotropic plasma considered in [107].

As for the dilepton production rate, the analysis is made more complicated by the presence of an extra parameter, the magnitude of the spatial part of the momentum, $\mathfrak{q}$. We have studied the total production rate, normalized with respect to an isotropic plasma at the same temperature, first as a function of the frequency $\mathfrak{w}$ for fixed values of $\mathfrak{q}$ (see Fig. 6.21), and then as a function of $\mathfrak{q}$ for fixed values of $\mathfrak{w}$ (see Fig. 6.22). For fixed values of $\mathfrak{q}$, we have seen that the anisotropic rate is higher than the isotropic counterpart at small frequencies (the larger the anisotropy the larger the deviation) and tends to the isotropic one at large frequencies. Moreover, the production for momenta along the anisotropic direction z is always larger than when the momenta are contained in the transverse xy-plane. Increasing the quark mass and/or $\mathfrak{q}$ increases the deviation from the corresponding isotropic results. For fixed values of $\mathfrak{w}$, we have found that for small spatial momentum the production rate does not depend on the quark mass nor on the angle, but only on the anisotropy and on $\mathfrak{w}$.

Production along the anisotropic direction is always an increasing function of $\mathfrak{q}$ (in the regime of values we have explored), whereas the production along the transverse plane can be increasing or decreasing, depending on the value of $\mathfrak{w}$.

The dependence of the dilepton production rate on the degree of anisotropy of the system is detailed in Figs. 6.23 and 6.24. We find that in general the anisotropic rate is larger than the isotropic one, but, if the quark mass and $\mathfrak{w}$ are large enough, there is a range of anisotropies where it might be smaller. The dependence on the angle is always monotonic, either increasing or decreasing depending on the specific quantity which is studied.

It is interesting to compare our results with what happens at weak coupling. Dilepton production in weakly coupled anisotropic plasmas has been studied in [128, 129], where an enhancement of the spectral functions with respect to the isotropic case has been reported, in agreement with the present work. However, dilepton production at weak coupling is suppressed along the forward direction [130], unlike what we observe in our strong coupling results shown in Figs. 6.21 to 6.24, where the suppression takes place along the transverse directions. In those works the dilepton production density per space-time volume and momentum space volume is computed using

$$\frac{dR^{\ell^+\ell^-}}{d^4P} = \int \frac{d\vec{p}_1}{(2\pi)^3}\frac{d\vec{p}_2}{(2\pi)^3} f_q(\vec{p}_1) f_{\bar{q}}(\vec{p}_2) v_{q\bar{q}} \sigma_{q\bar{q}}{}^{\ell^+\ell^-} \delta^{(4)}(P - p_1 - p_2), \tag{6.78}$$

where $f_{q,\bar{q}}$ are the phase space distribution functions of the quarks and antiquarks in the plasma, while $v_{q\bar{q}}$ and $\sigma_{q\bar{q}}{}^{\ell^+\ell^-}$ are their relative velocities and total cross section, respectively. The anisotropy of the plasma is modeled by including a parameter ξ

which encodes the type and strength of the anisotropy:

$$f_{q,\bar{q}}(\vec{p},\xi,p_{\rm hard}) = f_{q,\bar{q}}^{\rm iso}(\sqrt{\vec{p}^2+\xi\,(\vec{p}\cdot\hat{n})^2},p_{\rm hard}), \tag{6.79}$$

with $f_{q,\bar{q}}^{\rm iso}$ being the isotropic phase space distribution function, $p_{\rm hard}$ the hard momentum scale (which can be identified with the temperature T when $\xi = 0$), and $\hat{n}$ defining the anisotropic direction. What we provide in the present work is a non perturbative expression for the factors $f_{q,\bar{q}}(\vec{p},\xi,p_{\rm hard})$ used in the small coupling calculations. It is interesting to note that the enhancement of dilepton production appears to be a robust feature of anisotropic plasmas, which is present both at weak and strong coupling, unlike its dependence on the rapidity, which is sensitive to the strength of the coupling. Of course, the source of anisotropy in [128–130] is different than the one we have used in this paper, so that comparisons have to be taken with a grain of salt. Nonetheless, these comparisons certainly motivate further analysis.

As for the generality of our results, we observe that while we have used a very specific source of anisotropy, namely a non-trivial axion, we expect our results to be quite general. We observe in fact that the equations of motion for the gauge fields (6.23)-(6.26) are solely dependent on the metric and dilaton, meaning that any source of anisotropy that gives rise to similar metric and dilaton (and no Kalb-Ramond field) will produce qualitatively similar results for the photon and dilepton production rates. It would be interesting, nonetheless, to compute these quantities in as many anisotropic backgrounds as possible, including e.g. the one of [131, 132], to understand which features are really model-independent and therefore the most likely to be realized in the real-world QGP.

One thing we have left open is to determine what is the maximum value of $\psi_{\rm H}$

which results in a stable embedding of the flavor D7-branes. To address this question one needs to perform a careful analysis of the phase transition between the black hole and Minkowski embedding of the branes [121]. This requires comparing the free energy of the system in the two phases. To do that one would presumably need to perform from scratch the holographic renormalization process done in [133] for the axion-dilaton gravity, including this time also the DBI action for the branes. The UV limit ($\epsilon \to 0$) and the probe brane limit ($N_{\rm f}/N_{\rm c} \to 0$) do not in fact commute, in principle. This is because the dilaton of [10, 11] vanishes at the boundary and the introduction of additional D7-branes sources a dilaton that blows up before reaching the boundary; see e.g. [134]. This means that no matter how small $N_{\rm f}/N_{\rm c}$ is, it eventually overtakes the asymptotics and one cannot simply try to renormalize the D7-brane action in the fixed anisotropic background (as made evident by the fact that there do not seem to be enough counterterms to cancel all the divergences).

Appendix 6.A Solutions for $\mathbf{E_1}$ and $\mathbf{E_2}$

In this appendix we describe how to construct the two linearly independent solutions $\mathbf{E_1}$ and $\mathbf{E_2}$ used in subsection 6.3.3.

When solving the equation of motion for (6.72) near the horizon, we assume that the fields E_i behave like

$$E_i(u) = (u_{\rm H} - u)^{\nu} e_i(u)\,, \qquad i = x, z\,, \tag{6.80}$$

where $e_i(u)$ is some regular function at $u_{\rm H}$. We obtain that the exponent ν for both components of this vector is the same as that for the A_y mode, namely $\nu = \pm i\mathfrak{w}/2$.

After imposing the infalling wave condition (by choosing the minus sign for ν), the rest of the power series is linearly determined by the value of $\mathbf{E}$ at the horizon, $\mathbf{E}_{\rm H}$. Integrating from the horizon using any choice of such a vector $\mathbf{E}_{\rm H}$ would pick a particular solution to the equation of motion (6.73), which is linear. The general solution can then be written as a linear combination of any two linearly independent solutions $\mathbf{E}_a = (E_{x,a} \;\; E_{z,a})^{\rm T}$ and $\mathbf{E}_b = (E_{x,b} \;\; E_{z,b})^{\rm T}$. Using any two solutions $\mathbf{E}_a$ and $\mathbf{E}_b$ we can construct the matrix $\mathcal{E}$ that was needed in subsection 6.3.3:

$$\mathcal{E} \equiv (\mathbf{E_1} \;\; \mathbf{E_2}) = (\mathbf{E}_a \;\; \mathbf{E}_b)\mathcal{I}, \tag{6.81}$$

where the matrix $\mathcal{I}$ is given by

$$\mathcal{I} = (\mathbf{E}_a \;\; \mathbf{E}_b)^{-1}\big|_{\rm bdry}\,. \tag{6.82}$$

This makes $\mathcal{E}$ a matrix whose columns are solutions to (6.73) and that satisfies the desired property

$$\mathcal{E}\big|_{\rm bdry} = \begin{pmatrix} 1 & 0 \\ 0 & 1 \end{pmatrix}\,. \tag{6.83}$$

Using (6.81) and (6.76), we can write

$$\begin{aligned} \mathbf{E}_{\rm sol} &= (\mathbf{E}_a \;\; \mathbf{E}_b)\mathcal{I} \begin{pmatrix} E_x^{(0)} \\ E_z^{(0)} \end{pmatrix}\,, \\ \mathbf{E}'_{\rm sol} &= (\mathbf{E}'_a \;\; \mathbf{E}'_b)\mathcal{I} \begin{pmatrix} E_x^{(0)} \\ E_z^{(0)} \end{pmatrix}\,, \end{aligned} \tag{6.84}$$

and use it to write the boundary action (6.85) as

$$S_\epsilon = -2K_{\rm D7}\int dt\, d\vec{x}\left[(E_x^{(0)}\;\; E_z^{(0)})\mathcal{M}(\mathbf{E}'_a\;\; \mathbf{E}'_b)\mathcal{I}\begin{pmatrix} E_x^{(0)} \\ E_z^{(0)}\end{pmatrix}\right]_{u=\epsilon}, \tag{6.85}$$

where (6.83) was used. If we define the matrix

$$\mathcal{C} = \mathcal{M}(\mathbf{E}'_a\;\; \mathbf{E}'_b)\big|_{\rm bdry}\mathcal{I}\,, \tag{6.86}$$

we can see that

$$\begin{aligned}
\frac{\delta^2 S_\epsilon}{\delta E_x^{(0)2}} &= -4K_{\rm D7}\mathcal{C}^{xx}\,,\\
\frac{\delta^2 S_\epsilon}{\delta E_z^{(0)2}} &= -4K_{\rm D7}\mathcal{C}^{zz}\,,\\
\frac{\delta^2 S_\epsilon}{\delta E_z^{(0)}\delta E_x^{(0)}} &= -2K_{\rm D7}(\mathcal{C}^{zx}+\mathcal{C}^{xz})\,.
\end{aligned} \tag{6.87}$$

Using the technology developed in [127], we will now see how to obtain the imaginary parts of the components of $\mathcal{C}$ from u-independent quantities that can be computed at the horizon, so that all of the information of the boundary is encoded exclusively in $\mathcal{I}$. The first step is to show that the matrix $\tilde{\mathcal{C}} \equiv \mathcal{E}^\dagger\mathcal{M}\mathcal{E}' - \mathcal{E}^{\dagger\prime}\mathcal{M}\mathcal{E}$ is u-independent. To prove this, we start by multiplying (6.73) on the left by $\mathcal{M}$ to obtain

$$(\mathcal{M}\mathbf{E}')' + f(u)\mathcal{M}\mathbf{E} = 0, \tag{6.88}$$

which implies that the equation

$$(\mathcal{M}\mathcal{E}')' + f(u)\mathcal{M}\mathcal{E} = 0 \tag{6.89}$$

holds for the matrix $\mathcal{E}$. If we multiply (6.89) on the left by $\mathcal{E}^\dagger$ and subtract from it its transpose conjugate multiplied on the right by $\mathcal{E}$, we are left with

$$\mathcal{E}^\dagger\,(\mathcal{M}\mathcal{E}')' - \left(\mathcal{E}^{\dagger\prime}\mathcal{M}\right)'\mathcal{E} = 0\,. \tag{6.90}$$

Since

$$\mathcal{E}^\dagger\,(\mathcal{M}\mathcal{E}')' - \left(\mathcal{E}^{\dagger\prime}\mathcal{M}\right)'\mathcal{E} = \left(\mathcal{E}^\dagger\mathcal{M}\mathcal{E}' - \mathcal{E}^{\dagger\prime}\mathcal{M}\mathcal{E}\right)', \tag{6.91}$$

equation (6.90) proves that $\tilde{\mathcal{C}}$ is indeed u-independent. Notice now that, since $\mathcal{E}$ reduces to the identity matrix at the boundary, we have

$$\begin{aligned}
\tilde{\mathcal{C}} &= \left(\mathcal{E}^\dagger\mathcal{M}\mathcal{E}' - \mathcal{E}^{\dagger\prime}\mathcal{M}\mathcal{E}\right)\big|_{\text{H}} = \left(\mathcal{E}^\dagger\mathcal{M}\mathcal{E}' - \mathcal{E}^{\dagger\prime}\mathcal{M}\mathcal{E}\right)\big|_{\text{bdry}} \\
&= \left(\mathcal{M}\mathcal{E}' - \mathcal{E}^{\dagger\prime}\mathcal{M}\right)\big|_{\text{bdry}} \\
&= \mathcal{C} - \mathcal{C}^\dagger\,.
\end{aligned} \tag{6.92}$$

With (6.92) we can finally write

$$\tilde{\mathcal{C}}^{xx} = 2i\,\text{Im}\,\mathcal{C}^{xx}\,, \tag{6.93}$$

$$\tilde{\mathcal{C}}^{zz} = 2i\,\text{Im}\,\mathcal{C}^{zz}\,, \tag{6.94}$$

$$\tilde{\mathcal{C}}^{xz} + \tilde{\mathcal{C}}^{zx} = 2i\,\text{Im}\,(\mathcal{C}^{xz} + \mathcal{C}^{zx})\,, \tag{6.95}$$

which achieves the desired result of writing the imaginary parts of the correlators in

terms of $\mathcal{M}$ and $\mathcal{E}$ evaluated at the horizon, leaving only $\mathcal{I}$ to be evaluated at the boundary.

The final expression for $\chi_{(2)}$ can then be obtained by inserting (6.87) into (6.58), and using (6.93)-(6.95) to write

$$\chi_{(2)} = -4K_{\text{D7}} i \left((k_0^2 - q^2 \sin^2\vartheta)\tilde{\mathcal{C}}^{xx} + (k_0^2 - q^2\cos^2\vartheta)\tilde{\mathcal{C}}^{zz} - 2q^2 \cos\vartheta \sin\vartheta (\tilde{\mathcal{C}}^{xz} + \tilde{\mathcal{C}}^{zx}) \right). \tag{6.96}$$

Appendix 6.B Explicit near-boundary-expansion for the action (6.68)

We report here the explicit expression for the boundary action, eq. (6.68). The action reads

$$S_\epsilon = -2K_{\text{D7}} \int dt\, d\vec{x} \left[\mathcal{L}_1 + \mathcal{L}_2 + \mathcal{L}_3 + \ldots + O\left(u^2\right) \right]_{u=\epsilon} , \tag{6.97}$$

where

$$\begin{aligned}
\mathcal{L}_1 &= A_1\, E_x^{(0)2} + B_1\, E_z^{(0)2} + C_1\, E_x^{(0)}\, E_z^{(0)} , \\
\mathcal{L}_2 &= A_2\, E_x^{(0)}\, E_x^{(2)} + B_2\, E_x^{(0)}\, E_x^{(2)} + C_2\, E_x^{(0)}\, E_x^{(2)} + D_2\, E_x^{(0)}\, E_x^{(2)} , \\
\mathcal{L}_3 &= -\frac{\log u}{k_0^2} \left[(E_x^{(0)2} + E_z^{(0)2})\, k_0^2 + (E_x^{(0)} \cos\vartheta - E_z^{(0)} \sin\vartheta)^2\, q^2 \right] ,
\end{aligned} \tag{6.98}$$

and the various expansion coefficients are given by

$$\begin{aligned}
A_1 \;=\; & \frac{(q^2 - k_0^2)(2a^2 - 3(q^2 - k_0^2 + 8\psi_1^2))}{2(q^2 - k_0^2)(q^2 - k_0^2 + 8\psi_1^2) - 6a^2\, q^2 \cos^2\vartheta} + \\
& + \frac{6a^2 q^4 \cos^4\vartheta - q^2 \cos^2\vartheta [6(q^2 - k_0^2)(q^2 - k_0^2 + 8\psi_1^2) - a^2(4q^2 - 10k_0^2) + 3a^2 q^2 \cos^2\vartheta]}{4k_0^2 [(q^2 - k_0^2)(2a^2 - 3(q^2 - k_0^2 + 8\psi_1^2)) + 3a^2 q^2 \cos^2\vartheta]} ,
\end{aligned}$$

$$
\begin{aligned}
B_1 &= \frac{((5a^2+15q^2+48\psi_1^2-15k_0^2)(q^2-k_0^2)-3a^2q^2\cos^2\vartheta)\,(q^2\sin^2\vartheta-k_0^2)}{4k_0^2[(q^2-k_0^2)(2a^2-3(q^2-k_0^2+8\psi_1^2))+3a^2q^2\cos^2\vartheta]}\,,\\
C_1 &= \frac{q^2[3(7q^2-7k_0^2+32\psi_1^2)(q^2-k_0^2)-2a^2(q^2+2k_0^2)-6a^2q^2\cos 2\vartheta]\sin 2\vartheta}{8k_0^2((q^2-k_0^2)(2a^2-3(q^2-k_0^2+8\psi_1^2))+3a^2q^2\cos^2\vartheta)}\,,\\
A_2 &= \frac{2\cos\vartheta[3(q^2-2k_0^2)(q^2-k_0^2+8\psi_1^2)-a^2(5q^2-4k_0^2)-q^2(5a^2-3(q^2-k_0^2+8\psi_1^2))\cos 2\vartheta]}{k_0^2[6(q^2-k_0^2)(q^2+8\psi_1^2-k_0^2)-a^2(7q^2-4k_0^2)-3a^2q^2\cos 2\vartheta]}\,,\\
B_2 &= -\frac{48q^2\sin 2\vartheta}{k_0^2[6(q^2-k_0^2)(q^2-k_0^2+8\psi_1^2)-a^2(7q^2-4k_0^2)-3a^2q^2\cos 2\vartheta]}\,,\\
C_2 &= \frac{4q^2(5a^2-3(q^2-k_0^2+8\psi_1^2))\cos^2\vartheta\sin\vartheta}{k_0^2[6(q^2-k_0^2)(q^2-k_0^2+8\psi_1^2)-a^2(7q^2-4k_0^2)-3a^2q^2\cos 2\vartheta]}\,,\\
D_2 &= \frac{96(q^2\sin^2\vartheta-k_0^2)}{k_0^2[6(q^2-k_0^2)(q^2-k_0^2+8\psi_1^2)-a^2(7q^2-4k_0^2)-3a^2q^2\cos 2\vartheta]}\,.
\end{aligned}
\tag{6.99}
$$

Chapter 7

Chern-Simons diffusion rate from higher curvature gravity

In this chapter[1] we study the effects of higher curvature terms in the so-called Chern-Simons diffusion rate, $\Gamma_{\rm CS}$. This quantity parametrizes transitions among the different classical vacua of non-abelian gauge theories.

Gauge field configurations that produce transitions between different vacua through quantum tunneling are called instantons. The contribution of instantons to $\Gamma_{\rm CS}$ is exponentially suppressed in the coupling constant both at zero and finite temperature [135, 136].

At non-zero temperature classical thermal fluctuations can excite unstable gauge field configuration that give a contribution to $\Gamma_{\rm CS}$ upon decay. In the context of the electroweak theory, these excitations are called *sphalerons* [137–141]. Differently to the case of instantons, these classical thermal process are not exponentially suppressed

[1] In parts of this chapter we reproduce the text of arXiv:1403.2681v2 [hep-th], which is one of the papers published in this work.

[139].

In non-abelian gauge theories coupled to fundamental fermions a transition between different vacua is accompanied by flips of chirality that contributes to chiral anomalies in global symmetries. Because of that the Chern-Simons diffusion rate is relevant in the description of phenomena where there is a violation of the baryon number, like the baryogenesis process in the early universe [142, 143]. In the context of heavy-ion collisions a non-zero $\Gamma_{\rm CS}$ produces regions of net chirality that plays a role in the description of the so-called Chiral Magnetic Effect (CME) [144, 145].This effect is expected to take place in non-central heavy-ion collisions where the produced QGP has a magnetic field that acts in domains of non-zero net chirality producing an eletric current paralel to the magnetic field [146].

$\Gamma_{\rm CS}$ has been computed at weak coupling for a $SU(N_{\rm c})$ Yang-Mills theory and its parametric behavior has been found to be [147–150]

$$\Gamma_{\rm CS}^{\rm weak} \propto \lambda^5 \log\left(\frac{1}{\lambda}\right) T^4\,, \qquad \lambda \ll 1\,, \tag{7.1}$$

where $\lambda \equiv g_{\rm YM}^2 N_{\rm c}$ is the 't Hooft coupling and T is the temperature. Motivated by the strongly coupled nature of the quark-gluon plasma (QGP) produced in relativistic heavy ion collisions, this quantity has also been computed at strong coupling via holography in Einstein's gravity, with the result [103]

$$\Gamma_{\rm CS}^{\rm Einstein} = \frac{\lambda^2}{256\pi^3} T^4\,, \qquad N_{\rm c} \gg 1 \text{ and } \lambda \gg 1\,. \tag{7.2}$$

Other holographic studies of $\Gamma_{\rm CS}$ include [146, 151–153].

It is interesting to understand modifications to eq. (7.2) due to higher curvature

corrections. These are in principle dictated by string theory and would correspond, in the gauge theory, to corrections in $1/N_c$ and $1/\lambda$. In this chapter, we limit our attention to two specific types of higher curvature extensions of Einstein's gravity and compute the Chern-Simons diffusion rate in Gauss-Bonnet (GB) gravity [32–35][2] and in quasi-topological (QT) gravity [154].

These theories contain higher derivative terms, but are such that the equations of motion for the metric are still second order,[3] thus avoiding pathologies. It is not yet clear whether they emerge as a low energy solution of some string theory, so that their ultimate relevance is not yet established, but they do present very nice features. Besides being free of pathologies, as mentioned already, they possess a large class of black hole solutions and admit AdS boundary conditions, motivating their use in a 'bottom-up' approach to the study of strongly coupled plasmas.

Various physical observables relevant in the study of the QGP have already been computed from these theories. Notable examples are given by [156] and [155], where the shear viscosity to entropy ratio was studied. There it was found that higher derivative terms may violate the famous bound $\eta/s \geq 1/4\pi$ proposed in [9].

In the next section we made a brief introduction to the non-trivial topology of non-abelian gauge theories and introduce the concept of Chern-Simons number and give a precise definition to the Chern-Simons diffusion rate, $\Gamma_{\rm CS}$. In section 7.2 we introduce the higher curvatures gravity theories and present our results.

[2]For reviews of Gauss-Bonnet and, more generally, Lovelock gravity in the context of the AdS/CFT correspondence see e.g. [37, 38]. A nice overview of black hole solutions can be found in [41].

[3]For quasi-topological gravity this is true for the linearized equations in an AdS_5 background.

7.1 Topology of non-abelian gauge theories

A remarkable property of non-abelian gauge theories is the existence of a infinite number of degenerate classical vacua in these theories. In this section[4] we show that this is due to the non-trivial topology of these theories.

Consider a $(3+1)$-dimensional classical Yang-Mills theory with gauge group G and action

$$S_{\rm YM} = -\frac{1}{2}\int d^4x \,{\rm Tr}\left(F_{\mu\nu}F^{\mu\nu}\right) \tag{7.3}$$

where $F_{\mu\nu} = \partial_\mu A_\nu - \partial_\nu A_\mu + g_{\rm YM}\,[A_\mu, A_\nu]$ is the field strength and $A_\mu = A^a_\mu T^a$ is the gauge field, with T^a being the generators of G. Under gauge transformations $U(\mathbf{x},t) \in G$ these fields transform as

$$A_\mu \quad \to A'_\mu = U\,A_\mu\,U^\dagger + (\partial_\mu U)U^\dagger \tag{7.4}$$

$$F_{\mu\nu} \quad \to F'_{\mu\nu} = U\,F_{\mu\nu}U^\dagger. \tag{7.5}$$

The minimum energy of this theory is zero and is achieved by $F_{\mu\nu} = 0$. This is consistent with $A_\mu = 0$ and with gauge transformations of it. Then, the zero energy configuratons must be pure gauge

$$A'_\mu = \big(\partial_\mu U(\mathbf{x},t)\big)U^\dagger(\mathbf{x},t) \tag{7.6}$$

Let us now consider time-independent gauge transformation $U(\mathbf{x})$. For this transformations

$$A'_0 = 0, \quad \partial_0 A'_j = 0, \quad A'_j = \big(\partial_j U(\mathbf{x})\big)U^\dagger(\mathbf{x}). \tag{7.7}$$

[4]This section is based on the chapter 5 of [157].

This time-independent transformation define a map $U(\mathbf{x}) : \mathbb{R}^3 \to G$. If we further require that $U(\mathbf{x}) \to 1$ as $\mathbf{x} \to \infty$, the three-dimensional space $\mathbb{R}^3$ becomes topologically equivalent to a three-sphere S^3 for this class of transformations and we can write $U(\mathbf{x}) : S^3 \to G$.

The classification of the possible maps between S^3 and G reveal the non-trivial topological structure of Yang-Mills theories. From the mathematical point of view the gauge transformation $U(\mathbf{x})$ provides a map between two topological spaces, the 3-sphere and G. These maps can be classified in terms of *homotopy groups*, which record information about the topology (shapes and holes) of topological spaces.

The n-th homotopy group $\Pi_n(X)$ can be defined as follows. Consider the maps between the n-sphere and some topological space X. These maps can be collected into equivalence classes, called *homotopy classes*. Two maps are in the same equivalence class if they can be continuously deformed into each other. Maps in the same equivalence class are said to be *homotopic*. These homotopy classes form a group, which is the n-th homotopy group $\Pi_n(X)$.

Therefore, the gauge transformations $U(\mathbf{x})$ that can be continuously deformed into each other define a homotopy class. The corresponding homotopy group is $\Pi_3(G)$.

Consider two pure gauge configurations A'_μ and A''_μ obtained from $A_\mu = 0$ by the gauge transformations U' and U'', respectively. If U' and U'' belong to the same homotopy class, they can be continuously deformed into each other and, therefore, there is a gauge transformation connecting A'_μ and A''_μ. These gauge transformations are usually called *small gauge transformations* and they relate two different representations of the same classical vacua.

However, if U' and U'' belong to different homotopy classes, the gauge transformations connecting A'_μ and A''_μ are called *large gauge transformations*, and can be

viewed as relating two different classical vacua. As local gauge transformations cannot connect distinct physical situations, the presence of degenerate classical vacua leads to the notion of θ-vaccum, in which the true vaccum of the theory is given by a superposition of the classical vacua states [157].

For simplicity, let us consider the case where $G = SU(2)$. As $SU(2)$ is diffeomorphic to S^3 the above gauge transformations define a set of maps $U(\mathbf{x}) : S^3 \to S^3$. These maps can be classified by the so-called *winding number*, which counts the number of times the S^3 of the group space is swept as the S^3 of the coordinate space is swept once. It turns out that the winding number can be $n = 0, \pm 1, \pm 2, ...$, and so on. The negative values are allowed because the above maps are orientable [Shifman, 15]. This is mathematically expressed as $\Pi_3(SU(2)) = \Pi_3(S^3) = \mathbb{Z}$, where $\mathbb{Z}$ represents the set of integer numbers. Morover, one can show that $\Pi_3(SU(N)) = \mathbb{Z}$, for all N.

The above classification of the maps $U(\mathbf{x}) : S^3 \to SU(N)$ in terms of interger numbers is basically telling us that there is a non-trivial topology in the space of gauge field configurations. One can say that there is a "hole" in the space of gauge fields with non-contractible loops winding around this hole [Shifman].

To identify the degree of freedom corresponding to motion around this "hole" one defines the *Chern-Simons current*

$$K^{\mu} = 2\,\varepsilon^{\mu\nu\alpha\beta}\Big(A^a_{\nu}\partial_{\alpha}A^a_{\beta} + \frac{g_{\rm YM}}{3}f^{abc}A^a_{\nu}A^b_{\alpha}A^c_{\beta}\Big) \tag{7.8}$$

From it one defines the *Chern-Simons number*

$$N_{CS} = \frac{g^2_{\rm YM}}{32\pi^2}\int K_0(x)d^3\mathbf{x} \tag{7.9}$$

One can show that for pure gauge configurations $A'_\mu = \big(\partial_\mu U(\mathbf{x})\big)U^\dagger(\mathbf{x})$, obtained from a gauge transformation $U(\mathbf{x})$ with winding number n, the Chern-Simons number is equal to the winding number

$$N_{CS} = n, \quad \text{(winding number)} \tag{7.10}$$

This shows us the existence of a "direction" in the space of fields that has the topology of a circle, and N_{CS} counts the number of loops around this circle. Because of that N_{CS} can be used to classify different classical vacua states.

An analogy that helps to understand the hole of N_{CS} in Yang-Mills theories is the motion of a particle in a vertically oriented circle and in the presence of a gravitational field. Let us say that the position of the particle is specified by an angle θ, that is zero at the bottom of the circle. Classically, a particle with zero energy will stay at rest at the bottom of the circle, at $\theta = 0$. Quantum mechanically, zero-energy oscilations allows the particle to go around the circle via quantum tunneling, reaching the angular position $\theta = \pm 2\pi$. Of course these angular positions corresponds to the same physical point of $\theta = 0$, but there was a motion around the circle, and this is recorded by N_{CS}.

A possible way to represent these situation is to cut this circle and map it many times onto a straight line. If the line give the value of the Chern-Simons number, the potential energy of the system $V(N_{CS})$ must be zero for interger values of N_{CS}, as represented in Fig. 7.1.

A variation in the Chern-Simons number N_{CS} is given by

$$\Delta N_{\rm CS} = \frac{g^2_{\rm YM}}{8\pi^2}\int d^4x\, {\rm Tr} F\wedge F \,= \frac{g^2_{\rm YM}}{16\pi^2}\int d^4x\, {\rm Tr} F^{\mu\nu}\,\tilde{F}_{\mu\nu}\,, \tag{7.11}$$

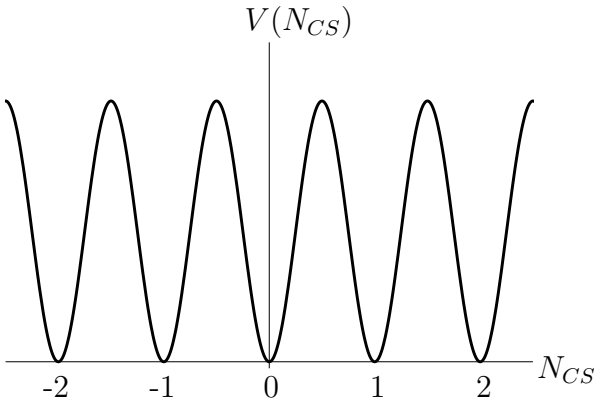

Figure 7.1: Schematic representation of the vacuum of non-abelian gauge theories. The Chern-Simons number, N_{CS}, labels the different classical vacua states.

where

$$\tilde{F}_{\mu\nu} = \frac{1}{2}\varepsilon_{\mu\nu\alpha\beta}F^{\alpha\beta} \tag{7.12}$$

We thus conclude that a variation in the Chern-Simons number is possible if add to the Yang-Mills lagrangian a θ-term

$$\mathcal{L}_{\rm YM} \to \mathcal{L}_{\rm YM} + \mathcal{L}_\theta \,. \tag{7.13}$$

where

$$\mathcal{L}_\theta = \theta \, \frac{g^2_{\rm YM}}{16\pi^2} \, {\rm Tr} F^{\mu\nu} \, \tilde{F}_{\mu\nu} \,, \tag{7.14}$$

The topological nature of the θ-term is evidenciated by the fact that it is a full derivative. Indeed, one can show that $\mathcal{L}_\theta \propto \partial_\mu K^\mu$, where K^μ is the Chern-Simons current. Threfore, this term will have an effect on the action only for gauge field configurations with non-trivial topology.

In Euclidean time, a gauge field configuration that interpolates between two vacua is called an *instanton*. Such configurations represents a quantum tunneling event

between two vacua and they produce a change in the Chern-Simons number.

At finite temperature, thermal fluctuations can produce an unstable gauge field configuration that has energy equal to the height of the barrier of potential energy that separates two classical vacua. Such a solution is called an *sphaleron*[5]. A sphaleron that interpolates between the classical vacua with Chern-Simons number equal to 0 and 1 has $N_{CS} = 1/2$. Just like the instantons, the sphalerons also produce a change in the Chern-Simons number.

The rate of change of $N_{\rm CS}$ per unit volume V and unit time t is a transport coefficient called the *Chern-Simons diffusion rate*, $\Gamma_{\rm CS}$, which is defined as

$$\Gamma_{\rm CS} \equiv \frac{\langle \Delta N_{\rm CS}^2 \rangle}{V \cdot t} = \left(\frac{g_{\rm YM}^2}{8\pi^2}\right)^2 \int d^4x \, \langle \mathcal{O}(x)\, \mathcal{O}(0) \rangle \,, \qquad \mathcal{O}(x) = ({\rm Tr} F \wedge F)(x) \,. \quad (7.15)$$

The "diffusion" that appears in the name of this coefficient occurs in the space of solutions, not in the space-time. The excitations (both thermal and quantum) of gauge field configurations connecting different classical vacua can be viewed as a propagation or diffusion in the space of fields of the theory.

7.2 Gravity setup and results

To study $\Gamma_{\rm CS}$ holographically we consider gravity in 5-dimensions with a negative cosmological constant and the inclusion of the GB and QT terms, with action given by

$$S = \frac{1}{16\pi G_5} \int d^5x \sqrt{-g} \left[R + \frac{12}{L^2} + \frac{L^2}{2} \lambda_{\rm GB}\, \mathcal{L}_2 + L^4 \mu\, \Xi_3 \right] + S_{\rm bdry} \,. \quad (7.16)$$

[5]This name cames from the Greek adjective *sphaleros* that means unstable, ready to fall.

Here L is a length scale, later to be related with the AdS radius, $\lambda_{\rm GB}$ and μ are two dimensionless couplings, the quadratic term $\mathcal{L}_2 = R^2 - 4R_{mn}R^{mn} + R_{mnrs}R^{mnrs}$ is the Euler density of GB gravity, and Ξ_3 is the cubic term of QT gravity, whose explicit expression [154] won't be needed in the following. $S_{\rm bdry}$ is a boundary term that makes the variational problem well posed. Remarkably, this action admits[6] planar AdS black hole solutions, given by [32–35, 154]

$$ds^2 = \frac{L^2}{z^2}\left(-a^2 f(z)dt^2 + \frac{dz^2}{f(z)} + \sum_{i=1}^{3} dx_i^2\right), \tag{7.17}$$

where $x^\mu = (t,\, x_i)$ are the gauge theory coordinates, z is the radial AdS coordinate, a is a constant, and $f(z)$ is a function that vanishes at the horizon, $z = z_{\rm H}$, and which will be given below. The AdS boundary is located at $z = 0$. Requiring $c = 1$ in the boundary theory fixes $a = f(0)^{-1/2}$. The black hole temperature is given by $T = a/\pi z_{\rm H}$.

In the AdS/CFT correspondence, the operator $\mathcal{O}(x)$ of eq. (7.15) is coupled to a bulk scalar field, $\chi(z, x^\mu)$, whose background value is zero in the present case. The (retarded) 2-point function of $\mathcal{O}(x)$ can be obtained by computing the fluctuations of this field, $\delta\chi(z, x^\mu)$, subject to infalling boundary conditions at the horizon and plugging the result into the corresponding boundary action, minimally coupled to eq. (7.16). This procedure is detailed in [103], where, as a first step, the definition (7.15) is rewritten in Fourier space as

$$\Gamma_{\rm CS} = -\left(\frac{g^2_{\rm YM}}{8\pi^2}\right)^2 \lim_{\omega\to 0}\frac{2T}{\omega}\,{\rm Im}\, G^{\rm R}(\omega, \mathbf{0})\,. \tag{7.18}$$

[6] This is true for appropriate values of the couplings. For example, it must be $\lambda_{\rm GB} < \frac{1}{4}$.

$G^{\rm R}(\omega,\mathbf{0})$ is the retarded Green's function associated to $\mathcal{O}(x)$, evaluated at zero spatial momentum. It can be calculated as

$$G^{\rm R}(\omega,\mathbf{0}) = \frac{N_{\rm c}^2}{8\pi^2 L^3}\sqrt{-g}g^{zz}f_{-k}(z)\partial_z f_k(z)\Big|_{z\to 0}\,, \tag{7.19}$$

where $f_k(z)$ is the Fourier mode of the scalar field fluctuation

$$\delta\chi(z,x^\mu) = \int \frac{d^4k}{(2\pi)^4}e^{ik\cdot x}f_k(z)\,, \tag{7.20}$$

which can be obtained as a solution of the equation

$$\frac{1}{\sqrt{-g}}\partial_z(\sqrt{-g}g^{zz}\partial_z f_k(z)) - g^{\mu\nu}k_\mu k_\nu f_k(z) = 0\,, \qquad k_\mu = (-\omega,\mathbf{k})\,. \tag{7.21}$$

It is convenient to work with the dimensionless coordinate u defined as $u = z^2/z_{\rm H}^2$, in terms of which we have (setting already $\mathbf{k}=0$)

$$\partial_u^2 f_k(u) + \left[\partial_u \ln\frac{f(u)}{u}\right]\partial_u f_k(u) + \frac{\mathfrak{w}^2}{uf(u)^2}f_k(u) = 0\,, \tag{7.22}$$

where we have defined for convenience the dimensionless frequency $\mathfrak{w}\equiv\omega/2\pi T$.

The 'blackening factor' $f(u)$ is defined implicitly through the cubic equation [154]

$$1 - f(u) + \lambda_{\rm GB}\,f(u)^2 + \mu\,f(u)^3 = u^2\,. \tag{7.23}$$

Out of the three solutions, we select the one which is regular when $\mu\to 0$ and reproduces the expression $f(u) = \left(1-\sqrt{1-4\lambda_{\rm GB}\,(1-u^2)}\right)/2\lambda_{\rm GB}$ of the GB case [39, 41].[7] We recall that the couplings $\lambda_{\rm GB}$ and μ are constrained by requirements of

[7] The GB case has also another solution for $f(u)$, with a plus sign in front of the square root,

unitarity, causality, and positivity of energy fluxes in the dual conformal field theory. It turns out that it must be [155][8]

$$-0.36 \lesssim \lambda_{\rm GB} \lesssim 0.12\,, \qquad |\mu| \lesssim 0.001\,. \tag{7.24}$$

In view of this, we will solve eqs. (7.22) and (7.23) exactly in $\lambda_{\rm GB}$, but only approximately to first order in small μ. This allows us to we write explicitly

$$\begin{aligned} f(u) \;=\; & \frac{1}{2\lambda_{\rm GB}}\left(1-\sqrt{1-4\lambda_{\rm GB}\,(1-u^2)}\right)+ \\ & +\frac{1-\sqrt{1-4\lambda_{\rm GB}\,(1-u^2)}-\lambda_{\rm GB}(1-u^2)\left(3-\sqrt{1-4\lambda_{\rm GB}\,(1-u^2)}\right)}{2\lambda_{\rm GB}^3\sqrt{1-4\lambda_{\rm GB}\,(1-u^2)}}\mu+O(\mu^2)\,. \end{aligned} \tag{7.25}$$

There is no known analytic solution to eq. (7.22), but this is not needed anyway, since only the small frequency behavior $\mathfrak{w}\to 0$ of the Green's function enters in the Chern-Simons diffusion rate. We can then make the following Ansatz:

$$f_k(u) = f(u)^{-i\frac{\mathfrak{w}}{2}}\left(F_0(u)+\mathfrak{w}\left(F_1^{(0)}(u)+\mu\,F_1^{(1)}(u)+O(\mu^2)\right)+O(\mathfrak{w}^2)\right)\,. \tag{7.26}$$

Here F_0, $F_1^{(0)}$, and $F_1^{(1)}$ are regular functions at the horizon, $u=1$. In fact, we can choose them to be such that

$$F_0(1)=1\,, \qquad F_1^{(0)}(1)=\frac{i}{2}\log 2\,, \qquad F_1^{(1)}(1)=0\,. \tag{7.27}$$

which is however known to be unstable and to contain ghosts; see e.g. [37, 38].

[8]The constraints on $\lambda_{\rm GB}$ and μ are not independent; see Fig. 1 of [155]. In particular, in the case of pure GB gravity ($\mu=0$), the allowed range of $\lambda_{\rm GB}$ is $-7/36\le\lambda_{\rm GB}\le 9/100$. For $\mu<0$ there are instabilities in the graviton tensor channel for momenta above a certain critical value [155]. Since $\Gamma_{\rm CS}$ is computed at $\mathbf{k}=0$ we do not worry about this here.

The exponent of $f(u)$ has been chosen to give infalling boundary conditions at the horizon, which correspond to having a retarded Green's function in the boundary. Expanding around $u = 1$, one finds in fact that $f_k(u) \sim (1-u)^{-i\frac{\mathfrak{w}}{2}}(1 + O(\mathfrak{w}^2))$. Plugging the Ansatz above in eq. (7.22), it is easy[9] to find the following solutions which respect the boundary conditions above:

$$\begin{aligned} F_0(u) &= 1\,, \qquad F_1^{(0)}(u) = \frac{i}{2}\left(1 + \log 2 - \sqrt{1 - 4\lambda_{\rm GB}(1-u^2)}\right)\,, \\ F_1^{(1)}(u) &= -\frac{i}{8\lambda_{\rm GB}^2}\frac{1 - 2\lambda_{\rm GB}(1-u^2) - 8\lambda_{\rm GB}^2(1-u^2)^2 - \sqrt{1-4\lambda_{\rm GB}(1-u^2)}}{1-4\lambda_{\rm GB}(1-u^2)} \end{aligned} \tag{7.28}$$

Using eqs. (7.18) and (7.19), and keeping only terms linear in μ, we finally arrive at

$$\Gamma_{\rm CS} = \Gamma_{\rm CS}^{\rm Einstein}\left(H^{(0)}(\lambda_{\rm GB}) + \mu\, H^{(1)}(\lambda_{\rm GB}) + O(\mu^2)\right)\,, \tag{7.29}$$

with

$$\begin{aligned} H^{(0)}(\lambda_{\rm GB}) &= \left(\frac{1-\sqrt{1-4\lambda_{\rm GB}}}{2\lambda_{\rm GB}}\right)^{3/2}\,, \\ H^{(1)}(\lambda_{\rm GB}) &= \frac{3}{4}\sqrt{\frac{1-\sqrt{1-4\lambda_{\rm GB}}}{2\lambda_{\rm GB}^7\,(1-4\lambda_{\rm GB})}}\left(1 - \sqrt{1-4\lambda_{\rm GB}} - \lambda_{\rm GB}\left(3 - \sqrt{1-4\lambda_{\rm GB}}\right)\right) \end{aligned} \tag{7.30}$$

We stress that this result is fully non-perturbative in $\lambda_{\rm GB}$, at any order in μ. We see that the Chern-Simons diffusion rate in GB and QT gravity is a rescaling of the result in eq. (7.2). The dependence on T is dictated by conformal invariance: $\Gamma_{\rm CS}$ must be proportional to T^4 for dimensional reasons, with the factor of proportionality depending solely on the dimensionless parameters, which are $\lambda_{\rm GB}$ and μ.[10] Fig. 7.2(Left)

[9] The equations simplify if one changes coordinates $u \to \sqrt{1-4\lambda_{\rm GB}(1-u^2)}$ in intermediate steps.

[10] An interesting context where this does not happen is Improved Holographic QCD [146], where the absence of conformal symmetry makes $\Gamma_{\rm CS}/\Gamma_{\rm CS}^{\rm Einstein}$ depend on T.

shows the two terms in $\Gamma_{\rm CS}$ as functions of $\lambda_{\rm GB}$. Both terms are finite, monotonically increasing and positive in the allowed range of $\lambda_{\rm GB}$, given in eq. (7.24). The GB contribution can be either smaller or larger than 1, depending on the sign of $\lambda_{\rm GB}$, and the corresponding Chern-Simons diffusion rate can be either smaller or larger than the result obtained from Einstein's gravity, but, in the allowed range of eq. (7.24), cannot get arbitrarily small.

Fig. 7.2(Right) displays the two contributions $H^{(0)}$ and $H^{(1)}$ as functions of the shear viscosity over entropy ratio, which is given by [155, 156]

$$\frac{\eta}{s} = \frac{1}{4\pi}\left[1 - 4\lambda_{\rm GB} - 36\mu(9 - 64\lambda_{\rm GB} + 128\lambda_{\rm GB}^2)\right] + O(\mu^2)\,. \tag{7.31}$$

We observe that $\Gamma_{\rm CS}$ for GB gravity decreases as η/s is increased (for QT gravity this depends on the sign of μ, whose contribution is however suppressed). It would be very interesting to understand if there is a microscopic interpretation of this behavior.

7.3 Discussion

Understanding corrections away from the infinite $N_{\rm c}$ and infinite λ limit is clearly of the utmost importance in order to make contact with realistic systems. Unfortunately, loop and stringy corrections are in general hard to compute, so that our philosophy in this note has been to consider two simple extensions of Einstein's gravity with higher curvature terms, just to gain a qualitative understanding of how such terms might modify the computation of an important observable in strongly coupled non-Abelian

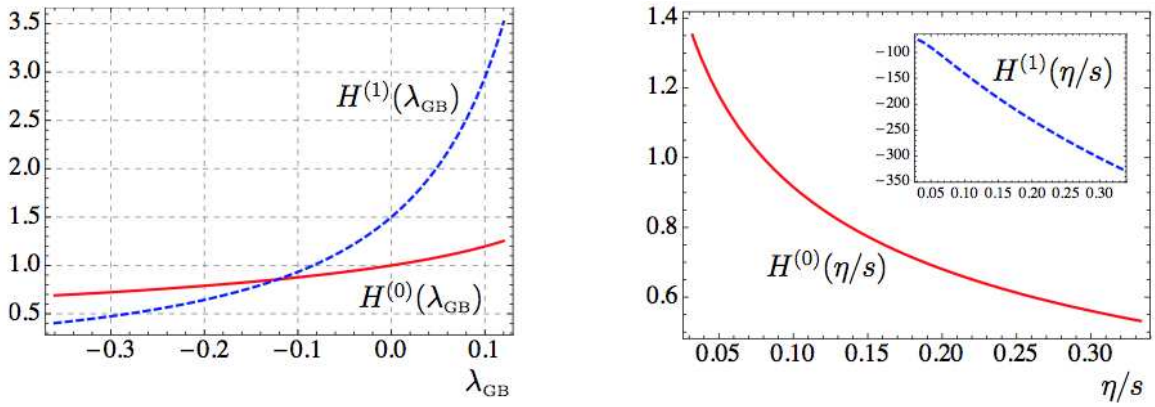

Figure 7.2: (Left) The factors $H^{(0)}(\lambda_{\rm GB})$ (red, solid curve) and $H^{(1)}(\lambda_{\rm GB})$ (blue, dashed curve) as functions of $\lambda_{\rm GB}$. (Right) The same factors as functions of η/s. The plots are exact in $\lambda_{\rm GB}$ and in η/s, whose allowed ranges are obtained from eqs. (7.24) and (7.31). In these ranges, the corrections to eq. (7.2) are finite and cannot make the diffusion rate arbitrarily small.

plasmas.[11] This is similar in spirit to what has been done, in [156] for GB gravity and in [155] for QT gravity, for the shear viscosity over entropy ratio, which turned out to be lower in these theories than what it is in Einstein's gravity. In [156] it was in fact found to be $\eta/s = (1 - 4\lambda_{\rm GB})/4\pi$ and in [155] to be $\eta/s \gtrsim 0.4140/4\pi$, both cases in violation of the bound proposed in [9].[12] It is interesting to observe that a subsequent computation [165] in a setting [166–168] where α'-corrections can be solved exactly yielded the same qualitative behavior, with the bound $\eta/s \geq 1/4\pi$ being violated.

The presence of the new gravitational couplings $\lambda_{\rm GB}$ and μ corresponds on the boundary to considering conformal field theories which are more generic than the ones usually studied. In particular, a non-vanishing $\lambda_{\rm GB}$ results in having independent

[11] Besides making things more realistic, the study of how higher derivative terms affect the computation of gauge theory observables might also be useful to put constraints on the string landscape, e.g. by excluding ranges of parameters that would produce pathologies in the dual gauge theory, as suggested in [40].

[12] See also, for instance, [158–163] and [10, 11, 13] for violations of the bound in an anisotropic plasma. A status report of the Kovtun-Son-Starinets conjecture can be found in [164].

central charges $a \neq c$ [169–171], whereas a non-vanishing μ also results in the breaking of supersymmetry [154]. For these reasons, these theories, even if they turn out to be just toy models without a UV completion, may still be useful in exploring situations which require an understanding of holography in non-trivial backgrounds.

Chapter 8

Anisotropic black branes in GB gravity theory

In this chapter[1] we consider a GB correction to Einstein-Hilbert gravity in five dimensions with a negative cosmological constant and a coupling to an axion-dilaton field. It is not clear whether this system might be obtained by some string theory compactification, so that our philosophy in this work is 'bottom-up'.

The first result of our analysis is a new solution of the equations of motion representing a black brane with a translationally invariant but anisotropic horizon. The force responsible for keeping the horizon in an anisotropic state is furnished by the axion field, which we take to have a fixed profile in the radial coordinate but to depend linearly in one of the horizon coordinates. This is similar to what has been done in [12] and later in [10, 11]. This new solution is interesting from a purely General Relativity point of view, for it opens up the possibility to study the thermodynam-

[1] In parts of this chapter we reproduce the text of arXiv:1411.5964v2 [hep-th] and 1510.03774v3 [hep-th], which are papers published in this work.

ics of a black brane which depends on several parameters (the temperature, the GB coupling and an anisotropy parameter), presumably giving rise to a rich phase space.

The GB coupling that we introduce here corresponds to allowing for different central charges, $a \neq c$, in the gauge theory [169–171]. We compute these two central charges for our particular solution, verifying that they are indeed different. On general grounds, looking at how higher derivative terms affect physical observables on the gauge theory might also be useful to constrain the string landscape, e.g. by excluding regions of parameters that would result in pathologies, as advocated for example in [40, 175]. As a final, concrete application of our geometry we compute the shear viscosity over entropy density ratio (in a few, equivalent ways), the eletric conductivities, the drag force, the jet quenching parameter, the quarkonium static potential and the photon production rate for the corresponding gauge theory plasma.

This chapter is organized as follows. In Sec. 8.1 we present our solution and compute its temperature and entropy density. In Sec. 8.2 we calculate the central charges a and c and we verify that $a \neq c$. In Sec. 8.3 we present the stress energy tensor of our solution and discuss the various features of energy density and pressures. In Sec. 8.4 we use the solution as a model for a strongly coupled anisotropic plasma and compute various physical observables. We finally discuss our results and outline possible future extensions of our work in Sec. 8.5. A series of appendices contains some of the more technical details of our computations, like the explicit derivation of the solution and the derivation of the shear viscosity tensor using alternative methods.

8.1 Action and solution

We are interested in five-dimensional gravity with a negative cosmological constant and the inclusion of a Gauss-Bonnet term, which we also couple to an axion-dilaton system in the following way

$$S = \frac{1}{16\pi G}\int d^5x\,\sqrt{-g}\left[R + \frac{12}{\ell^2} - \frac{1}{2}(\partial\phi)^2 - \frac{e^{2\phi}}{2}(\partial\chi)^2 + \frac{\ell^2}{2}\lambda_{\rm GB}\mathcal{L}_{\rm GB}\right] + S_{\rm GH}\,. \quad (8.1)$$

The scalar fields ϕ and χ are the dilaton and axion, respectively, $\lambda_{\rm GB}$ is the (dimensionless) Gauss-Bonnet coupling and

$$\mathcal{L}_{\rm GB} = R^2 - 4R_{mn}R^{mn} + R_{mnrs}R^{mnrs} \quad (8.2)$$

is the Gauss-Bonnet term. ℓ is a parameter with dimensions of length that we set to one in what follows, without loss of generality. We use the Latin indices $m, n, \ldots$ for the five-dimensional coordinates (t, x, y, z, u), with u being the radial coordinate. The term $S_{\rm GH}$ is the usual Gibbons-Hawking term, necessary to render the variational problem well posed. When $\lambda_{\rm GB} = 0$ the action above can be obtained from type IIB superstrings [10, 11], but this is no longer true when the Gauss-Bonnet coupling is turned on. In fact, it is not clear whether (8.1) can be obtained from any string theory compactification, so that our point of view in the present paper is 'bottom-up', as already discussed in the Introduction.

The field equations for the metric resulting from the action above are given by

$$R_{mn} - \frac{1}{2}g_{mn}R + \frac{\lambda_{\rm GB}}{2}\delta\mathcal{L}_{{\rm GB}mn} = \frac{1}{2}\partial_m\phi\,\partial_n\phi + \frac{1}{2}e^{2\phi}\partial_m\chi\,\partial_n\chi - \frac{g_{mn}}{4}\left[(\partial\phi)^2 + e^{2\phi}(\partial\chi)^2 - 12\right]\,, \quad (8.3)$$

where

$$\delta\mathcal{L}_{\mathrm{GB}mn} = -\frac{g_{mn}}{2}\mathcal{L}_{\mathrm{GB}} - 4R_m{}^r R_{rn} + 2R_{mn}R - 4R^{rs}R_{mrns} + 2R_m{}^{rst}R_{nrst} \tag{8.4}$$

is the variation of the Gauss-Bonnet term. The equations for the dilaton and axion read instead

$$\partial_m(\sqrt{-g}g^{mn}\partial_n\phi) = \sqrt{-g}e^{2\phi}(\partial\chi)^2\,, \qquad \partial_m(\sqrt{-g}e^{2\phi}g^{mn}\partial_n\chi) = 0\,. \tag{8.5}$$

We want to obtain a solution which displays a spatial anisotropy. This is achieved by singling out one direction, say the z-direction, which will be later identified with the 'beam direction' in a heavy ion collision experiment occurring in the boundary theory. To get an anisotropy between the z-direction and the xy-directions (the transverse plane to the beam), we consider the following Ansatz[2]

$$ds^2 = \frac{1}{u^2}\left(-FB\,dt^2 + dx^2 + dy^2 + H\,dz^2 + \frac{du^2}{F}\right). \tag{8.6}$$

All the metric components F, B, and H, as well as the dilaton ϕ, depend solely on the radial coordinate u. This guarantees that the solution be static. In this parametrization the boundary is located at $u = 0$. F is a 'blackening factor' that introduces an horizon in the geometry at $u = u_{\mathrm{H}}$, where $F(u_{\mathrm{H}}) = 0$. There is a scaling symmetry in the coordinates t and z that allows us to set $B_{\mathrm{bdry}}F_{\mathrm{bdry}} = H_{\mathrm{bdry}} = 1$, thus recovering a canonically normalized AdS metric in the UV region (with radius $1/\sqrt{F_{\mathrm{bdry}}}$). Here and in what follows we use the subscript 'bdry' to denote the value of the fields at $u = 0$.

[2]Note that this Ansatz is slightly different than the one used in [10, 11].

Following [10, 12] we consider an axion field which has a constant profile in the radial direction and depends linearly on z

$$\chi = a\, z\,. \tag{8.7}$$

The parameter a has dimensions of energy and controls the amount of anisotropy. It is clear that this is a solution of the axion equation, since the metric is diagonal and the metric and dilaton do not depend on z.

In this paper we limit ourselves to considering the case of small anisotropy, which will allow for an analytic solution of the equations of motion. To do this we expand all the fields around the (isotropic) Gauss-Bonnet black brane solution[3]

$$\begin{aligned} \phi(u) &= a^2\phi_2(u) + O(a^4)\,, \\ F(u) &= F_0(u) + a^2 F_2(u) + O(a^4)\,, \\ B(u) &= B_0\left(1 + a^2 B_2(u) + O(a^4)\right)\,, \\ H(u) &= 1 + a^2 H_2(u) + O(a^4)\,, \end{aligned} \tag{8.8}$$

where

$$F_0(u) = \frac{1}{2\lambda_{\rm GB}}\left(1 - \sqrt{1 - 4\lambda_{\rm GB}\left(1 - \frac{u^4}{u_{\rm H}^4}\right)}\right)\,, \qquad \lambda_{\rm GB} < \frac{1}{4}\,. \tag{8.9}$$

This is a solution of the equations of motion when $a = 0$. In order to have a unit speed of light at the boundary we set

$$B_0 = \frac{1}{2}\left(1 + \sqrt{1 - 4\lambda_{\rm GB}}\right)\,. \tag{8.10}$$

[3]See e.g. [156] or [37] for a review.

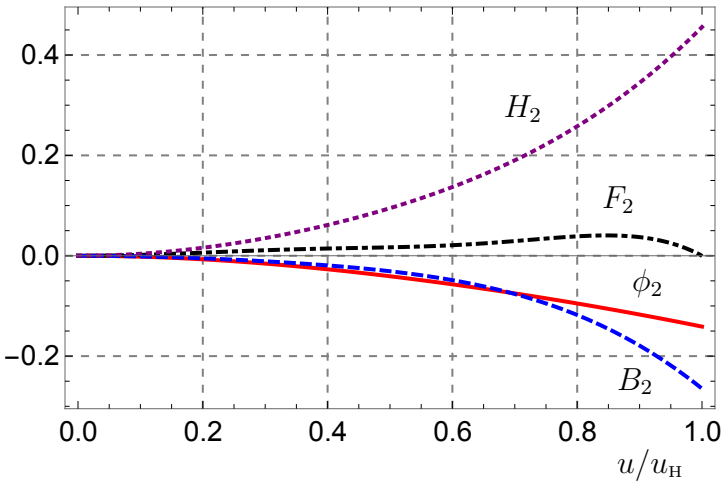

Figure 8.1: The metric functions at order $O(a^2)$. Here we have set $\lambda_{\rm GB} = 0.2$.

This is possible due to the scaling symmetry in t, which we have mentioned above. Note that only even powers of a can appear in the expansion because of the symmetry $z \to -z$.

Luckily it is possible to solve the equations analytically at order $O(a^2)$. The equations at this order and the explicit solutions are detailed in App. 8.A. A plot of representative solutions is contained in Fig. 8.1, where the regularity of the geometry is explicitly exhibited. Here we just mention that we have fixed the integration constants in such a way that all the metric functions are regular at the horizon and moreover

$$\phi_{2,\rm bdry} = F_{2,\rm bdry} = B_{2,\rm bdry} = H_{2,\rm bdry} = 0\,, \tag{8.11}$$

thus recovering AdS in the UV. A direct computation of the Kretschmann invariant $R_{mnpq}R^{mnpq}$ shows no singularity in the geometry except for $\lambda_{\rm GB} = 1/4$, which is however excluded, as can be seen from (8.9).

Unfortunately, we have not been able to find analytic solutions beyond order

$O(a^2)$ and most likely a numerical analysis will turn out to be necessary to go to higher anisotropies. This is however beyond the scope of the present work.

The temperature of the solution can be computed as usual from the standard requirement that the (Euclideanized) metric be regular at $u = u_{\rm H}$. One finds that

$$T = -\frac{F'(u)\sqrt{B(u)}}{4\pi}\Big|_{u=u_{\rm H}} . \tag{8.12}$$

Specializing to our solution this becomes[4]

$$T = \sqrt{B_0}\left(\frac{1}{\pi u_{\rm H}} - \frac{2B_0 - 6\lambda_{\rm GB} + \sqrt{\lambda_{\rm GB}}\log\left(\frac{1+2\sqrt{\lambda_{\rm GB}}}{1-2\sqrt{\lambda_{\rm GB}}}\right) - \log\left(\frac{4B_0}{\sqrt{1-4\lambda_{\rm GB}}}\right)}{48\pi(1-4\lambda_{\rm GB})} u_{\rm H} a^2 + O(a^4)\right) . \tag{8.13}$$

This equation can be easily inverted to find $u_{\rm H}$ as a function of T.

For planar black holes in GB gravity the entropy density is still given by the usual formula in terms of the area of the horizon. We find (here V_3 is the infinite volume $\int dx\, dy\, dz$)

$$s = \frac{A_{\rm hor}}{4GV_3} = \frac{\pi}{4GB_0^{3/2}}\left(\pi^2 T^3 + \frac{1}{8} T B_0 a^2 + O(a^4)\right) . \tag{8.14}$$

We notice that for $\lambda_{\rm GB} = 0$ this matches the result obtained in [10, 11].

A final comment on the IR behavior of the geometry is in order. The solution of [10, 11] was interpolating between AdS boundary conditions in the UV and a Lifshitz-like scaling solution [12] in the IR. We believe that the finite $\lambda_{\rm GB}$ generalization discussed here does not share this feature with [10, 11], although we have not been

[4]Note that this expression is valid, and real, even for negative $\lambda_{\rm GB}$.

able to prove this rigorously. More specifically, we have not been able to find a scaling solution in the IR (even for $T = 0$), as done in [12] for the case $\lambda_{\rm GB} = 0$. One obstruction might be that Lifshitz solutions in GB gravity seem to require to tune the cosmological constant in ways that are not compatible with our equations. For example, in the case of GB gravity coupled to a massive vector field the condition for a Lifshitz scaling is that the cosmological constant be half of the usual value [176].[5] It would certainly be interesting to settle this point, but this goes beyond the scope of this work.

8.2 Central charges

The trace of the stress energy tensor is related to the central charges a and c by the following expression[6]

$$\left\langle T_i^i \right\rangle = \frac{1}{16\pi^2}\left(c\,W - a\,E\right) + \dots\,, \tag{8.15}$$

where E is the four-dimensional Euler density

$$E = \mathcal{R}^2 - 4\mathcal{R}_{ij}\mathcal{R}^{ij} + \mathcal{R}_{ijkl}\mathcal{R}^{ijkl}\,, \tag{8.16}$$

W is the square of the Weyl tensor

$$W = C^{ijkl}C_{ijkl} = \frac{\mathcal{R}^2}{3} - 2\mathcal{R}_{ij}\mathcal{R}^{ij} + \mathcal{R}_{ijkl}\mathcal{R}^{ijkl}\,, \tag{8.17}$$

[5] A flow between a Lifshitz solution in the UV and an AdS solution in the IR for GB-gravity coupled to a massive vector field was discussed in [177].

[6] Notice that in this section a denotes one of the central charges and not the anisotropy parameter.

and where the ellipsis indicates the contribution by other fields (the axion-dilaton in our specific setting). The trace of the stress energy tensor [133] is given by

$$\left\langle T_i^i \right\rangle = \frac{1}{r\sqrt{-\gamma}} \mathcal{L}_{(4)} \,. \tag{8.18}$$

where $\mathcal{L}_{(4)}$, γ and r are defined in [43]. To isolate the metric contribution we set $\phi = \chi = 0$ in that expression and arrive at

$$\left\langle T_i^i \right\rangle = -\frac{1}{12}\mathcal{R}^2 + \frac{1}{4}\mathcal{R}_{ij}\mathcal{R}^{ij} + \left(\frac{19}{24}\mathcal{R}^2 + \frac{1}{2}\mathcal{R}_{ijkl}\mathcal{R}^{ijkl} - \frac{23}{8}\mathcal{R}_{ij}\mathcal{R}^{ij}\right)\lambda_{\rm GB} + O(\lambda_{\rm GB}^2) \,. \tag{8.19}$$

Comparing (8.15) and (8.19), we find that

$$a = \pi^2(2 - 15\,\lambda_{\rm GB}) + O(\lambda_{\rm GB}^2) \,, \qquad c = \pi^2(2 - 7\,\lambda_{\rm GB}) + O(\lambda_{\rm GB}^2) \,, \tag{8.20}$$

thus confirming that indeed $a \neq c$ for theories with GB corrections. These results are in perfect agreement with previous literature, see e.g. [178].

8.3 Boundary stress tensor

In this section we present the boundary stress tensor corresponding to our solution. This computation requires the machinery of holographic renormalization and it was performed in [43] using a Hamiltonian approach developed in [133]. We will only state the results, more details can be found in [43].

The obtained stress energy tensor is

$$\begin{aligned}
\langle T_{tt}\rangle &= 3\pi^4 T^4\left[1+\frac{1}{12\pi^2}\left(\frac{a}{T}\right)^2+\left(\frac{3}{2}+\frac{1}{24\pi^2}\left(\frac{a}{T}\right)^2\right)\lambda_{\rm GB}\right]+O(a^4,\lambda_{\rm GB}^2)\,,\\
\langle T_{xx}\rangle &= \langle T_{yy}\rangle=\pi^4 T^4\left[1+\frac{1}{4\pi^2}\left(\frac{a}{T}\right)^2+\left(\frac{3}{2}+\frac{1}{8\pi^2}\left(\frac{a}{T}\right)^2\right)\lambda_{\rm GB}\right]+O(a^4,\lambda_{\rm GB}^2)\,,\\
\langle T_{zz}\rangle &= \pi^4 T^4\left[1-\frac{1}{4\pi^2}\left(\frac{a}{T}\right)^2+\left(\frac{3}{2}-\frac{1}{8\pi^2}\left(\frac{a}{T}\right)^2\right)\lambda_{\rm GB}\right]+O(a^4,\lambda_{\rm GB}^2)\,. \qquad (8.21)
\end{aligned}$$

These quantities correspond to the energy density and pressures of the dual gauge theory

$$E=\frac{N_{\rm c}^2}{8\pi^2}\langle T_{tt}\rangle\,,\qquad P_\perp=\frac{N_{\rm c}^2}{8\pi^2}\langle T_{xx}\rangle\,,\qquad P_\parallel=\frac{N_{\rm c}^2}{8\pi^2}\langle T_{zz}\rangle\,, \qquad (8.22)$$

with $N_{\rm c}$ being the number of colors of the gauge theory and $P_\perp$ and $P_\parallel$ the pressures along the transverse plane and the longitudinal direction, respectively. The comparison with the energy density $E_0(T)=3\pi^2N_{\rm c}^2T^4/8$ and the pressure $P_0(T)=\pi^2N_{\rm c}^2T^4/8$ of an isotropic plasma at the same temperature and $\lambda_{\rm GB}=0$ is obvious from the expressions above. We see in particular that the anisotropy has the effect of increasing the energy density and perpendicular pressure compared to the isotropic case, while decreasing the longitudinal pressure. This is consistent with the findings of [10, 11] in the small anisotropy limit (whose results we reproduce for $\lambda_{\rm GB}=0$, see eq. (168) of [11]).

These results show that the system is really anisotropic in the z-direction, as $P_\perp\neq P_\parallel$. Notice that at this order in a, the trace of the stress tensor is vanishing

$$\left\langle T_i^i\right\rangle=O(a^4,\lambda_{\rm GB}^2)\,. \qquad (8.23)$$

This is in agreement with what found in [10, 11], where the conformal anomaly was

also vanishing at order $O(a^2)$ and appearing only at order $O(a^4)$ and beyond. We can also check some basic thermodynamic relations. In particular, the free energy $\mathcal{F} = E - Ts$, in the limit of $a = 0$, matches perfectly the value found in [156] from evaluating the Euclidean action on-shell. We can also check that $\mathcal{F} = -P_\perp$, as it should be [173].

8.4 Observables of the dual anisotropic plasma

As anticipated before one application of the solution we have found is modeling higher curvature effects on the dual gauge theory plasma. Generically, heavy ion collisions in experiments are non-central, resulting in a spatial anisotropy of the QGP formed in the collision. This represents one of the main motivations for our Ansatz.

In this section we compute several observables relevant to the study of the QGP. Most part of the analysis of our results involves a comparison with the isotropic $\mathcal{N} = 4$ SYM result, obtained by taking $a \to 0$ and $\lambda_{\rm GB} \to 0$. We limit ourselves to the comparison at the same temperature, for simplicity, but a comparison at the same entropy density is still possible, and it was done for the observables computed in the model of [10, 11].

In the following we will identify with z the anisotropic direction (or 'beam' direction), while x and y parametrize the plane transverse to the beam.

8.4.1 Shear viscosity to entropy ratios

An important quantity to compute in a plasma is the ratio of shear viscosity over entropy density.[7] This is a rather universal quantity for theories with an Einstein dual, which has been conjectured to obey the Kovtun-Son-Starinets (KSS) bound $\eta/s \geq 1/4\pi$ [9]. This bound can however be violated by the inclusion of higher derivative corrections [156] (see also [156, 158–160, 162, 163]) and by the breaking of spatial isotropy [13, 14]; see [164] for a status report on the viscosity bound.

In this section, we employ the *membrane paradigm*, proposed in [174] and used in [13] for the anisotropic plasma of [10], to compute η/s for our geometry (8.8).[8] Appendix 8.B contains two alternative derivations of the results in this section.[9] As in [13], we will be interested in two components of the shear viscosity tensor: η_{xyxy}, which is entirely in the transverse (isotropic) plane, and $\eta_{xzxz} = \eta_{yzyz}$, which mixes the anisotropic direction z with one of the directions in the transverse plane. We denote these two components as

$$\eta_\perp = \eta_{xyxy}\,, \qquad \eta_\parallel = \eta_{xzxz}\,. \tag{8.24}$$

To calculate these viscosities we consider the fluctuations h_{xy} and h_{xz} around the background (8.8). Given the symmetry in the transverse plane, we can take these fluctuations to depend solely on (t, y, z, u). The equations of motion for $\psi_\perp = h^x{}_y(t, y, z, u)$ and $\psi_\parallel = h^x{}_z(t, y, z, u)$ decouple from all other equations and from each other. In

[7] Other observables that have been computed in Einstein plus GB gravity can be found in, e.g., [42, 172].

[8] The computation of the shear viscosity in an anisotropic superfluid with a GB term has recently been presented in [179].

[9] Yet another way of doing the computation would be the so-called Riccati equation method, developed in [180] and revisited in [181]. This method allows to obtain the 2-point functions directly from the canonical momenta of Sec. 6.3, without deriving any effective action.

both cases, they have the following form

$$a(u)\psi'' + b(u)\psi' + c(u)\psi = 0\,, \tag{8.25}$$

where $a(u), b(u)$ and $c(u)$ are functions of the background fields and ψ stands for either $\psi_\perp$ or $\psi_\parallel$, depending on the case. Here the primes denote derivatives with respect to u. To use the membrane paradigm, we need to write an effective action for $\psi_\perp$ and $\psi_\parallel$. To this scope we write (8.25) in the form[10]

$$(n(u)\psi')' - m(u)\psi = 0\,, \tag{8.26}$$

with

$$n(u) = \exp\left(\int_u du' \frac{b(u')}{a(u')}\right)\,, \qquad m(u) = \frac{c(u)}{a(u)}\exp\left(\int_u du' \frac{b(u')}{a(u)}\right)\,. \tag{8.27}$$

The effective action that gives rise to the equation of motion above is

$$S_{\text{eff}} = -\frac{1}{2}\frac{1}{16\pi G}\int d^4x\, du\left[n(u)(\psi')^2 - m(u)\psi^2\right]\,. \tag{8.28}$$

To compare this action with the one of [174], we need to transform it to Fourier space. To do that, we write

$$\psi(t, y, z, u) = \int \frac{d\omega}{2\pi}\frac{d^3k}{(2\pi)^3}\psi(u)e^{-i\omega t + ik_y y + ik_z z}\,, \tag{8.29}$$

where we have used the axial symmetry to rotate $\mathbf{k} = (0, k_y, k_z)$. Plugging (8.29) into

[10]It is important to emphasize that $n(u)$ and $m(u)$ are not the same in the equations of motion for $\psi_\perp$ and $\psi_\parallel$. Here $n(u)$ stands for either $n_\perp$ or $n_\parallel$, and $m(u)$ stands for either $m_\perp$ or $m_\parallel$.

(8.28) and using Plancherel's theorem, it can be shown that

$$S_{\text{eff}} = -\frac{1}{2}\frac{1}{16\pi G}\int \frac{d\omega}{2\pi}\frac{d^3k}{(2\pi)^3}du\left[n(u)(\psi')^2 - m(u)\psi^2\right] . \tag{8.30}$$

Using the notation of [174], this can be recast in the following form

$$S_{\text{eff}} = -\frac{1}{2}\int \frac{d\omega}{2\pi}\frac{d^3k}{(2\pi)^3}du\sqrt{-g}\left[\frac{g^{uu}}{Q(u,k)}(\psi')^2 + P(u,k)\psi^2\right] , \tag{8.31}$$

with

$$\frac{1}{16\pi G}n(u) = \frac{\sqrt{-g}\,g^{uu}}{Q(u,k)} . \tag{8.32}$$

The shear viscosity is then obtained as [174]

$$\frac{\eta}{s} = \frac{1}{4\pi}\frac{16\pi G}{Q(u_{\text{H}}, k\to 0)} . \tag{8.33}$$

Writing the equations of motion for $\psi_\perp$ and $\psi_\parallel$, we can obtain explicit expressions for the $n(u)$'s and $m(u)$'s. Putting these together with (8.32) and (8.33), it is readily found that

$$\begin{aligned}\frac{\eta_\perp}{s} &= \frac{1}{4\pi}\left(\frac{g_{xx}}{g_{yy}} - \frac{\lambda_{\text{GB}}}{2}\frac{g_{xx}^2 g'_{tt}g'_{zz}}{g}\right) ,\\ \frac{\eta_\parallel}{s} &= \frac{1}{4\pi}\left(\frac{g_{xx}}{g_{zz}} - \frac{\lambda_{\text{GB}}}{2}\frac{g_{xx}^2 g'_{tt}g'_{yy}}{g}\right) .\end{aligned} \tag{8.34}$$

These results are completely generic for the system we have considered. In particular, we can check them against the known results from pure Einstein-Hilbert gravity with a GB term [156] and with the anisotropic background of [13], finding perfect agreement in both cases. In the first case, we need to take the limit of $a \to 0$ of the equations

above. We find

$$\frac{\eta_\perp}{s} = \frac{\eta_\parallel}{s} = \frac{1-4\lambda_{\rm GB}}{4\pi}\,, \tag{8.35}$$

as in [156]. To perform the second check we take the limit $\lambda_{\rm GB} \to 0$ and obtain[11]

$$\frac{\eta_\perp}{s} = \frac{1}{4\pi}\,, \qquad \frac{\eta_\parallel}{s} = \frac{1}{4\pi}\frac{1}{H(u_{\rm H})} = \frac{1}{4\pi} - \frac{\log 2}{16\pi^3}\left(\frac{a}{T}\right)^2 + O(a^4)\,. \tag{8.36}$$

Note how the longitudinal shear viscosity violates the KSS bound.

Specializing (8.34) to our solution (8.8) we find

$$\begin{aligned}
\frac{\eta_\perp}{s} &= \frac{1-4\lambda_{\rm GB}}{4\pi} + \frac{B_0}{24\pi^3}\frac{\lambda_{\rm GB}(3-4\lambda_{\rm GB})}{(1-4\lambda_{\rm GB})}\left(\frac{a}{T}\right)^2 + O\left(a^4\right)\,, \\
\frac{\eta_\parallel}{s} &= \frac{1-4\lambda_{\rm GB}}{4\pi} + \frac{B_0}{32\pi^3}G(\lambda_{\rm GB})\left(\frac{a}{T}\right)^2 + O(a^4)\,,
\end{aligned} \tag{8.37}$$

where $G(\lambda_{\rm GB})$ is given by

$$\begin{aligned}
G(\lambda_{\rm GB}) &= -1 + 2\lambda_{\rm GB}\left(\frac{8\lambda_{\rm GB}}{12\lambda_{\rm GB}-3}+1\right) + \sqrt{1-4\lambda_{\rm GB}} \\
&\quad + \sqrt{\lambda_{\rm GB}}\log\left(\frac{1+2\sqrt{\lambda_{\rm GB}}}{1-2\sqrt{\lambda_{\rm GB}}}\right) + \log\left(\frac{\sqrt{1-4\lambda_{\rm GB}}-1+4\lambda_{\rm GB}}{8\lambda_{\rm GB}}\right)
\end{aligned} \tag{8.38}$$

We emphasize that these results, despite being of second order in a, are fully non-perturbative in $\lambda_{\rm GB}$. The KSS bound might be violated in this setting both by the anisotropy and by the GB coupling.

[11] Note that to compare the expressions for $\eta_\parallel$ one needs to take into account the different factors of the dilaton in the Ansätze of [10, 13] and (8.6).

8.4.2 Conductivities

To calculate the plasma conductivities,[12] we need to introduce[13] a $U(1)$ gauge field A_m in the bulk, with a standard Maxwell action

$$S_{\rm Maxwell} = -\int d^5x\sqrt{-g}\frac{1}{4g^2_{\rm eff}(u)}F_{mn}F^{mn}\,, \tag{8.39}$$

where $g_{\rm eff}(u)$ is a generic u-dependent coupling constant. The conjugate momentum to the gauge field is given by[14]

$$j^i = -\frac{\sqrt{-g}}{g^2_{\rm eff}}F^{iu}\,. \tag{8.40}$$

The gauge field A_m is dual to a conserved current J^i in the boundary theory whose expectation value is equal to j^i evaluated at the boundary

$$\left\langle J^i(k)\right\rangle = j^i(u\to 0\,;k)\,. \tag{8.41}$$

The AC conductivity is given by the following relation between the spatial part of j^i and the electric field F_{jt}

$$\left\langle J^{i=x,y,z}(k)\right\rangle = \sigma^{ij}(k)F_{jt}(u\to 0)\,, \tag{8.42}$$

[12] For a related computation in an isotropic background with linear scalar fields and a GB term see [182].

[13] We introduce this field only in this section, solely for the purpose of computing the conductivities. Of course, the analysis of Sec. 6.3 would be modified by the inclusion of an extra field.

[14] In this section we keep denoting the boundary coordinates by the Latin indices $i, j, \ldots$, as in Sec. 6.3.

while the DC conductivity is defined by the zero momentum limit of $\sigma^{ij}(k)$

$$\sigma^{ij}_{\rm DC} = \lim_{k\to 0} \sigma^{ij}(k)\,. \tag{8.43}$$

It turns out that we can calculate these quantities doing a near horizon analysis [174]. Imposing infalling boundary conditions at the horizon implies that

$$F_{ui} = \sqrt{-\frac{g_{uu}}{g_{tt}}} F_{ti}\Big|_{u=u_{\rm H}}\,. \tag{8.44}$$

Combining (8.40) and (8.44) it can be readily shown that

$$j^i(u_{\rm H}) = \frac{1}{g^2_{\rm eff}} \sqrt{\frac{g}{g_{tt}g_{uu}}}\, g^{ij} F_{jt}(u_{\rm H})\,, \tag{8.45}$$

and that, in the zero momentum limit, this relation holds for all u [174]. Because of this, we can do the calculation at the horizon, instead of doing it at the boundary. Comparing (8.42) with (8.45) we see that the conductivity along the i-direction is

$$\sigma^{ii}_{\rm DC} = \frac{1}{g^2_{\rm eff}} \sqrt{\frac{g}{g_{tt}g_{uu}}}\, g^{ii}\Big|_{u_{\rm H}}\,. \tag{8.46}$$

For an isotropic background we have $\sigma^{ij}_{\rm DC} = \sigma\delta^{ij}$ (from now on we are going to use the symbol σ to represent the DC conductivity and will drop the subscript). When the background is anisotropic, there will be two different conductivities: $\sigma_\perp$ and $\sigma_\parallel$. The former corresponds to an electric field aligned along the x- and y-directions, resulting in a corresponding conductivity along the transverse plane, whereas the latter corresponds to electric field and conductivity along the beam direction. These

quantities are given by

$$\sigma_\perp = \frac{1}{g_{\rm eff}^2}\sqrt{\frac{g}{g_{tt}g_{uu}}}g^{xx}\Big|_{u_{\rm H}}\,, \qquad \sigma_\parallel = \frac{1}{g_{\rm eff}^2}\sqrt{\frac{g}{g_{tt}g_{uu}}}g^{zz}\Big|_{u_{\rm H}} = \frac{\sigma_\perp}{H(u_{\rm H})}\,. \tag{8.47}$$

Normalizing with the isotropic result, we get

$$\begin{aligned}\frac{\sigma_\perp}{\sigma_{\rm iso}} &= H(u_{\rm H})^{1/2} = 1 + \frac{a^2}{2}H_2(u_{\rm H}) + O(a^4)\,,\\ \frac{\sigma_\parallel}{\sigma_{\rm iso}} &= H(u_{\rm H})^{-1/2} = 1 - \frac{a^2}{2}H_2(u_{\rm H}) + O(a^4)\,.\end{aligned} \tag{8.48}$$

Since $H_2(u_{\rm H})$ is a positive quantity, we see that the anisotropy has the effect of enhancing the conductivity along the perpendicular directions, as compared to the isotropic case, while suppressing the one along the longitudinal direction, consistently with the findings of [27, 31].

8.4.3 Drag force

A heavy quark propagating through a strongly coupled plasma it loses energy due to the interaction with the medium. One quantity related to the dissipation of energy of the quark is the drag force. The study of drag force in a strongly coupled plasma was initiated in [183, 184] for the case of (isotropic) $\mathcal{N} = 4$ SYM and subsequently it was extended in several ways. See, for instance [185–204]. The two computations of the drag force closely related to the present work were done in [15, 205], corresponding to the limits $\lambda_{\rm GB} = 0$ and $a = 0$, respectively.

Following the standard prescription of the computation of the drag force, we consider an external heavy quark moving through the strongly coupled plasma with constant velocity v. Since the heavy quark loses energy due to the interaction with the

plasma, an external force is necessary to maintain the motion stationary. In the dual picture, we have a classical string with an endpoint in the quark (at the boundary) and the other endpoint in the bulk, in a picture usually referred to as "trailing string" [183, 184]. The derivation of the general formula is presented in Appendix 8.C. As a result, we first need to determine a critical point u_c by solving the equation

$$\left[\frac{2G_{tt}}{v^2} + G_{xx} + G_{zz} + (G_{zz} - G_{xx})\cos(2\varphi)\right]_{u=u_c} = 0, \tag{8.49}$$

where φ is the angle between the direction of motion of the quark and the z-direction. In the following, we will be interested in the cases where the motion of the quark is parallel ($||$) and transversal ($\perp$) to the direction of anisotropy, corresponding to $\varphi = 0$ and $\varphi = \pi/2$, respectively. Once the critical point is determined, it is straightforward to compute the drag force using

$$F^{||}_{\text{drag}} = e^{\phi/2} G_{zz} v\Big|_{u=u_c}, \qquad F^{\perp}_{\text{drag}} = e^{\phi/2} G_{xx} v\Big|_{u=u_c}. \tag{8.50}$$

Since we are working in the small anisotropy regime, the critical point can be written as

$$u_c = u_{0c} + a^2 u_{2c} + O(a^4). \tag{8.51}$$

For our particular background (8.6), the equation for the critical point (8.49) expanded to second order in a becomes

$$B_0 F_0 - v^2 + a^2 \left(B_0 B_2 F_0 + B_0 F_2 - v^2 \cos^2\varphi H_2 + B_0 u_{2c} F_0'\right)\Big|_{u_{0c}} = 0, \tag{8.52}$$

Solving the equation order by order gives

$$u_{0c} = u_{\rm H}\left(\frac{B_0^2 - v^2 B_0 + v^4\lambda_{\rm GB}}{B_0^2}\right)^{\frac{1}{4}},$$
$$u_{2c} = -\frac{B_0 B_2(u_{0c})F_0(u_{0c}) + B_0 F_2(u_{0c}) - v^2 H_2(u_{0c})\cos^2\varphi}{B_0 F_0'(u_{0c})}. \tag{8.53}$$

Plugging the solution for the critical point (8.53) into the formulas of the drag force (8.50), we obtain

$$F^{||}_{\rm drag} = \frac{v}{{u_{0c}}^2} + \frac{a^2 v}{2{u_{0c}}^2}\left(\phi_2(u_{0c}) - 4\frac{u_{2c}}{u_{0c}} + 2H_2(u_{0c})\right) + O(a^4),$$
$$F^{\perp}_{\rm drag} = \frac{v}{{u_{0c}}^2} + \frac{a^2 v}{2{u_{0c}}^2}\left(\phi_2(u_{0c}) - 4\frac{u_{2c}}{u_{0c}}\right) + O(a^4). \tag{8.54}$$

We do not report the full explicit expressions for the drag force here since they are too long and not very illuminating. Inverting the first relation of (8.13), the drag force can be expressed as a function of the temperature.[15] We can then check that in the limit $\lambda_{\rm GB} \to 0$ we recover the result of [15],

$$F^{||\,{\rm MT}}_{\rm drag} = \frac{\pi^2 T^2 v}{\sqrt{1-v^2}} + \frac{a^2 v\left(-v^2 + \sqrt{1-v^2} + (v^2+1)\log\left(\sqrt{1-v^2}+1\right)+1\right)}{24\left(1-v^2\right)^{3/2}},$$
$$F^{\perp\,{\rm MT}}_{\rm drag} = \frac{\pi^2 T^2 v}{\sqrt{1-v^2}} + \frac{a^2 v\left(-v^2 + \sqrt{1-v^2} + (4v^2-5)\log\left(\sqrt{1-v^2}+1\right)+1\right)}{24\left(1-v^2\right)^{3/2}}, \tag{8.55}$$

and in the limit $a \to 0$ we recover the result of [205]

$$F^{\rm GB}_{\rm drag} = \frac{\sqrt{2}\pi^2 T^2 v}{\sqrt{\left(v^2-1\right)\left(2\left(v^2+1\right)\lambda_{\rm GB} - \sqrt{1-4\lambda_{\rm GB}} - 1\right)}}. \tag{8.56}$$

[15] The easiest way to write the drag force in terms of the temperature is by noting that the critical point scales as $u_c = u_{\rm H}\gamma_0 + a^2 u_{\rm H}^3\gamma_2 + O(a^4)$, where γ_0 and γ_2 are quantities that do not depend on $u_{\rm H}$.

Of course, in the limit where both a and $\lambda_{\rm GB}$ go to zero we recover the isotropic $\mathcal{N}=4$ SYM result [183, 184]

$$F_{\rm drag}^{\rm iso}=\frac{\pi^2T^2v}{\sqrt{1-v^2}}. \tag{8.57}$$

In the analysis of our results, it is useful to normalize the drag force by the isotropic result (8.57). The normalized drag force here depends on $v, \lambda_{\rm GB}$ and a/T. The main result is shown in Fig. 8.2. Our results are, as expected, a combined effect of their limiting cases [15, 205]. The effect of the Gauss-Bonnet coupling is, in general, to enhance the drag force for $\lambda_{\rm GB} > 0$ and to decrease it for $\lambda_{\rm GB} < 0$, for both longitudinal and transversal motion. This is the same effect observed in the case of pure Gauss-Bonnet gravity [205], but it is different from what happens with corrections of type α'^3R^4, where the drag force is always enhanced [203]. The effect of the anisotropy is qualitatively the same found in [15]: for the transversal motion the drag force can increase or decrease, while for the parallel motion the drag force increases in general (except for sufficiently large negative values of $\lambda_{\rm GB}$). We also plotted the drag force as a function of the quark velocity (Fig. 8.3). In general, the drag is increased for larger velocities and there is a divergence in the limit $v \to 1$, similarly to what occurred in [15].

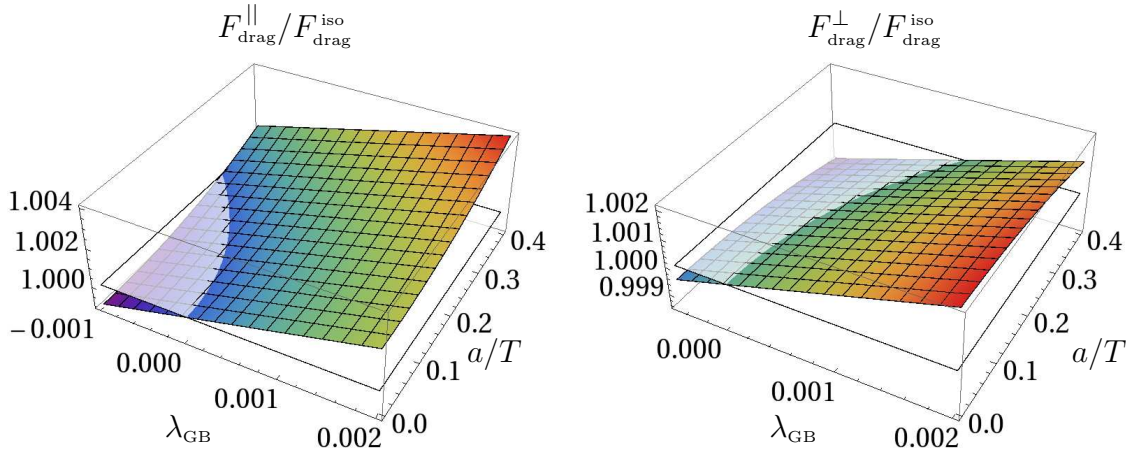

Figure 8.2: Drag force normalized by the isotropic result as a function of $(\lambda_{\rm GB}, \frac{a}{T})$. Here we have fixed $v = 0.3$. Left: Motion along the anisotropic direction. Right: Motion along the direction transversal to the anisotropy.

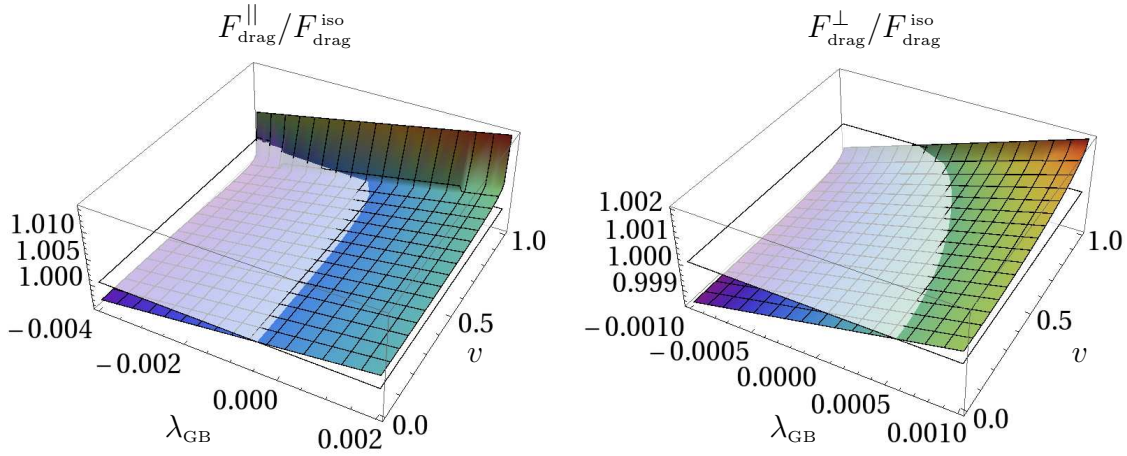

Figure 8.3: Drag force normalized by the isotropic result as a function of $(\lambda_{\rm GB}, v)$. Here we have fixed $\frac{a}{T} = 0.2$. Left: Motion along the anisotropic direction. Right: Motion along the direction transversal to the anisotropy. For other values of $\frac{a}{T}$ the results were qualitatively the same.

8.4.4 Jet quenching parameter

Results from RHIC [69–72] indicate a strong suppression of particles with high transversal momentum $p_{\rm T}$ in Au-Au collisions, but not in d-Au collisions. The explanation for this phenomenon is that in Au-Au collisions the hot and dense quark gluon plasma is produced, and the jets lose energy due to the interaction with this medium before hadronizing. This energy loss effect is called "jet quenching" and can give valuable information as regards the properties of the plasma. One important quantity related to jet quenching is the jet quenching parameter $\hat{q}$, which quantify the change of transverse momentum of the parton per unit length when suffering multiple scattering with the medium. The change in transverse momentum is usually referred to as

"momentum broadening".

The jet quenching parameter has been calculated at weak coupling for several models (see [206] for a review) and has been consistent with data [207]. However, the assumption of weak coupling is still not well justified, since different energy scales are involved in heavy ion collision experiments and thus a calculation at strongly coupling may be necessary. This motivates a non-perturbative definition of the jet quenching parameter. The non-perturbative definition of the jet quenching parameter and its first computation using holography was done in [208–210]. After that, it was extended in several directions.[16] See, for instance [215–217].

The non-perturbative definition of the jet quenching parameter $\hat{q}$ was inspired by its perturbative calculation in the so called dipole approximation [218]

$$\left\langle W^A(\mathcal{C})\right\rangle \simeq \exp\left[-\frac{L^-\ell^2}{4\sqrt{2}}\hat{q}\right], \tag{8.58}$$

where $W^A(\mathcal{C})$ is a rectangular light-like Wilson loop in the adjoint representation with sizes L^- and ℓ, with $L^- \gg \ell$. Using the holographic dictionary the jet quenching parameter is given in terms of the on-shell Nambu-Goto action whose string worldsheet boundary coincides with the Wilson loop[17]

$$\hat{q} = \frac{8\sqrt{2}}{L^-\ell^2} S^{\text{on-shell}}. \tag{8.59}$$

[16] There are also some attempts of non-perturbative computations of the jet quenching parameter on the lattice (see, for instance [211–213]).

[17] The extra factor of 2 comes from the fact that, for large N_c, the Wilson loop in the adjoint representation is roughly speaking the square of the Wilson loop in the fundamental representation.

In the case of pure (isotropic) $\mathcal{N}=4$ SYM, the result obtained was [208–210]

$$\hat{q}_{\rm iso} = \frac{\pi^{3/2}\Gamma(\frac{3}{4})}{\Gamma(\frac{5}{4})}\sqrt{\lambda}T^3. \tag{8.60}$$

Here we compute the jet quenching parameter for the anisotropic background with Gauss-Bonnet term (8.6). A detailed derivation of the formula we used here is presented in Appendix 8.D. The parameters involved are the Gauss-Bonnet coupling $\lambda_{\rm GB}$, the ratio of the anisotropy parameter to temperature a/T and the angles (θ,φ) associated with the direction of motion of the quark and the direction of the momentum broadening, respectively.[18]

Our results are summarized in Fig. 8.4. Similarly to the drag force computation of the previous subsection, the effect of the Gauss-Bonnet coupling is controlled by its sign: the jet quenching parameter is increased for $\lambda_{\rm GB} > 0$ and decreased for $\lambda_{\rm GB} < 0$. The effect of the anisotropy, in the small anisotropy limit, is to increase the jet quenching parameter as it occurred in [30, 186, 214], with the highest increase taking place when the quark moves in the anisotropic direction. We also verified that, for a fixed value of θ, the jet quenching parameter is slightly larger for the momentum broadening taking place in the anisotropic ($\varphi=\pi/2$) direction than in the transversal direction to the anisotropy ($\varphi=0$).

[18]More precisely, θ is the angle between the direction of motion of the quark and the anisotropic direction. The direction of the momentum broadening is transversal to the direction of motion of the quark and forms an angle φ with the y-axis. Note that the same symbols θ and φ were used for other observables, but with different meanings.

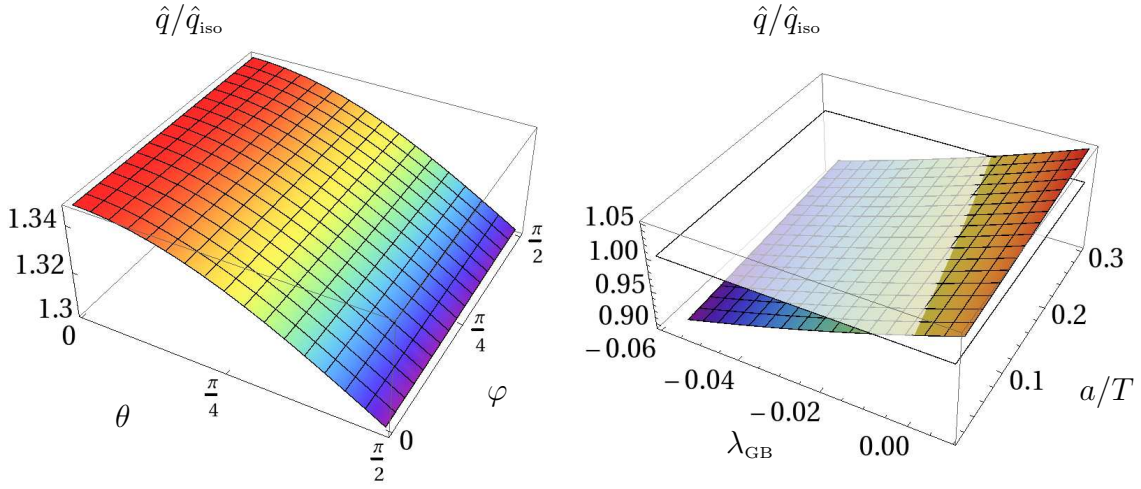

Figure 8.4: Left: Jet quenching parameter as a function of (θ, φ). We have set $\lambda_{\rm GB} = 0.1$ and $a/T = 0.33$. Right: The jet quenching parameter as a function of $(\lambda_{\rm GB}, \frac{a}{T})$. We have set $\theta = \varphi = \pi/4$. Both plots were normalized by the isotropic result (8.60).

As argued in [207], weak coupling models of jet quenching are in general lower than the value obtained at strong coupling for $\mathcal{N} = 4$ SYM (8.60). If we would expect a smooth interpolation between the weak and strong coupling values, the case $\lambda_{\rm GB} < 0$ would become particularly interesting since it decreases the $\mathcal{N} = 4$ SYM result. The same decreasing effect was also found in [219], where one considered fluctuations of the string worldsheet, and in [220], where curvature corrections of type $\alpha'^3 R^4$ in the AdS-Schwarzschild background were taken into account.

8.4.5 Quarkonium static potential

Quarkonium mesons are produced in the early stages of heavy ion collisions, before the creation of the QGP. As they are much more tightly bound and smaller than ordinary 'light' hadrons, they can survive as bound states in the QGP at temperatures above the deconfinement temperature up to some dissociation temperature. This property, together with the fact that their interaction with the thermal medium is comparatively stronger than their interaction with the hadronic matter formed after hadronization, makes the quarkonium mesons excellent probes to study the QGP formed in heavy ion collisions [67].

Here we study the static quarkonium potential in a strongly coupled plasma dual to the gravity theory described in Section 8.1. In particular, we analyze how the anisotropy and the higher derivative terms affect the potential energy and the screening length of a heavy quark-antiquark pair. The holographic studies of this quantity were initiated in [221, 222], for infinitely heavy quarks in the $\mathcal{N} = 4$ SYM theory, and since then several extensions of this work have been performed. See, for instance [223–234]. Higher derivative corrections to the quarkonium potential were considered in [223, 230] and the effects of anisotropy were taken into account in [186, 224].

The static quarkonium potential can be extracted from the expectation value of a Wilson loop

$$\lim_{\mathcal{T}\to\infty} \langle W(\mathcal{C})\rangle \sim e^{i\mathcal{T}\,(V_{Q\bar{Q}}+2M_Q)}, \tag{8.61}$$

where $\mathcal{C}$ is a rectangular loop with time extension $\mathcal{T}$ and spatial extension L, $V_{Q\bar{Q}}$ is the quark-antiquark potential energy and M_Q is the quark mass. The Wilson loop can be viewed as a static quark-antiquark pair separated by a distance L. In the gravity side, the pair is described by an open string with both endpoints attached

to a D7-brane sitting at some AdS radial position, which determines the quark mass ($M_Q \sim 1/u$). For simplicity, we will work in the case where the D7-brane is at the boundary of AdS and, consequently, the quark is infinitely heavy and non-dynamical.

In the large N_c and large λ limits the Wilson loop of Eq. (8.61) can be calculated in the gravity side by the expression

$$\lim_{\mathcal{T}\to\infty} \langle W(\mathcal{C})\rangle = e^{iS^{(\text{on-shell})}}, \tag{8.62}$$

where $S^{(\text{on-shell})}$ is the on-shell Nambu-Goto action of a U-shaped string whose world-sheet boundary coincides with the curve $\mathcal{C}$. The quarkonium potential is thus obtained as

$$V_{Q\bar{Q}} = \frac{S^{(\text{on-shell})}}{\mathcal{T}} - 2M_Q, \tag{8.63}$$

where the quark mass M_Q is determined by evaluating the Nambu-Goto action of a straight string connecting the boundary to the horizon. Given the rotational symmetry in the xy-plane, we can assume the quark-antiquark pair to lie in the xz-plane, forming an angle θ with the z-direction. Since we want to focus on the results, we leave the details of the calculation of $V_{Q\bar{Q}}(L)$ in Appendix 8.E.

First, let us discuss some general properties of $V_{Q\bar{Q}}(L)$. From Fig. 8.5, we see that $V_{Q\bar{Q}}$ only exists up to a maximum separation length L_{max}. For each value of $L \leq L_{\text{max}}$ there are two possible string configurations corresponding to the upper and lower parts of $V_{Q\bar{Q}}$. It turns out that only the lower part of $V_{Q\bar{Q}}$ represents a physical solution [225]. Note that $V_{Q\bar{Q}} = 0$ at some point $L = L_s$, usually referred to as "screening length". Since $V_{Q\bar{Q}}$ represents the difference between the energy and mass of the quarkonium, a negative value of the potential ($L \leq L_s$) represents a situation where the U-shaped string (bound state) is energetically favorable over the

configuration with two straight strings (unbound state). On the other hand, when the potential is positive ($L \geq L_s$), the opposite happens and the unbound configuration is energetically favorable.[19] Another point is that the screening of a plasma is weaker for large L_s and stronger for small L_s. This is because L_s represents the separation in which the interaction between the quark and the antiquark becomes completely screened by the medium.

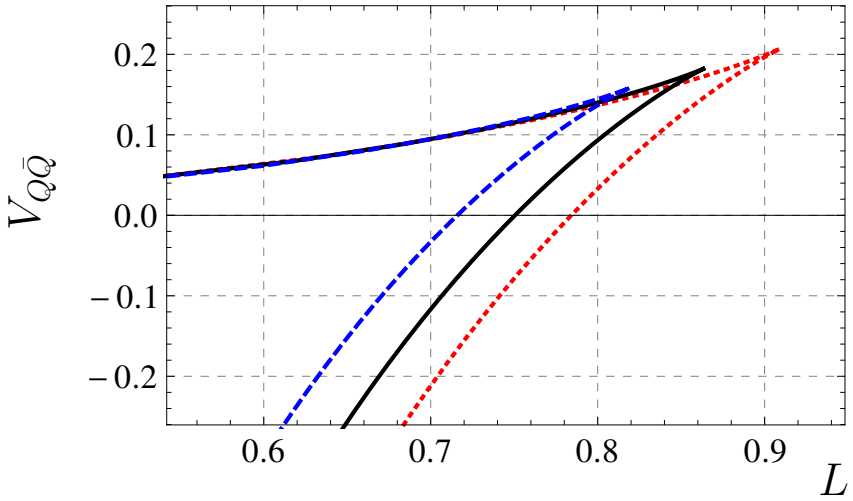

Figure 8.5: Quark-antiquark potential $V_{Q\bar{Q}}$ as a function of their separation L for different values of the Gauss-Bonnet coupling: $\lambda_{\rm GB} = -0.1$ (red, dotted), $\lambda_{\rm GB} = 0$ (black, solid) and $\lambda_{\rm GB} = 0.1$ (blue, dashed). For all curves $a/T \approx 0.3$ and $\theta = \pi/4$.

Fig. 8.5 shows that positive values of $\lambda_{\rm GB}$ decrease the screening length, while negative values of $\lambda_{\rm GB}$ increase this quantity. This effect can be better visualized in Fig. 8.6 (a), where the screening length is presented as a function of $(\lambda_{\rm GB}, a)$. Now let us discuss the effect of the anisotropy. First of all, Fig. 8.6 (b) shows that the

[19]However, we emphasize that the solution for $V_{Q\bar{Q}}$ is not valid when $L \geq L_s$. In this case the quark-antiquark interaction is completely screened by the presence of QGP between them and, as a consequence, their separation can be increased with no additional energy cost. This implies that the potential is actually constant for $L \geq L_s$. The dual gravity picture can be understood as follows: as we increase the quark-antiquark separation, the U-shaped string connecting the quarks eventually touches the horizon. At this point the string can minimize its energy by splitting into straight strings connecting the boundary of AdS to the horizon.

screening length for a quarkonium oriented along the anisotropic direction ($\theta = 0$) is always smaller than the corresponding quantity for a quarkonium oriented in the transverse plane ($\theta = \pi/2$). Second, the 2D plot of Fig. 8.7 reveals that the screening length always decrease as we increase a/T, for any orientation of the pair, at fixed $\lambda_{\rm GB}$. These anisotropic effects are also observed in holographic calculations at strong coupling when the anisotropy is introduced by a magnetic field [234] and at weak coupling in calculations based on "hard-thermal-loop" resummed perturbative QCD [235]. The limit $\lambda_{\rm GB} \to 0$ of the above results agrees with the calculations of [186]. We also checked that the limit $a \to 0$ for $V_{Q\bar{Q}}$ agrees with the results of [223] when the quasi-topological coupling constant is zero.[20]

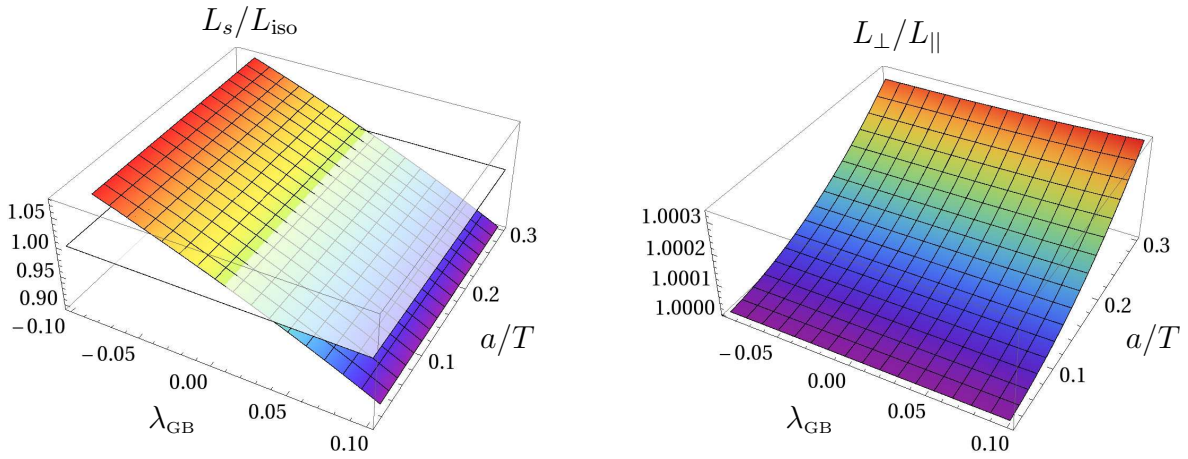

(a) (b)

Figure 8.6: (a) Screening length $L_s(\lambda_{\rm GB}, a)$ normalized with respect to the isotropic result $L_{\rm iso} = L_s(\lambda_{\rm GB} = 0, a = 0)$ for $\theta = 0$. (b) Ratio $L_\perp/L_{||}$, where $L_\perp$ is the screening length calculated at $\theta = \pi/2$, and $L_{||}$ is the screening length calculated at $\theta = 0$.

[20] In the comparison of our results with [223], one should note that the potential of [223] is normalized with $1/(\pi\alpha')$, while our results are normalized with $1/(2\pi\alpha')$.

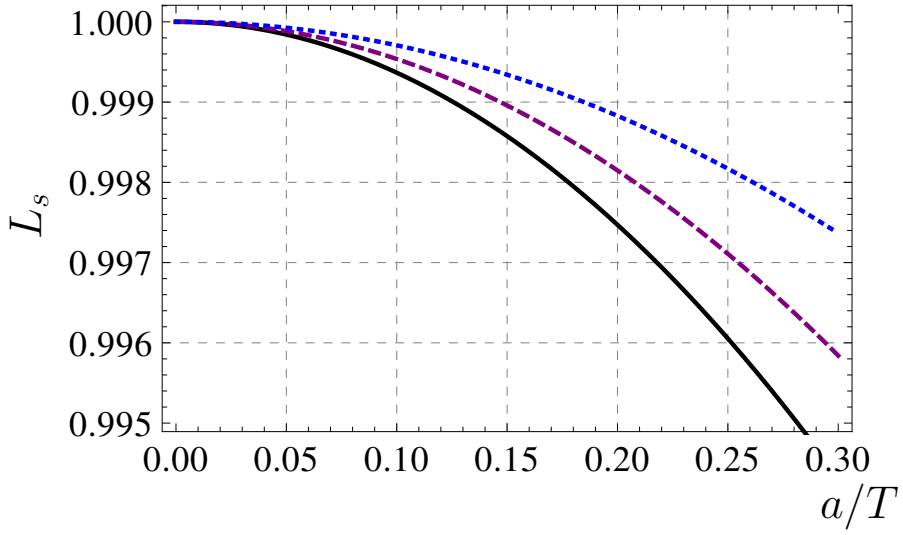

Figure 8.7: Screening length L_s as a function of a/T for three different quarkonium orientations: $\theta = 0$ (black, solid), $\theta = \pi/4$ (purple, dashed) and $\theta = \pi/2$ (blue, dotted). The Gauss-Bonnet coupling is fixed $\lambda_{\rm GB} = 0$.

8.4.6 Photon production

The limited extension of the QGP created in heavy ion collisions and the weakness of the electromagnetic interactions imply that this medium should be optically thin. Therefore, the photons produced in the plasma escape from it without subsequent interactions, providing an excellent probe of the conditions of the medium. The holographic studies of this quantity were initiated in [236] and extended in several directions, see, for instance [237–255]. In this section we study how the anisotropy and higher derivative corrections affect the photon production rate in the model described in Section 8.1.

Let $\mathcal{L}_0$ be the Lagrangian of the field theory dual to the gravity theory described by the action (8.1). The photon production rate is calculated by adding a dynamical

photon to $\mathcal{L}_0$ coupled to the electric charged matter fields, that is,

$$\mathcal{L} = \mathcal{L}_0 + eJ^{\rm EM}_\mu A^\mu - \frac{1}{4}F_{\mu\nu}F^{\mu\nu}, \tag{8.64}$$

where $F_{\mu\nu} = \partial_\mu A_\nu - \partial_\nu A_\mu$ is the field strength associated to the photon field A^μ, e is the electromagnetic coupling constant and $J^{\rm EM}_\mu$ is the electromagnetic current. At leading order in e, the number of photons emitted per unit time and unit volume is given by [119]

$$\frac{d\Gamma_\gamma}{d^3k} = \frac{e^2}{(2\pi)^3 2|\vec{k}|}\Phi(k)\,\eta^{\mu\nu}\chi_{\mu\nu}(k)\Big|_{k^0=|\vec{k}|}, \tag{8.65}$$

where $\eta^{\mu\nu} = \text{diag}(-+++)$ is the Minkowski metric, $k^\mu = (k^0, \vec{k})$ is the photon null momentum, $\Phi(k)$ is the distribution function and $\chi_{\mu\nu}$ is the spectral density. Assuming thermal equilibrium, the distribution function reduces to the Bose-Einstein distribution $n_B(k^0) = 1/(e^{k^0/T} - 1)$. The spectral density can be obtained as

$$\chi_{\mu\nu}(k) = -2\ \text{Im}\ G^{\rm R}_{\mu\nu}(k), \tag{8.66}$$

where

$$G^{\rm R}_{\mu\nu}(k) = -i\int d^4x\, e^{-ik\cdot x}\,\Theta(t)\big\langle[J^{\rm EM}_\mu(x), J^{\rm EM}_\nu(0)]\big\rangle \tag{8.67}$$

is the retarded correlator of two electromagnetic currents $J^{\rm EM}_\mu$ and the above expectation value is taken in the thermal equilibrium state. The Ward identity $k^\mu\chi_{\mu\nu} = 0$ for null k^μ implies that only the transverse spectral functions contribute in the calculation

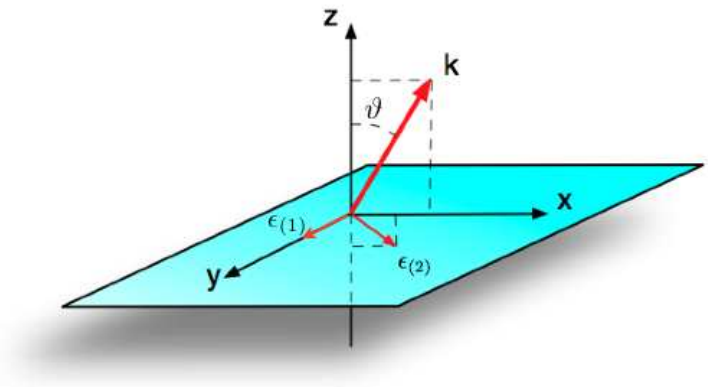

Figure 8.8: Momentum $\vec{k}$ and polarization vectors $\vec{\epsilon}_{(1)}$ and $\vec{\epsilon}_{(2)}$. The $SO(2)$ rotational symmetry in the xy-plane allows us to choose the momentum lying in the xz-plane, forming an angle ϑ with the z-direction. Both polarization vectors are orthogonal to $\vec{k}$. We chose $\vec{\epsilon}_{(1)}$ oriented along the y-direction and $\vec{\epsilon}_{(2)}$ contained in the xz-plane.

of the trace of the spectral density, that is,

$$\eta^{\mu\nu}\chi_{\mu\nu} = \sum_{s=1,2} \epsilon^{\mu}_{(s)}(\vec{k})\,\epsilon^{\nu}_{(s)}(\vec{k})\,\chi_{\mu\nu}(k)\Big|_{k^0=|\vec{k}|}\,. \tag{8.68}$$

Using the above formula, the differential photon production rate can be rewritten as

$$\frac{d\Gamma_\gamma}{d^3k} = \frac{e^2}{(2\pi)^3 2|\vec{k}|}\Phi(k)\sum_{s=1,2} \epsilon^{\mu}_{(s)}(\vec{k})\,\epsilon^{\nu}_{(s)}(\vec{k})\,\chi_{\mu\nu}(k)\Big|_{k^0=|\vec{k}|}\,, \tag{8.69}$$

where $\epsilon^{\mu}_{(1)}$ and $\epsilon^{\mu}_{(2)}$ are mutually orthogonal polarization vectors that are also orthogonal to k^μ. By the $SO(2)$ symmetry in the xy-plane of our model we can choose $\vec{k}$ to lie in the xz-plane – see Fig. 8.8. Following [238, 239], we set

$$\vec{k} = k_0(\sin\vartheta, 0, \cos\vartheta)\,. \tag{8.70}$$

With this choice of $\vec{k}$ the polarization vectors can be chosen as

$$\vec{\epsilon}_{(1)} = (0, 1, 0)\,, \qquad \vec{\epsilon}_{(2)} = (\cos\vartheta, 0, -\sin\vartheta)\,. \tag{8.71}$$

For later purposes we split the trace of the spectral density into two parts

$$\eta^{\mu\nu}\chi_{\mu\nu} = \chi_{(1)} + \chi_{(2)}, \tag{8.72}$$

where $\chi_{(s)}$ is proportional to the number of photons emitted with polarization $\vec{\epsilon}_{(s)}$. These quantities are given by

$$\begin{aligned}
\chi_{(1)} &= \epsilon^{\mu}_{(1)}\epsilon^{\nu}_{(1)}\chi_{\mu\nu} = \chi_{yy} \\
\chi_{(2)} &= \epsilon^{\mu}_{(2)}\,\epsilon^{\nu}_{(2)}\,\chi_{\mu\nu} = \cos^2\vartheta\,\chi_{xx} + \sin^2\vartheta\,\chi_{zz} - 2\cos\vartheta\sin\vartheta\,\chi_{xz}\,.
\end{aligned} \tag{8.73}$$

We now proceed to explain how to compute the retarded Green function of two electromagnetic currents using holography. It turns out that the gravity theory dual to the field theory described by the Lagrangian $\mathcal{L}$ is simply obtained by adding a $U(1)$ kinetic term to the action (8.1). As we are dealing with a bottom-up model, we consider a five-dimensional $U(1)$ kinetic term of the form,

$$S_{U(1)} = -K\int d^5x\, F_{mn}F^{mn}, \tag{8.74}$$

where $F_{mn} = \partial_m A_n - \partial_n A_m$ is the field strength associated to the gauge field A_m ($m = 0, 1, 2, 3, 4$) and K is a constant.[21] Let A_μ ($\mu = 0, 1, 2, 3$) denote the components

[21] In top-down calculations, K is proportional to the number of electrically charged degrees of freedom times the number of colors in the dual gauge theory. For instance, when photons are produced from adjoint matter we have $K \propto N_c^2$ [236], while for fundamental fields, $K \propto N_c N_f$ [238–240, 254]. In bottom-up models, this constant can be chosen freely and, since we are only interested in ratios of spectral densities (which are proportional to K), this constant will play no role in our analysis.

of this gauge field along the gauge theory coordinates $(t, \vec{x})$ and $A_4 = A_u$ denote the component along the radial coordinate of AdS. In order to simplify our calculations, we gauge fix $A_u = 0$. Our final results, however, will be written only in terms of gauge invariant quantities, in such a way that this gauge choice will not be relevant.

Given the translation invariance of our model, we can Fourier decompose the gauge field A_μ as

$$A_\mu(t, \vec{x}, u) = \int \frac{d^4k}{(2\pi)^4} e^{-ik^0 t + i\vec{k}\cdot\vec{x}} A_\mu(k^0, \vec{k}, u)\,. \tag{8.75}$$

The equations of motion derived from (8.74) are given by

$$\partial_\mu\big(\sqrt{-g} g^{\mu\alpha} g^{\nu\beta} F_{\alpha\beta}\big) = 0\,. \tag{8.76}$$

In terms of the gauge invariant quantities $E_i = \partial_0 A_i - \partial_y A_i$, the above equations of motion split into a decoupled equation for E_y,

$$E_y'' + \big(\log\sqrt{-g} g^{uu} g^{yy}\big)' E_y' - \frac{\overline{k}^2}{g^{uu}} E_y = 0\,, \tag{8.77}$$

and a system of two coupled equations for E_x and E_z,[22]

$$\begin{aligned}
&E_x'' + \left[\big(\log\sqrt{-g} g^{uu} g^{xx}\big)' - \left(\log\frac{g^{xx}}{g^{tt}}\right)' \frac{k_x^2}{\overline{k}^2} g^{xx}\right] E_x' - \frac{\overline{k}^2}{g^{uu}} E_x - \left(\log\frac{g^{xx}}{g^{tt}}\right)' \frac{k_z k_x}{\overline{k}^2} g^{zz} E_z' = 0\,,\\
&E_z'' + \left[\big(\log\sqrt{-g} g^{uu} g^{zz}\big)' - \left(\log\frac{g^{zz}}{g^{tt}}\right)' \frac{k_z^2}{\overline{k}^2} g^{zz}\right] E_z' - \frac{\overline{k}^2}{g^{uu}} E_z - \left(\log\frac{g^{zz}}{g^{tt}}\right)' \frac{k_z k_x}{\overline{k}^2} g^{xx} E_x' = 0\,,
\end{aligned} \tag{8.78}$$

[22] In the derivation of the equations of motion for E_x and E_z we used the constraint $g^{\alpha\beta} k_\alpha A_\beta' = 0$.

where the primes denote derivatives with respect to u and $\overline{k}^2 \equiv g^{\alpha\beta}k_\alpha k_\beta$. Note that the above equations are written in momentum space.

The action (8.74) can be written in terms of the gauge invariant fields E_i as

$$S_\epsilon = -2K \int dt\, d\vec{x}\, \frac{\sqrt{-g}g^{uu}}{k_0^2\overline{k}^2}\Big[\left(-g^{tt}k_0^2 - g^{zz}k_z^2\right) g^{xx}E_xE_x' - \overline{k}^2 g^{yy}E_yE_y' + \\ + g^{xx}g^{zz}k_xk_z\left(E_xE_z\right)' + \left(-g^{tt}k_0^2 - g^{xx}k_x^2\right) g^{zz}E_zE_z'\Big]_{u=\epsilon}. \quad (8.79)$$

The retarded correlators are obtained by taking functional derivatives of the above action with respect to the boundary values of the gauge fields $A^{\mu(0)}$. In the computation of $\chi_{(1)}$ and $\chi_{(2)}$ we only need the spatial correlators $G^{\rm R}_{xx}$, $G^{\rm R}_{yy}$, $G^{\rm R}_{zz}$, and $G^{\rm R}_{xz} = G^{\rm R}_{zx}$. This correlators can be obtained in terms of the E_i's as

$$G^{\rm R}_{ij} = \frac{\delta^2 S_\epsilon}{\delta A^{i(0)}\delta A^{j(0)}} = k_0^2 \frac{\delta^2 S_\epsilon}{\delta E_i^{(0)}\delta E_j^{(0)}}\,, \quad (8.80)$$

where $E_i^{(0)}$ is the boundary value of the gauge field E_i.

As the mode E_y does not couple to the other modes, the spectral density for photons with polarization $\vec{\epsilon}_{(1)}$ can be obtained by applying the prescription of [103]. The retarded correlator reads

$$G^{\rm R}_{yy} = k_0^2 \frac{\delta^2 S_\epsilon}{\delta E_y^{(0)2}} = -\frac{4K}{k_0^2}\sqrt{-g}g^{uu}g^{yy}\frac{E_y'(k,u)}{E_y(k,u)}\Big|_{u\to 0}. \quad (8.81)$$

The corresponding spectral density is then given by

$$\chi_{(1)} = \chi_{yy} = -2{\rm Im}\, G^{\rm R}_{yy} = \frac{8K}{k_0^2}{\rm Im}\left[\sqrt{-g}g^{uu}g^{yy}\frac{E_y'(k,u)}{E_y(k,u)}\right]_{u\to 0}. \quad (8.82)$$

The computation of $\chi_{(2)}$ is more involved, because of the coupling between E_x and E_z. We face this problem by following the technique developed in [238] to deal with mixed operators. First, we write a near-boundary expression for the fields E_x and E_z,

$$\begin{aligned} E_x &= E_x^{(0)} + u^2 E_x^{(2)} \cos\vartheta + u^4 E_x^{(4)} + O(u^6)\,, \\ E_z &= E_z^{(0)} - u^2 E_x^{(2)} \sin\vartheta + u^4 E_z^{(4)} + O(u^6)\,. \end{aligned} \tag{8.83}$$

The form of the second order coefficients was chosen such that the equations of motion (8.78) are satisfied. The equations of motion also determine the coefficients $E_x^{(4)}$ and $E_z^{(4)}$ in terms of the lower order coefficients,

$$\begin{aligned} E_x^{(4)} &= \frac{a^2 \lambda_{\text{GB}} \cos\vartheta}{96(1-B_0)(1-4\lambda_{\text{GB}})} \left(3k_0^2(B_0 - 2\lambda_{\text{GB}})E_x^{(0)} \cos\vartheta + 8(1-2B_0)E_x^{(2)}\right)\,, \\ E_z^{(4)} &= \frac{a^2}{192\sqrt{1-4\lambda_{\text{GB}}}} \left[3k_0^2(\lambda_{\text{GB}} - B_0)\left(E_x^{(0)} \sin\vartheta - E_z^{(0)} \cos\vartheta\right)\cos\vartheta - 8B_0 E_x^{(2)} \sin\vartheta\right]\,. \end{aligned} \tag{8.84}$$

The remaining coefficients $E_x^{(0)}$, $E_z^{(0)}$ and $E_x^{(2)}$ can be extracted from the numerical solution. With the above expressions the boundary action (8.79) takes the form

$$S_\epsilon = \sqrt{B_0} K \left[-\frac{1}{2}\left(E_x^{(0)} \sin\vartheta + E_z^{(0)} \cos\vartheta\right)^2 - \frac{4}{B_0 k_0^2}\left(E_x^{(0)} E_x^{(2)} \cos\vartheta + E_z^{(0)} E_x^{(2)} \sin\vartheta\right)\right]. \tag{8.85}$$

Finally, using (8.66), (8.73), and (8.80) we can show that

$$\chi_{(2)} = \frac{16K}{\sqrt{B_0}} \,\text{Im}\left[\frac{\delta E_x^{(2)}}{\delta E_x^{(0)}} \cos\vartheta - \frac{\delta E_x^{(2)}}{\delta E_z^{(0)}} \sin\vartheta\right], \tag{8.86}$$

where the functional derivatives $\delta E_x^{(2)}/\delta E_x^{(0)}$ and $\delta E_x^{(2)}/\delta E_z^{(0)}$ are calculated according to the prescription given in [238].

The trace of the spectral density $\chi^{\mu}_{\ \mu} = \chi_{(1)} + \chi_{(2)}$ is a function of the parameters $(\lambda_{\rm GB}, a, \vartheta, u_{\rm H}, k^0)$. In order to study the effects of the anisotropy parameter and the Gauss-Bonnet coupling, we computed $\chi^{\mu}_{\ \mu}$ for several values of $(\lambda_{\rm GB}, a, \vartheta)$, choosing as normalization the isotropic result

$$\chi_{\rm iso} = \chi^{\mu}_{\ \mu}(\lambda_{\rm GB} = 0, a = 0). \tag{8.87}$$

Our comparison with the isotropic result was made at fixed temperature $T_0 = 0.32$.[23] The results for the ratio $\chi^{\mu}_{\ \mu}/\chi_{\rm iso}$ as a function of the dimensionless frequency $\mathfrak{w} = k^0/2\pi T_0$ are presented in Fig. 8.9. For an anisotropic plasma, we have $\chi_{(1)} \neq \chi_{(2)}$. However, in our case the smallness of the anisotropy parameter a makes these two quantities almost equal, presenting a very similar behavior as a function of $\mathfrak{w}$, so we chose to plot only the total spectral density instead of plotting the two spectral densities separately. At least, we observed that $\chi_{(1)}$ is slightly bigger than $\chi_{(2)}$, as was the case in [238, 239]. We also verified that our results reproduce the calculations of [253] in the limit $a \to 0$ and that they are consistent with anisotropic calculations of [238] in the limit $\lambda_{\rm GB} \to 0$ and small values of a/T.

[23] Doing this, one must note that the temperature T of the system is a function of $(\lambda_{\rm GB}, a, u_{\rm H})$ and, consequently, it changes as we vary these parameters. Therefore, we need to adjust $u_{\rm H}$ in such a way that all the spectral densities are calculated at same temperature T_0, defined by $T_0 = T(\lambda_{\rm GB} = 0, a = 0, u_{\rm H} = 1)$.

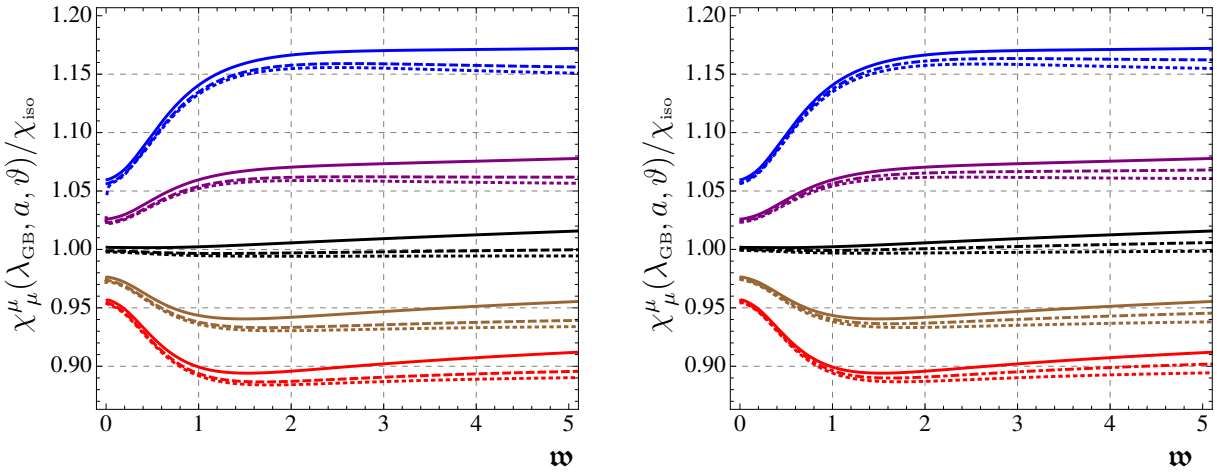

Figure 8.9: The trace of the spectral density $\chi^{\mu}_{\mu}(\lambda_{\rm GB}, a, \vartheta)$ normalized with respect to the isotropic result (8.87). All the spectral densities were calculated at the same temperature $T_0 = 0.316698$. The colors of the curves identify the value of the $\lambda_{\rm GB}$ parameter as: red curves ($\lambda_{\rm GB} = -0.1$), brown curves ($\lambda_{\rm GB} = -0.05$), black curves ($\lambda_{\rm GB} = 0$), purple curves ($\lambda_{\rm GB} = 0.05$) and blue curves ($\lambda_{\rm GB} = 0.1$). In (a), the angle of emission is fixed ($\vartheta = 0$) and we have solid curves ($a = 0.2$), dashed curves ($a = 0.1$) and dotted curves ($a = 0$). In (b), the anisotropy is fixed ($a = 0.2$) and we have solid curves ($\vartheta = 0$), dot-dashed curves ($\vartheta = \pi/4$), and dotted curves ($\vartheta = \pi/2$).

From Fig. 8.9 it is clear that the effect of the Gauss-Bonnet coupling is to increase or decrease the photon production rate, depending on whether $\lambda_{\rm GB} > 0$ or $\lambda_{\rm GB} < 0$, respectively. The main effect of the anisotropy parameter is to increase the photon production rate. At small frequencies, χ^{μ}_{μ} does not depend strongly on a. For generic frequencies, the χ^{μ}_{μ} is higher for photons with longitudinal wave vectors ($\vartheta = 0$) than for the ones with transverse wave vectors ($\vartheta = \pi/2$). One qualitative difference between the corrections introduced by $\lambda_{\rm GB}$ and a is their dependence on the frequency.

Looking at the curves for $a = 0$ in Fig. 8.9, we see that the Gauss-Bonnet correction reaches a constant value after a sufficiently large value of $\mathfrak{w}$. On the other hand, the effect of the anisotropy parameter a is enhanced as we increase $\mathfrak{w}$.

It is also interesting to analyze how the anisotropy and the Gauss-Bonnet term affects the total photon production (8.65), which can be expressed as

$$\frac{-1}{4Ke^2T_0^3}\frac{d\Gamma_\gamma}{d\cos\vartheta\, dk^0} = \frac{\mathfrak{w}}{32K\pi^3T_0^2}\frac{1}{e^{2\pi\mathfrak{w}}-1}\big(\chi_{(1)}+\chi_{(2)}\big) \tag{8.88}$$

This quantity is shown in Fig. 8.10, for different values of $\lambda_{\rm GB}$ and ϑ. From Fig. 8.10 we see that, for $\lambda_{\rm GB} > 0$, the peak in the spectrum of photons becomes higher, widens and gets shifted to the right. For $\lambda_{\rm GB} < 0$, the peak becomes smaller, sharpens and gets shifted to the left. This should be contrasted with the results of [248] for a top-down higher derivative correction of the form α'^3R^4, where the peak in the spectrum becomes higher, sharpens and gets shifted to the left, approaching the weak coupling result [236], which shows a very sharp peak at small $\mathfrak{w}$ in the photon spectrum. Therefore, the inclusion of the α'^3R^4 correction (which corresponds to a finite 't Hooft coupling correction in the gauge theory) goes into the direction of the weak coupling results, while this does not seems to be possible in the case of Gauss-Bonnet. However, a partial agreement between these two types of corrections is found when $\lambda_{\rm GB} < 0$, where the peak in the photon spectrum sharpens and moves to the left, but it also becomes smaller, contrary to what happens at weak coupling. We can understand this partial agreement noting that, for $\lambda_{\rm GB} < 0$, the ratio $\eta/s = (1-4\lambda_{\rm GB})/(4\pi)$ increases, which also happens with η/s when finite 't Hooft coupling corrections were taking into account. Since at weak coupling the shear viscosity over the entropy density ratio is proportional to the mean free path of momentum isotropization, we

can associate the approaching of the weak coupling results (negative $\lambda_{\rm GB}$ corrections or α'-corrections) with a larger mean free path in both cases.

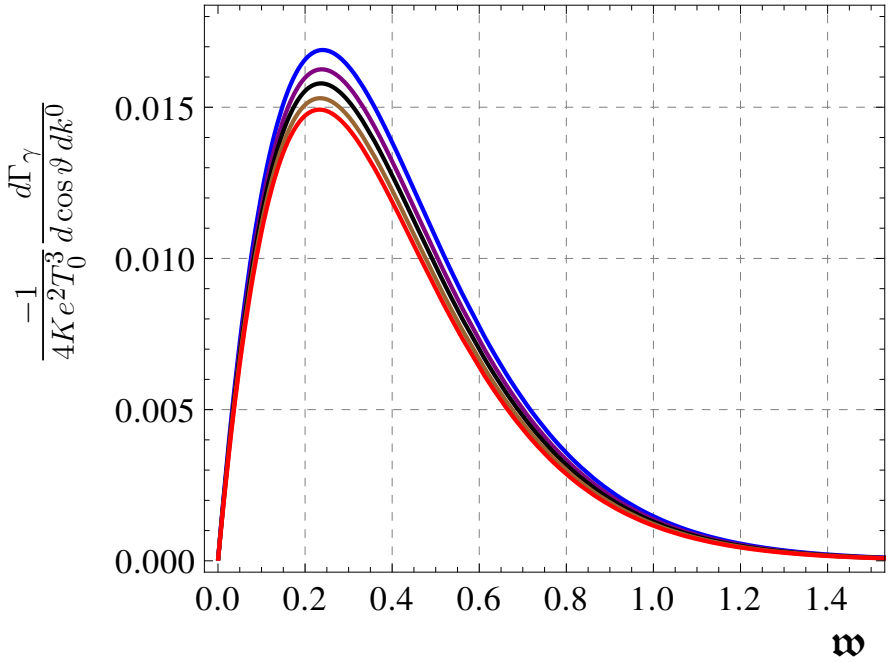

Figure 8.10: Total photon production rate as a function of $\mathfrak{w} = k^0/2\pi T_0$. From top to bottom, the value of the Gauss-Bonnet coupling is identified as $\lambda_{\rm GB} = 0.1$ (blue), $\lambda_{\rm GB} = 0.05$ (purple), $\lambda_{\rm GB} = 0$ (black), $\lambda_{\rm GB} = -0.05$ (brown), $\lambda_{\rm GB} = -0.1$ (red). We have fixed $\vartheta = 0$ and $a = 0.2$. The results for different angles are very similar to the plot above due to the smallness of the anisotropy.

8.5 Discussion

In this chapter we have explored the effects of higher curvature corrections (given by the inclusion of a GB term) in a system of AdS-gravity in five dimensions coupled to an axion-dilaton field. As we have explained above, these corrections correspond, on the gauge theory side, to considering cases that are more generic than the ones

usually considered, e.g. conformal field theories with independent central charges, $a \neq c$. It is still unclear whether our setup might be obtained in the low energy limit of some string theory, and our philosophy has been 'bottom-up'.

We have also considered a particular black brane Ansatz, in which the axion field is linearly dependent on one of the horizon coordinates, while being independent of the radial coordinate. This has resulted in finding an anisotropic black brane solution to the equations of motion, which is the GB-corrected equivalent of the geometry discovered in [10, 11]. As discussed in Sec. 8.1, one point that remains to be settled in our analysis is whether our solution might be interpreted as an interpolating solution between a Lifshitz-like scaling solution in the IR and an asymptotically AdS space, as was the case for the $\lambda_{\rm GB} = 0$ limit of [10, 11].

One of the most interesting applications of the present work would be a detailed study of the thermodynamics of this black brane and of its corresponding plasma. This analysis was carried out, in the canonical ensemble, for the case of vanishing $\lambda_{\rm GB}$ in [10, 11] and a rich phase diagram was discovered, with, in particular, the presence of instabilities that might turn out to be useful in understanding the fast thermalization time of the QGP. To this regard it is relevant to observe that part of the richness of the solution in [10, 11] was due to a conformal anomaly, appearing in the renormalization process at order $O(a^4)$ and beyond. In the present solution we also have an anomaly, which we expect to appear at the fourth order in the anisotropy parameter, but we are not able to capture with our analytic solution, which only goes up to second order. Extending our analytic solution to order $O(a^4)$ seems unviable and presumably numerical methods would have to be employed to explore larger values of the anisotropy. Given the large number of parameters in the game, this might be cumbersome, but it surely is something worth pursuing.

We also have studied how the anisotropy and higher curvature terms affect several observables relevant to the study of the QGP, namely, the shear viscosity over the entropy density ratio, the eletric conductivity, the drag force, the jet quenching parameter, the quarkonium static potential and the photon production rate.

We found that the KSS bound [9] for the shear viscosity over entropy density ratio is violated, as expected from previous works where either the case ($a = 0, \lambda_{\rm GB} \neq 0$) [156] or the case ($a \neq 0, \lambda_{\rm GB} = 0$) [13] were considered.

The effect of the Gauss-Bonnet term in our results are consistent with previous results [223, 253, 258, 259] and they are summarized in Table 8.1, where we specify if the value of the observable increases or decreases compared to the case of isotropic $\mathcal{N} = 4$ SYM. In this table we also present the result for the shear viscosity over entropy density obtained previously [43] and the finite 't Hooft corrections of type $\alpha'^3 R^4$ for these observables [185, 248, 261, 262].

Table 8.1: Summary of the effect of the Gauss-Bonnet coupling $\lambda_{\rm GB}$ on several observables. We also present the finite 't Hooft corrections of type $\alpha'^3 R^4$ [185, 248, 261, 262]. The comparison is taken w.r.t. the respective $\mathcal{N} = 4$ SYM result at same temperature.

	η/s	Drag force	Jet quenching	Screening length	Photon production
$\lambda_{\rm GB} > 0$	decrease	increase	increase	decrease	increase
$\lambda_{\rm GB} < 0$	increase	decrease	decrease	increase	decrease
$\alpha'^3 R^4$	increase	increase	decrease	decrease	increase

A possible heuristic interpretation of the increasing/decreasing in the above observables is to correlate these results with the changes in the ratio η/s. At weak coupling,

η/s is proportional to the mean free path of momentum isotropization of the plasma ($\eta/s \sim \ell_{\rm mfp}$). Imagining a situation where the mean free path is decreasing, we should expect an external probe to interact more with the medium, increasing the energy loss of the probe and its probability to suffer scattering. As a result, we would obtain an increase in the drag force and the jet quenching parameter. Moreover, a low mean free path would break the connection between a quark-antiquark pair more easily, resulting in a low value of screening length. Finally, a low mean free path would raise the number of collisions per time and, consequently, the number of photons produced in these interactions would increase. Note that this situation matches exactly the case of $\lambda_{\rm GB} > 0$. Of course, the opposite idea applies for $\lambda_{\rm GB} < 0$. Although this reasoning seems to be consistent for the Gauss-Bonnet, it does not work when applied to the $\alpha'^3 R^4$ correction.

The effect of the anisotropy is similar to what was found previously [15, 30, 186, 214, 224, 238]. The photon production rate and the quarkonium dissociation length in an anisotropic plasma are bigger than the corresponding quantities in an isotropic plasma at the same temperature. The drag force and the jet quenching parameter in an anisotropic plasma can be bigger or smaller than its isotropic counterparts, depending on several parameters like the quark velocity, the direction of the quark motion, and the direction of momentum broadening. Below we also summarize the effects of the anisotropy with a comparison between the value of the observables along the anisotropic direction ($||$) and along the transverse plane ($\perp$):

- Shear viscosity: $\eta_\perp > \eta_{||}$,
- Drag force: $F^\perp_{\rm drag} < F^{||}_{\rm drag}$,
- Jet quenching parameter: $\hat{q}_\perp < \hat{q}_{||}$,

- Screening length: $L_\perp > L_{||}$,
- Photon production rate: $\chi_\mu{}^\mu{}_\perp < \chi_\mu{}^\mu{}_{||}$.

The same interpretation in terms of the mean free path for the Gauss-Bonnet term can be applied here. Considering the mean free path in the anisotropic direction $\ell^{||}_{\rm mfp}$ and in the transverse plane $\ell^{\perp}_{\rm mfp}$, we note that the mean free path of an anisotropic system in the transverse plane is larger than the corresponding quantity in the anisotropic direction, because $\eta_\perp > \eta_{||}$. This can be associated with a smaller drag force, a smaller jet quenching parameter, less screening (larger screening length), a smaller drag force and less photon production in the transverse plane when compared with the corresponding quantities in the anisotropic direction.

It would be interesting to see how these observables behave for similar models. As far as we are aware, the only model that incorporates both the anisotropy and the higher curvature correction is [256]. Possible extensions of this work include the study of how the anisotropy and the higher derivative terms affect other observables like the imaginary part of the quarkonium potential, the quarkonium dissociation length in a plasma wind, Langevin diffusion coefficients, the dilepton production rate or the elliptic flow of photons and dileptons, to name a few.

Appendix 8.A Derivation of the solution

In this appendix we give some details on how we have found our solution (8.8) and present its explicit expression.

The Einstein equations (8.3) are diagonal, as a consequence of the fact that the metric only depends on u. We have then four equations for the metric (since the xx-

and yy-components are not independent) plus the equation for the dilaton in (8.5). There are four fields to solve for: ϕ, F, B, and H. Plugging the Ansatz (8.6)-(8.8) into the equations and expanding to order $O(a^2)$ one finds that the equation for $\phi_2(u)$ decouples. It reads

$$\phi_2'' + \frac{u\,F_0' - 3F_0}{u\,F_0}\phi_2' = \frac{1}{F_0}\,, \tag{8.89}$$

with F_0 given by (8.9). This can be readily solved changing coordinates as

$$u \to U(u) = \sqrt{1 - 4\lambda_{\rm GB}\left(1 - \frac{u^4}{u_{\rm H}^4}\right)} \tag{8.90}$$

in intermediate steps. The two integration constants are fixed in such a way that ϕ_2 is regular at the horizon and vanishes at the boundary, $\phi_{2,\rm bdry} = 0$. One finds

$$\begin{aligned}\phi_2(u) \;\; = \;\; & -\frac{u_{\rm H}^2}{8}\left[\alpha + U(u) + \log\left(1 + \frac{u^2}{u_{\rm H}^2}\right)^2\right. \\ & \left. -\sqrt{\lambda}_{\rm GB}\log\left(U(u) + 2\sqrt{\lambda}_{\rm GB}\frac{u^2}{u_{\rm H}^2}\right)^2 - \log\left(U(u) + 1 - 4\lambda_{\rm GB}\left(1 + \frac{u^2}{u_{\rm H}^2}\right)\right)\right]\,,\end{aligned} \tag{8.91}$$

where

$$\alpha \equiv -\sqrt{1 - 4\lambda_{\rm GB}} + \sqrt{\lambda}_{\rm GB}\log\left(1 - 4\lambda_{\rm GB}\right) + \log\left(1 - 4\lambda_{\rm GB} + \sqrt{1 - 4\lambda_{\rm GB}}\right)\,, \tag{8.92}$$

and $U(u)$ is defined as above. We notice that U is always positive (since $\lambda_{\rm GB} < 1/4$), and so is the argument of the last logarithm in (8.91). When $\lambda_{\rm GB} = 0$ we recover the result of [11], see eq. (164) of that paper.

To find H_2, we take the difference of the xx- and zz-components of (8.3). One

obtains a decoupled equation that reads

$$H_2''(u) + p(u)H_2'(u) = q(u)\,, \tag{8.93}$$

with

$$\begin{aligned} p(u) &= \frac{3(1-4\lambda_{\rm GB})(U(u)-1)+4\lambda_{\rm GB}(3U(u)-5)u^4/u_{\rm H}^4}{u\,U(u)^2\,(1-U(u))}\,, \\ q(u) &= \frac{2\lambda_{\rm GB}U(u)}{(1-4\lambda_{\rm GB})(1-U(u))}\,. \end{aligned} \tag{8.94}$$

This equation can be integrated readily via (8.90), fixing the integration constants as above. In particular we request that $H_{2,\rm bdry} = 0$. The final result is

$$\begin{aligned} H_2(u) = \frac{u_{\rm H}^2}{8(1-4\lambda_{\rm GB})}\Bigg[&\beta + U(u) + \log\left(1+\frac{u^2}{u_{\rm H}^2}\right) + 2\lambda_{\rm GB}\frac{u^2}{u_{\rm H}^2}\left(\frac{u^2}{u_{\rm H}^2}-2\right) \\ &-\sqrt{\lambda}_{\rm GB}\log\left(U(u)+2\sqrt{\lambda}_{\rm GB}\frac{u^2}{u_{\rm H}^2}\right)^2 - \log\left(\frac{U(u)+1-4\lambda_{\rm GB}\left(1+\frac{u^2}{u_{\rm H}^2}\right)}{U(u)-1+4\lambda_{\rm GB}\left(1+\frac{u^2}{u_{\rm H}^2}\right)}\right)^{1/2}\Bigg]\,, \end{aligned} \tag{8.95}$$

where, again, we have left $U(u)$ implicit in some places for compactness and where

$$\beta \equiv -\sqrt{1-4\lambda_{\rm GB}} + \sqrt{\lambda}_{\rm GB}\log(1-4\lambda_{\rm GB}) + \log\left(\frac{1+\sqrt{1-4\lambda_{\rm GB}}}{2\sqrt{\lambda}_{\rm GB}}\right)\,. \tag{8.96}$$

Similarly we can solve for the other fields. More specifically, now that we know ϕ_2 and H_2, we can use the tt-component of (8.3) to obtain F_2 and the uu-component to obtain B_2. One can finally check that the xx- and zz-components are also solved separately, as expected because of the Bianchi identities. The explicit expressions for the equations are not particularly illuminating, so that we limit ourselves to reporting

the final results for the remaining fields, which are given by

$$\begin{aligned} F_2(u) &= \frac{u_{\rm H}^2}{12(1-4\lambda_{\rm GB})U(u)}\left(\frac{u}{u_{\rm H}}\right)^4\left[\gamma+U(u)+(1-4\lambda_{\rm GB})\left(\frac{u_{\rm H}}{u}\right)^2\right. \\ &\quad +4\lambda_{\rm GB}\left(\frac{u}{u_{\rm H}}\right)^2-6\lambda_{\rm GB}\left(\frac{u}{u_{\rm H}}\right)^4+\log\left(1+\frac{u^2}{u_{\rm H}^2}\right)^2 \\ &\quad \left.-\sqrt{\lambda}_{\rm GB}\log\left(U(u)+2\sqrt{\lambda}_{\rm GB}\frac{u^2}{u_{\rm H}^2}\right)^2-\log\left(U(u)+1-4\lambda_{\rm GB}\left(1+\frac{u^2}{u_{\rm H}^2}\right)\right)\right], \end{aligned} \tag{8.97}$$

with

$$\gamma\equiv -2+6\lambda_{\rm GB}+\sqrt{\lambda}_{\rm GB}\log\left(1+2\sqrt{\lambda}_{\rm GB}\right)^2+\log\left(\frac{1-4\lambda_{\rm GB}}{2}\right), \tag{8.98}$$

and by

$$\begin{aligned} B_2(u) &= \frac{u_{\rm H}^2}{24(1-4\lambda_{\rm GB})}\left[\alpha+U(u)\frac{u_{\rm H}^2-u^2}{u_{\rm H}^2+u^2}+\log\left(1+\frac{u^2}{u_{\rm H}^2}\right)^2\right. \\ &\quad -\frac{2u^2}{u_{\rm H}^2+u^2}\left(1-2\lambda_{\rm GB}+\lambda_{\rm GB}\left(\frac{u}{u_{\rm H}}\right)^2+3\lambda_{\rm GB}\left(\frac{u}{u_{\rm H}}\right)^4\right) \\ &\quad \left.-\sqrt{\lambda}_{\rm GB}\log\left(U(u)+2\sqrt{\lambda}_{\rm GB}\frac{u^2}{u_{\rm H}^2}\right)^2-\log\left(U(u)+1-4\lambda_{\rm GB}\left(1+\frac{u^2}{u_{\rm H}^2}\right)\right)\right]. \end{aligned} \tag{8.99}$$

Again, we have fixed the integration constants in such a way that the fields be regular at the horizon and vanish at the boundary, $F_{2,\rm bdry}=B_{2,\rm bdry}=0$. Notice also that $F_2(u_{\rm H})=0$, as it should be for a blackening factor. One can check that when $\lambda_{\rm GB}=0$ the results from [10] are recovered.[24]

[24] In order to do so, one needs to take into account the different Ansätze and include a factor of the dilaton in (8.6), according to eq. (8) of [11].

Appendix 8.B Shear viscosity tensor

In this appendix we report two alternative derivations of the shear viscosity tensor (8.37).

8.B.1 Kubo formula

As is well known (see e.g. [103, 124–126]), the shear viscosity can be also computed using a Kubo formula

$$\eta = \lim_{\omega\to 0}\frac{1}{\omega}\mathrm{Im}\, G_{\mathrm{R}}(\omega, \vec{k}=0), \tag{8.100}$$

where $G_{\mathrm{R}}(k)$ is the retarded Green's function for the stress tensor. First, we take metric fluctuations h_{mn} around our solution and linearize the equations of motion. Here, we are interested in the modes $\psi_\perp = h^x_{\ y}$ and $\psi_\parallel = h^x_{\ z}$. In momentum space, we have

$$\psi(u,x) = \int \frac{d^4k}{(2\pi)^4} J(k)\psi(u;k)e^{-ik_i x^i}, \qquad k_i = (-\omega, \mathbf{k}), \tag{8.101}$$

where ψ denotes generically one of the modes $\psi_\perp$ or $\psi_\parallel$. The prescription tells us to solve the equation for $\psi(u;k)$ imposing infalling boundary conditions and regularity at the horizon and satisfying $\psi = 1$ at the boundary.

To compute the shear viscosity, we can restrict ourselves to zero spatial momentum and small frequency ω. For simplicity, we also consider small λ_{GB}. The linearized equations for $\psi(u;\omega)$ have the form

$$K_0(u)\psi'' + K_0'(u)\psi' = 0, \tag{8.102}$$

where for $\psi = \psi_\perp$ we have, up to orders $O(a^4, \lambda_{\rm GB}^2, \omega^2)$,

$$\begin{aligned} K_0^\perp(u) &= \frac{u^4\left(a^2u_{\rm H}^2\log 2+6\right)-a^2u_{\rm H}^6\log\left(1+\frac{u^2}{u_{\rm H}^2}\right)-6u_{\rm H}^4}{12u^3u_{\rm H}^4} \\ &\quad+\frac{\lambda_{\rm GB}}{12u^3u_{\rm H}^8}\Big[u^8\left(a^2u_{\rm H}^2(5-6\log 2)-18\right)-u^4u_{\rm H}^4\left(a^2u_{\rm H}^2(2-5\log 2)-6\right) \\ &\qquad -4a^2u^6u_{\rm H}^4+(12+a^2u^2)u_{\rm H}^8+a^2u_{\rm H}^2\left(3u^8-2u_{\rm H}^8\right)\log\left(1+\frac{u^2}{u_{\rm H}^2}\right)\Big], \end{aligned} \tag{8.103}$$

and for $\psi = \psi_\parallel$ we have

$$\begin{aligned} K_0^\parallel(u) &= K_0^\perp(u)+\frac{a^2\left(u_{\rm H}^4-u^4\right)\log\left(1+\frac{u^2}{u_{\rm H}^2}\right)}{8u^3u_{\rm H}^2} \\ &\quad+\frac{a^2\lambda_{\rm GB}\left(-7u^8+10u^6u_{\rm H}^2-u^4u_{\rm H}^4-2u^2u_{\rm H}^6+2\left(3u^8-5u^4u_{\rm H}^4+2u_{\rm H}^8\right)\log\left(1+\frac{u^2}{u_{\rm H}^2}\right)\right)}{16u^3u_{\rm H}^6}. \end{aligned} \tag{8.104}$$

The equations above can be solved by considering an Ansatz of the form

$$\psi(u;\omega)=\left(1-\frac{u^4}{u_{\rm H}^4}\right)^{-\frac{i\omega}{4\pi T}}\left[1+\omega\left(f_0(u)+\lambda_{\rm GB}(f_1(u)+a^2f_2(u))\right)+O(a^4,\lambda_{\rm GB}^2,\omega^2)\right], \tag{8.105}$$

where T is the temperature given by (8.13). The functions $f_0(u), f_1(u)$ and $f_2(u)$ can be determined by substituting the Ansatz into the linearized equation and solving order by order. The resulting expressions are not particularly illuminating and we do not report them here. The next step is to compute the quadratic on-shell action, which turns out to be a surface term of the form

$$S^{(2)}_{\text{on-shell}} = -\frac{1}{2}\int\frac{d^4k}{(2\pi)^4}J(k)\mathcal{F}(u;k)J(-k)\Big|_{u\to 0}^{u=u_{\rm H}}, \tag{8.106}$$

with $\mathcal{F}(u,k) = \frac{1}{16\pi G} K_0(u)\, \psi'(u;k)\psi(u;-k)$. The prescription of [103] instructs us to take only the contribution of the boundary. The retarded Green's function is then given by

$$G_{\rm R}(k) = \lim_{u\to 0} \mathcal{F}(u;k). \tag{8.107}$$

Finally, using (8.100) and the result for the entropy (8.14) we can compute the ratio of the shear viscosity over entropy density

$$\begin{aligned} \frac{\eta_\perp}{s} &= \frac{1-4\lambda_{\rm GB}}{4\pi} + a^2\lambda_{\rm GB}\frac{u_{\rm H}^2}{8\pi} + O(a^4,\lambda_{\rm GB}^2)\,, \\ \frac{\eta_\parallel}{s} &= \frac{1-4\lambda_{\rm GB}}{4\pi} + a^2\left(3\lambda_{\rm GB} - 2\log 2\right)\frac{u_{\rm H}^2}{32\pi} + O(a^4,\lambda_{\rm GB}^2)\,. \end{aligned} \tag{8.108}$$

These results agree with the ones obtained via the membrane paradigm expanded to first order in $\lambda_{\rm GB}$.

8.B.2 Near-horizon matching technique

In this appendix we calculate the viscosities $\eta_\perp$ and $\eta_\parallel$ using the near-horizon matching technique of [263]. We first solve the fluctuation equation for $\omega = 0$ and then expand the solution near the horizon. After that, we reverse the order of the operations, finding first a near-horizon solution and then expanding it for small ω. Matching the two solutions we obtain the retarded correlator $G_{\rm R}$ from which we can calculate $\eta_\perp$ and $\eta_\parallel$.

Consider a fluctuation ψ (again, ψ could be $\psi_\perp = h^x_{\ y}(t,y,z,u)$ or $\psi_{||} = h^x_{\ z}(t,y,z,u)$, as in the main body of this paper). The effective action and the equation of motion

for ψ have the following form

$$S_{\text{eff}} = -\frac{1}{2}\frac{1}{16\pi G}\int \frac{d\omega}{2\pi}\frac{d^3k}{(2\pi)^3}du\left[n(u)(\psi')^2 - m(u)\psi^2\right] ,$$
$$(n(u)\psi')' - m(u)\psi = 0\,, \qquad \psi = \psi(u,k)\,. \tag{8.109}$$

To be concrete, let us work out the case $\psi = \psi_\parallel$. For $\mathbf{k} = 0$, we have

$$\begin{aligned} n_\parallel(u) &= g^{uu}\sqrt{-g}\left(\frac{g_{xx}}{g_{zz}} - \frac{\lambda_{\text{GB}}}{2}\frac{g_{xx}^2 g'_{tt}g'_{yy}}{g}\right) , \\ m_\parallel(u) &= -\omega^2 g^{tt}\sqrt{-g}\frac{g_{xx}}{g_{zz}} - \frac{\lambda_{\text{GB}}}{2}\omega^2\left[\frac{g_{yy}g'_{uu}g'_{yy} + g'^2_{yy} - 2g_{yy}g'_{yy}}{\sqrt{g_{tt}g_{zz}}(g_{uu}g_{yy})^{3/2}}\right] g_{xx}^{3/2}\,. \end{aligned} \tag{8.110}$$

When $\omega = 0$ and $\mathbf{k} = 0$, we get that $m_\parallel(u) = 0$ and $(n(u)\psi')' = 0$. Hence $n(u)\psi' = C_2$, where C_2 is a constant. This implies that

$$\psi_\parallel = C_1 + C_2\int_0^u \frac{du'}{n_\parallel(u')}\,. \tag{8.111}$$

As $n_\parallel \propto g^{uu}$ and g^{uu} goes to zero at the horizon, we must have $C_2 = 0$ for $\omega = 0$. For small ω we can have a normalizable solution with $C_2 \propto \omega$. Using the prescription of [103] we calculate G_{R} as

$$G_{\text{R}} = -2\left[-\frac{1}{2}\frac{1}{16\pi G}n_\parallel(u)\psi_\parallel(u,-k)\partial_u\psi_\parallel(u,k)\right]_{u=0} , \tag{8.112}$$

where $\psi_\parallel$ should be equal to one at the boundary $u = 0$. Using (8.111) and (8.112) we can see that

$$G_{\text{R}} = \frac{C_2}{16\pi G}\,, \qquad (\text{small } \omega,\, \mathbf{k} = 0)\,. \tag{8.113}$$

We set $C_1 = 1$ in the equation above in order to have $\psi_\parallel(0,k) = 1$. Now we have to

determine C_2. Near the horizon, (8.111) can be written as

$$\psi_\parallel = 1 + C_2 \int_0^u \frac{du'}{n'_\parallel(u_{\rm H})(u-u_{\rm H})} = 1 + \frac{C_2}{n'_\parallel(u_{\rm H})} \log\left(1 - \frac{u}{u_{\rm H}}\right) . \tag{8.114}$$

We now find a near-horizon expression for $\psi_\parallel$ and expand it for small ω. The first thing we need to do is to write the $\psi_\parallel$ equation of motion in the limit $u \to u_{\rm H}$. In what follows, it will be convenient to work with the constants c_0 and c_1, defined by the near-horizon expansions for g_{tt} and g^{uu} as

$$g_{tt} = c_0(u-u_{\rm H})\,, \qquad g^{uu} = c_1(u-u_{\rm H})\,. \tag{8.115}$$

The near-horizon equation of motion is

$$(n_\parallel(u_{\rm H})(u-u_{\rm H})\psi'_\parallel)' - m_\parallel(u_{\rm H})\psi_\parallel = 0\,, \tag{8.116}$$

where

$$\begin{aligned} n_\parallel(u_{\rm H}) &= c_1\sqrt{-g}\left(\frac{g_{xx}}{g_{zz}} - \frac{\lambda_{\rm GB}}{2}\frac{g_{xx}^2 g'_{tt} g'_{yy}}{-g}\right)\Big|_{u_{\rm H}}\,, \\ m_\parallel(u_{\rm H}) &= -\frac{\omega^2}{c_0(u-u_{\rm H})}\sqrt{-g}\,\frac{g_{xx}}{g_{zz}}\Big|_{u_{\rm H}}\,. \end{aligned} \tag{8.117}$$

Plugging (8.117) into (8.116) and using the anzats $\psi_\parallel = (1-u/u_{\rm H})^\beta$ we can show that $\beta = \pm i\omega/\sqrt{c_0 c_1}$.[25] The general solution of (8.116) is then given by

$$\psi_\parallel = C_+\left(1-\frac{u}{u_{\rm H}}\right)^{\frac{i\omega}{\sqrt{c_0c_1}}} + C_-\left(1-\frac{u}{u_{\rm H}}\right)^{-\frac{i\omega}{\sqrt{c_0c_1}}}\,. \tag{8.118}$$

[25]Note that the temperature is given by $T = \frac{\sqrt{c_0c_1}}{4\pi}$, so that $\beta = \pm\frac{i\omega}{4\pi T}$.

We choose $C_+ = 0$ to impose infalling boundary conditions at the horizon. For small β, i.e. for $\omega \ll T$, we have

$$\psi_\parallel = C_- \left[1 + \frac{i\omega}{\sqrt{c_0 c_1}} \log\left(1 - \frac{u}{u_{\rm H}}\right)\right] . \tag{8.119}$$

Comparing (8.119) with (8.114) we can see that

$$\frac{C_2}{n_\parallel(u_{\rm H})} = \frac{-i\omega}{\sqrt{c_0 c_1}} , \tag{8.120}$$

and using (8.117) it is easy to show that

$$C_2 = -i\omega \sqrt{\frac{c_1}{c_0}} \sqrt{-g} \left(\frac{g_{xx}}{g_{zz}} - \frac{\lambda_{\rm GB}}{2} \frac{g_{xx}^2 g'_{tt} g'_{yy}}{-g}\right) \Big|_{u_{\rm H}} . \tag{8.121}$$

Plugging this result into (8.113) we have

$$G_{\rm R} = -\frac{i\omega}{16\pi G} \sqrt{\frac{c_1}{c_0}} \sqrt{-g} \left(\frac{g_{xx}}{g_{zz}} - \frac{\lambda_{\rm GB}}{2} \frac{g_{xx}^2 g'_{tt} g'_{yy}}{-g}\right) \Big|_{u_{\rm H}} . \tag{8.122}$$

According to the Kubo formula

$$\eta_\parallel = \lim_{\omega \to 0} \frac{1}{\omega} {\rm Im}\, G_{\rm R} = \frac{1}{16\pi G} \sqrt{\frac{c_1}{c_0}} \sqrt{-g} \left(\frac{g_{xx}}{g_{zz}} - \frac{\lambda_{\rm GB}}{2} \frac{g_{xx}^2 g'_{tt} g'_{yy}}{-g}\right) \Big|_{u_{\rm H}} . \tag{8.123}$$

The density entropy s is given by

$$s = \frac{1}{4G} \sqrt{\frac{g}{g_{tt} g_{uu}}} \Big|_{u_{\rm H}} = 4\pi \frac{\sqrt{-g}}{16\pi G} \sqrt{\frac{c_1}{c_0}} , \tag{8.124}$$

and we can finally calculate the ratio

$$\frac{\eta_{\parallel}}{s} = \frac{1}{4\pi}\left(\frac{g_{xx}}{g_{zz}} - \frac{\lambda_{\rm GB}}{2}\frac{g_{xx}^2 g'_{tt} g'_{yy}}{g}\right)\Big|_{u_{\rm H}}. \tag{8.125}$$

Doing the same for $\psi_\perp$ it is possible to show that

$$\frac{\eta_{\perp}}{s} = \frac{1}{4\pi}\left(\frac{g_{xx}}{g_{yy}} - \frac{\lambda_{\rm GB}}{2}\frac{g_{xx}^2 g'_{tt} g'_{zz}}{g}\right)\Big|_{u_{\rm H}}. \tag{8.126}$$

In both cases we find the same result (8.37) that we had obtained using the membrane paradigm.

Appendix 8.C Drag force for a general background and arbitrary direction

In this appendix we derive a formula for the drag force. The metric background is assumed to be of the form

$$ds^2 = G_{tt}dt^2 + G_{xx}(dx^2 + dy^2) + G_{zz}dz^2 + G_{uu}du^2. \tag{8.127}$$

We will only assume rotational symmetry in the xy directions and consider the metric to depend only on u. This is essentially what was done in [186], but here we consider the motion of the quark along an arbitrary direction, as in [15].

The Nambu-Goto action for the string is given by

$$S = -\frac{1}{2\pi\alpha'}\int d\tau d\sigma\, e^{\phi/2}\sqrt{-\det g} = \int d\tau d\sigma \mathcal{L}, \tag{8.128}$$

where $\phi = \phi(u)$ is the dilaton field. By rotational symmetry in the xy directions we can set $y = 0$. We choose static gauge $(t, u) = (\tau, \sigma)$ and let us consider the motion of the quark in the xz plane with a string embedding

$$x(t,u) = (vt + \xi(u)) \sin\varphi, \qquad z(t,u) = (vt + \zeta(u)) \cos\varphi, \tag{8.129}$$

where φ is the angle of the quark trajectory with the z axis, i.e., $\varphi = 0$ corresponds to the motion parallel with the anisotropic direction and $\varphi = \pi/2$ corresponds to the motion in the transversal direction. The boundary conditions are $\xi(u \to 0) = 0$ and $\zeta(u \to 0) = 0$, which are necessary in order to reproduce the stationary motion of the quark.

First, we need to compute the induced metric $g_{\alpha\beta} = G_{\mu\nu}\partial_\alpha x^\mu \partial_\beta x^\nu$ on the string worldsheet,

$$g_{\alpha\beta} = \begin{pmatrix} G_{tt} + v^2(G_{zz}\cos^2\varphi + G_{xx}\sin^2\varphi) & v\left(G_{zz}\zeta'(u)\cos^2\varphi + G_{xx}\xi'\sin^2\varphi\right) \\ v\left(G_{zz}\zeta'\cos^2\varphi + G_{xx}\xi'\sin^2\varphi\right) & G_{uu} + G_{zz}\zeta'^2\cos^2\varphi + G_{xx}\xi'^2\sin^2\varphi \end{pmatrix}, \tag{8.130}$$

where the prime denotes the derivative w.r.t. u. Ignoring factors of $\frac{1}{2\pi\alpha'}$, the Lagrangian takes the form

$$\begin{aligned}\mathcal{L} = -e^{\phi/2}\big[-G_{zz}\cos^2\varphi(\zeta'^2 G_{tt} + G_{uu}v^2 + G_{xx}v^2(\zeta' - \xi')^2\sin^2\varphi) - \\ -G_{xx}\sin^2\varphi(G_{tt}\xi'^2 + G_{uu}v^2) - G_{tt}G_{uu}\big]^{\frac{1}{2}}.\end{aligned} \tag{8.131}$$

We have the associated (conserved) momentum flow

$$\Pi_x = \frac{\delta \mathcal{L}}{\delta x'} = -\frac{e^{\phi} G_{xx} \sin\varphi}{\mathcal{L}} \left(G_{tt}\xi' - G_{zz} v^2 (\zeta' - \xi') \cos^2\varphi \right), \tag{8.132}$$

$$\Pi_z = \frac{\delta \mathcal{L}}{\delta z'} = -\frac{e^{\phi} G_{zz} \cos\varphi}{\mathcal{L}} \left(G_{tt}\zeta' + G_{xx} v^2 (\zeta' - \xi') \sin^2\varphi \right). \tag{8.133}$$

The values of the momenta will be fixed by imposing the requirement that ξ' and ζ' are both real. To do this, we invert the above expression, writing

$$\xi'(u) = \frac{G_{zz} N_x}{G_{xx} N_z} \zeta'(u), \tag{8.134}$$

where we have defined the quantities

$$N_x = G_{tt}\Pi_x \csc(\varphi) + G_{xx} v^2 (\Pi_x \sin(\varphi) + \Pi_z \cos(\varphi)), \tag{8.135}$$

$$N_z = G_{tt}\Pi_z \sec(\varphi) + G_{zz} v^2 (\Pi_x \sin(\varphi) + \Pi_z \cos(\varphi)). \tag{8.136}$$

Then we can use, for example, the expression for Π_z to obtain ζ'. The final expressions we found are given by

$$\xi' = \pm\sqrt{-\frac{2G_{uu}G_{zz}}{G_{tt}G_{xx}D}} N_x, \qquad \zeta' = \pm\sqrt{-\frac{2G_{uu}G_{xx}}{G_{tt}G_{zz}D}} N_z, \tag{8.137}$$

where

$$\begin{aligned} D = {} & 2G_{tt}\left(G_{xx}\Pi_z^2 + G_{zz}\Pi_x^2\right) + G_{xx}G_{zz}\left[G_{tt}e^{\phi}\left(2G_{tt} + v^2(G_{xx} + G_{zz})\right) + v^2\left(\Pi_x^2 + \Pi_z^2\right)\right] + \\ & + G_{xx}G_{zz}v^2\left[\left(-G_{tt}(G_{xx} - G_{zz})e^{\phi} - \Pi_x^2 + \Pi_z^2\right)\cos(2\varphi) + 2\Pi_x\Pi_z\sin(2\varphi)\right]. \end{aligned} \tag{8.138}$$

There is a sign ambiguity here, which we will fix later. The condition that ξ' and ζ' are always real can be satisfied only if D is positive for all u. But, in general, D has two zeros (turning points). Thus, in order to satisfy the positivity condition the two zeros should coincide at some critical point u_c. Also, the numerators N_x and N_z should vanish at the same point u_c, because otherwise ξ' and ζ' would diverge. We begin the analysis finding the zeros of the numerator. Imposing N_x and N_z to vanish at u_c gives us a relation between Π_x and Π_z,

$$\frac{\Pi_x}{\Pi_z} = \frac{G_{xx}}{G_{zz}} \tan\varphi\Big|_{u=u_c}. \tag{8.139}$$

Using this relation, we can find the two zeros of D at u_c. This gives us two equations; the first one is

$$\left[\frac{2G_{tt}}{v^2} + G_{xx} + G_{zz} + (G_{zz} - G_{xx})\cos(2\varphi)\right]_{u=u_c} = 0, \tag{8.140}$$

which can be used to fix the value of the critical point u_c. The second equation completely fixes the values of Π_x and Π_z and gives us the drag force

$$\Pi_x = e^{\phi/2} G_{xx} v \sin\varphi\Big|_{u=u_c}, \qquad \Pi_z = e^{\phi/2} G_{zz} v \cos\varphi\Big|_{u=u_c}. \tag{8.141}$$

We have fixed the sign of the momenta to be positive, thus ξ' and ζ' are both negative, which is consistent with the physical condition that the string "trails" behind the quark [183, 184] and not in front of it. Two special cases are obtained from (8.50) by setting $\varphi = 0$ and $\varphi = \pi/2$. This gives us the drag force parallel and transversal to

the direction of motion of the quark, respectively,

$$F^{||}_{\rm drag} = e^{\phi/2} G_{zz} v\Big|_{u=u_c}, \qquad F^{\perp}_{\rm drag} = e^{\phi/2} G_{xx} v\Big|_{u=u_c}. \tag{8.142}$$

Appendix 8.D Jet quenching parameter for an arbitrary motion

In this appendix we derive a formula for $\hat{q}$ considering a motion in an arbitrary direction and generic background. The steps are basically the same of [214], but here the computation is carried out in Einstein frame and the metric is left generic, with only a few assumptions, which we will specify below.

We assume a five-dimensional background displaying rotational symmetry in the xy directions,

$$ds^2 = G_{tt} dt^2 + G_{xx}(dx^2 + dy^2) + G_{zz} dz^2 + G_{uu} du^2. \tag{8.143}$$

From the rotational symmetry we can choose the direction of motion within the xz-plane. We define rotated coordinates

$$\begin{aligned} z &= Z\cos\theta - X\sin\theta, \\ x &= Z\sin\theta + X\cos\theta, \\ y &= Y. \end{aligned} \tag{8.144}$$

The new coordinates (X, Y, Z) are obtained from the old coordinates (x, y, z) by a rotation of an angle θ around the y-axis. We choose Z to be the direction of motion of

the quark. The direction of the momentum broadening takes place in the XY-plane and it forms an angle φ with the Y-axis. The prescription instructs us to consider a string with an endpoint moving at the speed of light along the Z direction. The other endpoint is separated by a small distance ℓ along the direction of the momentum broadening. Thus we have a string worldsheet whose boundary is a rectangular light-like Wilson loop with sizes L^- (along the Z^- direction) and ℓ, where L^- is assumed to be very large. Our task is to find a string worldsheet that minimizes the Nambu-Goto action satisfying this boundary condition. We then need to evaluate the on-shell Nambu-Goto action and expand it to second order in ℓ to obtain

$$\left\langle W^A(\mathcal{C})\right\rangle \simeq \exp\left[-\frac{L^-\ell^2}{4\sqrt{2}}\hat{q}\right], \tag{8.145}$$

from which we extract the jet quenching parameter. It is convenient to work in light-cone coordinates

$$t = \frac{Z^- + Z}{\sqrt{2}}, \quad Z = \frac{Z^- - Z^+}{\sqrt{2}}. \tag{8.146}$$

The metric in these new coordinates takes the form

$$G^{(LC)}_{\mu\nu} = \begin{pmatrix} G_{++} & G_{+-} & G_{X-} & 0 & 0 \\ G_{+-} & G_{++} & -G_{X-} & 0 & 0 \\ G_{X-} & -G_{X-} & G_{XX} & 0 & 0 \\ 0 & 0 & 0 & G_{xx} & 0 \\ 0 & 0 & 0 & 0 & G_{uu} \end{pmatrix}, \tag{8.147}$$

where

$$
\begin{aligned}
G_{++} &= \frac{1}{2}\left(G_{tt} + G_{xx}\sin^2\theta + G_{zz}\cos^2\theta\right), \\
G_{+-} &= \frac{1}{2}\left(G_{tt} - G_{xx}\sin^2\theta - G_{zz}\cos^2\theta\right), \\
G_{X-} &= \frac{\sin\theta\cos\theta}{\sqrt{2}}(G_{xx} - G_{zz}), \\
G_{XX} &= G_{xx}\cos^2\theta + G_{zz}\sin^2\theta.
\end{aligned}
\tag{8.148}
$$

We choose the static gauge $(\tau, \sigma) = (Z^-, u)$. Since we are assuming L^- to be very large, there is a translational symmetry in the Z^- direction, and we can fix the string embedding to only depend on u,

$$
Z^+ = Z^+(u), \quad X \to X(u)\sin\varphi, \quad Y \to Y(u)\cos\varphi. \tag{8.149}
$$

The induced metric on the string worldsheet, $g_{\alpha\beta} = G_{\mu\nu}\,\partial_\alpha x^\mu \partial_\beta x^\nu$, is given by

$$
\begin{aligned}
&g_{\tau\tau} = G_{++}, \qquad g_{\tau\sigma} = \sin\varphi\, G_{X-}X' + G_{+-}(Z^+)', \\
&g_{\sigma\sigma} = G_{uu} + \sin^2\varphi\, G_{XX}X'^2 - 2\sin\varphi\, G_{X-}(Z^+)'X' + \cos^2\varphi\, G_{xx}Y'^2 + G_{++}(Z^+)'^2,
\end{aligned}
\tag{8.150}
$$

where the primes denote the derivative w.r.t. u. We can now write the Nambu-Goto action,[26]

$$
S = -2\frac{L^-}{2\pi\alpha'}\int_0^{u_\mathrm{H}} du\, e^{\phi/2}\sqrt{-\det g} \equiv \frac{L^-}{\pi\alpha'}\int_0^{u_\mathrm{H}} du\, \mathcal{L}, \tag{8.151}
$$

[26]The extra factor of 2 comes from the two branches of the string worldsheet.

where $\phi = \phi(u)$ is the dilaton scalar field and

$$\begin{aligned}\mathcal{L} = - e^{\phi/2} \Big[& (G_{+-} + G_{++}) \left(2 G_{X-} X' (Z^+)' \sin\varphi - G_{XX} (Z^+)'^2 \right) \\ & - G_{++} \left(G_{uu} + G_{xx} Y'^2 \cos^2\varphi \right) + X'^2 \sin^2\varphi \left(G_{X-}^2 - G_{++} G_{XX} \right) \Big]^{\frac{1}{2}} .\end{aligned} \tag{8.152}$$

Since the Lagrangian does not depend on Z^+, X, and Y, we have three conserved quantities, given by the canonical conjugate momenta. Up to a constant factor, they are given by

$$\begin{aligned}\Pi_+ &= \frac{e^\phi}{\mathcal{L}} (G_{+-} + G_{++})(G_{X-} X' \sin\varphi - G_{XX} (Z^+)'), \\ \Pi_X &= \frac{e^\phi}{\mathcal{L}} \sin\varphi \left[G_{X-} (Z^+)' (G_{+-} + G_{++}) + X' \sin\varphi \left(G_{X-}^2 - G_{++} G_{XX} \right) \right], \\ \Pi_Y &= - \frac{e^\phi}{\mathcal{L}} G_{++} G_{xx} Y' \cos^2\varphi .\end{aligned} \tag{8.153}$$

We are interested in the limit where Π_+, Π_X, and Π_Y are small.[27] Working in first order in the Π_+, Π_X and Π_Y, we can invert the above expressions to obtain $(Z^+)'$, X' and Y', we find that

$$\begin{aligned}(Z^+)' &= c_{++} \Pi_+ + c_{+X} \Pi_X \csc\varphi, \\ X' &= c_{X+} \Pi_+ \csc\varphi + c_{XX} \Pi_X \csc^2\varphi, \\ Y' &= c_{YY} \Pi_Y \sec^2\varphi,\end{aligned} \tag{8.154}$$

[27] This is a consequence of ℓ be small, as explained in [214].

where

$$
\begin{aligned}
c_{++} &= \frac{e^{-\phi/2}G_{uu}\left(G_{X-}^2 - G_{++}G_{XX}\right)}{(G_{+-}+G_{++})\sqrt{-G_{++}G_{uu}}\left(G_{XX}^2 - 2G_{X-}^2\right)}, \\
c_{+X} = c_{X+} &= \frac{e^{-\phi/2}G_{uu}G_{X-}}{\sqrt{-G_{++}G_{uu}}\left(2G_{X-}^2 - G_{XX}^2\right)}, \\
c_{XX} &= -\frac{e^{-\phi/2}G_{uu}G_{XX}}{\sqrt{-G_{++}G_{uu}}\left(G_{XX}^2 - 2G_{X-}^2\right)}, \\
c_{YY} &= -\frac{e^{-\phi/2}G_{uu}}{G_{xx}\sqrt{-G_{++}G_{uu}}}.
\end{aligned}
\tag{8.155}
$$

Integration of $Z^{+\prime}$ gives zero. Integration of $X^\prime$ gives $\ell/2$. Integration of $Y^\prime$ also gives $\ell/2$. The conclusion is that

$$
\begin{aligned}
\Pi_+ &= \frac{\ell \sin\varphi \left(\int_0^{u_{\rm H}} c_{+X}(u)\,du\right)}{2\left(\left(\int_0^{u_{\rm H}} c_{+X}(u)\,du\right)^2 - \left(\int_0^{u_{\rm H}} c_{++}(u)\,du\right)\int_0^{u_{\rm H}} c_{+X}(u)\,du\right)}, \\
\Pi_X &= \frac{\ell \sin^2\varphi \left(\int_0^{u_{\rm H}} c_{++}(u)\,du\right)}{2\left(\int_0^{u_{\rm H}} c_{++}(u)\,du\right)\int_0^{u_{\rm H}} c_{+X}(u)\,du - 2\left(\int_0^{u_{\rm H}} c_{+X}(u)\,du\right)^2}, \\
\Pi_Y &= \frac{\ell\cos^2\varphi}{2\int_0^{u_{\rm H}} c_{YY}(u)\,du}.
\end{aligned}
\tag{8.156}
$$

The on-shell action then takes the form, up to second order in the momenta,

$$
S = 2i\frac{\sqrt{\lambda}L^-}{4\pi}\int_0^{u_{\rm H}} du\left[c_{++}\Pi_+^2 + \frac{1}{\sin^2\varphi}c_{XX}\Pi_X^2 + \frac{2}{\sin\varphi}c_{+X}\Pi_+\Pi_X + \frac{1}{\cos^2\varphi}c_{YY}\Pi_Y^2\right].
\tag{8.157}
$$

Using the expressions for the coefficients the action can be rewritten as

$$
S = 2i\frac{\sqrt{\lambda}L^-\ell^2}{16\pi}\left(\hat{P}(\theta)\sin^2\varphi + \hat{Q}(\theta)\cos^2\varphi\right),
\tag{8.158}
$$

where

$$\hat{P}(\theta) \equiv \frac{\int_0^{u_{\rm H}} c_{++}(u)\,du}{\left(\int_0^{u_{\rm H}} c_{++}(u)\,du\right)\int_0^{u_{\rm H}} c_{+X}(u)\,du - \left(\int_0^{u_{\rm H}} c_{+X}(u)\,du\right)^2}\,,$$
$$\hat{Q}(\theta) \equiv \frac{1}{\int_0^{u_{\rm H}} c_{YY}du}\,. \tag{8.159}$$

From this we immediately extract the jet quenching parameter

$$\hat{q} = \frac{\sqrt{2\lambda}}{\pi}\left(\hat{P}(\theta)\sin^2\varphi + \hat{Q}(\theta)\cos^2\varphi\right). \tag{8.160}$$

Appendix 8.E Quarkonium static potential in generic background

In this appendix we derive a formula for the static potential of a quark-antiquark pair (quarkonium).[28] Let L be the separation between the quarks and assume a generic background of the form (8.127). The dual picture corresponds to an U-shaped open string whose endpoints are located at the boundary and are identified with the quarks. Our task is to find the string worldsheet that minimizes the Nambu-Goto action (8.128). By rotational symmetry in the xy-plane we can assume the pair to live in the xz-plane. Putting the center of mass of the pair at the origin, let q be the polar radial coordinate and θ the angle between the pair and the z direction. We fix the gauge $(\tau,\sigma) = (t,q)$. In this way the string embedding has the form

$$X^\mu = (\tau, \sigma\sin\theta, 0, \sigma\cos\theta, u(\sigma)) \tag{8.161}$$

[28]This computation is similar to what was done in [186], generalizing the prescription of [257] for an anisotropic background.

The induced metric on the string worldsheet is given by

$$g_{\tau\tau} = G_{tt}, \quad g_{\sigma\sigma} = G_{pp} + G_{uu}u'^2, \quad g_{\tau\sigma} = 0, \tag{8.162}$$

where $G_{pp} \equiv G_{zz}\cos^2\theta + G_{xx}\sin^2\theta$ and the prime denotes derivative w.r.t. σ. The Nambu-Goto action takes the form

$$S = -\frac{\mathcal{T}}{2\pi\alpha'}\int_{-L/2}^{L/2} d\sigma\, e^{\phi/2}\sqrt{-G_{tt}\left(G_{pp} + G_{uu}u'^2\right)} \equiv \int_{-L/2}^{L/2} d\sigma\, \mathcal{L}. \tag{8.163}$$

Since the Lagrangian $\mathcal{L}$ does not depend explicitly on σ, the Hamiltonian is a constant of motion

$$H = \frac{\partial\mathcal{L}}{\partial\sigma'}\sigma' - \mathcal{L} = -\frac{\mathcal{T}}{2\pi\alpha'}\frac{e^{\phi/2}G_{tt}G_{pp}}{\sqrt{-G_{tt}\left(G_{pp} + G_{uu}u'^2\right)}}. \tag{8.164}$$

Evaluating the Hamiltonian at the turning point $u_0 \equiv u(0)$, where $u' = 0$, we find the value of the constant to be

$$C = \frac{\mathcal{T}}{2\pi\alpha'}e^{\frac{\phi}{2}}\sqrt{-G_{pp}G_{tt}}\Big|_{u=u_0}. \tag{8.165}$$

In order to simplify the expressions, it is useful to define the auxiliary quantities

$$P \equiv e^{\frac{\phi}{2}}\sqrt{-G_{pp}G_{tt}}\,, \qquad Q \equiv e^{\frac{\phi}{2}}\sqrt{-G_{tt}G_{uu}}\,. \tag{8.166}$$

Using (8.164) and(8.165) we can find an expression for u',[29]

$$u' = \pm\frac{P}{Q}\frac{\sqrt{P^2 - P_0^2}}{P_0}, \quad P_0 \equiv P|_{u=u_0}. \tag{8.167}$$

[29]One needs to be careful with the choice of sign here: when σ goes from 0 to $L/2$, then u goes from u_0 to 0 and thus $u' < 0$.

Integrating the above expression we find that the separation between the quarks is given by

$$L = -2\int_0^{u_0} \frac{d\sigma}{du} du = 2\int_0^{u_0} \frac{Q}{P}\frac{P_0}{\sqrt{P^2 - P_0^2}}\,. \tag{8.168}$$

Before we compute the on-shell Nambu-Goto action to find the potential energy that keeps the pair bounded, we need to take care of the ultraviolet divergence due to the infinite mass of the quarks. The mass term corresponds to a string hanging down straight from the boundary to the horizon. Note that in this case the string goes from 0 to $u_{\rm H}$ while σ is fixed, thus it effectively corresponds to $u' \to \infty$. Expanding the on-shell Nambu-Goto action in powers of $1/u'$ for this configuration we obtain

$$M_Q = -\frac{\mathcal{T}}{2\pi\alpha'}\int_0^{u_{\rm H}} du\, Q + O\left(\frac{1}{u'}\right). \tag{8.169}$$

Finally, computing the on-shell Nambu-Goto action for the U-shaped configuration with the mass subtraction we obtain the static potential

$$V_{Q\bar{Q}} = \frac{S^{(\text{on-shell})}}{\mathcal{T}} - 2M_Q = -\frac{1}{2\pi\alpha'}\left[P_0 L + 2\int_0^{u_0} du \frac{Q}{P}\left(\sqrt{P^2 - P_0^2} - P\right) - 2\int_{u_0}^{u_{\rm H}} du\, Q\right]. \tag{8.170}$$

Chapter 9

Conclusion

The main goal of this thesis is to apply the AdS/CFT correspondence to the study strongly coupled systems similar to the QGP formed in heavy ion collisions. The aim of the chapters 2-5 is to provide a basic introduction to some topics relevant for those who study applications of the AdS/CFT to the QGP. The Chapter 2 presents a brief introduction to QCD and its thermodynamics. In this chapter we present the strongly coupled deconfined phase of QCD known as QGP, which is our object of study in this work. In Chapters 3 and 4 we present some basic knowledge necessary to understand the gauge/gravity duality. Chapter 3 gives a brief introduction to conformal field theories, with emphasys to the $\mathcal{N} = 4$ SYM theory. Chapter 4 presents some basic aspects of string theory and D-branes. We then present an introduction to the AdS/CFT correspondence in Chapter 5. The chapters 6, 7, 8 contains the original work of this thesis.

In Chapter 6 we study the thermal production of photons and dileptons in a strongly coupled anisotropic plasma. We also compute the DC conductivity of this plasma. We compare the obtained results with the isotropic counterparts of a plasma

at the same temperature. This plasma was modeled using the anisotropic black brane solution found in [10, 11]. Despite being asymptotically AdS, this geometry is static and regular everywhere. The anisotropy is provided by a bulk axion field, linear in one of the gauge theory directions (z in our case).

The charged particles of this plasma are "quarks" (fields in the fundamental representation of the gauge group) provided by the introduction of flavor D7-branes. We consider non-equatorial embeddings of the flavor D7-branes, corresponding to quarks with non-vanishing masses, thus making a more realistic model.

The main results for the photon production rate may be summarized as follows: the anisotropic plasma glows brighter than its isotropic counterpart at the same temperature. The quark mass has the effect of decreasing the photon production rate and the DC conductivity of the plasma. The decrease is greater as we increase the quark mass, as expected on general grounds.

Generically, the dilepton production rate is larger than its isotropic counterpart at the same temperature, except for a small range of anisotropies, if the frequency and the quark mass are sufficiently large. Increasing the quark masses increases the deviation from the corresponding isotropic results.

The production of dileptons for momenta along the anisotropic direction is always larger than the production in the transverse plane. This is contrary to what is obtained for a weakly coupled anisotropic plasma, where there is a suppression along the forward direction [57,58,59]. However, the enhancement of the dilepton production rate in an anisotropic plasma appears to be a robust feature of this system, which is present both at weak and strong coupling.

All the quantities cited above were found to be monotonically dependent (either increasing or decreasing) on the angle between the momentum and the anisotropic

direction.

Finally, we expected our results concerning the effects of the anisotropy to be quite general, because the source of the anisotropy, the axion field, does not appear in the equation of motion of the gauge fields. However, it would be interesting to compute these quantities in other anisotropic models to understand which features are really model-independent and therefore more realistic.

In Chapter 7 we study how higher derivative terms affects the Chern-Simons diffusion rate. We compute this quantity in Gauss-Bonnet theory of gravity and also in Quasi-topological gravity theory. Let $\lambda_{\rm GB}$ be dimensionless coupling of the Gauss-Bonnet quadratic term and μ the dimensonless coupling of the Quasi-topological cubic term. This couplings corresponds to have more general conformal field theories on the boudary than the ones usually consider. The Gauss-Bonnet term results in having different central charges $a \neq c$ [169–171], while the Quasi-topological term results in the breaking of suersymmetry.

We compare our results with the result obtained in Einstein's theory of gravity (in which $\lambda_{\rm GB} = 0$ and $\mu = 0$). We found corrections that can be either smaller or greater than one, depending on the value of the parameters.

We conclude that, even if there isn't a UV completion for these higher derivative gravity theories, we can use it as toy models to investigate how the correspondence works in larger regions of the parameter space.

In Chapter 8 we found an anisotropic black brane solution (Eq. (8.8)) in five dimensional GB-gravity coupled to an axion-dilation field which incorporates both the effects of anysotropy and higher curvature corrections. The higher curvature correction is a Gauss-Bonnet term and the source of anisotropy is an axion field linearly dependent on one of the horizon coordinates. The solution found is the GB

corrected equivalent of the geometry discovered in [10, 11].

We have computed the shear viscosity over entropy density ratio for the dual plasma and found that the KSS bound [9] is violated, as expected from previous works where either the case ($a = 0$, $\lambda_{\rm GB} \neq 0$) [156] or the case ($a \neq 0$, $\lambda_{\rm GB} = 0$) [13] were considered. We also computed several other observables, like the eletric conductivity, the drag force, the jet quenching parameter, the quark-antiquark potential, and the photon production rate. The effects of anisotropy and of higher curvature term can be understood in terms of the corresponding effects on the mean free-path of medium, as explained the Section 8.5.

An interesting application of the solution (8.8) would be a detailed investigation of the thermodynamic properties of the dual plasma, as was done in [10, 11] for the $\lambda_{\rm GB} = 0$ case. The conformal anomaly plays an important role in such analysis, but this quantity only appears at order $O(a^4)$ while our solution is only valid up to second order. Then, it is necessary to extend our analytic solution to order $O(a^4)$ to achieve an interesting thermodynamic description of this system. This extension presumably requires the use of numerical methods to explore larger values of the anisotropy.

Bibliography

[1] J. M. Maldacena, "The Large N limit of superconformal field theories and supergravity," Adv. Theor. Math. Phys. **2**, 231-252 (1998) [hep-th/9711200].

[2] S. S. Gubser, I. R. Klebanov, A. M. Polyakov, "Gauge theory correlators from noncritical string theory," Phys. Lett. **B428**, 105-114 (1998) [hep-th/9802109].

[3] E. Witten, "Anti-de Sitter space and holography," Adv. Theor. Math. Phys. **2**, 253-291 (1998) [hep-th/9802150].

[4] J. Adams *et al.* [STAR Collaboration], "Experimental and theoretical challenges in the search for the quark gluon plasma: The STAR collaboration's critical assessment of the evidence from RHIC collisions," Nucl. Phys. A **757**, 102 (2005) [arXiv:nucl-ex/0501009].

[5] K. Adcox *et al.* [PHENIX Collaboration], "Formation of dense partonic matter in relativistic nucleus nucleus collisions at RHIC: Experimental evaluation by the PHENIX collaboration," Nucl. Phys. A **757**, 184 (2005) [arXiv:nucl-ex/0410003].

[6] Proceedings of Quark Matter 2011: J. Phys. GG **38**, number 12 (December 2011).

[7] E. Shuryak, "Why does the quark gluon plasma at RHIC behave as a nearly ideal fluid?," Prog. Part. Nucl. Phys. **53**, 273 (2004) [arXiv:hep-ph/0312227].

[8] E. V. Shuryak, "What RHIC experiments and theory tell us about properties of quark-gluon plasma?," Nucl. Phys. A **750**, 64 (2005) [arXiv:hep-ph/0405066].

[9] P. Kovtun, D. T. Son and A. O. Starinets, "Viscosity in strongly interacting quantum field theories from black hole physics," Phys. Rev. Lett. **94**, 111601 (2005) [hep-th/0405231].

[10] D. Mateos and D. Trancanelli, "The anisotropic N=4 super Yang-Mills plasma and its instabilities," Phys. Rev. Lett. **107**, 101601 (2011) [arXiv:1105.3472 [hep-th]].

[11] D. Mateos and D. Trancanelli, "Thermodynamics and Instabilities of a Strongly Coupled Anisotropic Plasma," JHEP **1107**, 054 (2011) [arXiv:1106.1637 [hep-th]].

[12] T. Azeyanagi, W. Li and T. Takayanagi, "On String Theory Duals of Lifshitz-like Fixed Points," JHEP **0906**, 084 (2009) [arXiv:0905.0688 [hep-th]].

[13] A. Rebhan and D. Steineder, "Violation of the Holographic Viscosity Bound in a Strongly Coupled Anisotropic Plasma," Phys. Rev. Lett. **108**, 021601 (2012) [arXiv:1110.6825 [hep-th]].

[14] K. A. Mamo, "Holographic Wilsonian RG Flow of the Shear Viscosity to Entropy Ratio in Strongly Coupled Anisotropic Plasma," JHEP **1210**, 070 (2012) [arXiv:1205.1797 [hep-th]].

[15] M. Chernicoff, D. Fernandez, D. Mateos and D. Trancanelli, "Drag force in a strongly coupled anisotropic plasma," JHEP **1208**, 100 (2012) [arXiv:1202.3696 [hep-th]].

[16] D. Giataganas, "Probing strongly coupled anisotropic plasma," JHEP **1207**, 031 (2012) [arXiv:1202.4436 [hep-th]].

[17] K. B. Fadafan and H. Soltanpanahi, "Energy loss in a strongly coupled anisotropic plasma," JHEP **1210**, 085 (2012) [arXiv:1206.2271 [hep-th]].

[18] B. Muller and D. -L. Yan, "Light Probes in a Strongly Coupled Anisotropic Plasma," Phys. Rev. D **87**, 046004 (2013) [arXiv:1210.2095 [hep-th]].

[19] M. Chernicoff, D. Fernandez, D. Mateos and D. Trancanelli, "Jet quenching in a strongly coupled anisotropic plasma," JHEP **1208**, 041 (2012) [arXiv:1203.0561 [hep-th]].

[20] A. Rebhan and D. Steineder, "Probing Two Holographic Models of Strongly Coupled Anisotropic Plasma," JHEP **1208**, 020 (2012) [arXiv:1205.4684 [hep-th]].

[21] S. Chakraborty and N. Haque, "Holographic quark-antiquark potential in hot, anisotropic Yang-Mills plasma," Nucl. Phys. B **874**, 821 (2013) [arXiv:1212.2769 [hep-th]].

[22] M. Chernicoff, D. Fernandez, D. Mateos and D. Trancanelli, "Quarkonium dissociation by anisotropy," JHEP **1301**, 170 (2013) [arXiv:1208.2672 [hep-th]].

[23] K. B. Fadafan, D. Giataganas and H. Soltanpanahi, "The Imaginary Part of

the Static Potential in Strongly Coupled Anisotropic Plasma," arXiv:1306.2929 [hep-th].

[24] D. Giataganas and H. Soltanpanahi, "Universal properties of the Langevin diffusion coefficients," arXiv:1310.6725 [hep-th].

[25] S. Chakrabortty, S. Chakraborty and N. Haque, "Brownian motion in strongly coupled, anisotropic Yang-Mills plasma: A holographic approach," arXiv:1311.5023 [hep-th].

[26] M. Ali-Akbari and H. Ebrahim, "Chiral Symmetry Breaking: To Probe Anisotropy and Magnetic Field in QGP," arXiv:1309.4715 [hep-th].

[27] L. Patino and D. Trancanelli, "Thermal photon production in a strongly coupled anisotropic plasma," JHEP **1302**, 154 (2013) [arXiv:1211.2199 [hep-th]].

[28] S. -Y. Wu and D. -L. Yang, "Holographic Photon Production with Magnetic Field in Anisotropic Plasmas," JHEP **1308**, 032 (2013) [arXiv:1305.5509 [hep-th]].

[29] G. Arciniega, P. Ortega and L. Patino, "Brighter Branes, enhancement of photon production by strong magnetic fields in the gauge/gravity correspondence," JHEP **1404**, 192 (2014) [arXiv:1307.1153 [hep-th]].

[30] D. Giataganas, "Observables in Strongly Coupled Anisotropic Theories," PoS Corfu **2012**, 122 (2013) [arXiv:1306.1404 [hep-th]].

[31] V. Jahnke, A. Luna, L. Patio and D. Trancanelli, "More on thermal probes of a strongly coupled anisotropic plasma," JHEP **1401**, 149 (2014) [arXiv:1311.5513 [hep-th]].

[32] D. Lovelock, "The Einstein tensor and its generalizations," J. Math. Phys. **12**, 498 (1971);

[33] B. Zwiebach, "Curvature Squared Terms and String Theories," Phys. Lett. B **156**, 315 (1985);

[34] D. G. Boulware and S. Deser, "String Generated Gravity Models," Phys. Rev. Lett. **55**, 2656 (1985);

[35] R. -G. Cai, "Gauss-Bonnet black holes in AdS spaces," Phys. Rev. D **65**, 084014 (2002) [hep-th/0109133].

[36] T. Padmanabhan and D. Kothawala, "Lanczos-Lovelock models of gravity," Phys. Rept. **531**, 115 (2013) [arXiv:1302.2151 [gr-qc]].

[37] J. D. Edelstein, "Lovelock theory, black holes and holography," Springer Proc. Math. Stat. **60**, 19 (2014) [arXiv:1303.6213 [gr-qc]].

[38] X. O. Camanho, J. D. Edelstein and J. M. Sanchez De Santos, "Lovelock theory and the AdS/CFT correspondence," Gen. Rel. Grav. **46**, 1637 (2014) [arXiv:1309.6483 [hep-th]].

[39] X. O. Camanho and J. D. Edelstein, "Causality in AdS/CFT and Lovelock theory," JHEP **1006**, 099 (2010) [arXiv:0912.1944 [hep-th]].

[40] X. O. Camanho, J. D. Edelstein, G. Giribet and A. Gomberoff, "Generalized phase transitions in Lovelock gravity," arXiv:1311.6768 [hep-th].

[41] X. O. Camanho and J. D. Edelstein, "A lovelock Lovelock black hole bestiary," Class. Quant. Grav. **30**, 035009 (2013) [arXiv:1103.3669 [hep-th]].

[42] V. Jahnke, A. S. Misobuchi and D. Trancanelli, "The Chern-Simons diffusion rate from higher curvature gravity," Phys. Rev. D **89**, 107901 (2014) [arXiv:1403.2681 [hep-th]].

[43] V. Jahnke, A. S. Misobuchi and D. Trancanelli, "Holographic renormalization and anisotropic black branes in higher curvature gravity," JHEP **1501**, 122 (2015) [arXiv:1411.5964 [hep-th]].

[44] V. Jahnke and A. S. Misobuchi, Eur. Phys. J. C **76**, no. 6, 309 (2016) doi:10.1140/epjc/s10052-016-4153-2 [arXiv:1510.03774 [hep-th]].

[45] J. Beringer *et al.* [Particle Data Group Collaboration], "Review of Particle Physics (RPP)," Phys. Rev. D **86**, 010001 (2012).

[46] D. J. Gross and F. Wilczek, "Ultraviolet Behavior of Nonabelian Gauge Theories," Phys. Rev. Lett. **30**, 1343 (1973).

[47] H. D. Politzer, "Reliable Perturbative Results for Strong Interactions?," Phys. Rev. Lett. **30**, 1346 (1973).

[48] S. R. Coleman and E. Witten, "Chiral Symmetry Breakdown in Large N Chromodynamics," Phys. Rev. Lett. **45**, 100 (1980).

[49] M. Gell-Mann, R. J. Oakes and B. Renner, "Behavior of current divergences under SU(3) x SU(3)," Phys. Rev. **175**, 2195 (1968).

[50] T. Schäfer, "Quark matter," [hep-ph/0304281].

[51] M. A. Stephanov, "QCD phase diagram: An Overview," PoS LAT **2006**, 024 (2006) [hep-lat/0701002].

[52] U. M. Heller, "Recent progress in finite temperature lattice QCD," PoS LAT **2006**, 011 (2006) [hep-lat/0610114].

[53] C. Schmidt, "Lattice QCD at finite density," PoS LAT **2006**, 021 (2006) [hep-lat/0610116].

[54] A. Ayala, A. Bashir, J. J. Cobos-Martinez, S. Hernandez-Ortiz and A. Raya, "The effective QCD phase diagram and the critical end point," arXiv:1411.4953 [hep-ph].

[55] M. G. Alford, "Color superconductivity in ultra-dense quark matter," PoS LAT **2006**, 001 (2006) [hep-lat/0610046].

[56] A. Adams, L. D. Carr, T. Schfer, P. Steinberg and J. E. Thomas, "Strongly Correlated Quantum Fluids: Ultracold Quantum Gases, Quantum Chromodynamic Plasmas, and Holographic Duality," New J. Phys. **14**, 115009 (2012) [arXiv:1205.5180 [hep-th]].

[57] E. V. Shuryak, "Theory of Hadronic Plasma," Sov. Phys. JETP **47**, 212 (1978) [Zh. Eksp. Teor. Fiz. **74**, 408 (1978)].

[58] E. V. Shuryak, "Quark-Gluon Plasma and Hadronic Production of Leptons, Photons and Psions," Phys. Lett. B **78**, 150 (1978) [Sov. J. Nucl. Phys. **28**, 408 (1978)] [Yad. Fiz. **28**, 796 (1978)].

[59] Y. Aoki, G. Endrodi, Z. Fodor, S. D. Katz and K. K. Szabo, "The Order of the quantum chromodynamics transition predicted by the standard model of particle physics," Nature **443**, 675 (2006) [hep-lat/0611014].

[60] A. M. Polyakov, "Thermal Properties of Gauge Fields and Quark Liberation," Phys. Lett. B **72**, 477 (1978).

[61] H. Satz, "The Quark-Gluon Plasma: A Short Introduction," Nucl. Phys. A **862-863**, 4 (2011) [arXiv:1101.3937 [hep-ph]].

[62] F. Karsch, "Lattice QCD at high temperature and density," Lect. Notes Phys. **583**, 209 (2002) [hep-lat/0106019].

[63] D. H. Rischke, "The Quark gluon plasma in equilibrium," Prog. Part. Nucl. Phys. **52**, 197 (2004) [nucl-th/0305030].

[64] A. Bazavov, T. Bhattacharya, M. Cheng, N. H. Christ, C. DeTar, S. Ejiri, S. Gottlieb and R. Gupta *et al.*, "Equation of state and QCD transition at finite temperature," Phys. Rev. D **80**, 014504 (2009) [arXiv:0903.4379 [hep-lat]].

[65] P. Di Francesco, P. Mathieu and D. Snchal, "Conformal Field Theory," Springer-Verlag, New York, 1997.

[66] M. G. Alford, Nucl. Phys. Proc. Suppl. **117**, 65 (2003) doi:10.1016/S0920-5632(03)01411-7 [hep-ph/0209287].

[67] H. Satz, "The Quark-Gluon Plasma: A Short Introduction," Nucl. Phys. A **862-863** (2011) 4 [arXiv:1101.3937 [hep-ph]].

[68] I. Y. Aref'eva, Phys. Usp. **57**, 527 (2014) [Usp. Fiz. Nauk **184**, no. 6, 569 (2014)]. doi:10.3367/UFNe.0184.201406a.0569

[69] I. Arsene *et al.* [BRAHMS Collaboration], "Transverse momentum spectra in Au+Au and d+Au collisions at s**(1/2) = 200-GeV and the pseudorapidity dependence of high p(T) suppression," Phys. Rev. Lett. **91**, 072305 (2003)

[70] S. S. Adler *et al.* [PHENIX Collaboration], "Absence of suppression in particle production at large transverse momentum in S(NN)**(1/2) = 200-GeV d + Au collisions," Phys. Rev. Lett. **91**, 072303 (2003) [nucl-ex/0306021].

[71] B. B. Back *et al.* [PHOBOS Collaboration], "Centrality dependence of charged hadron transverse momentum spectra in d + Au collisions at S(NN)**1/2 = 200 GeV," Phys. Rev. Lett. **91**, 072302 (2003) [nucl-ex/0306025].

[72] J. Adams *et al.* [STAR Collaboration], "Evidence from d + Au measurements for final state suppression of high p(T) hadrons in Au+Au collisions at RHIC," Phys. Rev. Lett. **91**, 072304 (2003) [nucl-ex/0306024].

[73] P. H. Ginsparg, "Applied Conformal Field Theory," hep-th/9108028.

[74] O. Aharony, S. S. Gubser, J. M. Maldacena, H. Ooguri and Y. Oz, "Large N field theories, string theory and gravity," Phys. Rept. **323**, 183 (2000) [hep-th/9905111].

[75] L. Brink, J. H. Schwarz and J. Scherk, "Supersymmetric Yang-Mills Theories," Nucl. Phys. B **121**, 77 (1977).

[76] F. Gliozzi, J. Scherk and D. I. Olive, "Supersymmetry, Supergravity Theories and the Dual Spinor Model," Nucl. Phys. B **122**, 253 (1977).

[77] W. Nahm, "Supersymmetries and their Representations," Nucl. Phys. B **135**, 149 (1978).

[78] E. Kiritsis, "String theory in a nutshell," Princeton, USA: Univ. Pr. (2007).

[79] G. 't Hooft, "A Planar Diagram Theory for Strong Interactions," Nucl. Phys. B **72**, 461 (1974).

[80] T. Goto, "Relativistic quantum mechanics of one-dimensional mechanical continuum and subsidiary condition of dual resonance model," Prog. Theor. Phys. **46**, 1560 (1971).

[81] Y. Nambu, Notes prepared for the Copenhagen High Energy Symposium (1970).

[82] K. Becker, M. Becker and J. Schwarz, "String Theory and M-Theory: A Modern Introduction," Cambridge University Press, 2007.

[83] D. Tong, "String Theory," arXiv:0908.0333 [hep-th].

[84] P. Ramond, "Dual Theory for Free Fermions," Phys. Rev. D **3**, 2415 (1971).

[85] A. Neveu and J. H. Schwarz, "Factorizable dual model of pions," Nucl. Phys. B **31**, 86 (1971).

[86] M. B. Green and J. H. Schwarz, "Supersymmetrical Dual String Theory," Nucl. Phys. B **181**, 502 (1981).

[87] M. B. Green and J. H. Schwarz, "Supersymmetrical Dual String Theory. 2. Vertices and Trees," Nucl. Phys. B **198**, 252 (1982).

[88] N. Berkovits, "Super Poincare covariant quantization of the superstring," JHEP **0004**, 018 (2000) [hep-th/0001035].

[89] J. H. Schwarz and P. C. West, "Symmetries and Transformations of Chiral N=2 D=10 Supergravity," Phys. Lett. B **126**, 301 (1983).

[90] J. H. Schwarz, "Covariant Field Equations of Chiral N=2 D=10 Supergravity," Nucl. Phys. B **226**, 269 (1983).

[91] M. Ammon and J. Erdmenger,

[92] J. Polchinski, "Dirichlet Branes and Ramond-Ramond charges," Phys. Rev. Lett. **75**, 4724 (1995) [hep-th/9510017].

[93] J. Casalderrey-Solana, H. Liu, D. Mateos, K. Rajagopal and U. A. Wiedemann, "Gauge/String Duality, Hot QCD and Heavy Ion Collisions," arXiv:1101.0618 [hep-th].

[94] J. Polchinski, "Introduction to Gauge/Gravity Duality," arXiv:1010.6134 [hep-th].

[95] R. C. Myers and S. E. Vazquez, "Quark Soup al dente: Applied Superstring Theory," Class. Quant. Grav. **25**, 114008 (2008) [arXiv:0804.2423 [hep-th]].

[96] B. Zwiebach, "A first course in string theory," Cambridge University Press, 2004.

[97] A. V. Ramallo, "Introduction to the AdS/CFT correspondence," Springer Proc. Phys. **161**, 411 (2015) [arXiv:1310.4319 [hep-th]].

[98] G. W. Gibbons and K. i. Maeda, "Black Holes and Membranes in Higher Dimensional Theories with Dilaton Fields," Nucl. Phys. B **298**, 741 (1988).

[99] G. T. Horowitz and A. Strominger, "Black strings and P-branes," Nucl. Phys. B **360**, 197 (1991).

[100] H. Nastase, "Introduction to AdS-CFT," arXiv:0712.0689 [hep-th].

[101] E. D'Hoker and D. Z. Freedman, "Supersymmetric gauge theories and the AdS / CFT correspondence," hep-th/0201253.

[102] K. Skenderis, "Lecture notes on holographic renormalization," Class. Quant. Grav. **19**, 5849 (2002) [hep-th/0209067].

[103] D. T. Son and A. O. Starinets, "Minkowski space correlators in AdS/CFT correspondence: Recipe and applications," JHEP **0209**, 042 (2002) [hep-th/0205051].

[104] N. Iqbal and H. Liu, "Real-time response in AdS/CFT with application to spinors," Fortsch. Phys. **57**, 367 (2009) [arXiv:0903.2596 [hep-th]].

[105] S. Caron-Huot, P. Kovtun, G. D. Moore, A. Starinets and L. G. Yaffe, "Photon and dilepton production in supersymmetric Yang-Mills plasma," JHEP **0612**, 015 (2006) [hep-th/0607237].

[106] A. Parnachev and D. A. Sahakyan, "Photoemission with Chemical Potential from QCD Gravity Dual," Nucl. Phys. B **768**, 177 (2007) [hep-th/0610247].

[107] D. Mateos and L. Patiño, "Bright branes for strongly coupled plasmas," JHEP **0711**, 025 (2007) [arXiv:0709.2168 [hep-th]].

[108] A. Nata Atmaja and K. Schalm, "Photon and Dilepton Production in Soft Wall AdS/QCD," JHEP **1008**, 124 (2010) [arXiv:0802.1460 [hep-th]].

[109] Y. Y. Bu, "Photoproduction and conductivity in dense holographic QCD," Phys. Rev. D **86**, 026003 (2012); "Electromagnetic signature in holographic plasma with B field," Phys. Rev. D **87**, 026005 (2013).

[110] K. Jo and S. -J. Sin, "Photo-emission rate of sQGP at finite density," Phys. Rev. D **83**, 026004 (2011) [arXiv:1005.0200 [hep-th]].

[111] B. Hassanain and M. Schvellinger, "Plasma conductivity at finite coupling," JHEP **1201**, 114 (2012) [arXiv:1108.6306 [hep-th]].

[112] B. Hassanain and M. Schvellinger, "Diagnostics of plasma photoemission at strong coupling," Phys. Rev. D **85**, 086007 (2012) [arXiv:1110.0526 [hep-th]].

[113] R. Baier, S. A. Stricker, O. Taanila and A. Vuorinen, "Production of Prompt Photons: Holographic Duality and Thermalization," Phys. Rev. D **86**, 081901 (2012) [arXiv:1207.1116 [hep-ph]].

[114] D. Steineder, S. A. Stricker and A. Vuorinen, "Holographic Thermalization at Intermediate Coupling," Phys. Rev. Lett. **110**, no. 10, 101601 (2013) [arXiv:1209.0291 [hep-ph]].

[115] B. Hassanain and M. Schvellinger, "Plasma photoemission from string theory," JHEP **1212**, 095 (2012) [arXiv:1209.0427 [hep-th]].

[116] H. -U. Yee, "Flows and polarization of early photons with magnetic field at strong coupling," Phys. Rev. D **88**, 026001 (2013) [arXiv:1303.3571 [nucl-th]].

[117] D. Steineder, S. A. Stricker and A. Vuorinen, "Probing the pattern of holographic thermalization with photons," JHEP **1307**, 014 (2013) [arXiv:1304.3404 [hep-ph]].

[118] B. Schenke and M. Strickland, "Photon production from an anisotropic quark-gluon plasma," Phys. Rev. D **76**, 025023 (2007) [hep-ph/0611332].

[119] M. Le Bellac, "Thermal Field Theory," Cambridge University Press (1996).

[120] S. S. Gubser, I. R. Klebanov and A. W. Peet, "Entropy and temperature of black 3-branes," Phys. Rev. D **54**, 3915 (1996) [hep-th/9602135].

[121] D. Mateos, R. C. Myers and R. M. Thomson, "Thermodynamics of the brane," JHEP **0705**, 067 (2007) [hep-th/0701132].

[122] A. Karch and L. Randall, "Open and closed string interpretation of SUSY CFT's on branes with boundaries," JHEP **0106**, 063 (2001) [hep-th/0105132].

[123] A. Karch and E. Katz, "Adding flavor to AdS / CFT," JHEP **0206**, 043 (2002) [hep-th/0205236].

[124] G. Policastro, D. T. Son and A. O. Starinets, "From AdS/CFT correspondence to hydrodynamics," JHEP **0209**, 043 (2002) [arXiv:hep-th/0205052].

[125] G. Policastro, D. T. Son and A. O. Starinets, "From AdS/CFT correspondence to hydrodynamics. 2. Sound waves," JHEP **0212**, 054 (2002) [hep-th/0210220].

[126] P. K. Kovtun and A. O. Starinets, "Quasinormal modes and holography," Phys. Rev. D **72**, 086009 (2005) [hep-th/0506184].

[127] M. Kaminski, K. Landsteiner, J. Mas, J. P. Shock and J. Tarrio, "Holographic Operator Mixing and Quasinormal Modes on the Brane," JHEP **1002**, 021 (2010) [arXiv:0911.3610 [hep-th]].

[128] M. Martinez and M. Strickland, "Measuring QGP thermalization time with dileptons," Phys. Rev. Lett. **100**, 102301 (2008) [arXiv:0709.3576 [hep-ph]].

[129] M. Martinez and M. Strickland, "Pre-equilibrium dilepton production from an anisotropic quark-gluon plasma," Phys. Rev. C **78**, 034917 (2008) [arXiv:0805.4552 [hep-ph]].

[130] M. Martinez and M. Strickland, "Suppression of forward dilepton production from an anisotropic quark-gluon plasma," Eur. Phys. J. C **61**, 905 (2009) [arXiv:0808.3969 [hep-ph]].

[131] R. A. Janik and P. Witaszczyk, "Towards the description of anisotropic plasma at strong coupling," JHEP **0809**, 026 (2008) [arXiv:0806.2141 [hep-th]].

[132] A. Rebhan and D. Steineder, "Electromagnetic signatures of a strongly coupled anisotropic plasma," JHEP **1108**, 153 (2011) [arXiv:1106.3539 [hep-th]].

[133] I. Papadimitriou, "Holographic Renormalization of general dilaton-axion gravity," JHEP **1108**, 119 (2011) [arXiv:1106.4826 [hep-th]].

[134] A. Magana, J. Mas, L. Mazzanti and J. Tarrio, "Probes on D3-D7 Quark-Gluon Plasmas," JHEP **1207**, 058 (2012) [arXiv:1205.6176 [hep-th]].

[135] E. V. Shuryak, Phys. Lett. B **79**, 135 (1978). doi:10.1016/0370-2693(78)90453-7

[136] D. J. Gross, R. D. Pisarski and L. G. Yaffe, Rev. Mod. Phys. **53**, 43 (1981). doi:10.1103/RevModPhys.53.43

[137] N. S. Manton, Phys. Rev. D **28**, 2019 (1983). doi:10.1103/PhysRevD.28.2019

[138] F. R. Klinkhamer and N. S. Manton, "A Saddle Point Solution in the Weinberg-Salam Theory," Phys. Rev. D **30**, 2212 (1984);

[139] P. B. Arnold and L. D. McLerran, "The Sphaleron Strikes Back," Phys. Rev. D **37**, 1020 (1988);

[140] D. Kharzeev, R. D. Pisarski and M. H. G. Tytgat, "Possibility of spontaneous parity violation in hot QCD," Phys. Rev. Lett. **81**, 512 (1998);

[141] G. D. Moore and M. Tassler, "The Sphaleron Rate in SU(N) Gauge Theory," JHEP **1102**, 105 (2011).

[142] V. A. Kuzmin, V. A. Rubakov and M. E. Shaposhnikov, Phys. Lett. B **155**, 36 (1985). doi:10.1016/0370-2693(85)91028-7

[143] P. B. Arnold and L. D. McLerran, Phys. Rev. D **36**, 581 (1987). doi:10.1103/PhysRevD.36.581

[144] D. E. Kharzeev, L. D. McLerran and H. J. Warringa, "The Effects of topological charge change in heavy ion collisions: 'Event by event P and CP violation'," Nucl. Phys. A **803**, 227 (2008);

[145] K. Fukushima, D. E. Kharzeev and H. J. Warringa, "The Chiral Magnetic Effect," Phys. Rev. D **78**, 074033 (2008).

[146] U. Gürsoy, I. Iatrakis, E. Kiritsis, F. Nitti and A. O'Bannon, "The Chern-Simons Diffusion Rate in Improved Holographic QCD," JHEP **1302**, 119 (2013) [arXiv:1212.3894 [hep-th]].

[147] P. B. Arnold, D. Son and L. G. Yaffe, "The Hot baryon violation rate is O (alpha-w**5 T**4)," Phys. Rev. D **55**, 6264 (1997) [hep-ph/9609481];

[148] P. Huet and D. T. Son, "Long range physics in a hot nonAbelian plasma," Phys. Lett. B **393**, 94 (1997) [hep-ph/9610259];

[149] D. Bodeker, "On the effective dynamics of soft nonAbelian gauge fields at finite temperature," Phys. Lett. B **426**, 351 (1998) [hep-ph/9801430];

[150] G. D. Moore, "Do we understand the sphaleron rate?," hep-ph/0009161.

[151] G. Koutsoumbas, E. Papantonopoulos and G. Siopsis, "Shear Viscosity and Chern-Simons Diffusion Rate from Hyperbolic Horizons," Phys. Lett. B **677**, 74 (2009) [arXiv:0809.3388 [hep-th]].

[152] G. Basar and D. E. Kharzeev, "The Chern-Simons diffusion rate in strongly coupled N=4 SYM plasma in an external magnetic field," Phys. Rev. D **85**, 086012 (2012) [arXiv:1202.2161 [hep-th]].

[153] B. Craps, C. Hoyos, P. Surowka and P. Taels, "Chern-Simons diffusion rate in a holographic Yang-Mills theory," JHEP **1211**, 109 (2012) [Erratum-ibid. **1302**, 087 (2013)] [arXiv:1209.2532 [hep-th]].

[154] R. C. Myers and B. Robinson, "Black Holes in Quasi-topological Gravity," JHEP **1008**, 067 (2010) [arXiv:1003.5357 [gr-qc]].

[155] R. C. Myers, M. F. Paulos and A. Sinha, "Holographic studies of quasi-topological gravity," JHEP **1008**, 035 (2010) [arXiv:1004.2055 [hep-th]].

[156] M. Brigante, H. Liu, R. C. Myers, S. Shenker and S. Yaida, "Viscosity Bound Violation in Higher Derivative Gravity," Phys. Rev. D **77**, 126006 (2008) [arXiv:0712.0805 [hep-th]]; "The Viscosity Bound and Causality Violation," Phys. Rev. Lett. **100**, 191601 (2008) [arXiv:0802.3318 [hep-th]].

[157] M. Shifman, "Advanced topics in quantum field theory. : A lecture course,"

[158] Y. Kats and P. Petrov, "Effect of curvature squared corrections in AdS on the viscosity of the dual gauge theory," JHEP **0901**, 044 (2009) [arXiv:0712.0743 [hep-th]].

[159] A. Buchel, R. C. Myers and A. Sinha, "Beyond eta/s = 1/4 pi," JHEP **0903**, 084 (2009) [arXiv:0812.2521 [hep-th]].

[160] R. -G. Cai, Z. -Y. Nie, N. Ohta and Y. -W. Sun, "Shear Viscosity from Gauss-

Bonnet Gravity with a Dilaton Coupling," Phys. Rev. D **79** (2009) 066004 [arXiv:0901.1421 [hep-th]].

[161] J. Noronha and A. Dumitru, "The Heavy Quark Potential as a Function of Shear Viscosity at Strong Coupling," Phys. Rev. D **80**, 014007 (2009) [arXiv:0903.2804 [hep-ph]];

[162] J. de Boer, M. Kulaxizi and A. Parnachev, "AdS(7)/CFT(6), Gauss-Bonnet Gravity, and Viscosity Bound," JHEP **1003**, 087 (2010) [arXiv:0910.5347 [hep-th]].

[163] X. O. Camanho, J. D. Edelstein and M. F. Paulos, "Lovelock theories, holography and the fate of the viscosity bound," JHEP **1105**, 127 (2011) [arXiv:1010.1682 [hep-th]].

[164] S. Cremonini, "The Shear Viscosity to Entropy Ratio: A Status Report," Mod. Phys. Lett. B **25**, 1867 (2011) [arXiv:1108.0677 [hep-th]].

[165] J. Polchinski and E. Silverstein, "Large-density field theory, viscosity, and '$2k_F$' singularities from string duals," Class. Quant. Grav. **29**, 194008 (2012) [arXiv:1203.1015 [hep-th]].

[166] J. M. Maldacena and H. Ooguri, "Strings in AdS(3) and SL(2,R) WZW model 1.: The Spectrum," J. Math. Phys. **42**, 2929 (2001) [hep-th/0001053].

[167] J. M. Maldacena, H. Ooguri and J. Son, "Strings in AdS(3) and the SL(2,R) WZW model. Part 2. Euclidean black hole," J. Math. Phys. **42**, 2961 (2001) [hep-th/0005183].

[168] J. M. Maldacena and H. Ooguri, "Strings in AdS(3) and the SL(2,R) WZW model. Part 3. Correlation functions," Phys. Rev. D **65**, 106006 (2002) [hep-th/0111180].

[169] M. J. Duff, "Observations on Conformal Anomalies," Nucl. Phys. B **125**, 334 (1977).

[170] S. 'i. Nojiri and S. D. Odintsov, "On the conformal anomaly from higher derivative gravity in AdS / CFT correspondence," Int. J. Mod. Phys. A **15**, 413 (2000) [hep-th/9903033].

[171] M. Blau, K. S. Narain and E. Gava, "On subleading contributions to the AdS / CFT trace anomaly," JHEP **9909**, 018 (1999) [hep-th/9904179].

[172] K. B. Fadafan, "Charge effect and finite 't Hooft coupling correction on drag force and Jet Quenching Parameter," Eur. Phys. J. C **68**, 505 (2010) [arXiv:0809.1336 [hep-th]].

[173] M. M. Caldarelli, R. Emparan and B. Van Pol, "Higher-dimensional Rotating Charged Black Holes," JHEP **1104**, 013 (2011) [arXiv:1012.4517 [hep-th]].

[174] N. Iqbal and H. Liu, "Universality of the hydrodynamic limit in AdS/CFT and the membrane paradigm," Phys. Rev. D **79**, 025023 (2009) [arXiv:0809.3808 [hep-th]].

[175] X. O. Camanho, J. D. Edelstein, J. Maldacena and A. Zhiboedov, "Causality Constraints on Corrections to the Graviton Three-Point Coupling," arXiv:1407.5597 [hep-th].

[176] M. H. Dehghani and R. B. Mann, "Lovelock-Lifshitz Black Holes," JHEP **1007**, 019 (2010) [arXiv:1004.4397 [hep-th]].

[177] M. Park and R. B. Mann, "Deformations of Lifshitz holography with the Gauss-Bonnet term in $(n+1)$ dimensions," JHEP **1308**, 003 (2013) [arXiv:1305.5578 [hep-th]].

[178] L. Y. Hung, R. C. Myers and M. Smolkin, "On Holographic Entanglement Entropy and Higher Curvature Gravity," JHEP **1104**, 025 (2011) [arXiv:1101.5813 [hep-th]].

[179] A. Bhattacharyya and D. Roychowdhury, "Viscosity bound for anisotropic superfluids in higher derivative gravity," arXiv:1410.3222 [hep-th].

[180] I. Papadimitriou and K. Skenderis, "Correlation functions in holographic RG flows," JHEP **0410**, 075 (2004) [hep-th/0407071].

[181] I. Papadimitriou and A. Taliotis, "Riccati equations for holographic 2-point functions," JHEP **1404**, 194 (2014) [arXiv:1312.7876 [hep-th]].

[182] L. Cheng, X.-H. Ge, Z.-Y. Sun, "Thermoelectric DC conductivities with momentum dissipation from higher derivative gravity," arXiv:1411.5452 [hep-th].

[183] S. S. Gubser, "Drag force in AdS/CFT," Phys. Rev. D **74**, 126005 (2006) [hep-th/0605182].

[184] C. P. Herzog, A. Karch, P. Kovtun, C. Kozcaz and L. G. Yaffe, "Energy loss of a heavy quark moving through N=4 supersymmetric Yang-Mills plasma," JHEP **0607**, 013 (2006) [hep-th/0605158].

[185] K. B. Fadafan, "Charge effect and finite 't Hooft coupling correction on drag force and Jet Quenching Parameter," Eur. Phys. J. C **68** (2010) 505 [arXiv:0809.1336 [hep-th]].

[186] D. Giataganas, "Probing strongly coupled anisotropic plasma," JHEP **1207**, 031 (2012) [arXiv:1202.4436 [hep-th]].

[187] J. Casalderrey-Solana and D. Teaney, "Heavy quark diffusion in strongly coupled N=4 Yang-Mills," Phys. Rev. D **74** (2006) 085012 [hep-ph/0605199].

[188] C. P. Herzog, "Energy Loss of Heavy Quarks from Asymptotically AdS Geometries," JHEP **0609** (2006) 032 [hep-th/0605191].

[189] E. Caceres and A. Guijosa, "Drag force in charged N=4 SYM plasma," JHEP **0611** (2006) 077 [hep-th/0605235].

[190] S. J. Sin and I. Zahed, "Ampere's Law and Energy Loss in AdS/CFT Duality," Phys. Lett. B **648** (2007) 318 [hep-ph/0606049].

[191] T. Matsuo, D. Tomino and W. Y. Wen, "Drag force in SYM plasma with B field from AdS/CFT," JHEP **0610** (2006) 055 [hep-th/0607178].

[192] P. Talavera, "Drag force in a string model dual to large-N QCD," JHEP **0701** (2007) 086 [hep-th/0610179].

[193] E. Antonyan, "Friction coefficient for quarks in supergravity duals," hep-th/0611235.

[194] A. Karch and A. O'Bannon, "Metallic AdS/CFT," JHEP **0709** (2007) 024 [arXiv:0705.3870 [hep-th]].

[195] C. P. Herzog and A. Vuorinen, "Spinning Dragging Strings," JHEP **0710** (2007) 087 [arXiv:0708.0609 [hep-th]].

[196] M. Chernicoff and A. Guijosa, "Energy Loss of Gluons, Baryons and k-Quarks in an N=4 SYM Plasma," JHEP **0702** (2007) 084 [hep-th/0611155].

[197] S. S. Gubser, "Momentum fluctuations of heavy quarks in the gauge-string duality," Nucl. Phys. B **790** (2008) 175 [hep-th/0612143].

[198] J. Casalderrey-Solana and D. Teaney, "Transverse Momentum Broadening of a Fast Quark in a N=4 Yang Mills Plasma," JHEP **0704** (2007) 039 [hep-th/0701123].

[199] M. Chernicoff and A. Guijosa, "Acceleration, Energy Loss and Screening in Strongly-Coupled Gauge Theories," JHEP **0806** (2008) 005 [arXiv:0803.3070 [hep-th]].

[200] F. Bigazzi, A. L. Cotrone, J. Mas, A. Paredes, A. V. Ramallo and J. Tarrio, "D3-D7 Quark-Gluon Plasmas," JHEP **0911** (2009) 117 [arXiv:0909.2865 [hep-th]].

[201] A. Guijosa and J. F. Pedraza, "Early-Time Energy Loss in a Strongly-Coupled SYM Plasma," JHEP **1105** (2011) 108 [arXiv:1102.4893 [hep-th]].

[202] A. Nata Atmaja and K. Schalm, "Anisotropic Drag Force from 4D Kerr-AdS Black Holes," JHEP **1104** (2011) 070 [arXiv:1012.3800 [hep-th]].

[203] J. F. Vazquez-Poritz, "Drag force at finite 't Hooft coupling from AdS/CFT," arXiv:0803.2890 [hep-th].

[204] L. Cheng, X. H. Ge and S. Y. Wu, "Drag force of Anisotropic plasma at finite $U(1)$ chemical potential," arXiv:1412.8433 [hep-th].

[205] K. B. Fadafan, "R**2 curvature-squared corrections on drag force," JHEP **0812**, 051 (2008) [arXiv:0803.2777 [hep-th]].

[206] A. Majumder and M. Van Leeuwen, "The Theory and Phenomenology of Perturbative QCD Based Jet Quenching," Prog. Part. Nucl. Phys. A **66**, 41 (2011) [arXiv:1002.2206 [hep-ph]].

[207] K. M. Burke *et al.* [JET Collaboration], "Extracting the jet transport coefficient from jet quenching in high-energy heavy-ion collisions," Phys. Rev. C **90**, no. 1, 014909 (2014) [arXiv:1312.5003 [nucl-th]].

[208] H. Liu, K. Rajagopal and U. A. Wiedemann, "Calculating the jet quenching parameter from AdS/CFT," Phys. Rev. Lett. **97**, 182301 (2006) [hep-ph/0605178].

[209] H. Liu, K. Rajagopal and U. A. Wiedemann, "Wilson loops in heavy ion collisions and their calculation in AdS/CFT," JHEP **0703**, 066 (2007) [hep-ph/0612168].

[210] F. D'Eramo, H. Liu and K. Rajagopal, "Transverse Momentum Broadening and the Jet Quenching Parameter, Redux," Phys. Rev. D **84**, 065015 (2011) [arXiv:1006.1367 [hep-ph]].

[211] M. Panero, K. Rummukainen and A. Schfer, "Lattice Study of the Jet Quenching Parameter," Phys. Rev. Lett. **112**, no. 16, 162001 (2014) [arXiv:1307.5850 [hep-ph]].

[212] M. Panero, K. Rummukainen and A. Schfer, "Jet quenching from the lattice," Nucl. Phys. A **931** (2014) 393 [arXiv:1407.2963 [hep-lat]].

[213] M. Panero, K. Rummukainen and A. Schfer, "Investigating jet quenching on the lattice," arXiv:1407.2233 [hep-lat].

[214] M. Chernicoff, D. Fernandez, D. Mateos and D. Trancanelli, "Jet quenching in a strongly coupled anisotropic plasma," JHEP **1208**, 041 (2012) [arXiv:1203.0561 [hep-th]].

[215] K. Bitaghsir Fadafan, B. Pourhassan and J. Sadeghi, "Calculating the jet-quenching parameter in STU background," Eur. Phys. J. C **71** (2011) 1785 [arXiv:1005.1368 [hep-th]].

[216] J. Sadeghi and B. Pourhassan, "Jet-quenching of the rotating heavy meson in a $\mathcal{N}$=4 SYM plasma in presence of a constant electric field," Int. J. Theor. Phys. **50** (2011) 2305 [arXiv:1001.0706 [hep-th]].

[217] D. Li, J. Liao and M. Huang, "Enhancement of jet quenching around phase transition: result from the dynamical holographic model," Phys. Rev. D **89** (2014) 12, 126006 [arXiv:1401.2035 [hep-ph]].

[218] B. G. Zakharov, "Radiative energy loss of high-energy quarks in finite size nuclear matter and quark - gluon plasma," JETP Lett. **65**, 615 (1997) [hep-ph/9704255].

[219] Z. q. Zhang, D. f. Hou and H. c. Ren, "The finite 't Hooft coupling correction on jet quenching parameter in a $\mathcal{N} = 4$ Super Yang-Mills Plasma," JHEP **1301**, 032 (2013) [arXiv:1210.5187 [hep-th]].

[220] N. Armesto, J. D. Edelstein and J. Mas, "Jet quenching at finite 't Hooft coupling and chemical potential from AdS/CFT," JHEP **0609**, 039 (2006) [hep-ph/0606245].

[221] J. M. Maldacena, "Wilson loops in large N field theories," Phys. Rev. Lett. **80** (1998) 4859 [hep-th/9803002].

[222] S. J. Rey and J. T. Yee, "Macroscopic strings as heavy quarks in large N gauge theory and anti-de Sitter supergravity," Eur. Phys. J. C **22** (2001) 379 [hep-th/9803001].

[223] K. B. Fadafan, "Heavy quarks in the presence of higher derivative corrections from AdS/CFT," Eur. Phys. J. C **71**, 1799 (2011) [arXiv:1102.2289 [hep-th]].

[224] M. Chernicoff, D. Fernandez, D. Mateos and D. Trancanelli, "Quarkonium dissociation by anisotropy," JHEP **1301** (2013) 170 [arXiv:1208.2672 [hep-th]].

[225] S. J. Rey, S. Theisen and J. T. Yee, "Wilson-Polyakov loop at finite temperature in large N gauge theory and anti-de Sitter supergravity," Nucl. Phys. B **527** (1998) 171 [hep-th/9803135].

[226] A. Brandhuber, N. Itzhaki, J. Sonnenschein and S. Yankielowicz, "Wilson loops in the large N limit at finite temperature," Phys. Lett. B **434** (1998) 36 [hep-th/9803137].

[227] E. Witten, "Anti-de Sitter space, thermal phase transition, and confinement in gauge theories," Adv. Theor. Math. Phys. **2** (1998) 505 [hep-th/9803131].

[228] M. Chernicoff, J. A. Garcia and A. Guijosa, "The Energy of a Moving

Quark-Antiquark Pair in an N=4 SYM Plasma," JHEP **0609** (2006) 068 [hep-th/0607089].

[229] H. Liu, K. Rajagopal and U. A. Wiedemann, "An AdS/CFT Calculation of Screening in a Hot Wind," Phys. Rev. Lett. **98** (2007) 182301 [hep-ph/0607062].

[230] J. Noronha and A. Dumitru, "The Heavy Quark Potential as a Function of Shear Viscosity at Strong Coupling," Phys. Rev. D **80** (2009) 014007 [arXiv:0903.2804 [hep-ph]].

[231] S. I. Finazzo and J. Noronha, "Estimates for the Thermal Width of Heavy Quarkonia in Strongly Coupled Plasmas from Holography," JHEP **1311** (2013) 042 [arXiv:1306.2613 [hep-ph]].

[232] S. I. Finazzo and J. Noronha, "Thermal suppression of moving heavy quark pairs in a strongly coupled plasma," JHEP **1501** (2015) 051 [arXiv:1406.2683 [hep-th]].

[233] S. I. Finazzo and J. Noronha, "Debye screening mass near deconfinement from holography," Phys. Rev. D **90** (2014) 11, 115028 [arXiv:1411.4330 [hep-th]].

[234] R. Rougemont, R. Critelli and J. Noronha, "Anisotropic heavy quark potential in strongly-coupled $\mathcal{N} = 4$ SYM in a magnetic field," Phys. Rev. D **91** (2015) 6, 066001 [arXiv:1409.0556 [hep-th]].

[235] A. Dumitru, Y. Guo and M. Strickland, "The Heavy-quark potential in an anisotropic (viscous) plasma," Phys. Lett. B **662** (2008) 37 [arXiv:0711.4722 [hep-ph]].

[236] S. Caron-Huot, P. Kovtun, G. D. Moore, A. Starinets and L. G. Yaffe, "Photon and dilepton production in supersymmetric Yang-Mills plasma," JHEP **0612**, 015 (2006) [hep-th/0607237].

[237] A. Parnachev and D. A. Sahakyan, "Photoemission with Chemical Potential from QCD Gravity Dual," Nucl. Phys. B **768**, 177 (2007) [hep-th/0610247].

[238] L. Patiño and D. Trancanelli, "Thermal photon production in a strongly coupled anisotropic plasma," JHEP **1302**, 154 (2013) [arXiv:1211.2199 [hep-th]].

[239] V. Jahnke, A. Luna, L. Patiño and D. Trancanelli, "More on thermal probes of a strongly coupled anisotropic plasma," JHEP **1401**, 149 (2014) [arXiv:1311.5513 [hep-th]].

[240] D. Mateos and L. Patiño, "Bright branes for strongly coupled plasmas," JHEP **0711**, 025 (2007) [arXiv:0709.2168 [hep-th]].

[241] A. Nata Atmaja and K. Schalm, "Photon and Dilepton Production in Soft Wall AdS/QCD," JHEP **1008**, 124 (2010) [arXiv:0802.1460 [hep-th]].

[242] Y. Y. Bu, "Photoproduction and conductivity in dense holographic QCD," Phys. Rev. D **86**, 026003 (2012); "Electromagnetic signature in holographic plasma with B field," Phys. Rev. D **87**, 026005 (2013).

[243] K. Jo and S. -J. Sin, "Photo-emission rate of sQGP at finite density," Phys. Rev. D **83**, 026004 (2011) [arXiv:1005.0200 [hep-th]].

[244] B. Hassanain and M. Schvellinger, "Plasma conductivity at finite coupling," JHEP **1201**, 114 (2012) [arXiv:1108.6306 [hep-th]].

[245] B. Hassanain and M. Schvellinger, "Diagnostics of plasma photoemission at strong coupling," Phys. Rev. D **85**, 086007 (2012) [arXiv:1110.0526 [hep-th]].

[246] R. Baier, S. A. Stricker, O. Taanila and A. Vuorinen, "Production of Prompt Photons: Holographic Duality and Thermalization," Phys. Rev. D **86**, 081901 (2012) [arXiv:1207.1116 [hep-ph]].

[247] D. Steineder, S. A. Stricker and A. Vuorinen, "Holographic Thermalization at Intermediate Coupling," Phys. Rev. Lett. **110**, no. 10, 101601 (2013) [arXiv:1209.0291 [hep-ph]].

[248] B. Hassanain and M. Schvellinger, "Plasma photoemission from string theory," JHEP **1212**, 095 (2012) [arXiv:1209.0427 [hep-th]].

[249] H. -U. Yee, "Flows and polarization of early photons with magnetic field at strong coupling," Phys. Rev. D **88**, 026001 (2013) [arXiv:1303.3571 [nucl-th]].

[250] D. Steineder, S. A. Stricker and A. Vuorinen, "Probing the pattern of holographic thermalization with photons," JHEP **1307**, 014 (2013) [arXiv:1304.3404 [hep-ph]].

[251] B. Muller, S. Y. Wu and D. L. Yang, "Elliptic flow from thermal photons with magnetic field in holography," Phys. Rev. D **89** (2014) 2, 026013 [arXiv:1308.6568 [hep-th]].

[252] D. L. Yang and B. Mller, "Collective flow of photons in strongly coupled gauge theories," arXiv:1507.04232 [hep-th].

[253] Y. Bu, "Gauss-Bonnet correction to the R-current correlator in $\mathcal{N} = 4$ theory at strong coupling," Phys. Rev. D **89**, no. 8, 086008 (2014).

[254] S. Y. Wu and D. L. Yang, "Holographic Photon Production with Magnetic Field in Anisotropic Plasmas," JHEP **1308** (2013) 032 [arXiv:1305.5509 [hep-th]].

[255] S. I. Finazzo and R. Rougemont, "Thermal photon and dilepton production and electric charge transport in a baryon rich strongly coupled QGP from holography," arXiv:1510.03321 [hep-ph].

[256] A. Bhattacharyya and D. Roychowdhury, "Viscosity bound for anisotropic superfluids in higher derivative gravity," JHEP **1503**, 063 (2015) [arXiv:1410.3222 [hep-th]].

[257] Y. Kinar, E. Schreiber and J. Sonnenschein, "Q anti-Q potential from strings in curved space-time: Classical results," Nucl. Phys. B **566** (2000) 103 [hep-th/9811192].

[258] M. Ali-Akbari and K. Bitaghsir Fadafan, "Rotating mesons in the presence of higher derivative corrections from gauge-string duality," Nucl. Phys. B **835**, 221 (2010) [arXiv:0908.3921 [hep-th]].

[259] M. Ali-Akbari and K. B. Fadafan, "Conductivity at finite 't Hooft coupling from AdS/CFT," Nucl. Phys. B **844**, 397 (2011) [arXiv:1008.2430 [hep-th]].

[260] K. B. Fadafan, D. Giataganas and H. Soltanpanahi, "The Imaginary Part of the Static Potential in Strongly Coupled Anisotropic Plasma," JHEP **1311**, 107 (2013) [arXiv:1306.2929 [hep-th]].

[261] K. B. Fadafan and S. K. Tabatabaei, "The Imaginary Potential and Thermal Width of Moving Quarkonium from Holography," arXiv:1501.00439 [hep-th].

[262] K. B. Fadafan and S. K. Tabatabaei, "Thermal Width of Quarkonium from Holography," Eur. Phys. J. C **74**, 2842 (2014) [arXiv:1308.3971 [hep-th]].

[263] U. Gürsoy, I. Iatrakis, E. Kiritsis, F. Nitti and A. O'Bannon, "The Chern-Simons Diffusion Rate in Improved Holographic QCD," JHEP **1302**, 119 (2013) [arXiv:1212.3894 [hep-th]].